UNIVERSITY OF BIRMINGHAM

IMAGING THE INJURED BEATING HEART INTRAVITALLY AND THE VASCULOPROTECTION AFFORDED BY HAEMATOPOIETIC STEM CELLS IN MYOCARDIAL ISCHAEMIA/REPERFUSION INJURY

By

Adam Bin Lokman

A thesis submitted to the University of Birmingham

for the degree of

DOCTOR OF PHILOSOPHY

College of Medical and Dental Sciences

School of Clinical and Experimental Medicine

The University of Birmingham

March 2020

Abstract

Myocardial ischaemia/reperfusion (IR) injury is a major contributor to the clinical mortality and morbidity in patients who have suffered a myocardial infarction (MI). Although stem cell (SC)-based therapy for MI holds promise, clinical success has been poor. This may be due to a lack of knowledge of whether systemically infused SCs efficiently home and adhere within the injured heart and whether therapeutic mechanisms involve SCs conferring vasculoprotection in damaged coronary microvessels. Indeed, the microcirculatory perturbations that occur during myocardial IR injury itself are not well understood, as pre-clinical research has been incapable of routinely and reliably directly imaging the beating heart *in vivo*. This study has presented a novel technique for visualising these disturbances through the use of intravital microscopy (IVM) alongside ventricular blood flow assessment. Laser speckle contrast imaging (LSCI) showed a sustained hyperaemic ventricular response during reperfusion that was not transmitted downstream, as IVM of the coronary microcirculation showed heterogenic flow with patchy, disorganised reperfusion and reduced functional capillary density. This was accompanied by a thrombo-inflammatory response leading to aggregates of microthrombi that occluded coronary capillaries. There was a significant and rapid increase in adherent platelets, neutrophils and monocytes in the IR injured heart. HSC therapy produced a remarkable reverse in these phenomena in IR injured hearts, alleviating the thrombo-inflammatory response and restoring the microcirculation to an organised state. Surprisingly, this was achieved without the need for HSCs to home to the injured heart. This suggest an important paracrine role in HSC therapy that confers vasculoprotection to the microvessels of the heart, likely through a reduction in oxidative stress-induced endothelial cell damage, which was characterised by a reduction in levels of 8-OHdG (a marker for oxidative damage) and endothelial adhesion molecules (ICAM-1 & VCAM-1). This is also the first study to show the pro-inflammatory effects of topical application of IL-36 isoforms on the beating heart, with promising potential for the IL-36 receptor antagonist to reduce the inflammatory infiltration observed in IR injured hearts.

Publications Arising from this Thesis:

Papers:

Dean PJ Kavanagh*, Adam B Lokman*, Georgiana Neag, Abigail MM Colley, Neena Kalia

Imaging the injured beating heart intravitally and the vasculoprotection afforded by haematopoietic stem cells, Cardiovascular Research, Volume 115, Issue 13, 1 November 2019, Pages 1918–1932, https://doi.org/10.1093/cvr/cvz118 * Joint first authors

Oral Presentations:

Institute of Cardiovascular Sciences Away Day 2018, University of Birmingham, UK

Adam B Lokman, Dean PJ Kavanagh, Neena Kalia

Imaging the vasculoprotective effects of haematopoietic stem cells (HSCs) following myocardial ischaemia-reperfusion (IR) injury in the murine beating heart

HONOURABLE MENTION

68th Meeting of the British Microcirculation Society 2018, University of Nottingham, UK

Adam B Lokman, Dean PJ Kavanagh, Georgiana Neag, Neena Kalia

Imaging the vasculoprotective effects of haematopoietic stem cells (HSCs) following myocardial ischaemia-reperfusion (IR) injury in the murine beating heart

ORAL PRIZE WINNER

2nd Midlands Academy of Medical Sciences Research Festival 2017, University of Warwick, UK

Adam B Lokman, Dean PJ Kavanagh, Abigail MM Colley, Neena Kalia

Intravital imaging of leukocyte and stem cell trafficking in the cardiac microcirculation following myocardial ischaemia-reperfusion injury

Poster Presentations:

3rd Midlands Academy of Medical Sciences Research Festival 2018, Loughborough University, UK

Adam B Lokman, Dean PJ Kavanagh, Abigail MM Colley, Neena Kalia

Vascuoloprotective effects of haematopoietic stem cells in combatting a heart attack

Inaugural Open Scientific Meeting, Midlands Cardiovascular Research Network 2017, University of Leicester, UK

Adam B Lokman, Dean PJ Kavanagh, Abigail MM Colley, Neena Kalia

Utilising intravital imaging to determine the vasculoprotective effects of haematopoietic stem cells in myocardial ischaemia/reperfusion injury

POSTER PRIZE WINNER

67th Meeting of the British Microcirculation Society 2017, University of Birmingham, UK

Adam B Lokman, Dean PJ Kavanagh, Abigail MM Colley, Neena Kalia

Intravital imaging of leukocyte, platelet and stem cell trafficking in vivo in the cardiac microcirculation following myocardial ischaemia-reperfusion injury

Published Conference Proceedings:

Adam Lokman, Dean Kavanagh, Georgiana Neag, Neena Kalia. PP7. Intravitally imaging endogenous monocyte trafficking in the injured murine beating heart and assessing whether HSC and interleukin-36 modify their presence. ***Microcirculation*** 2020, 27:e12589 (69th British Microcirculation Society Conference, Exeter 2019)

A. Lokman, D.P.J. Kavanagh, G.Neag, N. Kalia. P7: Imaging the vasculoprotective effects of haematopoietic stem/progenitor cells (HSPCs) following myocardial ischaemia-reperfusion (IR) injury in the murine beating heart. ***Cardiovascular Drugs and Therapy*** 2019; 33:261-274. (British Society of Cardiovascular Research Autumn Conference, Cambridge 2019)

Adam Lokman, Dean Kavanagh, Georgiana Neag, Asif Iqbal, Neena Kalia. 117 Intravital imaging of vasculoprotective effects of haematopoietic stem/progenitor cells following myocardial ischaemia-reperfusion injury in the beating mouse heart. ***Journal of Vascular Research*** 2019; 56(suppl 1):1-134 (3rd Joint ESM-EVBO Conference, Maastricht 2019)

A. Lokman, D.P.J. Kavanagh, G. Neag, N. Kalia. OP11. Imaging the vasculoprotective effects of haematopoietic stem cells (HSCs) following myocardial ischaemia-reperfusion (IR) injury in the murine beating heart. ***Microcirculation*** 2018, 25:e12489 (68th British Microcirculation Society Conference, Nottingham 2018)

Dean Kavanagh, Adam Lokman, Neena Kalia. 142. Intravital imaging of leukocyte, platelet and stem cell trafficking in vivo in the cardiac microcirculation following myocardial ischaemia-reperfusion injury. ***Heart*** 2017; 103:A106-A107. (Joint BAS/BSCR/BCS Conference, Manchester 2017)

N. Kalia, A. Lokman, D. Kavanagh. 5A-01. Imaging of leukocyte and stem cell trafficking in vivo in the beating mouse heart microcirculation following myocardial ischaemia-reperfusion injury. ***Journal of Vascular Research*** 2017; 54(suppl 1):1-80 (2nd Joint ESM-EVBO Conference, Geneva 2017)

K. Bumroongthai, A. Lokman, D.P.J. Kavanagh, N. Kalia. PC36. Expansion in 3D culture alters the morphology and adhesive capability to the injured heart of mesenchymal and haematopoietic stem cells. ***Microcirculation*** 2017; 24:e12391. (67th British Microcirculation Society Conference, Birmingham 2017)

D. Kavanagh, A. Lokman, N. Kalia. OC6. Intravital imaging of leukocyte, platelet and stem cell trafficking in vivo in the beating mouse heart microcirculation following myocardial IR injury. ***Microcirculation*** 2017; 24:e12391. (67th BMS Conference, Birmingham 2017)

D.P.J. Kavanagh, A. Lokman, N. Kalia. PP31. *In vivo* imaging of microcirculatory disturbances associated with the ageing and ischaemically injured mouse heart. ***Microcirculation*** 2017; 24:e12287. (66th British Microcirculation Society Conference, Newcastle 2016)

“A Silent Wish”

In memory of

Uncle Mike

&

Uncle Don

Thank you for the memories. Sorry that I didn’t do more. InsyaAllah, we’ll meet again.

“My Mercy Mirror” (Within Temptation)

“Time is a cruel healer. For it doesn’t remedy, it simply abandons”

“Nothing more to say, nothing left to break.

Nothing more to give, nothing left to take”

(Lady Antebellum)

“and (God) is with you wheresoever you may be”

(Qur’an – 57:4)

Acknowledgements

First and foremost, I must give a huge thanks to Dr. Neena Kalia for your guidance throughout my PhD and with the write-up of my thesis. It was an amazing opportunity to be allowed to conduct this work. I, however, have not been the easiest person to guide and have caused too much trouble to many, including you. I apologise for that. Thank you for your patience. Huge thanks must go to Dr. Dean Kavanagh as well, for your help in training me and being a reliable science 'spotter'. That first year we spent bashing our heads against walls optimising this work is baked in memory. Of course, you re-kindled my love for 80s music when I had all but forgotten it! The last thing I thought I'd be doing in this PhD was belting out Michael Bolton hits with you, or getting hyped about marble racing, but it was seriously fun. Sorry if I was ever rude and thanks for being a friend.

Thank you to the little guys that gave up so much to make this work, and ultimately research as a whole, bear fruition.

To everyone I met on this journey, whether it be Team Kalia groupmates, fellow PhD students, lab co-workers, office buddies or people I met elsewhere, thank you all too. When I first started, I wasn't sure I'd complete 3 months, let alone 3 years, due to health reasons. It was hard at times. But everyone close made me easily forget my issues; I honestly think it helped me recover quicker, even if you guys didn't know. Even when other health issues would crop up, affecting me on a daily basis at times – yet again, the people around me just made me forget. Honestly, I had a lot of fun with everyone, especially during long, hard days. You guys made a lot of difference. At times, I have not been the easiest person to work with or just be around personally. I'm sorry for not being helpful at times or for being selfish often. I can only hope I did some good for you guys. I wish you all the best.

To my mom, dad and sister, and my extended family, I owe you all so much. Thank you for your patience and for your support. None of my accomplishments are ever just mine, they are ours. I'm sorry for being a burden at times and for not doing more. I don't think I could ever repay the debt of gratitude, but hopefully I'll do better.

To God, thank You. I wasn't quite sure what to expect undertaking this chapter in life, but it has been an immense rollercoaster ride. Thank You for the experience. A friend once asked what I thought God might be "saying" to me after prayers. After some thought, I replied "to not give up". I ask that You help everyone else to not give up.

Table of Contents

1. General Introduction **01-57**

- **1.1 Myocardial Ischaemia-Reperfusion (IR) Injury** **02-10**
  - 1.1.1 Cardiac Ischaemia 03-04
  - 1.1.2 Post-Ischaemic Reperfusion of Cardiac Tissue 04-09
  - 1.1.3 Global Effects of Myocardial IR Injury 09-10
- **1.2 Cardiac Damage Resulting from IR Injury** **11-14**
  - 1.2.1 Myocardial Stunning 11
  - 1.2.2 No-Reflow Phenomenon 12
  - 1.2.3 Reperfusion Arrhythmias 13
  - 1.2.4 Lethal Reperfusion Injury 14
- **1.3 Coronary Microcirculation in Myocardial IR Injury** **15-19**
  - 1.3.1 Endothelial Cells 19
- **1.4 Oxidative Stress in Myocardial IR Injury** **20-24**
  - 1.4.1 Sources of ROS 21-22
  - 1.4.2 Pre-clinical Studies of Antioxidant Therapy in Myocardial IR Injury 22-23
  - 1.4.3 Clinical Trials of Antioxidant Therapy in Myocardial IR Injury 23-24
- **1.5 Pro-thrombogenic Microenvironment in Myocardial IR Injury** **25-28**
- **1.6 Inflammatory Response during Myocardial IR Injury** **28-45**
  - 1.6.1 Pro-inflammatory Cytokines 29-37
  - 1.6.2 Leukocyte Trafficking 37-42
  - 1.6.3 Innate Immune Response 42-47
- **1.7 Stem Cells as a Therapeutic Option Myocardial IR Injury** **47-54**
  - 1.7.1 Haematopoietic Stem Cells (HSCs) 49-50
  - 1.7.2 Mesenchymal Stem Cells (MSCs) 51-52
- **1.8 Imaging the Beating Mouse Heart In Vivo – Intravital Microscopy (IVM)** **55-56**
- **1.9 Summary** **56-57**
- **1.10 Aims and Hypotheses** **58-59**

2. Materials & Methods **60-103**

- **2.1 Materials** **61-63**
- **2.2 Animal Usage** **63**
- **2.3 Cell Culture, Cell Isolation, Labelling of Cells and Preparation of Cultured Media** **64-72**
  - 2.3.1 Culturing of Murine Vena Cava Endothelial Cells 64-65
  - 2.3.2 Culturing of Haematopoietic Progenitor Cell-7s (HPC-7s) 65-66
  - 2.3.3 Culturing of Mesenchymal Stem Cells 66-67

- 2.3.4 Preparation of CFSE-Labelled Fluorescent Cells 68-72
- **2.4 *In Vivo* Studies – Murine Myocardial IR Injury 72-74**
  - 2.4.1 Pre-surgery Preparation 72
  - 2.4.2 Inducing Murine Myocardial IR Injury 73-74
  - 2.4.3 Laser Speckle Contrast Imaging (LSCI) 74
- **2.5 Intravital Microscopy Based Studies 75-85**
  - 2.5.1 Murine Myocardial IR Injury 75-81
  - 2.5.2 Murine Cardiac Thermal Ablation Injury 81-82
  - 2.5.3 Murine Cardiac Topical Injury 82-83
  - 2.5.4 Analysis of IVM and Laser Speckle Contrast Images 83-85
- **2.6 *In Vitro* Studies – Assessment of Myocardial IR Injury 85-93**
  - 2.6.1 Frozen Tissue Sections 85-90
  - 2.6.2 Plasma Cytokine Measurements 90
  - 2.6.3 Triphenyl Tetrazolium Chloride (TTC) Staining 92-93
- **2.7 *In Vitro* Studies – Endothelial-Stem Cell Co-Culture 93-98**
  - 2.7.1 Endothelial-Stem Cell Co-Culture Assay Setup 94
  - 2.7.2 Reactive Oxygen Species (Superoxide; $O2^{-}$) Staining Protocol using Dihydroethidium 95
  - 2.7.3 Oxidative Damage Staining Protocol (Anti-8-OHdG) 96-97
  - 2.7.4 Analysis of Endothelial-Stem Cell Co-Culture Assays 97
- **2.8 Flow Cytometry Based Studies 97-102**
  - 2.8.1 Isolation of Cells from Digested Mouse Hearts 97-98
  - 2.8.2 Assessing Oxidative Damage Levels in the Murine Heart 98-99
  - 2.8.3 Assessing Upregulation of Adhesion Molecules on ECs after Myocardial IR Injury 100
  - 2.8.4 Assessing HPC-7 Recruitment to Various Organs during Myocardial IR Injury 100
  - 2.8.5 Assessing Efficacy of Labelling Circulating Monocytes via Fluorescent Microbeads 101
  - 2.8.6 Assessing Monocyte Population in the Murine Heart after IR Injury 101-102
  - 2.8.7 Assessment of Whole Blood Counts 102
  - 2.8.8 Analysis of Flow Cytometry and Whole Blood Counts 102
- **2.9 Statistical Analysis 103**

3. Vasculoprotective Effects of Stem Cells – *In Vitro* Studies 104-139

- **3.1 Introduction 105-107**
  - 3.1.1 Hypotheses and Aims 106-107
- **3.2 Methods 107-108**
- **3.3 Results 109-124**
  - 3.3.1 Stress and Inflammatory Markers on IR Injured Murine Heart Tissue are Increased 109

- 3.3.2 Adhesion Capabilities of Different Stem Cell Types to Murine Heart Tissue Sections Varies *in vitro* 111
- 3.3.3 Correlation between Stem Cell Adhesion and 8-OHdG Expression 111-112
- 3.3.4 Correlation between Stem Cell Adhesion and VCAM-1 Expression 112
- 3.3.5 Endothelial-Stem Cell Co-Culture: Protective Effects of HPC-7s as Determined by ROS Generation at 24 & 72 Hours 116
- 3.3.6 Endothelial-Stem Cell Co-Culture: Protective Effects of BM MSCs as Determined by ROS Generation at 24 & 72 Hours 118
- 3.3.7 Endothelial-Stem Cell Co-Culture: Protective Effects of HPC-7s as Determined by Oxidative Stress Induced in Endothelial Cells at 24 & 72 Hours 118-119
- 3.3.8 Endothelial-Stem Cell Co-Culture: Protective Effects of BM MSCs as Determined by Oxidative Stress Induced in Endothelial Cells at 24 & 72 Hours 119
- 3.3.9 Endothelial-Stem Cell Co-Culture: WJ MSCs Disrupt the Endothelial Cell Monolayer 123
- 3.3.10 Stem Cell Morphology 123-124

- **3.4 Discussion 124-139**
  - 3.4.1 Establishing a Myocardial Ischaemia/Reperfusion Injury Mouse Model 127-129
  - 3.4.2 Haematopoietic Stem Cells 129-134
  - 3.4.3 Mesenchymal Stem Cells 134-138
  - 3.4.4 Shape Considerations of HPC-7s, BM MSCs and WJ MSCs 138
  - 3.4.5 Conclusion 139

4. Vasculoprotective Effects of Stem Cells – *In Vivo* Studies 140-197

- **4.1 Introduction 141-144**
  - 4.1.1 Hypotheses and Aims 143-144
- **4.2 Methods 145-146**
- **4.3 Results 147-178**
  - 4.3.1 Developing a Successful Protocol for Imaging the Mouse Beating Heart Coronary Microcirculation *in vivo* 147-148
  - 4.3.2 HPC-7s Therapy Reduces Infarct Size after Myocardial IR Injury 148
  - 4.3.3 Analysing Regional Blood Flow Dynamics in Beating Mouse Hearts using Full Field Laser Speckle Contrast Imaging 151-152
  - 4.3.4 Laser Speckle Contrast Imaging Revealed a Sustained Reactive Myocardial Hyperaemia in Response to IR Injury Alone and IR Injury + HPC-7s 152-153

- 4.3.5 Intravital Microscopy Revealed Myocardial IR Injury was Associated with Impaired Capillary Perfusion which was Improved with HPC-7s 153-154
- 4.3.6 Intravital Microscopy Revealed an Increase in Endogenous Neutrophil Adhesion Following Myocardial IR Injury but these did not Appear to Compromise Blood Flow 159-160
- 4.3.7 Intravital Microscopy Revealed that Platelet Microthrombi Contributed to Microvascular Occlusive Events Following Myocardial IR Injury 160-161
- 4.3.8 Intravital Microscopy Revealed an Increase in Individual Platelet Adhesion Following Myocardial IR Injury 168
- 4.3.9 HPC-7s Therapy Attenuates the Significant and Rapid Increase in both Neutrophil and Platelet Recruitment Following Myocardial IR Injury 168-169
- 4.3.10 Intravital Microscopy Revealed Myocardial IR Injury was Associated with Increased Monocyte Recruitment which was Decreased with HPC-7s 169-170
- 4.3.11 Detecting Macrophages in the Mouse Heart 170-171
- 4.3.12 Balloon Ligation as an Alternative Method in Ligating the LAD Artery 171-172
- 4.3.13 Myocardial Sterile Burn Injury Induces a Visible Inflammatory Response which could be Detected using Intravital Microscopy 172-173

- **4.4 Discussion 179-197**
  - 4.4.1 Establishing a Model for Intravital Imaging of the Murine Beating Heart 180-182
  - 4.4.2 Mismatch between Global Hyperaemia and Microcirculatory Flow Heterogeneity 182-184
  - 4.4.3 Rapid and Sustained Inflammatory Response 184-187
  - 4.4.4 Intravital Imaging of Monocyte Trafficking in the Beating Mouse Heart *in vivo* 175-189
  - 4.4.5 Remarkable Thrombotic Events within IR Injured Coronary Capillaries 189-190
  - 4.4.6 Stem Cells Confer Vasculoprotection in the IR Injured Beating Heart 190-194
  - 4.4.7 Technical Limitations of the Study 194-196
  - 4.4.8 Conclusion 197

5. Mechanisms Explaining HSC Vasculoprotective Effects 198-248

- **5.1 Introduction 199-203**
  - 5.1.1 Hypotheses and Aims 202-203
- **5.2 Methods 203-205**
- **5.3 Results 206-233**

- 5.3.1 HPC-7s Demonstrate Low Levels of Adhesion within the Coronary Microcirculation following Myocardial IR Injury 206
- 5.3.2 Non-Specific HPC-7s Retention Identified within Non-Injured Lungs and Liver 206-207
- 5.3.3 HPC-7s Cultured Media (CM) Is Not Vasculoprotective 208
- 5.3.4 Flow Cytometric Analysis of Oxidative Stress and ICAM-1/VCAM-1 in Whole Hearts 212-213
- 5.3.5 Endothelial Cells are More Susceptible to Oxidative Stress than Cardiomyocytes following IR Injury – HPC-7s Therapy Reduces this Oxidative Damage in Endothelial Cells 213-214
- 5.3.6 Myocardial IR Injury Induces an Upregulation of ICAM-1 and VCAM-1 in Endothelial Cells-HPC-7s Therapy Reduces this Adhesion Molecule Upregulation 214-215
- 5.3.7 HPC-7s Therapy Reduces Plasma Levels of Multiple Inflammatory Cytokines but Increased Levels of IL-10 215
- 5.3.8 Circulating Cell Profile in Murine Peripheral Blood following Myocardial IR Injury 222
- 5.3.9 Verification of Circulating Monocytes Population Labelling with Fluorescent Latex Microparticles 222-223
- 5.3.10 Myocardial IR Injury Causes Recruitment of Pro-Inflammatory Monocyte Sub-Population but HPC-7s Therapy Induces a Generalised Reduction of all Monocytes 223-224
- 5.3.11 Topical Application of Either IL-36 α or β to the Beating Mouse Heart Promotes Monocyte Recruitment *in vivo* while IL-36β + HPC-7s Therapy Inhibited this Effect 225
- 5.3.12 Topical Application of Either IL-36 α or β to the Beating Mouse Heart Promotes Neutrophil Recruitment *in vivo* while IL-36β + HPC-7s Therapy did not Inhibit this Effect 230
- 5.3.13 IL-36RA Treatment Reduces Inflammatory Recruitment following Myocardial IR Injury 231

5.4 Discussion 234-248

- 5.4.1 HPC-7s do not Adhere within the Heart during Reperfusion 235-238
- 5.4.2 Cellular Mechanisms by which HPC-7s Confer Vasculoprotection 238-247
- 5.4.3 Conclusion 248

6. General Discussion 249-264

- **6.1 Summary of Main Findings 250-260**
- **6.2 Imaging the Beating Mouse Heart with Intravital Microscopy 260-261**
- **6.3 Future Work 262-264**
- **6.4 Concluding Remarks 264**

7. References 265-279

Abbreviations

$^{\cdot}OH$	Hydroxyl Radical
8-OHdG	8-Hydroxy-2'-Deoxyguanosine
AAR	Area At Risk
ab	Antibody
ACD	Acid Citrate Dextrose
ANG-1	Angiopoeitin-1
ASPA	Animals Scientific Procedures Act
ATP	Adenosine Triphosphate
BH_4	Tetrahydrobiopterin
BM	Bone Marrow
BP	Blood Pressure
BSA	Bovine Serum Albumin
Ca^{2+}	Calcium Ion
CAT	Catalase
CCR	C-C Chemokine Receptor
CFDA-SE	Carboxyfluorescein Diacetate Succinimidyl Ester
CFSE	Carboxyfluorescein Succinimidyl Ester
CMR	Cardiac Magnetic Resonance
cTnT	Cardiac Troponin T
DAMP	Damage-Associated Molecular Patterns
DC	Dendritic Cell
DHE	Dihydroethidium
DMEM	Dulbecco's MEM
DMSO	Dimethyl Sulphoxide
DSS	Dextran Sulphate Sodium
EC	Endothelial Cell
ECG	Electrocardiographic
eNOS	Endothelial Nitric Oxide Synthase
ER	Endoplasmic Reticulum
ESC	Embryonic SC
ESL-1	E-selectin ligand-1
FBS	Foetal Bovine Serum
FCD	Functional Capillary Density
FGF-2	Fibroblast Growth Factor-2
hsCRP	High-Sensitivity C-Reactive Protein
H^+	Hydrogen Ion
H_2O_2	Hydrogen Peroxide
HPC	Haematopoietic Progenitor Cell
HSC	Haematopoietic Stem Cell
ICAM-1	Intercellular Adhesion Molecule-1

IFN-γ	Interferon-gamma
IgSF	Immunoglobulin Superfamily
IHC	Immunohistochemistry
IL	Interleukin
IMR	Index of Microcirculatory Resistance
iPSC	Induced Pluripotent SC
IR	Ischaemia/Reperfusion
IVIS	In Vivo Imaging System
IVM	Intravital Microscopy
JAM-A	Junctional Adhesion Molecule-A
LAD	Left Anterior Descending
LBRC	Lateral Border Recycling Compartment
LFA-1	Lymphocyte Function-Associated Antigen 1
LSCI	Laser Speckle Contrast Imaging
Ly6	Lymphocyte Antigen 6
MAO	Monoamine Oxidase
MAP	Mitogen-Activated Protein
MEM	Modified Eagle's Media
Mg^{2+}	Magnesium Ion
MI	Myocardial Infarction
MMP	Matrix Metalloprotease
MP	Microparticle
MPO	Myeloperoxidase
MPTP	Mitochondrial Permeability Transition Pores
MSC	Mesenchymal Stem Cell
NADPH	Nicotinamide Adenine Dinucleotide Phosphate
NCA	N-acetyl cysteine
NCE	Sodium-Calcium Exchanger
NF-kB	Nuclear Factor kappa-light-chain-enhancer of Activated B Cells
NHE	Sodium-Hydrogen Exchanger
NO_3^-	Nitrate
NOX	NADPH Oxidase
Nrf2	Nuclear factor erythroid 2-related factor 2
O_2^-	Superoxide
OCT	Optimal Cutting Temperature
P/S	Penicillin/Streptomycin
PBMC	Primary Bone Marrow Cell
PBS	Phosphate Buffer Solution
PCA	Percutaneous Coronary Angioplasty
PCI	Percutaneous Coronary Intervention
PDGFR- α	Platelet-Derived Growth Factor Receptor alpha
PECAM-1	Platelet-EC Adhesion Molecule-1

PET	Positron Emission Tomography
PGI_2	Prostaglandin I_2
PKSOD	Microparticles Encapsulating SOD
PMCA	Plasma Membrane Calcium Ion-ATPase
PRP	Platelet-Rich Plasma
PSGL-1	P-selectin glycoprotein ligand-1
RNS	Reactive Nitrogen Species
ROS	Reactive Oxygen Species
SC	Stem Cell
Sca-1	Stem Cell Antigen-1
SCF	Stem Cell Factor
SEM	Standard Error of the Mean
SOD	Superoxide Dismutase
SpAn	Basic Speckle Analysis
SPS	StemPro Suppliment
SR	Sarcoplasmic Reticulum
TGF-β	Transforming Growth Factor-beta
TIMI	Thrombolysis In MI
TNBS	2,4,6-Trinitro Benzene Sulphonic Acid
TNF-α	Tumour Necrosis Factor-alpha
TTC	Triphenyl Tetrazolium Chloride
TUNEL	Terminal Deoxynucleotidyl Transferase dUTP Nick End Labelling
UPA	Urokinase-type Plasminogen Activator
VAP-1	Vascular Adhesion Protein-1
VCAM-1	Vascular Cell Adhesion Molecule-1
VCEC	Vena Cava EC
VE-Cadherin	Vascular Endothelial Cadherin
VEGF-A	Vascular Endothelial Growth Factor-A
VLA-4	Very Late Antigen-4
WJ	Wharton's Jelly
WT	Wild-Type
XO	Xanthine Oxidase

CHAPTER 1:

GENERAL INTRODUCTION

1.1 Myocardial Ischaemia-Reperfusion (IR) Injury

Myocardial infarction (MI), also known as a heart attack, is the leading cause of death worldwide and accounts for nearly 70,000 deaths per annum in the UK [1]. Coronary artery disease accounts for the majority of cases of MI due to atherosclerotic plaque rupture and subsequent thrombus formation. The sudden thrombus formation can rapidly block the lumen of a coronary artery, obstructing blood flow downstream [2]. Prolonged cessation of blood flow to cells in the cardiac tissue of the region affected will inevitably cause cellular injury and death. MI in and of itself can be lethal depending on its severity, as lack of oxygen and nutritional supply to cardiac tissue can cause irreversible damage on a time-dependant scale. Current treatment strategies for MI focusses on rapidly re-establishing myocardial perfusion following blockage in one or more of the coronary arteries. This can be achieved through pharmacological therapy or minor and major surgery [3]. Most commonly, this is achieved by a procedure called a primary percutaneous coronary intervention (PCI) or stent placement to open the culprit artery. This is combined with dual anti-platelet therapy which aims to prevent thrombotic events taking place in the stent and the re-occurrence of future MI or stroke.

As stated previously, there still exists a high rate of extensive muscle damage and heart failure and thus severe morbidity and mortality associated with MI even in patients given optimal therapy such as PCI. Hence, there is a need for more research into this area. Several studies have shown that while reperfusing the heart is vital, the initial period of reperfusion itself can inflict additional damage onto cardiac tissue [4]. Myocardial ischaemia/reperfusion (IR) injury is the term used to define cardiac tissue injury triggered by a period of ischaemia to the heart followed by paradoxical tissue injury driven by the initial period of reperfusion as coronary

blood flow is restored [5]. Indeed, restoration of normal epicardial blood vessel flow but with sub-optimal myocardial perfusion, can be observed in as high as 50% of PCI patients, leading to worse outcomes than in patients with full perfusion recovery [6-9]. This paradoxical response is therefore an area of interest as cardioprotective treatments administered at the point of reperfusion have the potential to improve the prognosis following an MI [10, 11].

1.1.1 Cardiac Ischaemia

Reduction of blood flow to cardiac tissue will result in the switching of cells to perform anaerobic metabolism instead of aerobic metabolism [5]. This switch is essential in prolonging cell function via production of adenosine triphosphate (ATP) during periods of ischaemia. However, cells can only maintain this change for short periods of time. During anaerobic metabolism, the pH level of cells reduce and the production of ATP generated is typically not sufficient to maintain the function of ATP-reliant enzymes such as the plasma membrane calcium ion (Ca^{2+})-ATPase (PMCA) [12]. In order to compensate for the fall in pH, hydrogen ions (H^+) are transported out of the cell via the sodium ion/hydrogen ion (Na^+/H^+) exchanger (NHE), resulting in increased intracellular Na^+ [13]. In order to compensate for the increased intracellular Na^+, the Na^+/Ca^{2+} exchanger (NCE) in turn transports Na^+ out of the cell whilst transporting Ca^{2+} into the cell. The net effect of the various altered ion exchange processes and ATP depletion is an overload of Ca^{2+} intracellularly during ischaemia. Ca^{2+} overload can cause damage to cellular structures either directly via proteolytic pathological events or indirectly by initiating pro-inflammatory cytokine release such as tumour necrosis factor-alpha (TNF-α) [12]. The mitochondria within cells are also affected by ischaemia. Mitochondria

exhibit slight structural changes such as swelling and cristae disruption during ischaemia however, this belies the important changes that occur within mitochondria [5]. Ischaemia causes a decrease in cytochrome c and cardiolipin content within mitochondria which leads to activation of steps promoting cell death and also causes leakage in the electron transport chain which in turn promotes reactive oxygen species (ROS) production [14, 15]. These changes favour the opening of mitochondrial permeability transition pores (MPTPs) during the phase of reperfusion, leading to cell death [16].

1.1.2 Post-Ischaemic Reperfusion of Cardiac Tissue

Rapid restoration of blood flow to the ischaemic region of the heart is of paramount importance as the degree of blood flow reduction and duration have been shown to affect the extent of cellular death [17]. As such, reperfusion of blocked coronary arteries is still the primary therapeutic goal, whether achieved via pharmaceutical or surgical methods. Unfortunately, as was first shown by Jennings et al in 1960, reperfusion itself can paradoxically inflict damage onto the cardiac tissue resulting in additional cellular necrosis [18]. This has led to further research investigating the pathological events underpinning this phenomenon, where reperfusion of ischaemic hearts has been found to initiate a cascade of events that can lead to cell death. As reperfusion is still vitally important long-term, this was obviously an area that required more research in order to minimise its damaging side-effects.

Research into the reperfusion stage of IR injury, also known as lethal reperfusion injury, has shown that the initial period (~ first hour) of reperfusion can inflict a higher degree of cellular death than pure ischaemia [3]. However, this does not last long as the benefits of reperfusion

generally curtails further damage after the first hour. Non-reperfused hearts will ultimately develop severe damage over time. In animal studies, 30-50% of the final infarct size after myocardial IR injury is attributable to lethal reperfusion injury, making it an important area of research for therapeutic intervention ***(Figure 1.1)*** [4].

A summary of the pathological events underpinning lethal reperfusion injury ***(Figure 1.2)*** is described as follows.

1.1.2.1 pH Paradox

As mentioned earlier, during ischaemia, intracellular pH levels fall. In order to compensate this acidic tendency, H^+ are transported out of the cell. This leads to an accumulation of H^+ in the extracellular space. When reperfusion commences, the extracellular space is replenished with fluid, removing the H^+ present. The acidic environment during the period of ischaemia actually helps to slow down certain pathophysiological processes such as MPTP opening. As such, the return to normal pH levels during reperfusion can have adverse effects on cell health [19]. The removal of H^+ also creates an ionic imbalance between the intracellular and extracellular space and thus promotes further H^+ transport outside of the cell [20]. As with during ischaemia, this continues the cascade of events that leads to further intracellular Ca^{2+} overload.

1.1.2.2 Oxygen Paradox

During ischaemia, there is an accumulation of pro-oxidant enzymes such as xanthine oxidase (XO) and its substrate hypoxanthine [21]. Reperfusion of previously ischaemic sites allows for the return of aerobic respiration as oxygen supply is re-established. Paradoxically however, leakage of the electron transport chain in the mitochondria and the accumulation of pro-oxidant enzymes during ischaemia permits the generation of ROS with the re-introduced oxygen [22]. ROS is dangerous as it can alter the structure of molecules such as proteins, lipids and nucleic acid within the cell, leading to adverse effects and ultimately damage. Similar to the pH paradox phenomenon, this oxygen paradox also leads to further intracellular Ca^{2+} overload as damage to membrane structures promotes Ca^{2+} accumulation within the cell [5]. Uncontrolled ROS generation, as seen during reperfusion, can have a profound effect on ischaemic tissue and the neighbouring cells.

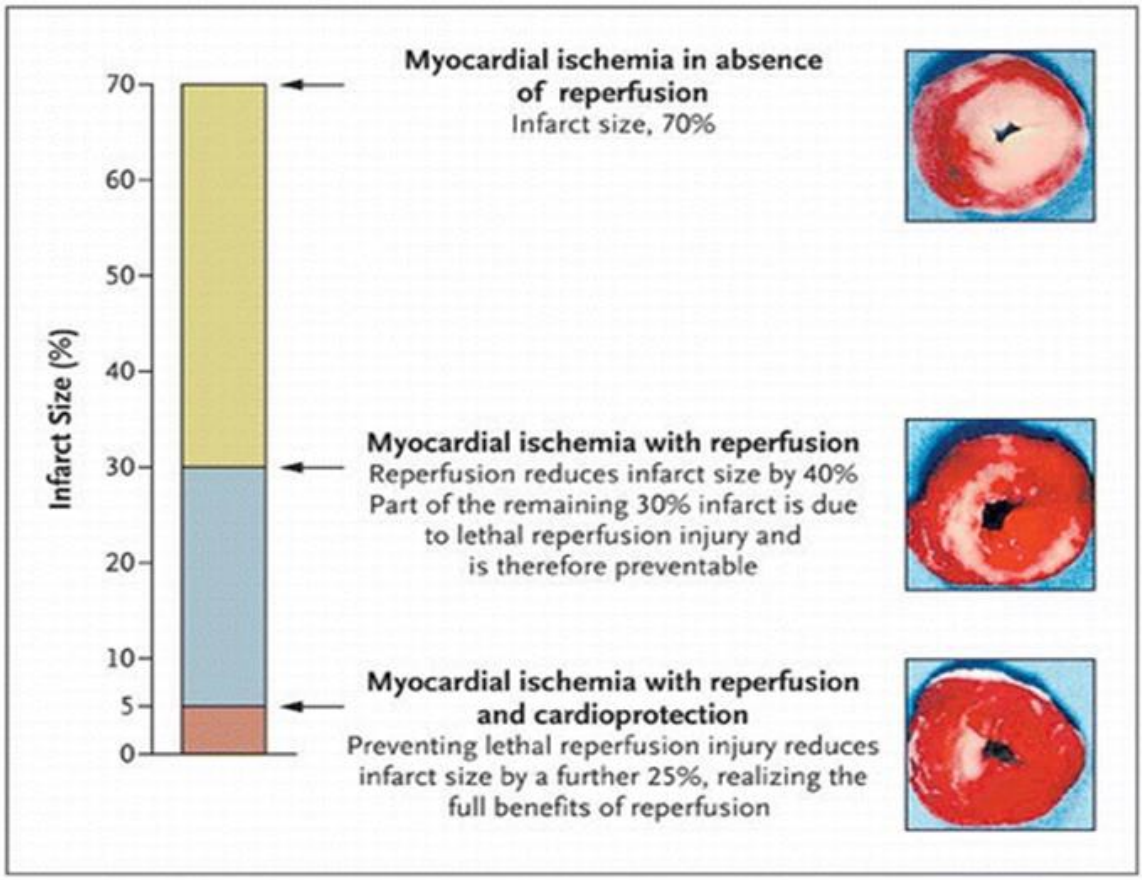

Figure 1.1: Effect of reperfusion injury on myocardial infarct size. *While early reperfusion of an ischaemic heart is important and leads to a smaller final infarct size, an extra 30% on the final infarct size is further preventable by alleviating the effects of lethal reperfusion injury.*

Source: Yellon & Hausenloy 2007; New England Journal of Medicine.

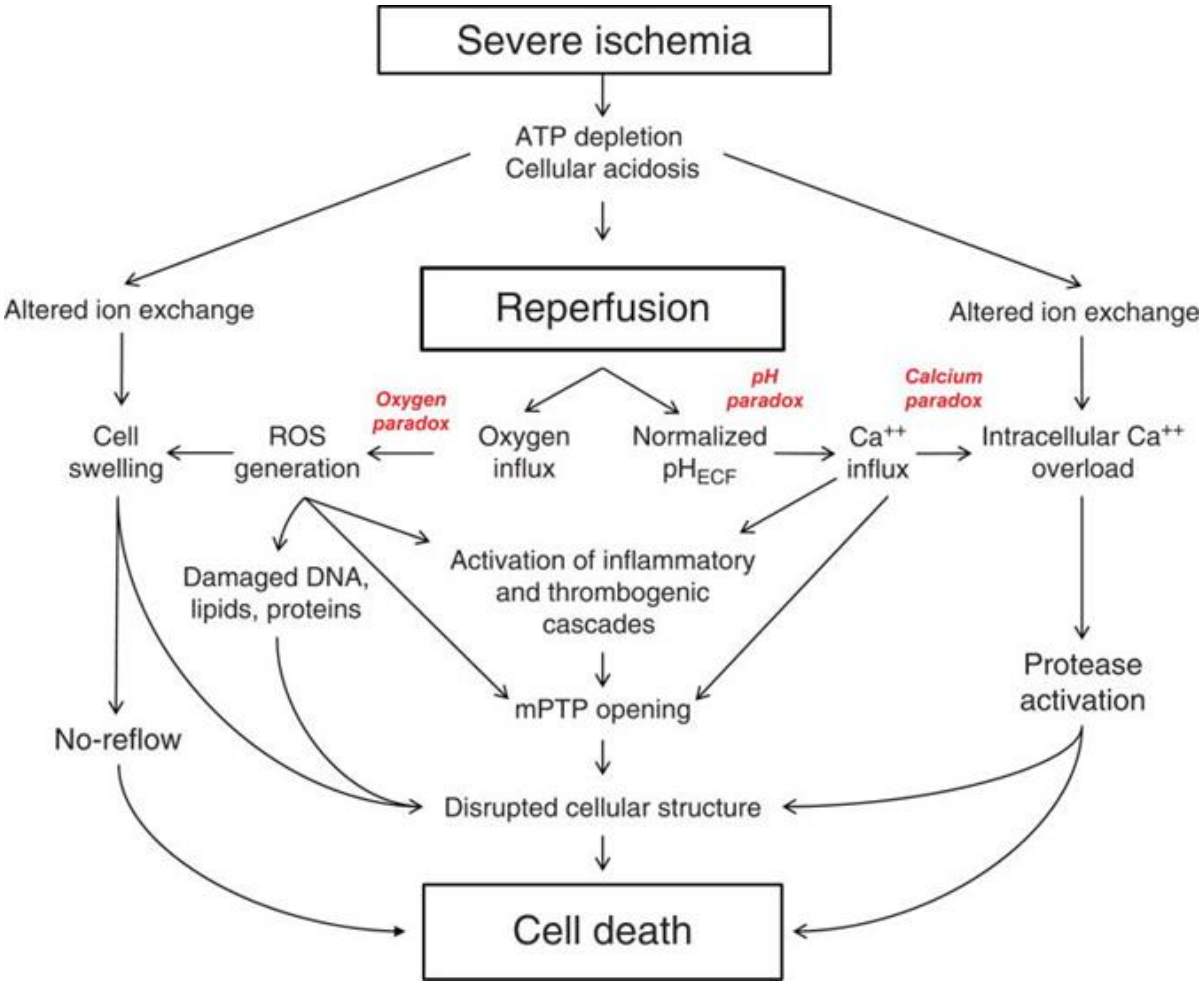

Figure 1.2: Pathologic events in ischaemia/reperfusion injury. *IR injury involves a cascade of events that will ultimately lead to cell death if left unchecked. Resumption of blood flow to the ischaemic tissue is still vitally important and as such, research into safe and effective means of inhibiting these mechanisms is needed.*

Source: Kalogeris 2016; Comprehensive Physiology.

1.1.2.3 Ca^{2+} Overload

A major consequence of reperfusing ischaemic tissue is the increase in intracellular Ca^{2+} concentrations. Ca^{2+} overload is initiated during the period of ischaemia and further increases during reperfusion, rather than subsiding. As previously mentioned, ionic imbalances favour the transport of Ca^{2+} into the cell however, this is not the only mechanism for Ca^{2+} overload. Damage to membrane bound enzymes on intracellular organelles such as the endoplasmic (ER) and sarcoplasmic reticulum (SR) inhibit Ca^{2+} sequestration into these compartments. Ryanodine receptors are conversely activated to pump out Ca^{2+} from these compartments during reperfusion. This increase in intracellular Ca^{2+} levels promotes the transport of Ca^{2+} into the mitochondria [12, 23]. An increase in mitochondrial levels of Ca^{2+} then promotes the opening of MPTPs, initiating steps leading towards cell death.

This Ca^{2+} overload can directly trigger the inflammatory response by producing Ca^{2+} complexes that activate inflammasomes. Pro-inflammatory cytokines such as interleukin-1β (IL-1β) and TNF-α are generated which either directly promote inflammatory infiltration into the injured site or indirectly by instigating the generation of other pro-inflammatory cytokines [24, 25]. Inflammatory infiltration into IR injured tissue is another potent method by which additional damage is inflicted upon IR injured tissue.

1.1.3 Global Effects of Myocardial IR Injury

The cellular changes that occur during IR injury are profound in and of itself however, the structural changes will have an impact upon the overall tissue function as well. During myocardial IR injury, intracellular swelling and interstitial oedema can develop. This can

effectively ‘squeeze’ the microvasculature of the heart, reducing the lumen size of vessels that may proceed to trap circulating inflammatory cells. This can lead to blocked vessels downstream of the initial thrombotic event which has been termed the ‘no-reflow’ phenomenon [26]. The no-reflow phenomenon refers to the lack of blood flow into ischaemic tissue even after reperfusion has been initiated, such as through PCI interventions or thrombolytic therapy. Excess extracellular fluid also increases the travel or diffusion distance of metabolites to and from cells, delaying the return of normal function [5].

The attraction of inflammatory cells to the site of injury can exacerbate damage to the heart. Although the presence of inflammatory cells is important for tissue repair, the cytotoxic effect of inflammatory cells can induce damage on surrounding, healthy tissue. Therefore, a balance is important to rescue the viable cells in the injured heart and is discussed in more detail later.

Another important side-effect of myocardial IR injury is the disruption of myocardial electrical conduction. The changes discussed above, such as ion imbalances, myocyte structural damage and cell death can contribute to the impairment of electrical conduction in the heart [27, 28]. The development of fibrosis over time that replace damaged cells will also contribute to further impairment of this system. The development of arrhythmias is not an uncommon complication after an MI and can be fatal.

1.2 Cardiac Damage Resulting from IR Injury

There are four main types of clinically observable cardiac damage that arises from myocardial IR injury. These are generally referred to as myocardial stunning, no-reflow phenomenon, reperfusion arrhythmias and lethal reperfusion injury [4].

1.2.1 Myocardial Stunning

Myocardial stunning refers to the contractile dysfunction that occurs after cardiac IR despite the absence of irreparable damage and the reestablishment of regular blood flow to the myocardium [29]. Myocardial stunning is generally considered a mild dysfunction as the period of ischaemia is very brief and consequently the damage that occurs is fully reversible after several days or weeks. The pathogenesis of myocardial stunning is not yet well established. The concepts stated earlier that may help explain this phenomenon are the generation of ROS and a transient Ca^{2+} imbalance [30]. Free radicals such as ROS directly damage myocytes and render them less able to perform contractions adequately. Myocytes also rely heavily on Ca^{2+} in order to contract properly. As such, the presence of a Ca^{2+} imbalance during myocardial IR can directly cause myocardial stunning. Furthermore, the two theories can overlap where damage induced by free radicals will render myocytes less responsive to Ca^{2+}, thus bringing about the state of myocardial stunning. As the period of ischaemia is brief however, these changes are short-lived and reversible. There is also an absent inflammatory response in this condition that would otherwise exacerbate the injury. If required, treatments provided to manage myocardial stunning include ionotropic agents and insertion of an intra-aortic balloon pump [30].

1.2.2 No-Reflow Phenomenon

Another cardiac dysfunction resulting from reperfusion is known as the no-reflow phenomenon. The no-reflow phenomenon essentially involves the microvasculature downstream of a coronary blockage that becomes impeded after reperfusion is initiated [31]. This leads to a small extended area of ischaemia or infarction in the heart. As cardiac reperfusion generally involves the disintegration of a plaque in a large arterial vessel, smaller segments of the aforementioned plaque can travel downstream and subsequently block smaller vessels [32]. These microemboli are one reason behind the no-reflow phenomenon. However, the interstitial oedema, cellular swelling and thromboinflammatory cell infiltration can all occur during an infarction and these events can also lead to microvascular compression and blockage and thus contribute to no-reflow as well [33]. Reperfusion of a damaged area can exacerbate the structural damage seen with further infiltration of inflammatory cells, generation of free radicals and resumption of normal contractions in neighbouring myocytes [31]. Patients who develop the no-reflow phenomenon during the reperfusion period after an MI tend to develop more complications as regions of no-reflow are not able to heal adequately, whether naturally or through pharmacological intervention [9]. Clinical treatments must be aimed at managing the no-reflow phenomenon itself. Aggressive anti-platelet strategies and introduction of cardioprotective agents have been shown to improve microvascular function, which reduce the effect of the no-reflow phenomenon [34]. Another strategy is to induce vasculogenesis and angiogenesis through mobilisation of bone-marrow resident precursor cells [35]. These precursor cells have the ability to restore capillary integrity and blood flow to areas of no-reflow [35].

1.2.3 Reperfusion Arrhythmias

An important research finding in the field of myocardial IR injury was the separation of ischaemic arrhythmias and reperfusion arrhythmias into two distinct entities [36]. Reperfusion arrhythmias refer specifically to cardiac arrhythmias that arise during the period of cardiac reperfusion. While the arrhythmias originate during the reperfusion phase, the type of arrhythmia is still dependent on the duration of ischaemia prior. Cardiac ischaemia of very short durations, for instance due to a coronary spasm that lasts for a few seconds, can induce arrhythmias such as ventricular tachycardia and ventricular fibrillation during the reperfusion stage. These arrhythmias may account for the occurrence of sudden cardiac death. Cardiac ischaemia of moderate duration, minutes to hours such as seen during cardiopulmonary bypass surgery, can in turn induce supraventricular tachycardia and ventricular fibrillation. Cardiac ischaemia of a long duration, hours to days such as after an acute myocardial infarction, can induce premature ventricular beats and atrial fibrillation. Finally, cardiac ischaemia of an extreme duration, days to weeks such as from the generation of new blood supply to an otherwise ischaemic region, can induce electrocardiographic (ECG) abnormalities leading to sudden cardiac death [36]. Theories behind the genesis of arrhythmias during cardiac reperfusion include the state of ionic imbalances such as with Ca^{2+} and magnesium (Mg^{2+}) and the presence of free radicals disrupting cellular integrity [37]. Treatments available to manage reperfusion arrhythmias generally involve anti-arrhythmia drugs.

1.2.4 Lethal Reperfusion Injury

Lethal reperfusion injury is defined as the death of previously-viable myocytes inflicted by cardiac reperfusion [38]. Lethal reperfusion injury can exacerbate the damage inflicted during cardiac ischaemia and increase the final infarct size. In animal studies, 30-50% of the final size of an MI is attributable to lethal reperfusion injury ***(Figure 1.1)*** [4]. There are a number of factors that facilitate the genesis of lethal reperfusion injury. Oxidative stress induced by free radicals and Ca^{2+} imbalances play roles in this form of cardiac damage as they have in the other forms mentioned previously. Similarly, their actions within the cellular environment mean that myocytes are not able to function normally and die due to events such as hypercontraction, mitochondrial dysfunction and overactive inflammation [39]. Neutrophils, as part of the inflammatory response, exacerbate the condition by increasing free radical presence and activating further inflammatory components [39]. Therapeutic strategies involve, among others, ischaemic post-conditioning. Ischaemic post-conditioning is the process of introducing intermittent ischaemia and reperfusion during the reperfusion phase [40]. In this scenario, the detrimental effects of constant reperfusion are broken up by the short repetitive bursts of ischaemia, allowing cells to recover from reperfusion injury. This treatment, however, is difficult to conduct during an acute myocardial infarction due to the unpredictable nature of the ischaemic attack and also the invasiveness of the procedure.

1.3 Coronary Microcirculation in Myocardial IR Injury

Despite successful reperfusion of blocked vessels via thrombolytic therapy or PCI following an MI, it has been observed that nearly 50% of patients still exhibit signs of reduced myocardial perfusion [9, 41]. As such, it is not a surprise that a significant number of patients progress to heart failure even after successful therapy. As mentioned earlier, microcirculatory disturbances such as that observed in the no-reflow phenomenon contribute heavily to the damage incurred in the cardiac tissue during IR injury ***(Figure 1.3)***. It is thus surprising that research into the role of the coronary microcirculation in cardiovascular disease has largely been avoided. There exist several obvious difficulties in trying to investigate the coronary microcirculation in real-time clinically. The microvessels of interest are small, <200 µm in diameter, making imaging modalities such as cardiac magnetic resonance (CMR) and positron emission tomography (PET) unsuitable due to their limited spatial resolution [42]. Hence, little is known about the full range of cardiac microcirculatory responses to IR injury clinically and importantly the mechanisms contributing to them.

More recently, progressive loss of distal microvessel perfusion at the tissue level has been clinically demonstrated in patients post-MI using PET scanning [42]. Furthermore, a role for microcirculatory perturbations has also recently been demonstrated using CMR imaging, which provide new insights into the significant impact microvascular obstruction and intramyocardial haemorrhage has on clinical MI outcomes [43]. Functional readouts, such as local blood flow and pressure determined clinically using a Doppler flow wire inserted into the coronary artery or assessed using thrombolysis in MI (TIMI) flow or myocardial blush, have also indicated a lack of perfusion in microvessels downstream of an opened epicardial artery.

The index of microcirculatory resistance (IMR), a pressure-temperature sensor guidewire-based measurement, has recently been proposed for quantitatively assessing coronary microvessel functional status indirectly post-PCI in the territory surrounding the artery from which the measurement is made [44]. However, these various anatomical and functional assessments are mainly of the larger coronary vessels as the current clinical imaging tools such as x-ray angiography, CMR and PET cannot spatially resolve blood vessels less than 200µm in diameter as stated earlier. Hence actual visualisation of the coronary microcirculation, let alone any detrimental thromboinflammatory events taking place within them, remains impossible with current clinical imaging tools.

The importance of studying in detail the cardiac microcirculation response to IR injury is gathering pace, although somewhat slowly. It is accepted that multiple microcirculatory and inflammatory perturbations, initiated in the immediate reperfusion period, are responsible for inducing tissue damage [45]. Hence, myocardial IR injury can be considered a multifaceted microvascular pathology which explains why targeting just one microvascular disturbance has not been a successful therapeutic option. Microcirculatory and inflammatory perturbations initiated in a reperfused heart include neutrophil and platelet activation/aggregation, microvascular obstruction/congestion, ROS production, capillary damage and thus a reduction in the functional capillary density. Inflammatory damage and impaired vasodilation of coronary arterioles, which physiologically modulate local blood flow, also impacts detrimentally on cardiac perfusion [38]. Collectively, these microvascular complications enhance heart muscle damage caused by an MI and contribute to the no-reflow phenomenon. Indeed, in patients with MI, coronary microvascular dysfunction is responsible for the no-reflow phenomenon, which is associated with a worse outcome than in patients in whom

blood perfusion is restored [41]. Since the extent of these disturbances determine infarct size, restoring microvascular integrity is essential. However, little is known about the full range of cardiac microcirculatory responses to IR injury that take place *in vivo* in preclinical studies, limited by an inability to directly image these events in the beating heart. It is becoming increasingly accepted that since the extent of these disturbances determine infarct size, restoring microvascular integrity is essential.

Most of our knowledge has been obtained from heart tissue imaged histologically for morphological deterioration, inflammatory cells infiltration, and infarct size etc. However, these static snapshots provide no indication of the real-time kinetics of deleterious cell recruitment *in vivo* in the presence of pathophysiological flow, nor information on microvessel integrity post-injury. Lack of mechanistic understanding underlying microvascular dysfunction has led some to suggest the creation of an international "coronary microcirculatory observatory"; an EU-wide virtual facility, utilising techniques such as intravital microscopy (IVM) to properly interrogate coronary microvascular dysfunction [46].

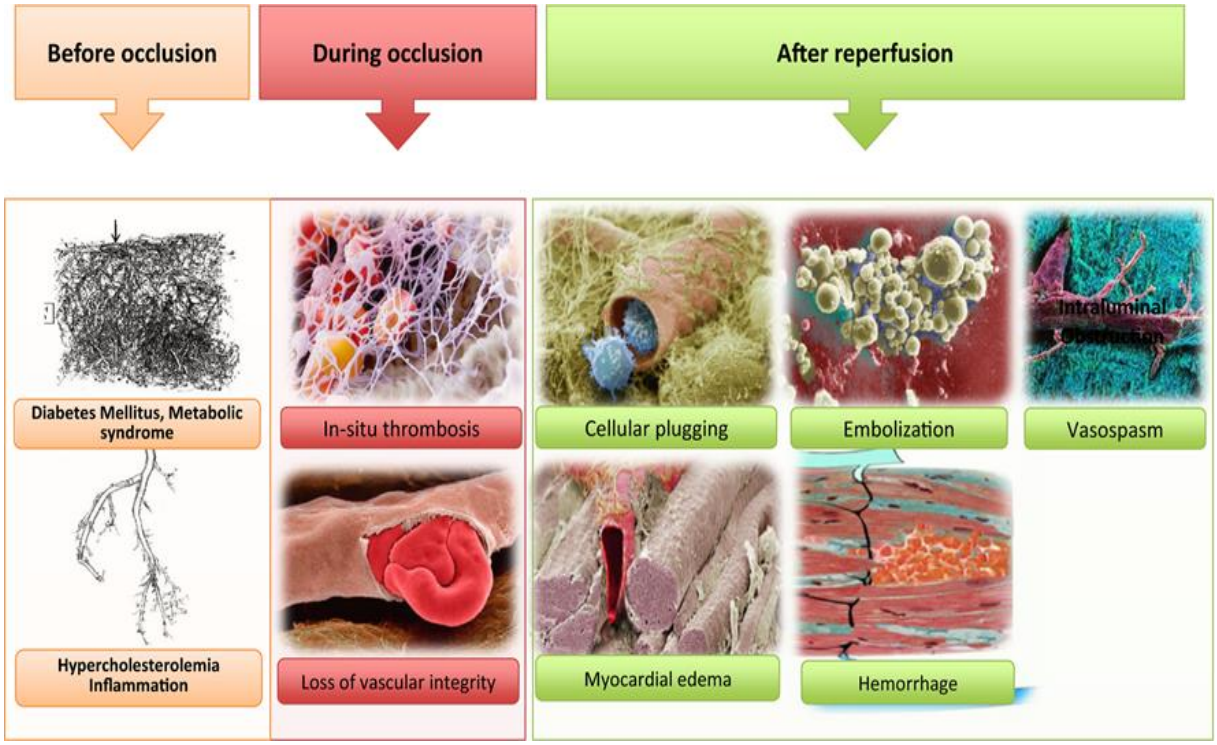

Figure 1.3: Microcirculatory pertubations in myocardial IR injury on a temporal scale. *Pre-existing conditions such as diabetes and hypercholesterolemia lead to the presence of underlying microvascular damage. During ischemic occlusion, microthrombi may form in the microvessels and vascular integrity may become damaged. During reperfusion, returning blood flow allows for cellular plugs to form, embolization of microthrombi and vasospasms. Vascular leakage will also result in myocardial oedema and haemorrhage.*

Source: Umman 2018; Journal of the American Heart Association.

1.3.1 Endothelial cells

Endothelial cells (ECs) are an important component of the coronary microcirculation. During cardiac ischaemia, these cells can become dysfunctional and die due to a lack of oxygen and nutrition, just like other cells in the affected region. During reperfusion, they are the first point of contact for the returning blood flow. Damage to ECs during myocardial IR injury induces microvascular permeability changes, promotes vasoconstriction, thrombogenesis, inflammatory infiltration and cytoskeletal derangements [5].

Damage to ECs can either be direct or indirect. IR injury can directly cause necrosis of ECs that results in their detachment and vasculature breakdown. Indirectly, IR injury will produce a cascade of cytokines that modify ECs into becoming more porous [47]. Regardless of the mechanism, this can result in fluid and cells leaking out of the vasculature and into the surrounding tissue. Interstitial oedema can cause narrowing of blood vessels and delay the delivery of oxygen and nutrition during reperfusion. Swelling of ECs and increased production of endothelin can also cause blood vessels to narrow and thus leukocyte plugging [48]. Platelets exposed to either the extracellular matrix or pro-thrombogenic stimuli will become activated and aggregate, attempting to stem any leakage. Activated platelets will unfortunately further promote a pro-thrombogenic environment and can induce leukocyte accumulation and infiltration [49].

As ECs play an important role in the microcirculation of the heart – they are also sources of ROS – it is vitally important to understand their dysfunction and their potential to exacerbate myocardial IR injury. Ultimately, they may present alternative therapeutic avenues by which IR injury can be limited.

1.4 Oxidative Stress in Myocardial IR injury

As has been discussed previously, oxidative stress is an important mediator for cardiac dysfunction as a result of IR injury. In the steady-state, free radical production is normal however, the presence of free radicals and non-radicals in the tissue microenvironment is maintained by the antagonistic actions of pro- and antioxidants [15]. A proper balance mediates the deleterious effects of free radicals and non-radicals. An imbalance of this model favouring pro-oxidants is known as oxidative stress. Free radicals and non-radicals can exist in the form of ROS and reactive nitrogen species (RNS) [50]. During ischaemia, a host of events occur that favour the generation of free radicals which include the build-up of pro-oxidant enzymes such as XO, the build-up of substrates such as hypoxanthine and a build-up of electrons intracellularly, especially in the mitochondria, due to leakage in the electron transport chain [15]. During reperfusion, the missing piece of the puzzle, molecules such as oxygen and nitrate, are fed back into the microenvironment; a rich supply of free radicals and non-radicals such as superoxide (O_2^-), hydrogen peroxide (H_2O_2), the hydroxyl radical ($^{\cdot}OH$) and peroxynitrite (NO_3^-) are thus produced [51]. An excess of ROS within the cellular space can have detrimental effects on the cell. Cellular structure and function can be damaged by ROS as they target lipids, proteins and DNA. Intrinsically, cells will try to eliminate excess ROS using antioxidant enzymes such as superoxide dismutase (SOD) and catalase (CAT) [52]. In the scenario of myocardial IR injury however, the cell is overwhelmed by excess ROS and cannot eliminate them effectively.

1.4.1 Sources of ROS

In myocardial IR injury, there exists a number of sources from which ROS formation may occur. Damaged mitochondria are a rich source of ROS formation due to electron leaks in the electron transport chain (ETC) during ischaemia. The electron leaks occur primarily at complex I and complex III in the ETC. Mitochondria also host enzymes such as monoamine oxidase (MAO) which produces H_2O_2 and has been shown to contribute to oxidative stress in myocardial IR injury [14].

Other enzymatic sources of ROS include XO, as mentioned previously, and nicotinamide adenine dinucleotide phosphate (NADPH) oxidases (NOX). Endothelial sources of XO have been shown to contribute to ROS production during IR injury and can even be released into the vasculature, affecting sites neighbouring the IR injured tissue [5]. In general, there are two forms of NOX, those derived from leukocytes and those derived from non-leukocytes. NOX derived from leukocytes form the majority of ROS generation in myocardial IR injury and are known as phagocytic NOX. The role of inflammation in myocardial IR injury will be discussed later however, the exacerbation of oxidative stress is an important component of the inflammatory response. Briefly, the infiltration of neutrophils into the site of injury promotes a substantial release of ROS, generated within the neutrophil itself, into the interstitial space [22]. This release of ROS not only damages surrounding cells directly, but also promotes further inflammatory infiltrates, exacerbating the injury. Non-phagocytic NOX plays a lesser role in ROS generation however, it does still contribute to the overall production of ROS and is mediated by the microvasculature, being produced by the endothelium and vascular smooth muscle cells [53].

Endothelial nitric oxide synthase (eNOS) also contributes to the production of ROS when it becomes uncoupled from producing NO and instead favours the production of ROS, such as during IR injury [54, 55]. Whilst the production of ROS through eNOS does occur in the steady-state, this is often at low levels and the benefits of NO production far outweigh its impact. Unfortunately, during IR injury eNOS becomes another important source for ROS generation.

1.4.2 Pre-clinical Studies of Antioxidant Therapy in Myocardial IR injury

Support for the concept that oxidative stress plays a key role in myocardial IR injury is shown by pre-clinical studies that ameliorate injury to the heart and maintain cardiac function with antioxidant therapy. One such example was a study by Masano et al. who showed that treatment using tetrahydrobiopterin (BH_4), a cofactor for NO production through eNOS, was able to reduce MI ventricular remodelling in rats by reducing ROS formation through uncoupled eNOS [56]. This study used Sprague-Dawley rats and inflicted a permanent MI via ligation of the left anterior descending (LAD) coronary artery and proceeded to recover these animals for 4 weeks. Oral BH_4 supplementation (10 mg/kg.day) was initiated 3 days prior to surgery and maintained for the duration of the experiment. Another group of rats were fed a normal chow diet for the same duration. The results of this experiment showed that the BH_4 treated rats developed significantly less cardiac hypertrophy and maintained better cardiac function with greater fractional shortening following MI compared to the rats on a normal chow diet. This group went on to show that the use of L-NAME, a NOS inhibitor, reduced superoxide production in the rats fed a normal chow diet following an MI.

Another study by Seshadri et al. showed that the delivery of microparticles encapsulating SOD1 (PKSOD) was able to reduce cardiomyocyte death and improve cardiac fractional shortening following IR injury in rats compared to non-treated IR injured rats [57]. In this study, myocardial IR injury was induced in Sprague-Dawley rats via ligation of the LAD for 30 minutes followed by reperfusion and recovery of animal for 3 days. PKSOD (10 mg/ml) was injected into the perimeter of the ischaemic zone immediately following reperfusion. Another group of rats were inflicted with myocardial IR injury without any treatments. This study showed a significant reduction in cardiomyocyte death, measured using Terminal deoxynucleotidyl transferase dUTP nick end labelling (TUNEL) staining, and improved cardiac function, measured using echocardiography in rats treated with PKSOD following myocardial IR injury.

These studies helped to solidify the argument that oxidative stress plays a key role in myocardial IR injury.

1.4.3 Clinical Trials of Antioxidant Therapy in Myocardial IR injury

Unfortunately, treatment strategies involving antioxidants have yielded mixed results in clinical trials [58]. A variety of approaches have been tested. Randomised clinical trials looking at the benefits of therapies such as vitamins C and E have returned inconclusive or ineffective results when used for either primary or secondary prevention of cardiovascular disease.

Ramos et al. conducted a clinical study looking into the benefits of ascorbate therapy in patients presenting to hospital with an acute MI [59]. Ascorbate works by reducing ROS generation through NOX downregulation, and by increasing NO production, through eNOS.

Patients were assigned into two groups that received either intravenous sodium ascorbate (320 mmol/l) or placebo prior to reperfusion via percutaneous coronary angioplasty (PCA). After PCA, therapy was continued in oral form. They found that there was no significant difference in infarct size or ejection fraction after 3 months between both groups, as measured by cardiac magnetic resonance. This study did state however that although there was no outright difference in ejection fraction, the patients receiving ascorbate therapy had better ejection fraction recovery over time compared to the patients on placebo.

On the other hand, Tsujita et al. conducted a clinical study which found that treating patients who had presented to hospital with an acute MI with edaravone, a free radical scavenger, prior to reperfusion improved patient clinical outcomes [60]. They assigned patients into two groups, one receiving 30 mg of edaravone intravenously with the other receiving a placebo. They found that the group which received edaravone had better long-term clinical outcomes, as determined by refractory angina, non-fatal MI, ischaemic stroke, cardiac death or heart failure when compared to the placebo group over the course of ~4 years. This was alongside a reduction in oxidative stress as measured by serum levels of thioredoxin. This was a small-scale study however, with only 101 participants, making it difficult to extrapolate the findings to a wider population.

Research utilising selective antioxidants that target the mitochondria, such as MitoQ, is currently ongoing as an alternative to conventional antioxidant therapies in order to provide more effective protection to mitochondria in situ. As mitochondria are a major source of free radicals, this is an exciting treatment strategy with promising early results [61].

1.5 Pro-thrombogenic Microenvironment in Myocardial IR Injury

The accumulation and aggregation of platelets in myocardial IR injury has been well documented. Under steady-state conditions, platelets circulate through the blood vessels harmlessly. As such, there must exist an environment within the cardiac tissue during IR injury that promotes the activation and shape-change of platelets, leading towards their accumulation. Most studies have shown that the presence of platelets in myocardial IR injury is extremely damaging in nature [62]. A study by Barrabes et al. showed that direct tissue damage can occur due to the presence of platelets within coronary blood vessels [63]. In this study, they used a Langendorff rat heart model of IR injury perfused with human platelets isolated from healthy or MI patients. Interestingly, they did not image the coronary macro- or microvessels histologically, but found anti-platelets reduced infarct size and improved functional contractile readouts induced by MI patients' platelets. Others have shown that the 'sticky' nature of activated platelets not only promotes platelet-platelet and platelet-EC adhesion, but also platelet-leukocyte adhesion [64]. This interaction can be damaging to the microenvironment as it promotes inflammation in the tissue. A study by Husain et al. has also shown that activated platelets may release potent vasoconstrictors such as serotonin and thromboxane A2, leading to more tissue damage [65]. As such, the general consensus is that the presence of activated platelets in myocardial IR injury is detrimental and promotes more damage to cardiac tissue.

The mechanisms behind platelet activation in myocardial IR injury is not fully known. However, the evidence of microvasculature disturbances, from damaged ECs to collagen exposure, likely create a pro-thrombogenic environment [66]. Once activated, platelets have been shown to

have a direct impact on infarct size after myocardial IR injury. A study by Xu et al. eloquently showed that the transfer of platelet-rich plasma from transgenic mice with a global knockout of the P-selectin gene into wild-type mice undergoing myocardial IR injury resulted in significantly smaller cardiac infarct sizes after 30 minutes of ischaemia and 60 minutes of reperfusion compared to platelet-rich plasma transferred from wild-type counterparts [49]. Since P-selectin is expressed on activated platelets, a role for activated rather than non-activated platelets was identified. Again, the primary output measured in this study was infarct size and time course of platelet deposition assessed immunohistochemically. They also showed that platelets gradually accumulated in cardiac tissue during ischaemia, with the presence of platelets seen in wild-type mice after 45 minutes of ischaemia, but not at 20 minutes. They concluded that platelets, specifically activated platelets, play an important role in myocardial IR injury.

A recent study has gone further and shown that while platelets can slowly accumulate during cardiac ischaemia, the majority of tissue infiltration occurs during reperfusion. Ziegler et al. used positron emission tomography (PET) scans with a radiotracer against GPIIb/IIIa, a highly specific marker for activated platelets, to locate platelets in mice undergoing myocardial IR injury. They showed a significantly higher degree of activated platelets in mice undergoing 60 minutes of cardiac ischaemia followed by 2 hours of reperfusion in comparison to mice undergoing 60 minutes of cardiac ischaemia followed by 5 minutes of reperfusion [67]. This study also went on to confirm that the accumulation of activated platelets occurred at sites of ischaemia and necrosis in the heart, providing further proof of the detrimental effects of platelets in myocardial IR injury. The PET images presented in this paper identified platelets appearing as a radioactive flare, occupying a single, large area corresponding to the infarct.

Certainly, individual platelets or even discrete areas of radiotracer occupying vessel-like structures were not resolved using this technique.

How do platelets exit the microcirculation and infiltrate the cardiac tissue? As mentioned previously, activated platelets can adhere to circulating leukocytes. This process helps to tether leukocytes such as neutrophils and monocytes at the site of injury. As the activated platelets have essentially 'latched' onto the leukocytes, migrating leukocytes carry the activated platelets along with them into the tissue [68]. In the cardiac tissue, activated platelets can continue releasing exosomes or microvesicles rich in pro-inflammatory cytokines or vasoconstrictors, promoting further damage. The role of platelets in facilitating the inflammatory response is vital as studies have shown that infiltration of inflammatory cells is lower and infarct size is reduced after myocardial IR injury in mice models of attenuated circulating platelets [69, 70]. Again, these mechanistic mouse studies have focussed on imaging platelets in the myocardium histologically and at single time points during ischaemia or reperfusion. Furthermore, the primary endpoint assessed for the impact of various cellular, genetic or pharmacological manipulations include infarct size or levels of myocardial injury markers such as troponin.

An exciting avenue for therapeutic intervention in myocardial IR injury and ultimately in MI is the ability to provide pharmacological treatments directly to the site of injury by targeting activated platelets. Ziegler et al. showed in a mouse model that successfully linking the active form of platelet GPIIb/IIIa to stem cell antigen-1 (Sca-1) receptor found on peripheral blood mononuclear cells (PBMCs) via antibodies led to the successful delivery of the latter to cardiac tissue after IR injury, resulting in a reduction in infarct size [71]. Homing of platelet-attached

PBMCs was imaged at 3- and 24-hours post-reperfusion in the mouse using a whole animal *in vivo* imaging system (IVIS). Another study by Ziegler et al. however, showed that induced vascular progenitor cells incubated with the linked antibodies mentioned did not accumulate in cardiac tissue after myocardial IR injury, instead becoming trapped in the pulmonary microvasculature [72]. These cells did however still manage to provide a beneficial effect on cardiac tissue by again reducing infarct size and fibrosis after IR injury, most likely through a paracrine effect, when compared to induced vascular progenitor cells not incubated with the linked antibodies delivered in myocardial IR injury.

1.6 Inflammatory Response during Myocardial IR Injury

Inflammation plays a key role in myocardial IR injury. Although platelets appear to have a critical role, it is argued that inflammation accounts for a large portion of injury that occurs during reperfusion, ultimately affecting final infarct size [4, 5]. As such, many consider there to be a therapeutic benefit in limiting the inflammatory response in myocardial IR injury. This is anticipated due to the fact that preclinical studies involving myocardial IR injury with attenuation of inflammatory cell subsets have shown a reduction in final infarct size [73, 74]. This confirms that too much inflammation at the affected area exacerbates the injury. Whilst some inflammatory infiltration may occur during the period of ischaemia, the majority of infiltration occurs during the period of reperfusion [5, 75]. As blood supply returns to the damaged area of the heart, circulating inflammatory cells of the innate immune system become exposed to a rich supply of activation markers such as pro-inflammatory cytokines and an increase in EC adhesion molecules. These events, coupled together with the pro-

thrombogenic platelet response, provide an environment ripe for the activation of inflammatory cells and initiate the cascade of events that make up the process of leukocyte trafficking. This response is rapid, providing 'protection' during the early stages of an insult and comprises neutrophils, eosinophils, monocytes, macrophages, dendritic cells (DC) and other granulocytes.

An inflammatory response that is not initiated by an infection is termed sterile inflammation and myocardial IR injury would be classified as such. The general consensus in the research community with regards to the sequential infiltration of inflammatory cells begins with the migration of neutrophils into the site of injury during the first few hours of reperfusion, peaking at day 1 [76]. Monocytes and macrophages then play an important role in intensifying the immune response by clearing out dead or damaged cells and then by switching to a resolution phase to promote angiogenesis, wound healing and tissue remodelling. Other cells that may be recruited into the injured site to help promote the resolution stage include DCs and T-lymphocytes. A more in-depth review of the inflammatory response will be addressed below.

1.6.1 Pro-inflammatory Cytokines

The damage that occurs during the period of ischaemia initiates a variety of pathways that eventually lead to the infiltration of inflammatory cells. The production of ROS, the release of damage-associated molecular patterns (DAMPs) and activation of the complement cascade are all events that trigger activation of the inflammatory response [77]. This can be achieved in a number of ways. Toll-like receptors recognise the DAMPs and induce pro-interleukin-1β

(IL-1β) mediators [78]. Inflammasomes regulate the inflammatory response and when activated by DAMPs or ROS, will activate caspase-1 [79, 80]. This increases production of pro-inflammatory cytokines such as IL-1β and interleukin-18 (IL-18). IL-1β then acts as an inducer for other pro-inflammatory cytokines. The presence of DAMPs can also promote an inflammatory response by mediating the release of TNF-α and Nuclear Factor kappa-light-chain-enhancer of activated B cells (NF-kB) activation [81]. These events do not just lead to the activation of inflammatory cells, but also encourage recruitment via vasoconstriction and via inducing upregulation of adhesion molecules by ECs ***(Figure 1.4)***.

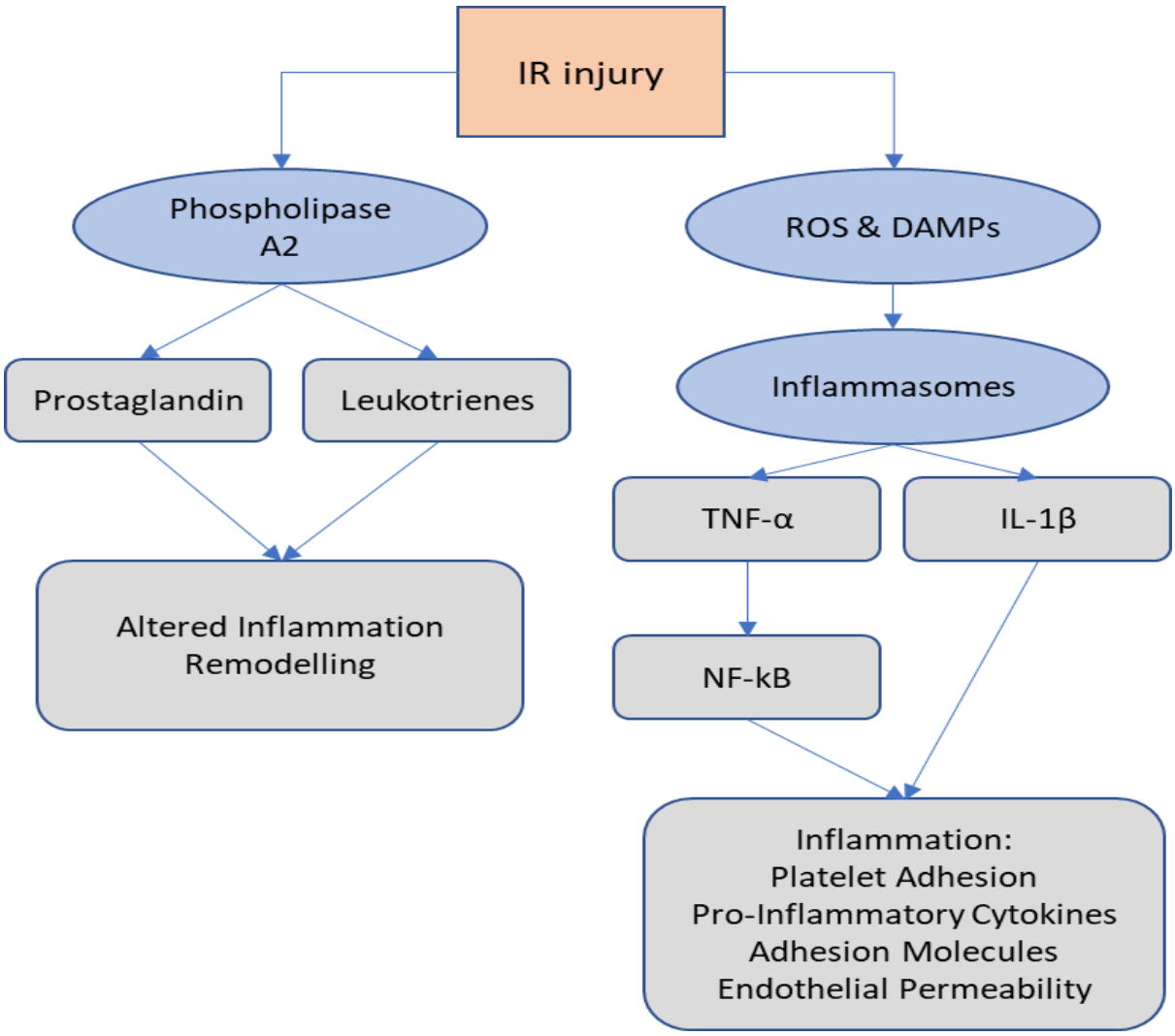

Figure 1.4: IR injury induces inflammation. *IR injury can promote inflammation by increasing phospholipase A2 activity which in turn promotes prostaglandin and leukotriene production. ROS and DAMPs produced during IR injury will activate inflammasomes into increasing production of TNF-α and IL-1β. This will promote inflammation through the release of pro-inflammatory cytokines, upregulation of adhesion molecules and by activating platelets. This can occur through NF-kB activation*

Adapted: Rosenzwieg 2012; Circulation Research.

1.6.1.1 Interleukin-1 (IL-1) Family

The main cytokine involved in mediating the inflammatory response in an MI is IL-1. The IL-1 family consists of a number of cytokines, 11 in total, some of which are pro-inflammatory whilst others are anti-inflammatory. The most commonly studied members are IL-1α and IL-1β [82]. These cytokines produce a strong inflammatory response and have a natural antagonist known as IL-1 receptor antagonist (IL-1Ra). Preclinical studies have shown that overexpression of IL-1Ra in the heart resulted in a smaller infarct size after myocardial IR injury [83, 84]. Unfortunately, clinical trials using human recombinant IL-1Ra (Anakinra) have produced disappointing results where the drug was reported to have increased major adverse cardiac effects and did not prevent recurrent ischaemic events [85].

In 2017, Ridker and colleagues conducted a clinical trial to directly test the possibility that inflammation plays a critical role in MI – known as the '*Inflammatory Hypothesis'*. This was the first major randomised double-blind trial of canakinumab, a therapeutic monoclonal antibody targeting IL-1ß – now famously known as the CANTOS trial [86]. The trial involved 10,061 patients with a previous history of MI receiving the anti-IL-1ß antibody subcutaneously every 3 months. The main endpoints, non-fatal MI/stroke or cardiovascular death, were measured approximately 3.7 (median) years later. Patients receiving canakinumab demonstrated modest, yet significant, beneficial effects with regards to these cardiovascular outcomes. A 15% decrease in the above primary end points and a 39% reduction in high-sensitivity C-reactive protein (hsCRP), a circulating inflammatory marker, was demonstrated. Importantly, this was independent of any lipid or blood pressure (BP)-lowering effects. This study sparked a renewed interest in the role of inflammation in MI. In 2018, Ridker and

colleagues further scrutinised the data from the CANTOS trial to determine which specific patient group benefited most from the treatment [87]. This re-analysis study confirmed the potential use of canakinumab as an adjunctive post-MI therapy but further found that all patient sub-groups (which took into consideration age, diabetes, BMI, CRP, triglycerides, cholesterol levels etc.) achieved similar relative risk reductions. Not surprisingly, they also found that patients who better responded to the drug, as evidenced by substantial reductions in hsCRP levels, achieved better reduced risk for primary adverse endpoints.

Some experts interpreted the results of the CANTOS trial as evidence that anti-inflammatory drugs, particularly those targeting the IL-1ß pathway, and not just cholesterol-lowering medications, could effectively prevent subsequent cardiovascular events. Despite these results, the United States Food and Drug Administration (USFDA) recently rejected approving the indications for canakinumab to include cardiovascular risk reduction among MI patients. This was based on the modest benefit it had, the high cost of the antibody drug ($16,000/injection), and importantly the increased risk of a fatal infection noted in some patients. Trial organisers, including Professor Paul Ridker, and experts in the field have tasked the cardiovascular research community to find alternative approaches to inflammation inhibition that are as effective if not better in MI.

1.6.1.2 Interleukin-36 (IL-36)

The IL-1 family (IL-1F) consists of 11 pro- and/or anti-inflammatory cytokines, some of which have been studied extensively (eg. IL-1α, IL-1β, IL -1Ra), whilst others have received less attention [88]. These are frequently the first and most upstream cytokines produced in response to injury, thus good targets for intervention such as in the CANTOS trial [89]. In the last decade, genes encoding a novel cytokine cluster, namely IL-36, with structural and functional similarities to IL-1 were discovered [90, 91]. IL-36, a collective name for three agonist ligands, IL-36α (IL-1F6), IL-36β (IL-1F8) and IL-36γ (IL-1F9), is fast emerging as a novel player regulating both innate and adaptive immune responses in acute and chronic disorders. As well as amplifying IL-1 effects, it is also a mediator of inflammation in its own right. Indeed, its critical role in psoriasis, equalling if not surpassing that of IL-1, is well established with emerging roles in Crohn's disease, airway infections and rheumatoid arthritis recently identified [92-94]. IL-36 cytokines can be released from many sources including epithelial cells, macrophages, monocytes, lymphocytes and microparticles, with neutrophils identified as an IL-36 source more recently [95-98]. Its presence in epithelial cells has made it an important cytokine in the progression of diseases such as psoriasis, systemic lupus erythematosus and inflammatory bowel disease [99, 100]. All agonists signal through the IL-36 receptor (IL-36R), a heterodimer formed of IL-1Rrp2 (IL-1RL2) and a co-receptor accessory protein IL-1RacP [101]. Downstream intracellular signaling results in NF-κB and mitogen-activated protein (MAP) kinases activation and subsequent secretion of multiple potent pro-inflammatory mediators (eg. IL-6, IL-8) in susceptible cells ***(Figure 1.5)***.

As with other members of the IL-1 superfamily, activation of the various IL-36 isoforms requires the cleavage of its inactive, precursor form into a more truncated version. This is carried out via proteolytic enzymes. Studies have shown that enzymes derived from neutrophil granules such as elastase, proteinase-3 and cathepsin G can carry this out [102]. Therefore, IL-36 not only mediates neutrophil recruitment, but once recruited they can further enhance the potency of IL-36 inactive precursors by 500 to 1000-fold [102]. While the role of neutrophils will be discussed later, this is a particularly novel, if unsurprising, mechanism by which neutrophils can escalate inflammation. IL-36 not only recruits inflammatory cells but is also capable of triggering the production of additional cytokines from many cell types, such as macrophages, epithelial cells and ECs. Indeed, a study by Vigne et al. showed that IL-36 stimulation of bone marrow-derived dendritic cells resulted in an increase in the production of other pro-inflammatory cytokines such as IL-6, IL-1β and TNF-α and, importantly, this effect was a more potent stimulatory effect than that induced by other IL-1 cytokines [103].

IL-36 is also known to play a role in tissue remodelling and fibrosis. A study conducted by Scheibe et al. in mice models showed that anti-IL-36 treatment can prevent and treat experimental intestinal fibrosis brought on by either dextran sulphate sodium (DSS) or 2,4,6-trinitro benzene sulphonic acid (TNBS) [104]. They also showed that stimulation of IL-36R in fibroblast from both humans and mice resulted in significant expression of genes that regulate fibrosis and tissue remodelling.

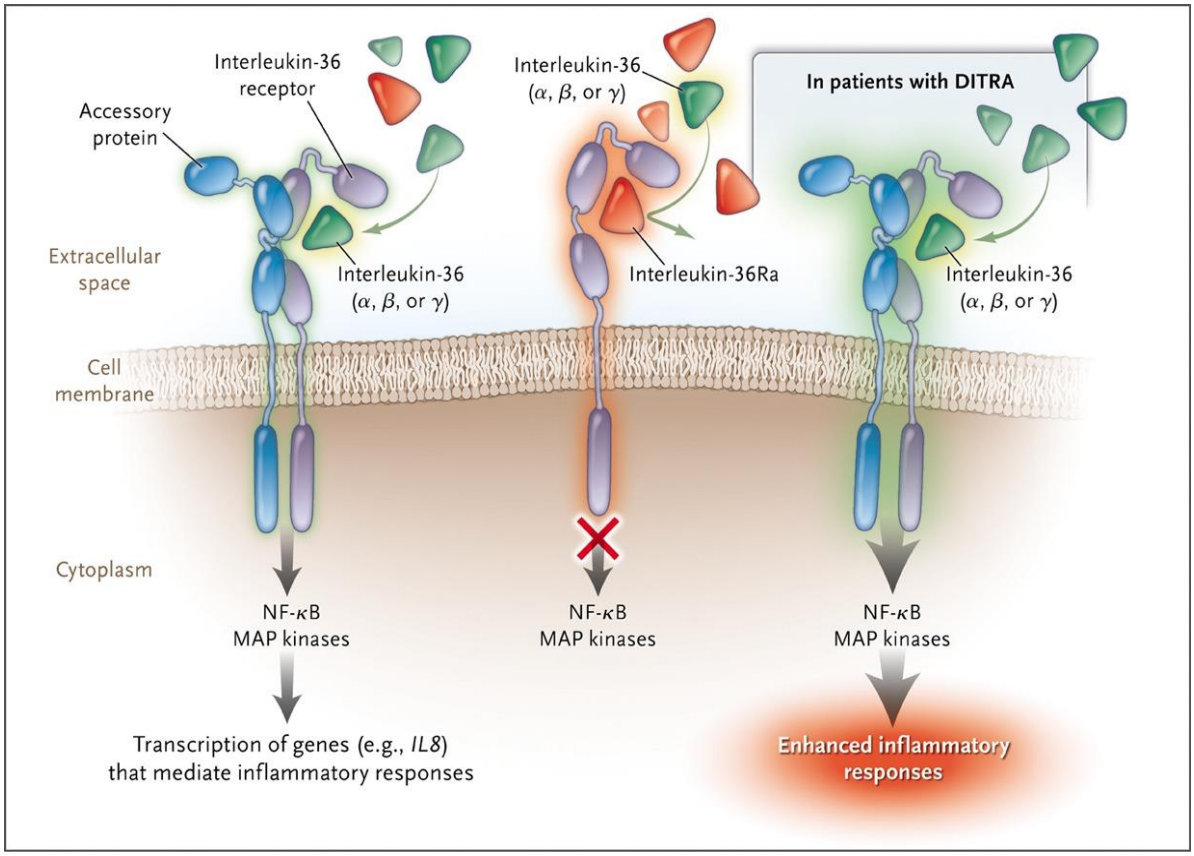

Figure 1.5: Interleukin-36. *IL-36 agonists promote inflammation through the NF-κB and MAP kinases pathways. Binding promotes the formation of a heterodimer of the IL-1RL2 and IL-1RacP. IL-36RA blocks this formation, inhibiting the inflammatory response. In patients deficient in IL-36RA (DITRA), IL-36 agonists can elicit and enhanced inflammatory response.*

Source: Douangpanya 2011; New England Journal of Medicine.

Although we know the IL-36/IL36R pathway is highly pro-inflammatory in skin and lungs, we are still at a very early stage in our current understanding of its *in vivo* biology and certainly no studies have investigated a role for this pathway in the heart. As the escalation of inflammation and adverse tissue remodelling are important aspects that tend to favour a worse prognosis in patients after an MI, IL-36 may play a key therapeutic role in the setting of myocardial IR injury. This makes it an exciting candidate for investigation.

1.6.2 Leukocyte Trafficking

The pro-inflammatory environment that exists during IR injury leads to the activation of circulating inflammatory cells and the vasculature, particularly the EC lining. This thus allows for the initiation of leukocyte trafficking. Trafficking of inflammatory cells from the vasculature into the injured tissue can be divided into a number of steps which comprise the 'adhesion cascade' ***(Figure 1.6)*** and include: i) Tethering and rolling – ii) Arrest and firm adhesion – iii) Transmigration [105].

1.6.2.1 Tethering and Rolling

The initial stage of leukocyte trafficking involves the capture of cells from the blood vessel lumen onto the endothelial surface. This stage is mostly mediated by selectins and integrins where bonds are formed with their respective ligands – the formation and dissociation of these bonds helps to reduce the velocity of circulating leukocytes until capture [106, 107]. There are 3 types of selectins, known as P-selectin, E-selectin and L-selectin. E-selectin and P-

selectin are present on ECs while L-selectin is present on leukocytes. P-selectin can also be found on platelets.

In the steady-state, there is only a slight expression of E- and P-selectin on the endothelium. The presence of pro-inflammatory cytokines such as TNF-α and IL-1β will increase the expression of selectins very rapidly such as during IR injury [108].

Capture of circulating leukocytes is mediated by selectins and their corresponding ligands. A higher expression of E- and P-selectin on the stimulated endothelium enables capture of leukocytes through binding with P-selectin glycoprotein ligand-1 (PSGL-1) and E-selectin ligand-1 (ESL-1), among others [109, 110]. Leukocytes also utilise L-selectin during the process of tethering through L-selectin-E-selectin interactions and via L-selectin binding to proteoglycans on the endothelium [111]. As the accumulation of leukocytes on the vessel wall reduces the surface area of exposed endothelial cells, further capture is permitted by PSGL-1 interaction with L-selectin, facilitating adhesion of leukocytes onto one another [112].

Functional integrins are heterodimers comprised of a large α-subunit (120-180kDa) and a small β-subunit (90-110kDa) [113]. The subunit combination determines the type of integrin produced. Integrins also play a role in leukocyte capture. This has been shown with integrins such as lymphocyte function-associated antigen-1 (LFA-1; $\alpha_L\beta_2$) and very late antigen-4 (VLA-4; $\alpha_4\beta_1$), which mediate this via their respective ligands intercellular adhesion molecule-1 (ICAM-1) and vascular cell adhesion molecule-1 (VCAM-1) [114].

Studies investigating the role of selectins in myocardial IR injury have focussed on histological assessments of injury. For instance, the role that P-selectin plays in mediating the early phase of leukocyte-EC adhesion was shown in studies that administered antibodies or carbohydrate

ligands against P-selectin in the setting of myocardial IR injury, leading to a reduction in injury [115, 116]. However, how these mechanisms truly function in real-time *in vivo* is unknown as assumptions of leukocyte trafficking in the heart are made due to difficulties in visualising the beating heart microcirculation.

1.6.2.2 Arrest and Firm Adhesion

Activation of leukocytes occurs during the process of 'slow-rolling', where the leukocyte is exposed to local factors closely surrounding and on the surface of the endothelium. Cytokines such as IL-1 and TNF-α can aid in the priming of leukocytes for firm adhesion [105]. Chemokines are cytokines that produce a chemotactic gradient that allows inflammatory cells to home in towards the site of injury. They consist of different motifs that relate to cysteine crosslinks and amino acid sequences, namely C, CC, CXC and CX3C. The chemokines CXC ligand-1 (CXCL1) and CC ligand-2 (CCL2) are well-known examples and their function is to activate leukocytes [117, 118]. Activation of leukocytes during the process of slow-rolling allows for the further priming of adhesion molecules, namely the integrins. Priming of integrins results in a conformational change where they transform from an inactive state (low affinity) to an active state (high affinity) in order to facilitate binding of leukocytes to the endothelium. Integrins such as LFA-1, VLA-4, VLA-5 etc. play an important role in arresting and instigating firm adhesion of leukocytes onto the endothelial surface [119]. Ligands for integrins are part of the immunoglobulin superfamily (IgSF) which are expressed on the endothelial surface. Examples of these include ICAM-1, ICAM-2, VCAM-1 etc.

The majority of studies investigating the role of integrins in myocardial IR injury have been conducted via histological assessment. Metzler et al. showed that using β1 integrin knockout mice ($\beta1^{-/-}$) resulted in reduction of neutrophil infiltration into ischaemic regions of the mouse heart but did not reduce myocardial damage [120]. Such a finding would no doubt benefit from being able to directly image the heart and visualise neutrophil trafficking.

Non-integrins may also play a role in arresting leukocytes. The selectins, especially E-selectin, mentioned previously still play a role during firm adhesion [105]. CD44 has also been shown to mediate firm adhesion of leukocytes through binding with hyaluronan (HA) or VLA-4 [121, 122].

1.6.2.3 Transmigration

In order for inflammatory cells to home towards an injured site, they need to leave the vasculature, which is usually 'impermeable' to cells. Activated leukocytes that are firmly adherent onto the endothelium can now start to transmigrate out towards the site of injury. Transmigration of leukocytes through the endothelial layer can occur via two routes. It is believed that leukocytes preferably transmigrate at sites of least resistance, which may partly determine their route of choice [123]. The paracellular route involves leukocytes crawling on the endothelium in order to reach an appropriate junction between adjacent ECs that will facilitate their migration out of the blood vessel [105]. Integrins remain important in transmigration too, where clustering of LFA-1 and VLA-4 at docking sites on ECs (clustering of ICAM-1 and VCAM-1) mediates transmigration [107, 124]. Integrin clustering helps to initiate events that lead to transmigration by phosphorylation of vascular endothelial cadherin (VE-

cadherin), by inducing slight EC contraction and by inducing EC surface transfer of the lateral border recycling compartment (LBRC) [106]. The junction between ECs consists of adhesion molecules, such as VE-cadherin, that oppose transmigration and hold the ECs together. Phosphorylation of VE-cadherin loosens the inter-endothelial bond and it is then translocated away from the EC junction [106, 125]. A number of adhesion molecules that favour leukocyte transmigration, such as platelet-EC adhesion molecule-1 (PECAM-1/CD31), CD99 and junctional adhesion molecule-A (JAM-A), then play a pivotal role in transmigration and become concentrated at the EC junction [105]. Corada et al. showed that JAM-A knockout mice (JAM $A^{-/-}$) undergoing myocardial IR injury experienced neutrophils that could adhere to the vessel wall, but could not transmigrate into the tissue (histological analysis) and ultimately resulted in reduced cardiac function as recorded during echocardiography [126]. Integrins have also been shown to interact with JAMs during transmigration, where LFA-1 was shown to bind to JAM-A and likely promote transmigration [107]. As mentioned earlier, PECAM-1 on ECs can bind to PECAM-1 on leukocytes in order to facilitate transmigration as well [107]. These molecules are present at the EC junction but are also found in abundance in the LBRC. The LBRC is a membrane compartment that resides just below the plasma membrane in the EC and houses unbound pro-transmigration adhesion molecules [106]. The trafficking of the LBRC to the EC surface at the site of the adherent leukocyte and the expansion of its membrane around the leukocyte thus facilitates transmigration [127]. The other mechanism of transmigration involves a leukocyte directly migrating through an EC in order to escape the vasculature (transcellular). The transcellular route shares many similarities with the paracellular route such as pivotal adhesion molecules however, the transcellular route takes more time to complete and is rarer [105].

Once pass the endothelial layer, leukocytes still need to migrate through the sub-endothelial layer. The adhesion molecules that play an important role during transmigration continue to do so in this stage as well [128, 129]. As this layer is composed of laminins, collagen and proteoglycans, leukocytes will break down these components in order to facilitate traversal. This can be conducted via enzymes such as matrix metalloproteinases (MMPs) [130]. Again, as leukocytes favour the path of least resistance, they prefer to traverse areas with low expression of extracellular macromolecules [131]. The presence of chemokines within the tissue help to guide leukocytes towards the site of injury.

1.6.3 Innate Immune Response

The innate immune response during myocardial IR injury is generally slow during the period of ischaemia but ramps up in effect during reperfusion. Within an hour of reperfusion, there is already an increase in the infiltration of the innate immune cells [5]. The innate immune response is comprised of a number of cell types such as neutrophils, eosinophils, basophils, monocytes, macrophages and dendritic cells. Experiments investigating the role of the innate immune system in myocardial IR injury are generally conducted using immunofluorescence, histology, gene expression assays or flow cytometry after IR injury of the heart taken at various time points [132-135]. These have primarily been conducted in mice and rats, although experiments in rabbits, cats and dogs have also been undertaken.

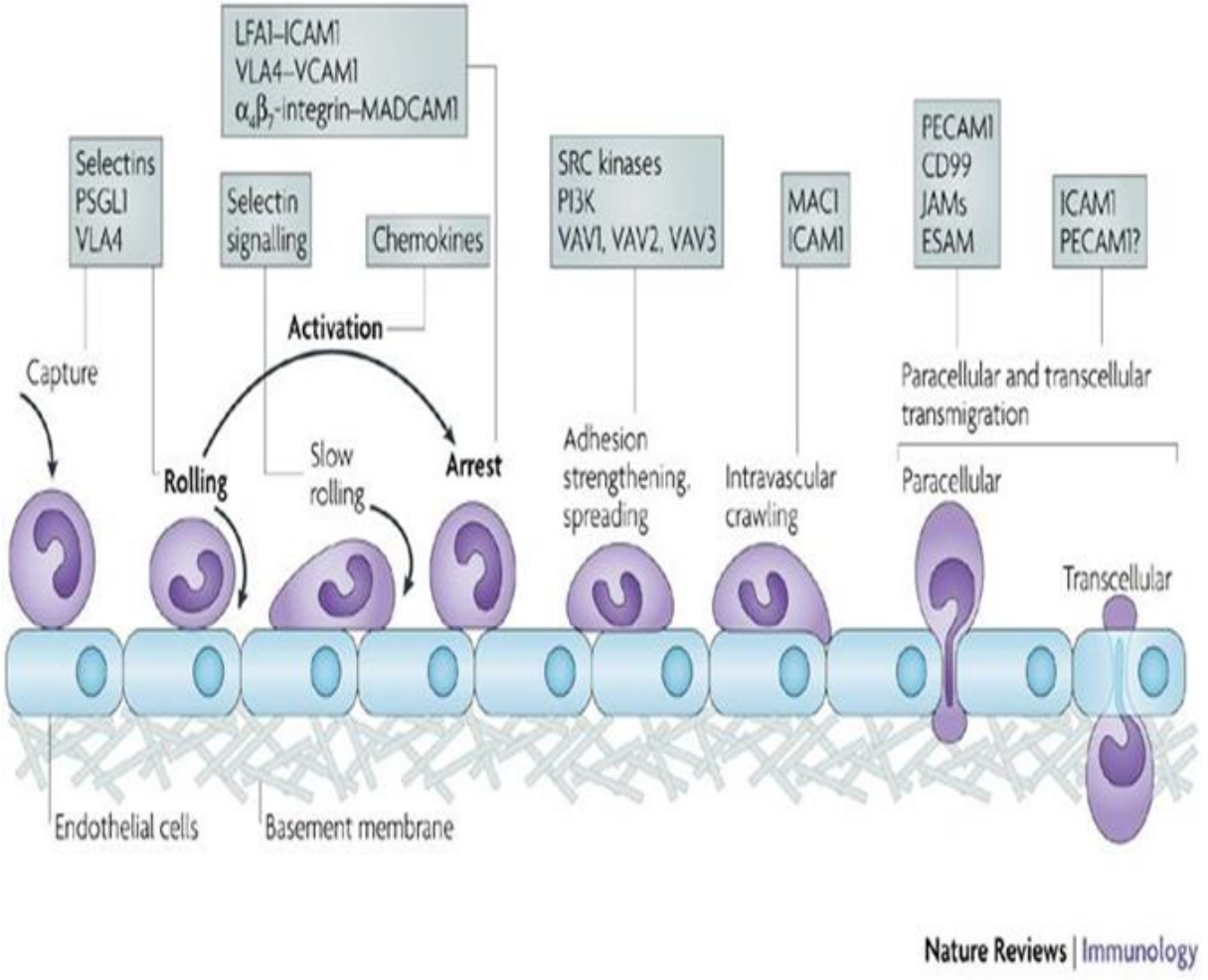

Figure 1.6: Leukocyte trafficking (leukocyte adhesion cascade). *The capture (tethering) and subsequent migration of free-flowing leukocytes out of the vasculature is an important process mediated by a number of cytokines and adhesion molecules. This process is also important in understanding the homing potential of cellular therapies.*

Source: Ley 2007; Nature Reviews Immunology.

1.6.3.1 Neutrophils

Our classical understanding of the role that the innate immune system plays in inflammation begins with the activation of neutrophils as the first line of defence. Neutrophils are the most abundant white blood cell in humans. They contain secretory granules – thus are part of the granulocyte family – and are easily identified by their multi-lobular nucleus. During an infection, activated neutrophils function to remove the invading microbe. During sterile inflammation, activated neutrophils function to remove debris and damaged/dead cells via the same mechanisms. These mechanisms include the generation and release of ROS, degranulation and the release of stored cytokines or enzymes, phagocytosis and formation of neutrophil extracellular traps (NETs) [136].

The primary ROS molecule generated by neutrophils is superoxide. Stimulated neutrophils rely on NOX2 in order to produce superoxide [22]. As superoxide is a precursor to other ROS molecules, the cascade by which other, more potent, ROS can be produced is initiated. The majority of ROS formation that occurs during myocardial IR injury is generated by the innate immune system [137]. While the primary function of ROS in this instance is to help degrade non-viable cells, the abundance of ROS present leads to damage of healthy cells as well. As such, the deleterious effects of oxidative stress, covered earlier, can be tied to the presence of the innate immune cells at the injury site. Neutrophils also store enzymes that can mediate ROS production and promote extracellular matrix degradation. For instance, myeloperoxidase (MPO) promotes further inflammation into the site of injury by encouraging inflammatory infiltration [138].

Whilst neutrophils are not as phagocytically active as monocytes and macrophages, they have the capacity to engulf debris and damaged cells in order to promote clearing of the injured area [139]. Engulfed components are further broken down by ROS and enzymes stored in the granules of neutrophils.

The formation of neutrophil extracellular traps is a relatively newfound function of neutrophils. NETs are weblike structures that are made up of DNA components, making them 'sticky'. Primarily seen as a method to capture agile microbes during an infection, its role in sterile inflammation is less understood. Research has found that the process of NET formation, NETosis, still occurs even in the context of sterile inflammation such as myocardial IR injury, where its role is said to be pro-thrombotic [140]. The release of NETs into the blood vessel activates platelets and provides bedding for the capture of red blood cells and white blood cells. These microthrombi that form due to NETs may help explain the no-reflow phenomenon described earlier as well.

Once in the tissue and they have carried out their function, neutrophils die off quickly through apoptosis. Whilst this was previously seen as just a consequence of inflammation, it is now known that the removal of apoptotic neutrophils by macrophages acts as a marker or checkpoint which shifts the inflammatory response from a pro-inflammatory state into a reparative state [141]. As such, treatment strategies looking at inhibiting the neutrophil response in myocardial IR injury need to be mindful of a potential impairment towards resolution of the injury. The role of the other granulocytes is not as well understood as neutrophils however, an increase in the presence of other granulocytes in cardiac tissue during IR injury is not uncommon [142].

1.6.3.2 Monocytes and Macrophages

Circulating monocytes in the blood make up around 10% of blood leukocytes in humans. They exist either as classical inflammatory monocytes ($CD14^{++}CD16^{-}$), non-classical monocytes ($CD14^{+}CD16^{++}$) and intermediate monocytes ($CD14^{++}CD16^{+}$). In mice, they are split into two groups known as $Ly6C^{high}$ (pro-inflammatory) and $Ly6C^{low}$ (anti-inflammatory) monocytes. In the steady-state, circulating monocytes survey the blood and tissue and scavenge debris as required without differentiating into macrophages or dendritic cells [143].

During an insult however, monocytes can readily extravasate into the tissue and differentiate into macrophages or dendritic cells. Pro-inflammatory monocytes tend to differentiate into pro-inflammatory macrophages (M1 macrophages) while anti-inflammatory monocytes tend to differentiate into anti-inflammatory macrophages (M2 macrophages). There exists a high degree of plasticity amongst these cells however, meaning that they can rapidly shift between both states based on environmental cues [144]. Of note, recent research suggest that the nomenclature of M1 and M2 macrophages is too rigid, based primarily on an *in vitro* classification of macrophages, and that the existence of a spectrum of macrophage activation states is more accurate *in vivo* [145]. In the early stages of myocardial IR injury, pro-inflammatory monocytes/macrophages dominate as there exist a need to clear damaged/dead cells rapidly. This is carried out primarily via phagocytosis, monocytes and macrophages being more aggressive phagocytes compared to neutrophils, but also by ROS generation and the release of proteolytic enzymes [143]. This is similar in function to that of neutrophils.

As mentioned earlier, the phagocytosis of apoptotic neutrophils by macrophages initiates signals from the macrophage that promotes a shift in the inflammatory response from pro-inflammatory to reparative. This is done by inhibiting pro-inflammatory cytokines and promoting anti-inflammatory cytokines such as interleukin-10 (IL-10) and transforming growth factor-beta (TGF-β) [141]. Anti-inflammatory monocytes and macrophages thereafter play a dominant role in repairing post-reperfusion injured tissue through several mechanisms such as by promoting angiogenesis, regulating the extracellular matrix and by promoting the formation of myofibroblasts [146].

Macrophages in cardiac tissue can arise from blood monocytes, known as infiltrating macrophages, or can be tissue resident macrophages. Unlike infiltrating macrophages, tissue resident macrophages arise from the yolk sac during embryogenesis [147]. During myocardial IR injury, tissue resident macrophages may become necrotic and thus not contribute to the inflammatory process. If they do survive, they function similarly to the infiltrating macrophages, reliant on environmental cues.

1.7 Stem Cells as a Therapeutic Option in Myocardial IR injury

Stem cells (SCs) have emerged as one of the leading candidates for cardiovascular disease therapy, particularly for limiting or reversing myocardial damage caused by an MI. Although initial studies in the heart were conducted using bone marrow (BM)-derived haematopoietic SCs (HSCs), mesenchymal SCs (MSCs) have emerged as an alternative candidate for cell therapy as well. The exact mechanisms by which SCs confer a protective action are unknown. A plethora of more recent studies now point to the paracrine release of therapeutic factors as

an important mechanism. This includes the production and secretion of a broad variety of anti-inflammatory and immunomodulatory cytokines, angiogenic factors, anti-apoptotic factors and antioxidant elements (IL-6, IL-10, PGE_2, SOD etc), which act in a paracrine manner to ensure cytoprotection [148]. Although some clinical trials demonstrate improvements in infarction size, ejection fraction and myocardial perfusion, benefits with exogenously injected SCs have been either minor or transitory with regards to reduction of adverse outcomes [149]. This may be due to a lack of knowledge of whether systemically infused SCs efficiently home and adhere within the injured heart coronary microvessels. Again, the generation of such information has been hampered by the lack of an imaging technique that can track SCs in the beating heart at a cellular level. Previous studies from the Kalia group have shown that the efficacy of cellular therapy appears to depend on successful SC homing to injury sites following their systemic delivery into the bloodstream [150, 151]. Certainly, poor homing and entrapment within non-injured sites, such as the lungs, contributes to their limited clinical success [72]. Furthermore, it is not clear whether the therapeutic mechanisms of cellular therapy for myocardial IR injury involve SCs conferring vasculoprotection and inhibiting any thromboinflammatory processes in coronary microvessels. These problems underscore and prioritise the need for finding ways to improve SC delivery and recruitment to the heart and identify whether coronary vasculoprotection underpins their therapeutic benefits.

More importantly, we still remain unsure as to which SC population would home to the heart more effectively and confer the greatest therapeutic effect. Indeed, no study has compared the adhesive and therapeutic effectiveness of HSCs and MSCs in the IR injured heart. We now know that MSCs can be isolated from various sites in the body and studies show these MSCs are structurally and functionally different. Indeed, even MSCs isolated from the same site

show heterogeneity in their behaviour [152]. The prospective identification, isolation and expansion of discrete functional SC subsets which show the greatest therapeutic promise for heart disease is undoubtedly the real future of SC scientific and therapeutic use.

As mentioned earlier, clinical trials utilising SCs as a form of cell therapy in MI studies have returned inconclusive results. Whilst some studies have shown beneficial impacts (infarct reduction, preserved left ventricular function) of SC therapy utilising HSCs, MSCs, induced pluripotent stem cells (iPSCs) or embryonic stem cells (ESCs), these results have not been consistently reproducible and any benefit observed has not translated into improvements in clinical outcomes [149]. Reasons behind this range from a lack in standardised methodologies (cell isolation protocols, timing of cell delivery etc.), trial designs lacking in rigorous attention to detail (inclusion criteria with regards to patient characteristics), small patient samples and a lack of long-term follow-up of patients. Little is known as to how SCs can confer vasculoprotection in the injured heart, requiring more research in order to understand the role that SCs can play in clinical applications.

1.7.1 Haematopoietic Stem Cells (HSCs)

HSCs are the progenitor cells for the entire blood cell lineage. In order to achieve this, HSCs are multipotent cells capable of long-term self-renewal and differentiating into blood cells as required [153]. HSCs contribute to the generation of erythroid, myeloid, lymphoid and megakaryocyte cells ***(Figure 1.7)*** [154]. They are primarily resident in the bone marrow (BM) although some cells do circulate in the peripheral blood [155]. HSCs can be mobilised from the BM into the peripheral blood system in order to reach target organs of interest. These organs

can be targeted due to injury or insult, where the presence of HSCs can provide a stabilising and reparative action. HSCs store a number of cytokines that help promote angiogenesis, neovascularisation and EC health and proliferation [156]. Examples of the cytokines released by HSCs to promote tissue revitalisation include angiopoietin-1 (ANG-1), fibroblast growth factor-2 (FGF-2) and vascular endothelial growth factor-A (VEGF-A) [157]. HSCs have also been shown to exhibit anti-inflammatory and anti-platelet properties as well, both of which would help aid damage reduction during an insult such as during myocardial IR injury [150].

Some research groups have suggested the possibility of HSCs differentiating into endothelial progenitor cells and directly influencing tissue healing [157]. Such an ability would allow for HSCs to incorporate themselves into the vasculature and directly repair or replace damaged ECs cells. Evidence of this in preclinical trials has not been favourable, as even though HSCs have been shown attach themselves within the blood vessel wall and exhibit endothelial markers, they do not tend to permanently relocate there [157]. Utilisation of HSCs in preclinical experiments is undoubtedly important. They can be obtained from many species, including human and murine, with primary HSCs isolated from either the bone marrow or, in lesser numbers, the peripheral blood system. Human HSCs exhibit CD34 and CD90 molecules and can be purified from samples via these markers and maintained in culture [158]. Mouse immortalised cell lines have also been established such as haematopoietic progenitor cell-5 and -7 (HPC-5; HPC-7) [151]. As immortalised cells, they are easier to obtain in large numbers as they can proliferate *in vitro* continuously.

1.7.2 Mesenchymal Stem Cells (MSCs)

MSCs are multipotent stromal cells capable of self-replicating and can differentiate into mesoderm, endoderm and ectoderm lineages [159]. They were first identified and isolated from BM as plastic adherent cells that were capable of differentiating into bone cells (osteoblasts), fat cells (adipocytes) and cartilage (chondrocytes) but were later shown to be able to form muscle and neurons as well ***(Figure 1.8)***. MSCs are primarily located in the BM, similar to HSCs, but can also be isolated from adipose tissue, muscle, connective tissue and also birth or neonatal tissue including from the umbilical cord (Wharton's jelly (WJ)) and umbilical cord blood [159]. Early studies in the heart focussed on BM-derived MSCs while recent experimental studies have also investigated the therapeutic potential of umbilical cord, umbilical cord blood and adipose tissue MSCs. Although less investigated, these cells have shown promising potential for treating degenerative and inflammatory disease. Interestingly, MSCs isolated from different sites vary with regards to surface marker expression and proliferative, differentiation and immunomodulatory capacity. Certainly, birth or neonatal tissue MSCs appear to have better proliferative/differentiation potential and engraftment capacity than adult cells [160]. Interestingly, same site MSCs also vary - for example, BM-derived MSC cultures, even from the same donor, can present as a heterogeneous population that show differing morphology, differentiation and migratory capacity.

No unique cell surface marker unequivocally distinguishes MSCs from other HSCs, which makes a uniform definition difficult. However, the definition of MSCs, as agreed to by the International Society for Stem Cell Research, include the three following criteria [160] (i) MSCs are plastic adherent cells in standard *in vitro* culturing conditions (ii) MSCs must be able to tri-

differentiate into adipocytes, chondrocytes and osteoblast *in vitro* and (iii) MSCs must express markers for CD73, CD90 and CD105 while not expressing markers for CD11b, CD14, CD34, CD45, CD79a and HLA-DR. An interesting aspect of MSCs are their ability to avoid detection by a host's immune system as they express few HLA class I markers and no HLA class II markers [161]. They possess several advantages over other SCs, including their ease of isolation and growth in culture and low immunogenicity. This makes MSCs a potentially powerful therapeutic tool in the clinical field.

As mentioned previously, there are many sources from which MSCs can be obtained. Different sources of MSCs confer different advantages. BM MSCs are highly proliferative and have been shown to help reduce the final size of a myocardial infarct, reduce myocardial hypertrophy and repair damaged tissue [160]. WJ MSCs share certain properties with embryonic stem cells and thus are less likely to cause immunorejection but, unlike ESCs, are also less likely to trigger teratoma formation [162]. The advantages of specific sources of MSCs and their specialised target organ effects should be taken into account when setting up an experimental design. However, it is important to state that the homing and specifically the vasculoprotective potential of different MSC types or sub-types has not previously been investigated in the injured heart *in vivo*.

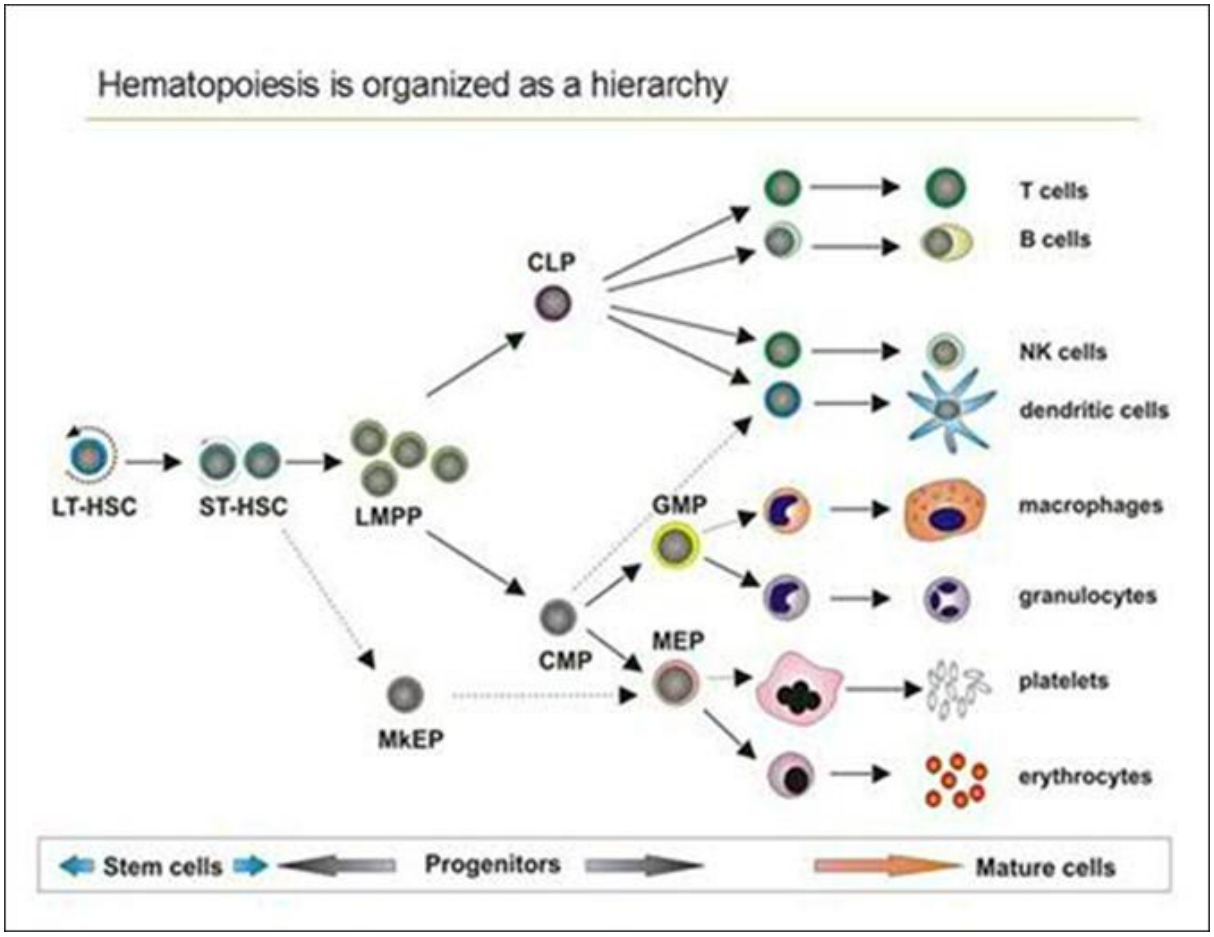

***Figure 1.7: Haematopoietic Stem Cell Lineage**. Haematopoietic stem cells differentiate along a set pathway and ultimately are able to form all specialised blood cells.*

Source: Schuringa 2015; University of Groningen.

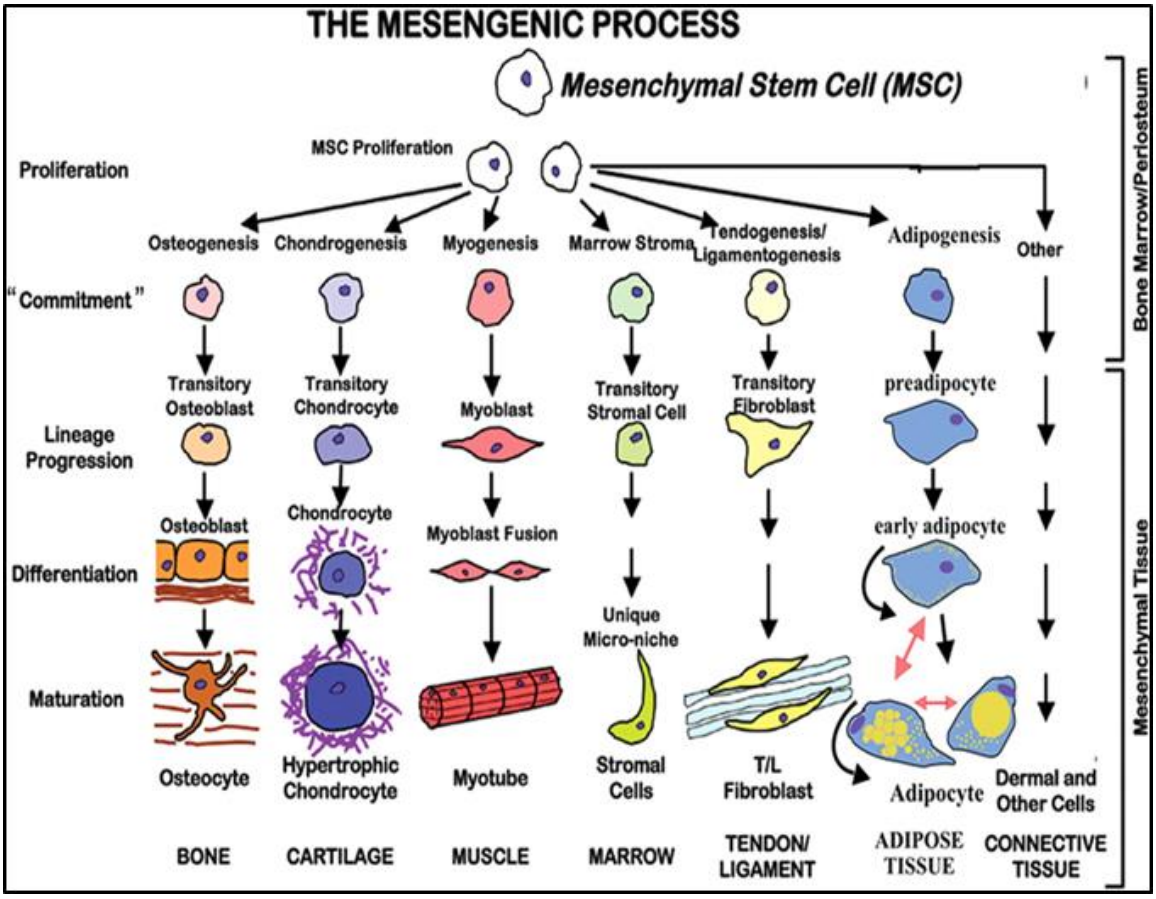

Figure 1.8: Mesenchymal Stem Cell Lineage*. MSCs differentiate into mesoderm, endoderm and ectoderm lineages and form specialised cells such as bone cells, fat cells, muscle and cartilage.*

Source: Caplan 2010; Cartilage.

1.8 Imaging the Beating Mouse Heart *In Vivo* – Intravital Microscopy (IVM)

Intravital microscopy is an imaging technique that has been used extensively to image the microcirculation of a number of different rodent solid organs (liver, kidney etc.) and also transparent tissues such as the mesentery and cremaster muscle. Indeed, much of our existing knowledge of the impact of IR injury on the microcirculation and thromboinflammatory response has been obtained using mesenteric and cremasteric preparations [163-165]. However, as mentioned earlier, investigating the dynamic events that occur in the coronary microcirculation in real-time during an insult to the heart has been very challenging due to beating and respiratory related movements. In this regard, preclinical studies have been hampered either by technology or the inability to adequately gain high-quality images depicting the coronary microcirculation [46]. This is especially true in animal models relating to mice. Such studies have been commonplace in other organs however, such as the liver and kidney. Recent advancements in technology has meant that carrying out IVM to investigate dynamic events of the coronary microcirculation is now more feasible.

Currently, *in vitro* cellular assays and immunohistochemistry of frozen or paraffin embedded tissue sections are the primary methods by which the molecular, cellular and structural changes that occur during cardiovascular diseases are investigated. However, these static snapshots provide no indication of real-time kinetics of deleterious cell recruitment in the presence of pathophysiological flow, nor information on microvessel integrity. Whilst these provide valuable insights and are still important in understanding the underlying disease process, there exists a need to investigate these changes in whole tissue. Langendorff heart preparations are used to fill in this knowledge gap. However, this comes at the expense of the

native physiological parameters that are present in a fully systemic system. As such, real-time *in vivo* measurements are the ideal complement to these current methods.

Vinegoni et al. elegantly showed that attaching a 3D printed tissue stabiliser to the exposed mouse heart allowed for motion artefact-free measurements to be obtained at single-cell resolution in real-time [166]. This study looked at visualising various structures such as capillary networks, blood flow, cardiomyocytes and inflammatory cells. However, this was only conducted on healthy, uninjured mice hearts, not in the setting of myocardial IR injury. Labelling of inflammatory cells was not specific either, using Rhodamine-6G for generalised labelling of circulating leukocytes. High-resolution microscopes, such as laser scanning and spinning disk confocal microscopes, can be used to obtain high quality images through this method. The use of fluorescent markers has meant that this achievement opens up a variety of potential investigative avenues in understanding pathophysiology of cardiovascular diseases. Dynamic events such as microvascular physiology, leukocyte trafficking, cell-cell interactions and the acute production of injury markers are amongst the novel research investigations that can be undertaken with IVM [167].

1.9 Summary

In summary, MI poses a considerable health issue globally that requires further investigation in order to develop effective treatment strategies, particularly those that target the immediate period post-reperfusion. The high mortality and morbidity associated with the disease also places a huge financial burden on healthcare systems worldwide. The need to conduct more in-depth research into this field is paramount.

A key missing element into cardiovascular research is the inability to adequately visualise the coronary microcirculation of the heart during injury. This is true in the clinical setting and the pre-clinical setting. Current modern imaging techniques in the clinical field do not allow us to adequately interrogate the coronary microcirculation in real-time. In the pre-clinical research setting however, steps have been taken to allow researchers to acquire high-quality images from the beating heart of experimental animal models. This has been very difficult to achieve especially when using mice models. Intravital microscopy of the beating mouse heart is a novel technique that can now allow researchers to interrogate the microcirculation of the heart with respect to different injury models, such as IR injury. This will open up our understanding of the important role that the microcirculation plays in myocardial IR injury and ultimately in MI. As researchers have begun to appreciate the complex nature of the microcirculation of the heart, opportunities will arise that may allow us to find other therapeutic options for the treatment of reperfusion mediated injury in MI.

One such treatment option would be via delivery of cellular therapy. Although SCs have been used in clinical trials as therapy for MI, their results have been underwhelming. By combining our knowledge of the cardiac microcirculation, through the use of IVM, with the use of SCs as a form of cell therapy, we will be able to better understand the impact that SCs can have in the disease state. Specifically, we will be able to determine whether their therapeutic efficacy and mechanisms of action involves protecting the coronary microcirculation. Our understanding of how SCs home to the heart and exert their protective effects may allow us to refine our delivery techniques in order to achieve a much better therapeutic outcome.

1.10 Aims and Hypotheses

This thesis aimed to characterise in detail the impact of myocardial IR injury on the mouse beating heart coronary microcirculation *in vivo* using fluorescent, confocal-based intravital imaging. In order to do this, we aimed to establish a novel method whereby myocardial stabilisation of a small region of the beating heart left ventricle would subsequently allow real-time intravital imaging of the coronary microcirculation *in vivo*. The second major aim is to investigate whether the ability of SCs to potentially be beneficial relied on a vasculoprotective mechanism of action. More specifically, the two main aims and hypotheses of this thesis are:

- **AIM:** Optimise the surgical and stabilisation techniques to allow for IVM assessment of the murine beating heart coronary microcirculation *in vivo.* Image the healthy and IR injured coronary microcirculation and quantitate changes in ventricular blood perfusion, functional capillary density and recruitment of endogenous inflammatory cells (neutrophils, platelets, monocytes and macrophages). **HYPOTHESIS:** Myocardial IR injury leads to tissue infarction by promoting a thrombo-inflammatory response specifically within the coronary microvessels and through causing disorganisation of microvessels of the heart. These multiple events would lead to a decrease in effective ventricular blood perfusion in the injured area due to a decrease in the functional capillary density.

- **AIM:** Firstly determine, using *in vitro* assays, the most suitable SC to use as cell therapy in *in vivo* myocardial IR injury murine models. Further investigate, both *in vitro* and *in vivo,* whether SCs provide benefit to the IR injured beating heart through effects on the microcirculation. **HYPOTHESIS:** SCs will reduce infarct size in the IR injured heart by inhibiting any thrombo-inflammatory events, protect the structural integrity of the microvessels and increase regional blood flow perfusion through the heart. SCs will achieve this vasculoprotective benefit partly by effectively homing to the murine heart during IR injury.

CHAPTER 2:

MATERIALS & METHODS

2.1 Materials

A list of the antibodies and materials used from can be found below:

Experiment	Antibody	Conj.	Clone	Origin	Target	Company	Conc.
Flow Cytometry	anti-CD31	PE	390	Rat	Mouse	Biolegend	0.2 mg/ml
	IgG2a Control	PE	RTK2758	Rat	Mouse	Biolegend	0.2 mg/ml
	anti-cardiac TnT	PE	REA400	NS	Mouse	Miltenyi Biotech	NS
	REA Control	PE	REA293	NS	Mouse	Miltenyi Biotech	NS
	anti-8-OHdG	-	NS	Goat	SI	Abcam	NS
	IgG Control	-	NS	Goat	SI	Abcam	5 mg/ml
	anti-goat IgG	AF488	NS	Donkey	Goat	Abcam	2 mg/ml
	anti-ICAM-1	FITC	YN1/1.7.4	Rat	Mouse	Biologend	0.5 mg/ml
	IgG2b Control	FITC	RTK4530	Rat	Mouse	Biolegend	0.5 mg/ml
	anti-VCAM-1	PE-Cy7	429	Rat	Mouse	Biolegend	0.2 mg/ml
	IgG2a Control	PE-Cy7	RTK2758	Rat	Mouse	Biolegend	0.2 mg/ml
	anti-CD115	PE-Cy7	AFS98	Rat	Mouse	Invitrogen	0.2 mg/ml
	IgG2a Control	PE-Cy7	eBR2a	Rat	Mouse	Invitrogen	0.2 mg/ml
	anti-CD115	PE	AFS98	Rat	Mouse	Biolegend	0.2 mg/ml
	anti-Ly6C (Gr-1)	PE-Cy7	HK1.4	Rat	Mouse	Biolegend	0.2 mg/ml
IHC & *In Vitro*	anti-8-OHdG	-	NS	Goat	SI	Abcam	NS
	IgG Control	-	NS	Goat	SI	Abcam	5 mg/ml
	anti-goat IgG	AF488	NS	Donkey	Goat	Abcam	2 mg/ml
	anti-goat IgG	AF647	NS	Donkey	Goat	Abcam	2 mg/ml
	anti-VCAM-1	AF647	429	Rat	Mouse	Biolegend	0.5 mg/ml
	anti-CD31	FITC	390	Rat	Mouse	Biolegend	0.5 mg/ml
Blocking	anti-CD16/CD32	-	93	Rat	Mouse	Biolegend	0.5 mg/ml
Intravital	anti-CD31	PE	390	Rat	Mouse	Biolegend	0.2 mg/ml
	anti-CD41	APC	MWReg30	Rat	Mouse	Biolegend	0.2 mg/ml
	anti-Ly6G (Gr-1)	APC	RB6-8C5	Rat	Mouse	Thermo Fisher Scientific	0.2 mg/ml
	anti-Ly6G (Gr-1)	PE	RB6-8C5	Rat	Mouse	Thermo Fisher Scientific	0.2 mg/ml
	anti-F4/80	APC	BM8	Rat	Mouse	Biolegend	0.2 mg/ml

* NS = Not Specified; SI = Species Independent

Product	Abbreviation	Company	Location
0.9% Sodium Chloride	Saline	Sigma	Poole, UK
2,3,5-Triphenyltetrazolium Chloride	TTC	Serva	Heidelberg, Germany
5-0 Suture	-	Ethicon	New Jersey, USA
8-0 Suture	-	Ethicon	New Jersey, USA
Acetone	-	Thermo Fisher Scientific	Paisley, UK
ACK Lysing Buffer	-	Thermo Fisher Scientific	Paisley, UK
Carboxyfluorescein Diacetate Succinimidyl Ester	CFDA-SE	Thermo Fisher Scientific	Paisley, UK
Chlorhexidine	-	Medipal	Leicestershire, UK
Citric Acid	-	Sigma	Poole, UK
Collagenase Type I	-	Wako Chemicals	Osaka, Japan
Dihydroethidium	DHE	Thermo Fisher Scientific	Paisley, UK
Dimethyl Sulphoxide	DMSO	Sigma	Poole, UK
DMEM High Glucose	-	Sigma	Poole, UK
DMEM Low glucose	-	Biosera	East Sussex, UK
D-Valine MEM	-	US Biological	Leicestershire, UK
Ethanol	-	VWR Chemicals	Pennsylvania, USA
Evans Blue	-	MP Biomedicals	California, USA
FITC-Conjugated Bovine Serum Albumin	FITC-BSA	Thermo Fisher Scientific	Paisley, UK
Fluoresbrite Yellow-Green Microspheres (1µm)	-	Polysciences	Pennsylvania, USA
Foetal Bovine Serum (Heat-Inactivated)	FBS	Sigma	Poole, UK
Formalin (10% Neutral Buffered)	-	Sigma	Poole, UK
Glucose	-	Sigma	Poole, UK
Heparin Sodium	-	Wockhardt	Wrexham, UK
HEPES Solution	HEPES	Sigma	Poole, UK
Hydrogen Peroxide	H_2O_2	Sigma	Poole, UK
Hydromount	-	National Diagnostics	Georgia, USA
Interferon-gamma	IFN-γ	Creative Biolabs	New York, USA
Interleukin-36 (alpha, beta, gamma)	Il-36 (α, β, γ)	R&D Systems	Minnesota, USA
Interleukin-36 Receptor Antagonist	IL-36RA	R&D Systems	Minnesota, USA
Isofluorane	-	Abbott	Maidenhead, UK
Ketamine Hydrochloride	-	Vetoquinol	Northamptonshire, UK
L-Glutamine	-	Sigma	Poole, UK
Magnesium Chloride	$MgCl_2$	Sigma	Poole, UK
Medetomidine Hydrochloride	-	Pfizer	New York, USA

MEM Alpha Modification	-	Sigma	Poole, UK
MEM Non-Essential amino acids	-	Sigma	Poole, UK
MEM Vitamin Solution	-	Sigma	Poole, UK
Optimal Cutting Temperature	OCT	Sakura Finetek	Tokyo, Japan
Penicillin/Streptomycin Solution	P/S	Thermo Fisher Scientific	Paisley, UK
Phosphate Buffer Solution	PBS	Sigma	Poole, UK
Potassium Chloride	KCl	Sigma	Poole, UK
Prostaglandin I2	PGI2	Cayman Chemicals	Michigan, USA
Sodium Bicarbonate	$NaHCO_3$	Sigma	Poole, UK
Sodium Chloride	NaCl	Sigma	Poole, UK
Sodium Citrate	-	Sigma	Poole, UK
Sodium Phosphate Dibasic	Na_2HPO_4	Sigma	Poole, UK
Sodium Phosphate Monobasic	NaH_2PO_4	Sigma	Poole, UK
Stem Cell Factor	SCF	Thermo Fisher Scientific	Paisley, UK
StemPro Supplement	-	Thermo Fisher Scientific	Paisley, UK
StemPro-34 Media	-	Thermo Fisher Scientific	Paisley, UK
Trypsin-EDTA	-	Sigma	Poole, UK
VEET Hair Removal Cream	VEET	Reckitt Benckiser	Slough, UK
Vetbond	-	3M	Minnesota, USA

2.2 Animal Usage

Wild-type (WT; Harlem) and CD68-eGFP (kindly provided by Prof. David Greaves, University of Oxford and Dr. Asif Iqbal, University of Birmingham) male mice (8-12 weeks) on a C57BL/6 background were used in all experiments within this thesis with adherence to the Animals (Scientific Procedures) Act of 1986 (ASPA 1986) under project licence: P552D4447 (Dr. Neena Kalia).

2.3 Cell Culture, Cell Isolation, Labelling of Cells and Preparation of Cultured Media

The cell types utilised in this study that required culturing were murine vena cava ECs, embryonic-derived murine HSC line HPC-7s, BM-derived murine MSCs and WJ-derived human MSCs. These cell types required different culturing conditions which are detailed below. Some experiments involved utilising the adoptive transfer of labelled murine platelets and so their isolation and labelling process is also detailed below.

2.3.1 Culturing of Murine Vena Cava Endothelial Cells

The ECs used in this study were immortalised murine vena cava ECs (VCECs) which were kindly provided by Dr Jonathan S Alexander (Health Sciences Centre, Louisiana State University, USA). These cells were thawed from stock as required and cultured in modified eagle medium (MEM) D-Valine media topped with 10% heat-inactivated foetal bovine serum (FBS), 0.22% sodium bicarbonate, 1% penicillin/streptomycin (P/S), 1% MEM non-essential amino acids, 1% vitamin mix and 10 units/ml interferon-γ (IFN-γ) at a pH of 7.4 [168]. This media was used to expand the cells and was labelled as endothelial cell (EC) expansion media. Cells were seeded in appropriate tissue culture flasks (T25/T75) and cultured at 33.5^{o}C in a humidified, 5% CO_2 controlled incubator. The cells were split at a ratio of 1:3 when confluent and centrifuged at 1200 rpm for 5 minutes at room temperature during the sub-culturing process. When actual experiments were conducted utilising VCEC, a different culture media was used instead of the expanding media. During experiments, ECs were cultured in high glucose Dulbecco's MEM

(DMEM) media topped with 10% heat-inactivated FBS and 1% P/S. This media was labelled as EC experimental media.

2.3.2 Culturing of Haematopoietic Progenitor Cell-7s (HPC-7s)

The HSCs used in this study were the immortalised murine embryonic-derived cell line haematopoietic progenitor cell-7 (HPC-7) which were kindly provided by Prof Leif Carlsson (Umeå Centre for Molecular Medicine, Umeå University, Sweden). These cells have been routinely used by the Kalia lab to investigate HSC homing to various organs *in vivo* and to track them intravitally. Intravital studies monitoring HSC trafficking have been limited due to difficulties in isolating sufficient numbers for *in vivo* experimentation. As a result, many HSC trafficking studies have relied heavily on HSC lines. HPC-7 cells were generated by transfecting murine embryonic SCs with the LIM-Homeobox gene LHx2 [169]. HPC-7s display many characteristics of primary HSCs, including early haematopoietic transcription markers such as SCL, c-myb, GATA-1 and PU.1, express common cell surface markers and are lineage negative. In addition, the Kalia lab has demonstrated previously that HPC-7s express adhesion molecules known to be present on primary HSCs and have previously used HPC-7s to model hepatic HSC recruitment [170]. These cells were thawed from stock as required and cultured in StemPro-34 serum free media topped with 10% heat-inactivated FBS, 1% P/S, 2mM L-glutamine, 2.5% StemPro Supplement (SPS) and 0.02% Stem Cell Factor (SCF) [151]. Cells were seeded in a T25 tissue culture flask at a density of 1 x 10^6 cells/ml in suspension and maintained as such on a daily basis. The cells were centrifuged at 1200 rpm for 5 minutes at room temperature during the sub-culturing process and cultured at 37^{o}C in a humidified, 5% CO_2 controlled incubator.

2.3.2.1 Preparation of HPC-7 Cultured/Conditioned Media

As culturing of HPC-7s occurred on a daily basis, acquisition of HPC-7 cultured/conditioned media was only conducted when HPC-7s that were seeded between 3 to 5 x 10^6 cells in 3 to 5ml (1 x 10^6 cells/ml) of fresh culture media experienced a 2-fold growth after a single day. As such, only when cells had successfully reached 2 x 10^6 cells/ml after culturing for a day was the media then collected. Media was collected after the cells were centrifuged as per **section 2.3.2**, the supernatant being labelled as HPC-7 cultured media and stored at -80^{o}C.

2.3.2.2 Preparation of hydrogen peroxide (H_2O_2) pre-activated HPC-7s

Where experiments required the pre-activation of HPC-7s in order to stimulate a more robust therapeutic response, H_2O_2 was used as the activation agent. 2 x 10^6 cells/ml HPC-7s were incubated in 200µl of 100µM H_2O_2 on ice for 1 hour prior to their injection into a mouse. After 1 hour, the cells were centrifuged at 1000 rpm for 5 minutes at room temperature and resuspended in 100µl of phosphate buffer solution (PBS). The cells were then injected intra-arterially as described in **section 2.5.1.1**.

2.3.3 Culturing of Mesenchymal Stem Cells

Two different types of MSCs were used in this study. The first were primary MSCs obtained from the bone marrow of mice (BM MSC), which were kindly provided by the research group of Prof Philip Newsome (Centre for Liver Research, University of Birmingham). Briefly, the tibia and femur were collected from 8-12 weeks adult male C57Bl/6 mice and the bone marrow

was obtained by crushing of bone fragments and mechanical dissociation. Primary MSCs were isolated through flow cytometric cell sorting of live bone marrow cells based on positive staining for platelet-derived growth factor receptor α (PDGFR- α) and stem cell antigen 1 (Sca-1) alongside negative staining for TER-119 and CD45 [171, 172]. These cells were thawed from stock as required and cultured in MEM alpha modification media topped up with 10% heat-inactivated FBS, 1% P/S and 2mM L-glutamine [173]. The cells were seeded in appropriate tissue culture flasks (T75/T175) and cultured at 37^{o}C in a humidified, 5% CO_2 controlled incubator. The cells were split at a ratio of 1:3 when confluent and centrifuged at 1200 rpm for 5 minutes at room temperature during the passaging process. The cells were used at passages 7-8 in experiments in this study.

The second type of MSCs used in this study were Wharton's Jelly derived MSCs (WJ MSC) obtained from the umbilical cord of humans which were kindly provided by the research group of Prof Gerard Nash (Institute of Cardiovascular Sciences, University of Birmingham). These cells were used in compliance with the ethical standards subscribed to by Professor Nash and his group. Briefly, fresh human umbilical cords are dissected to expose the blood vessels which are then resected. The remaining cord tissue is cut into 2-3 mm^3 pieces and enzymatic digestion is used to obtain a single cell suspension. The cell suspension is cultured in WJ MSC culture medium in order to facilitate proliferation of WJ MSCs [174]. These cells were thawed from stock as required and cultured in DMEM low glucose media topped up with 10% heat-inactivated FBS and 1% P/S [174]. The cells were seeded in appropriate tissue culture flasks (T25/T75) and cultured at 37^{o}C in a humidified, 5% CO_2 controlled incubator. The cells were split at a ratio of 1:3 when confluent and centrifuged at 400 g for 5 minutes at room

temperature during the sub-culturing process. The cells were used at passages 6-8 in experiments in this study.

2.3.4 Preparation of CFSE-Labelled Fluorescent Cells

Stem cells were routinely fluorescently stained to ensure visibility when analysing experimental images. Carboxyfluorescein diacetate succinimidyl ester (CFDA-SE) is a highly cell permeable substance that, when present intracellularly, is cleaved by intracellular esterase enzymes into carboxyfluorescein succinimidyl ester (CFSE), which is impermeable to the cell membrane, locking it within the cell [175]. CFSE is a strongly fluorescent intracellular dye that is useful in staining a number of different cell types, including stem cells [176]. When stained properly, cells will appear green on imaging (488nm emission wavelength). In this study, cells stained with CFSE were used within 2 days of staining.

2.3.4.1 Preparation of CFSE stained HPC-7s

HPC-7s are non-adherent to tissue culture flasks, thus, they were stained whilst in suspension. The protocol used to stain HPC-7s with CFSE was as follows:

- Desired number of HPC-7s (1-5 x 10^6 cells) were removed from culture, placed into a 15ml centrifuge tube, and centrifuged at 1200 rpm for 5 minutes at room temperature.
- The resulting supernatant was removed and the cell pellet washed with PBS and centrifuged again at 1200 rpm for 5 minutes at room temperature.

- The resulting supernatant was removed and the cell pellet was resuspended in 5ml of 5µM CFDA-SE (diluted in PBS). The solution was mixed gently and incubated for 10 minutes at 37^{o}C and away from light sources.
- After the incubation period, an excess of culture media was added to the solution to neutralise surplus CFDA-SE. The cells were then centrifuged again at 1200 rpm for 5 minutes at room temperature.
- The resulting supernatant was removed and the cell pellet washed with PBS and centrifuged again at 1200 rpm for 5 minutes at room temperature.
- Cells were resuspended at the desired cell dilution, ready for an experiment, or cultured as described earlier to be used at a later time point.

2.3.4.2 Preparation of CFSE stained BM MSCs and WJ MSCs

Unlike HPC-7s, BM MSCs and WJ MSCs are both adherent to tissue culture flasks, thus, they were stained when >80% confluent. The protocol used to stain BM MSCs and WJ MSCs with CFSE was as follows:

- When the cells had reached >80% confluence in a tissue culture flask, the culture media was removed and the cells were washed with PBS.
- After washing, 5µM of CFDA-SE (diluted in PBS) was added to the tissue culture flask at an appropriate volume, making sure to coat the cells fully with the solution.
- The cells were incubated for 10 minutes at 37^{o}C and away from light sources.
- After the incubation period, the CFDA-SE solution was removed and the cells were washed with PBS to remove surplus CFDA-SE.

- The cells could then be harvested using 1x trypsin-EDTA and collected for use in an experiment or they could be sub-cultured into a new passage to be used at a later time point.

2.3.4.3 Murine Platelet Isolation and CFSE Staining

In some intravital experiments, donor platelets were used to image singular platelet kinetics and gain an indication of blood flow in mice undergoing myocardial IR injury. Donor mice were anaesthetised by inducing them with 5% isoflurane. Once the mice were fully anaesthetised (absence of a pedal reflex), a laparotomy was performed to open the abdomen and reveal the intestines. The intestines were then softly brushed aside to reveal the inferior vena cava. A 1ml syringe was preloaded with 100µl of acid citrate dextrose (ACD; 120mM sodium citrate, 110mM glucose, and 80mM citric acid) and attached to a 25G needle. Blood was drawn into the syringe via a puncture through the vena cava. 800µl-1ml of blood was collected per mouse. The blood was then transferred to a 1.5ml Eppendorf preloaded with 200µl of modified Tyrode's solution (134mM NaCl, 2.9mM KCl, 0.34mM Na_2HPO_4, 12mM $NaHCO_3$, 1mM $MgCl_2$, 5mM glucose, and 20mM HEPES; pH adjusted to 7.3) and kept at room temperature. Mice were culled using schedule 1 techniques once bleeding had been performed. Platelet isolation from whole blood was conducted as follows:

- Whole blood obtained from the terminal bleeding process (in 1.5ml Eppendorf) was centrifuged at 2000 rpm for 5 minutes at room temperature.
- After centrifugation, the platelet rich plasma (PRP) was removed along with 1/3 of the remaining blood products and placed into a new 1.5ml Eppendorf.

- The PRP + 1/3 blood was then centrifuged at 1000 rpm for 6 minutes at room temperature.
- After centrifugation, the PRP was removed and placed into another new Eppendorf and placed to the side. 200µl of modified Tyrode's solution was added to the remaining blood products and centrifuged again at 1000 rpm for 6 minutes at room temperature to obtain further PRP.
- After centrifugation, the PRP was removed and mixed together with the PRP obtained earlier.
- The PRP solution was topped up to 1ml with modified Tyrode's solution. 10µg/ml of prostaglandin I_2 (PGI_2) was added to the PRP solution in order to inhibit platelet aggregation.
- The PRP solution was centrifuged immediately at 2750 rpm for 6 minutes at room temperature.
- After centrifugation, the supernatant was discarded (if more platelets were required, the supernatant obtained was centrifuged again as prior).
- The pellet obtained is resuspended in 500µl of 5µM CFDA-SE (diluted in PBS) solution and incubated at room temperature for 20 minutes.
- At the same time, 5µl of the resuspended platelets is taken for counting which is used to determine the dilution factor at the end of the protocol.
- After incubating the platelets for 20 minutes, the solution was topped up to 1ml with modified Tyrode's solution. 10µg/ml of PGI_2 was added again to the solution.

- The solution was immediately centrifuged at 2750 rpm for 6 minutes at room temperature.
- The supernatant was discarded and the pellet was resuspended in PBS at the dilution required.

For intravital experiments utilising donor platelets, 100µl of 1 x 10^8 cells were injected intra-arterially 5 minutes prior to reperfusion to allow for the cells to readily circulate in the blood stream prior to imaging.

2.4 *In Vivo* Studies – Murine Myocardial IR Injury

2.4.1 Pre-surgery Preparation

All equipment to be used during surgical procedures was sterilised either by autoclaving (i.e. surgical instruments) or by disinfecting workbench equipment (i.e. microscope, downdraft surgical table etc.) using chlorhexidine. An induction dose of a ketamine hydrochloride (100mg/kg) and medetomidine hydrochloride (100mg/kg) was delivered to the mouse via intraperitoneal administration in order to anaesthetise the mouse. Maintenance anaesthesia was subsequently delivered via gaseous isoflurane (2%) in 98.5% medical oxygen at a rate of 0.3 litres/minute. Prior to surgery, hair over the neck and left thoracic regions of the mouse was removed using hair removal cream (VEET). Once exposed, the underlying skin was disinfected using chlorhexidine. The mouse was then placed on a surgical board, which contained a heating pad linked to a temperature monitor ***(Figure 2.1A)***.

2.4.2 Inducing Murine Myocardial IR Injury

The anaesthetised mouse was artificially ventilated using a small rodent ventilator (Minivent, Biochrom Ltd., Harvard Apparatus) which allowed the user to control respiratory stroke volume and rate. To connect the ventilator to the mouse, an incision was performed at the neck region to expose the trachea. The anterior aspect of a tracheal cartilage was cut to expose the inner side of the trachea. A respiratory tube that was attached to the ventilator was passed into the trachea towards the lungs, allowing the ventilator to control lung function. A knot made with a 5-0 suture was used to ensure the connecting tube remained within the trachea. The mouse was then ventilated with medical oxygen via the small rodent ventilator at a stroke volume of 220µl and a respiratory rate of 130 breaths per minute.

Once artificial ventilation had been achieved, the left carotid artery was then exposed. After the vagus nerve was separated from the artery, a 5-0 suture was placed at the end closest to the head and tied off. The other end of the artery was clamped using a mini arterial clamp. A small incision was made in the artery in between the clamp and suture. A cannula, which was attached to a 1ml syringe and filled with PBS, was then passed into the artery and securely tied in place. The mini arterial clamp was then removed. This intra-arterial cannula allowed for the injection of fluids or cells into the mouse as and when required.

Once the intra-arterial cannula had been placed, an incision was made in the left thoracic region to expose the left pectoral muscles covering the left ribcage and chest wall. The pectoral muscles in this region were removed using a cautery pen in order to gain access to the 3rd and 4th chest ribs. A further incision was made between the 3rd and 4th ribs to expose the underlying heart and kept open using a retractor. The surrounding pericardial sac was then

removed from the heart. The left anterior descending (LAD) coronary artery was located and an 8-0 suture was passed gently through the muscle underneath it. The LAD was then tied off using the suture against a small piece of plastic tubing protecting the heart from direct damage from the suture ***(Figure 2.1B)***. This induced ischaemia to downstream regions of the heart supplied by the LAD. The ischaemia period was allowed to persist for 45 minutes after which the ligation was removed to begin reperfusion. The reperfusion period was allowed to persist for 2 hours and then mice were culled via an appropriate Schedule 1 method. Tissue harvesting was conducted on organs of interest (e.g. heart, lungs, liver etc.) to be utilised in experiments detailed later. Sham mice underwent the same surgery as the IR injured mice except the LAD ligation was not applied. In myocardial IR injured mice treated with HSCs, 2 x 10^6 HPC-7s were injected intra-arterially within 5 minutes of reperfusion. When the homing and trafficking capabilities of HPC-7s were investigated using IVM, the HPC-7s were injected intra-arterially during the first imaging timepoint. This was done in order to allow for assessment of the initial pass of the HPC-7s through the heart.

2.4.3 Laser Speckle Contrast Imaging (LSCI)

Imaging the perfusion of the heart was performed using a moorFLPI-2 laser speckle contrast imager (Moor Instruments; UK) on exposed mice hearts ***(Figure 2.2A)***. Surgery was conducted as described in **section 2.4.2**. At certain periods of time, a laser speckle contrast video was obtained during the surgical process. 1000 frames (~40-second videos) were obtained during pre-ischaemia, ischaemia and immediately following reperfusion. 40-second videos were then taken every 15 minutes for 120 minutes.

2.5 Intravital Microscopy Based Studies

Intravital microscopy (IVM) experiments formed the foundation of this thesis and was integral to investigating the beneficial role that HPC-7s could play in alleviating the microcirculatory disturbances induced by myocardial IR injury. Intravital imaging of the coronary microcirculation was performed using a Nipkow spinning disk confocal head (Yokogawa CSU, Japan) attached to an upright Olympus BX61WI microscope with an Evolve EMCCD camera (Photometrics, USA) and a 10x objective (Olympus; Japan) ***(Figure 2.2B)***. This provided capture of images at 100x magnification which allowed for visualisation of adherent and free flowing cells, but was not strong enough to accurately delineate cells that are rolling (via velocity measurements) due to a limited resolution. Listed below are a number of novel in-house designed procedures performed in order to conduct intravital imaging.

2.5.1 Murine Myocardial IR Injury

Murine myocardial IR injury was performed as described in **section 2.4.2**. Within 5 minutes of reperfusion being initiated, a 3D printed stabiliser was carefully mounted, using a micro-manipulator, onto a region of the beating left ventricle downstream from the site of LAD ligation (area at risk of infarction). The same region was identified in sham hearts. It was permanently fixed to the heart using a thin layer of clinical grade Vetbond biological glue applied to its underside ***(Figure 2.3A-C)***. The 3D printed stabiliser was a small ring-shaped structure, designed and 3D printed in-house, which allowed for imaging to be conducted through a window in its centre. It had internal and external diameters of 2.25mm and 4mm respectively. This allowed a small region of the left ventricle to be stabilised and have

sufficiently reduced motion such that high-quality imaging of the epicardial coronary microvasculature could be obtained. Importantly, the rest of heart continued to beat normally. The stabiliser was a modified version of one previously described by Lee and colleagues [177]. The central area was kept moist by application of 0.9% saline with the surrounding area covered with saran wrap to prevent loss of moisture. As it took ~20-30 minutes before the beating heart was ready for imaging, the first recording lasting 2 minutes took place from a pre-selected field of view at 30 minutes post-reperfusion. This also allowed for consistency between experiments. 2-minute videos were subsequently taken every 15 minutes from the same area for 120 minutes. All data was captured, stored and analysed using Slidebook 6 software (Intelligent Imaging Innovations, USA). Once the intravital experiment was complete, tissue harvesting was conducted on organs of interest (heart etc.) to be utilised in experiments detailed later.

The 3D printed stabiliser mentioned here and used throughout experiments was created using Tinkercad (Autodesk, USA) 3D printing software and printed using a MakerBot (Stratasys, USA) 3D printer. Modifications to the stabiliser were made using Tinkercad until a suitable version was obtained. A 1.75mm bioplastic polylactic acid filament was fitted to the MakerBot 3D printer and this material was used to print our 3D stabiliser ***(Figure 2.3B)***. Briefly, a nozzle/extruder in the MakerBot 3D printer melts the filament at 220^{o}C and prints the bottom-most layer of the object. Once that first layer quickly becomes dry, the next layer is printed. This continues until the object is fully printed.

2.5.1.1 Fluorescent Labelling for IVM studies

Several different parameters were imaged *in vivo* in the beating mouse heart during IVM experiments. This required fluorescent labelling of either endogenous targets of interest or labelling of exogenous cells that were introduced into the experimental mouse. In addition to existing expertise within the Kalia lab, a number of additional resources were used in identifying reliable labelling techniques [178-180]. Endogenous targets of interest included platelets, neutrophils, monocytes, macrophages and endothelial cells. Platelets, neutrophils, macrophages and endothelial cells were all labelled using antibodies against specific cell surface markers. 20µl of a specific cell surface antibody (ab) was added to 80µl of PBS and injected intra-arterially 5 minutes prior to the initiation of reperfusion in IR injury experiments.

Endogenous platelets were fluorescently labelled with APC-conjugated rat anti-mouse CD41 antibody. Endogenous neutrophils were labelled with PE-conjugated or APC-conjugated rat anti-mouse Gr-1 (Ly6G) antibody. Endogenous macrophages were labelled with APC-conjugated rat anti-mouse F4/80 antibody. Endothelial cells were labelled *in vivo* with PE-conjugated rat anti-mouse CD31 antibody. For monocytes, we employed a method described by Haka and colleagues which labelled endogenous monocytes with non-degradable fluorescent latex beads to intravitally image them in mouse models of atherosclerosis *in vivo* [179]. 100µl of 1µm diameter Fluoresbrite® FITC-dyed Yellow-Green Microspheres (4.55×10^{10} particles/ml; excitation: 441nm; emission: 486 nm) were injected intra-arterially at a concentration of 1.15×10^{10} particles/ml 10 minutes prior to ischaemia in IR injury experiments. The premise behind this method was that circulating monocytes would become labelled after phagocytic uptake of the latex beads.

A

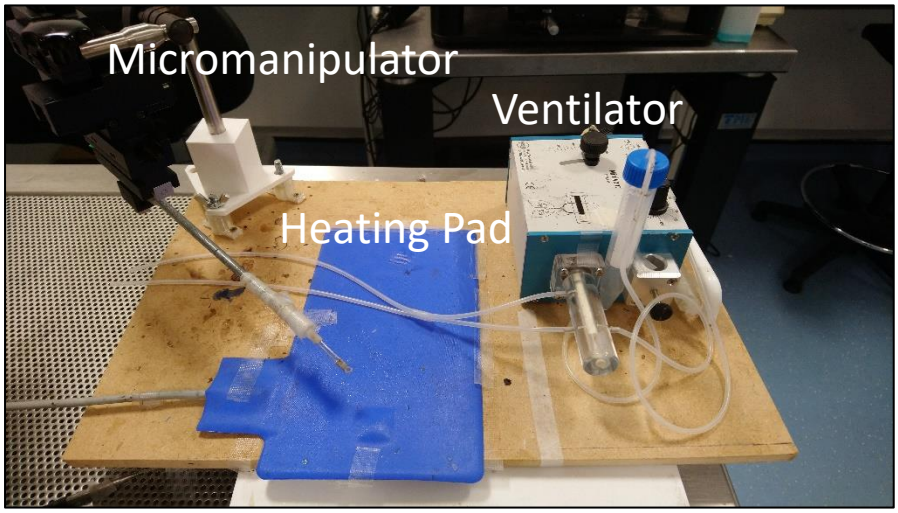

B

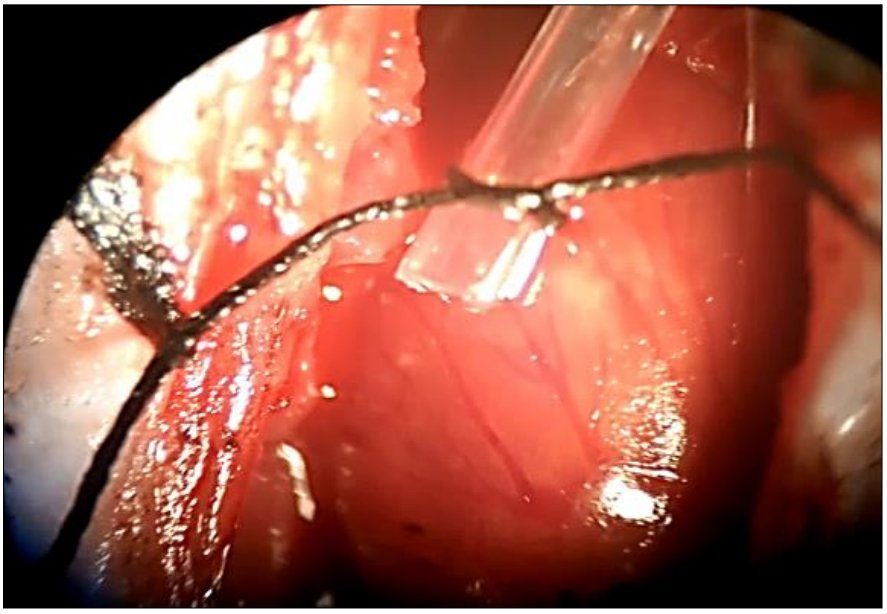

Figure 2.1: (A) Specialised surgical board. *In order to perform open heart surgery on mice and also aid the easy transfer of the prepared mouse to the microscope stage, an in-house surgical board was created.* ***(B) To induce ischaemia in the beating mouse heart, a suture ligature was placed around the LAD artery and tied in place.*** *To avoid damage to the heart muscle or the coronary artery, a piece of plastic tubing was used against which the suture is tied.*

A

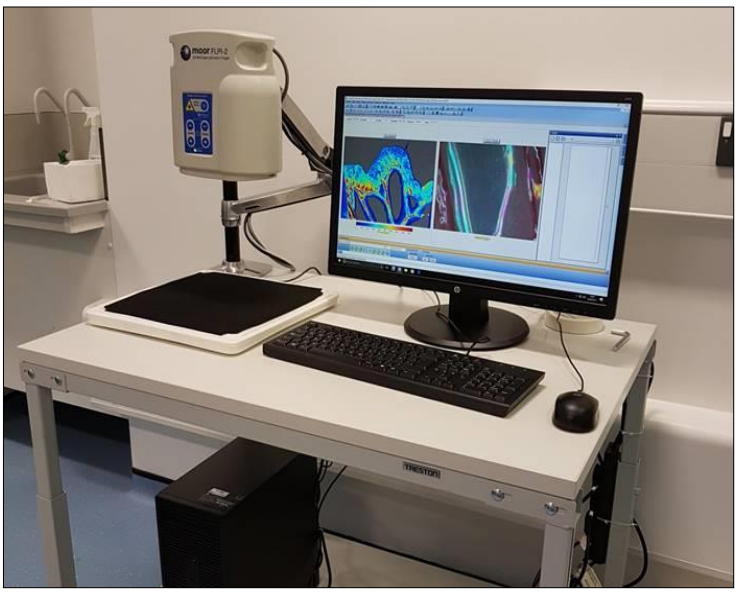

B

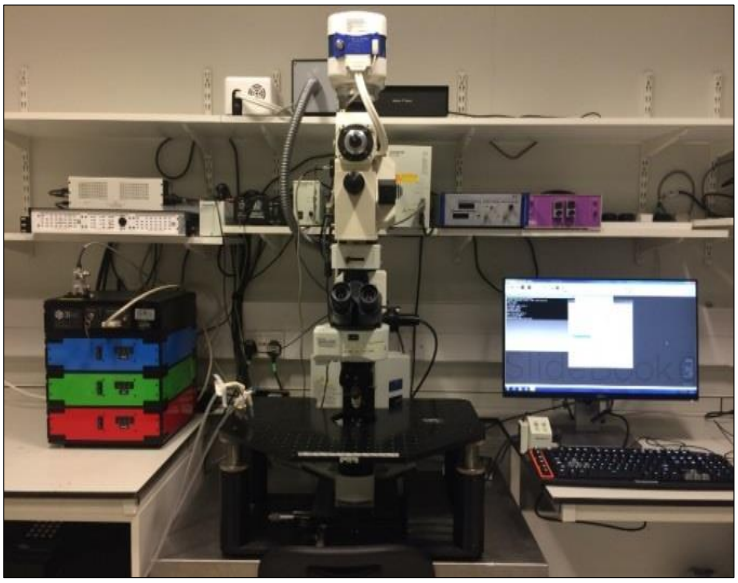

Figure 2.2: (A) Laser speckle contrast imager. *Left ventricular perfusion was imaged using a moorFLPI-2 laser speckle contract imager.* ***(B) Nipkow Spinning-disk confocal-based intravital microscope.*** *Intravital microscopy was carried out using an Olympus microscope with confocal capabilities. A spinning Nipkow disk confocal head attached to the microscope allowed real-time comnfocal imaging to be aquired. The green/blue/red laser stack allowed more than one fluorescent dye to be imaged in the same mouse heart simultaneously thus allowing more than one cell type to be imaged. This allowed for a thorough investigation of the cardiac microcirculation in a mouse.*

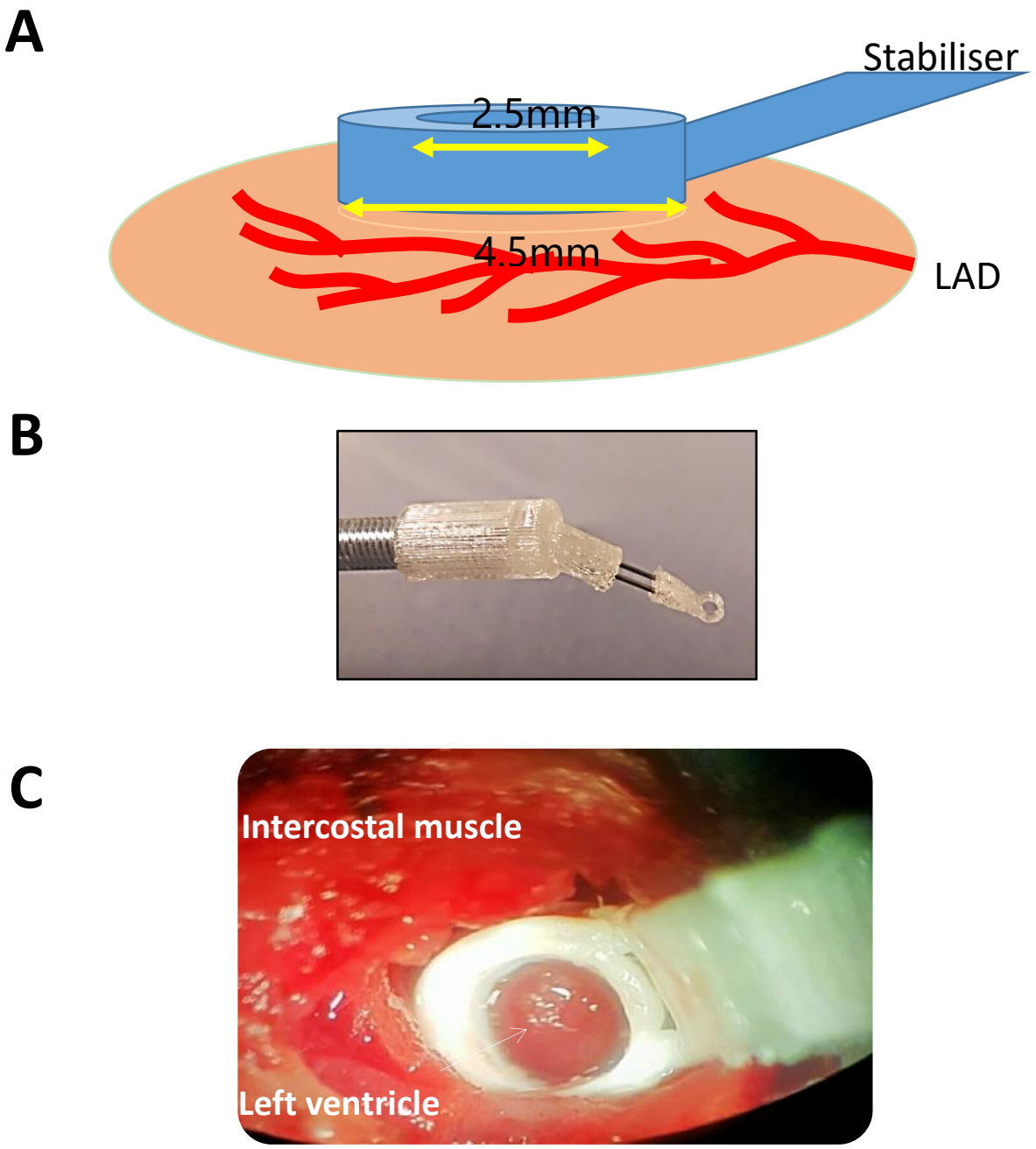

Figure 2.3: (A) Cartoon mock-up of a 3D printed stabiliser attached to a mouse heart. *An in-house designed 3D printed stabiliser was vet-bonded to the beating left ventricle of the anaesthetised mouse allowing Spinning Nipkow confocal based intravital imaging in its centre. In LAD ligated and reperfused hearts, the stabiliser was attached downstream of the ligated site allowing for imaging of the region at risk. The stabiliser carefully approached the exposed heart with the aid of a precision micromanipulator. The internal and external diameter of the stabiliser were 2.25mm and 4mm respectively and so only a small surface of the heart had its motion reduced or stabilised sufficiently enough to permit imaging. The central region was kept moist by topical application of warmed saline.* ***(B) Photo of the 3D printed stabiliser.*** *In order to provide stability, the 3D printed stabiliser was attached to a metal arm that connected it to a micro-manipulator.* ***(C) Stabiliser vet-bonded to a beating left ventricle.*** *Once attached to the heart, a stable region of the left ventricle is obtained, allowing for high-resolution imaging.*

Exogenous cells were also prepared and labelled prior to systemic injection in some IVM experiments. Considering the sheer numbers of endogenous platelets, labelling all of them made it difficult to subsequently quantitate singular platelet events. Therefore, in some experiments, $1x10^8$ CFSE-labelled donor mouse platelets were injected intra-arterially into the experimental mouse within 5 minutes of reperfusion in IR injury experiments. This resulted in a labelled fraction in the recipient mouse of ~5% of all circulating platelets, a value low enough to allow individual platelets to be imaged. Donor platelets were isolated and labelled with CFSE as per **section 2.3.4.3**. For experiments investigating the homing capabilities of HSCs, 2 x 10^6 HPC-7s – cultured and labelled as per **section 2.3.4.1** – were injected intra-arterially during the first imaging session at 30 minutes post reperfusion. This was done in order to image the first instance of HPC-7s trafficking through the cardiac microcirculation, before the cells completed their first pass through the systemic circulation.

In some experiments, the microcirculation was interrogated using FITC-conjugated bovine serum albumin (FITC-BSA). When introduced systemically, it is retained within the vasculature, thereby facilitating easy visualisation of the vasculature and confirming the presence of blood flow [181]. 200µl of FITC-BSA was injected into the mouse intra-arterially at the end of certain intravital experiments to ascertain functional capillary density.

2.5.2 Murine Cardiac Thermal Ablation Injury

Preliminary experiments were conducted to investigate the efficacy of labelling endogenous monocytes using fluorescent latex microbeads and whether this method impacted on the recruitment capabilities of monocytes. Thermal ablation injury has been utilised by

researchers to determine the inflammatory response in other organs, such as the liver, during IVM experiments to good effect [182]. In order to test this out this novel technique, surgery was performed similar to **section 2.4.2** up until the mouse heart was exposed and the pericardial sac removed. Thereafter, a 3D printed stabiliser was immediately attached to the heart. An initial 2-minute video was obtained as a control or pre-ablation assessment. Once completed, a cautery pen was used to make a micro-ablation on the surface of the heart within the region stabilised (i.e. within the central window of the stabiliser). Another 2-minute video was captured immediately following successful ablation injury. This was repeated every 20 minutes for 120 minutes.

With regards to fluorescent labelling in this set of experiments, only endogenous neutrophils and monocytes were targets of interest. These were labelled as described in **section 2.5.1.1**. Delivery of antibodies or fluorescent microbeads was conducted 10 minutes prior to the first imaging time point.

2.5.3 Murine Cardiac Topical Injury

Some IVM experiments in this thesis aimed to understand the real-time effects of pro-inflammatory cytokines, specifically IL-36 isoforms, upon the cardiac microcirculation when the cytokines were directly applied onto the heart surface. In order to achieve this novel technique, surgery was performed as described in **section 2.5.2**. Once the 3D printed stabiliser was attached to the heart, 3µl of PBS was added within the central region of the 3D printed stabiliser and left for 20 minutes. Since the stabiliser was essentially a ring with some height, it was able to contain the solution within its centre. As the 3D printed stabiliser was glued

onto the heart surface, a water impermeable seal was created, allowing for the topical application of fluid for an extended period of time. After 20 minutes, the PBS was carefully removed using a paper towel and a 2-minute intravital video was captured. This was assigned as a vehicle control or pre-stimulation assessment. Once completed, 3µl of the IL-36 cytokine of interest (α, β or γ; 100ng/ml) was added onto the stabilised region instead and again left for 20 minutes. Thereafter, the IL-36 solution was carefully removed and a 2-minute video was again captured. This was repeated every 20 minutes for 120 minutes.

With regards to fluorescent labelling in this set of experiments, only endogenous neutrophils, monocytes and endothelial cells were targets of interest. These were labelled as described in **section 2.5.1.1**. Delivery of antibodies or fluorescent microbeads was conducted 10 minutes prior to PBS treatment.

2.5.4 Analysis of IVM and Laser Speckle Contrast Images

2.5.4.1 Analysis of IVM images

Once IVM experiments were completed, videos and images obtained were analysed using SlideBook 6.0 analysis software. The number of free-flowing neutrophils, monocytes or HPC-7s that trafficked through the field of view without adhering was manually counted. Neutrophil, donor platelet and stem cell adhesion were quantitated by manual counting of cells that remained stationary for $\geq$30 seconds during the 2-minute recording period at a given time point. This data was collected for each time point of the experiment. Free-flowing neutrophils and platelets were identified as those that passed through the coronary microcirculation in the field of view without making adhesive interactions. The trafficking of

donor platelets was measured using manual counting similar to analysis of neutrophils. However, the number of donor platelets that could be visualised circulating through the field of view was much higher than endogenous neutrophil counts. Due to this high volume, trafficking was determined by analysing free flowing donor platelets in one quadrant of the overall field of view for 1 minute only.

Labelling of endogenous platelets allowed platelet aggregates/microthrombi to be quantitated using ImageJ (NIH; USA) software. A mask was placed around CD41 positive areas and integrated fluorescence density, which took into account area size and flourescence intensity, was calculated. Briefly, images were loaded into the software and areas of absent or low intensity colour (background fluorescence) were eliminated from analysis through a threshold modifier. The area size and the mean value of the remaining high intensity colour was multiplied to form a standard value that could be compared between experimental groups (Area of Fluorescence Intensity * Mean Fluorescence Intensity = Mean Integrated Fluorescence Intensity). This method was reliable at detecting and quantitating the aggregates of endogenous platelets that developed in IR injured hearts.

2.5.4.2 Analysis of Laser Speckle images

Once LSCI experiments were completed, videos and images obtained were analysed using manufacturer supplied imaging software mFLPI-2Measure V2.0 and mFLPIReview V5.0 (Moor Instruments; UK). An area downstream of the LAD ligation site was demarcated during image capture and flux data was obtained at 25Hz using spatial processing (sliding window, time constant: 0.1s). In-house developed software – *Basic Speckle Analysis* (SpAn) – was used to

collate flux values during diastole over the whole imaging period. More detail on the method of analysis is described later in Chapter 4.

2.6 *In Vitro* Studies – Assessment of Myocardial IR Injury

2.6.1 Frozen Tissue Sections

Following sham surgery or myocardial IR injury, with or without HPC-7s therapy, the heart was removed and snap frozen in liquid nitrogen and stored at -80^{o}C until ready for use. To perform Stamper-Woodruff or static tissue adhesion assays or immunohistochemistry (IHC) assays, frozen heart tissues were embedded in optimal cutting temperature (OCT) compound and 10µm sections were cut from the left ventricle incorporating the area of injury utilising a cryostat machine. An initial 50µm section of the heart was removed prior to collection of the first suitable section. These sections were then mounted onto adhesive coated microscope slides. Due to the relatively small sizes of the sections, two sections were mounted onto one microscope slide. The sections were then allowed to air dry for 10 minutes before being fixed in 100% Acetone for another 10 minutes. Once fixed, the sections were allowed to air dry again for 10 minutes. After this period was completed, the microscope slides were wrapped in research-grade aluminium foil and stored at -20^{o}C until they were required for experiments.

2.6.1.1 Static Tissue Adhesion Assay

Static tissue adhesion assays based on the Stamper Woodruff protocol were conducted to examine *in vitro* the cell adhesion capabilities of the HPC-7s, BM MSCs and WJ MSCs to snap

frozen tissue sections of IR injured and sham murine hearts. Details of the protocol used was as follows [151]:

- Snap frozen heart tissue sections on microscope slides were brought to room temperature.
- Wax was used to encircle the sections using a wax pen.
- For experiments using stained HPC-7s (as per **section 2.3.4.1**), 1 x 10^5 cells / 100µl culture media was carefully placed on each tissue section. For experiments using stained BM MSCs and WJ MSCs (as per **section 2.3.4.2**), 5 x 10^4 cells / 100µl culture media (respectively) was carefully placed on each tissue section.
- The slides were loosely covered with foil to avoid light interference and allowed to incubate at room temperature for 30 minutes.
- After 30 minutes, the slides were submerged in PBS to wash away non-adherent cells and the culture media.
- The slides were then fixed in 100% Acetone for 5 minutes and then submerged in PBS to remove excess acetone.
- Once dry, the tissue sections were mounted with a non-fluorescing aqueous medium (Hydromount) and covered with an appropriate coverslip.
- The slides were then be imaged straight away or stored at 4^{o}C until imaging was required.

2.6.1.2 Immunohistochemistry (IHC) Assay

IHC assays were conducted to examine the expression of certain markers for cellular stress/trauma on frozen tissue sections. 8-hydroxy-2'-deoxyguanosine (8-OHdG) is a marker of oxidative DNA damage, used to confirm the extent of injury produced specifically by ROS. During IR injury the production of free radicals such as $O_2^{\cdot -}$ and $OH^{\cdot}$ can attack the DNA and lead to the production of modified DNA bases. More than 20 different oxidation products of DNA have been characterized including 8-OHdG, a major oxidation product of guanine. 8-OHdG is a sensitive and stable marker of oxidative damage in cellular DNA and its corresponding antibody anti-8-OHdG makes it very suitable for co-locating DNA damage with oxidative stress. The antibodies anti-8-OHdG and anti-VCAM-1 were used to examine cellular oxidative damage and cellular upregulation of adhesion molecules respectively. Details of the protocol used for IHC assays was as follows [151]:

- Snap frozen heart tissue sections on microscope slides were brought to room temperature.
- Wax was used to encircle the sections using a wax pen.
- 100µl of a blocking agent was carefully applied to the tissue sections and left to incubate for 30 minutes at room temperature to block non-specific binding of immunoglobulins to Fc receptors. The blocking agent used in this experiment was the anti-CD16/CD32 antibody diluted to a ratio of 1:500.
- After 30 minutes, the slides were washed in PBS.

- The primary antibody for either unconjugated anti-8-OHdG or AF647-conjugated anti-VCAM-1 was diluted to a ratio of 1:200. 100µl of the corresponding solution was carefully added to the tissue sections.
- The slides were loosely covered with foil to avoid light interference and allowed to incubate at room temperature for 1 hour.
- As the anti-8-OHdG antibody was unconjugated, after incubating with the primary anti-8-OHdG antibody, the slides were washed in PBS. The secondary antibody for anti-8-OHdG, AF647-conjugated donkey anti-goat IgG antibody was diluted to a ratio of 1:200. 100µl of the corresponding solution was carefully added to the tissue sections. The slides were loosely covered again with foil to avoid light interference and allowed to incubate at room temperature for 1 hour.
- After all antibody staining steps were completed, the slides were washed in PBS.
- The protocol then mirrors **section 2.6.1.1** from when slides were then fixed in 100% Acetone.

Some frozen tissue sections would already have contained within them cells pre-labelled with antibodies delivered during surgery as mentioned in **section 2.5.1.1**. This allowed further quantification of specific cells and their presence within the heart without the need to perform any additional staining procedures. In such cases, frozen tissue sections on microscope slides would be directly imaged after bringing them to room temperature, mounting the tissue using Hydromount and covering the slides with the appropriate coverslips.

2.6.1.3 Stem Cell-Injury Antibody Correlation Assay

Correlation analyses experiments were performed to investigate the correlation between stem cell adhesion and antibody expression on snap frozen heart tissue sections. These allowed us to determine whether the extent of stem cell adhesion was directly proportional to the degree of oxidative stress or adhesion molecule expression on hearts regardless of whether the hearts had undergone IR injury or were sham counterparts. The protocol for this experiment involved initially conducting the IHC antibody staining procedure, for both anti-8-OHdG or anti-VCAM-1 antibodies, as described in **section 2.5.2** followed by the Stamper Woodruff static adhesion protocol as described in **section 2.5.1**. The one consideration that was taken into account was that the tissue sections were fixed in 100% Acetone only when both protocols were completed. As such, the Stamper Woodruff static adhesion protocol was carried out straight away after the primary, for anti-VCAM-1, or secondary, for anti-8-OHdG, antibody staining had been washed with PBS.

2.6.1.4 Analysis of Frozen Tissue Sections

Once the protocols described in **section 2.6.1** were completed, the tissue sections were ready for imaging. Imaging was carried out utilising an EVOS Fluorescent Cell Imaging System microscope (Thermo Fisher Scientific) with a 20x objective lens (Olympus). Five regions per tissue section were imaged for analytical purposes. The central field of view was imaged and then 4 additional regions above, below and to the left and right of this field were also imaged. This allowed for the avoidance of bias ***(Figure 2.4)***. If a region was too damaged or had

excessive dead space, slight adjustments to the selected region were made to allow for better image quality. If this was not possible, that particular region was not included in analysis.

IHC image analysis was performed using ImageJ software, similar to **section 2.5.4.1**.

2.6.2 Plasma Cytokine Measurements

At the end of surgical experiments, blood was harvested through the inferior vena cava from mice that had undergone sham, myocardial IR injury or myocardial IR injury + HPC-7 cell therapy surgeries. As described in **section 2.3.4.3**, around 500µl of blood was collected via a 1ml syringe attached to a 25G needle pre-washed with 100U heparin. The blood was then transferred to a sterile Eppendorf pre-loaded with 50µl of 100U heparin. Plasma was isolated from the blood by centrifugation at 2000 rpm for 10 minutes at room temperature. The plasma was then collected into a new sterile Eppendorf and stored at -80^{o}C until required.

Measurement of circulating cytokines was conducted using Bio-Plex pro mouse cytokine 23-plex assay plate (Bio-Rad Laboratories; USA) and analysed using a Luminex 200 plate reader (Bio-Rad Laboratories; USA). Samples were loaded in triplicates and the protocol supplied by the manufacturer for mouse cytokine assay preparation and analysis was followed for accurate measurements.

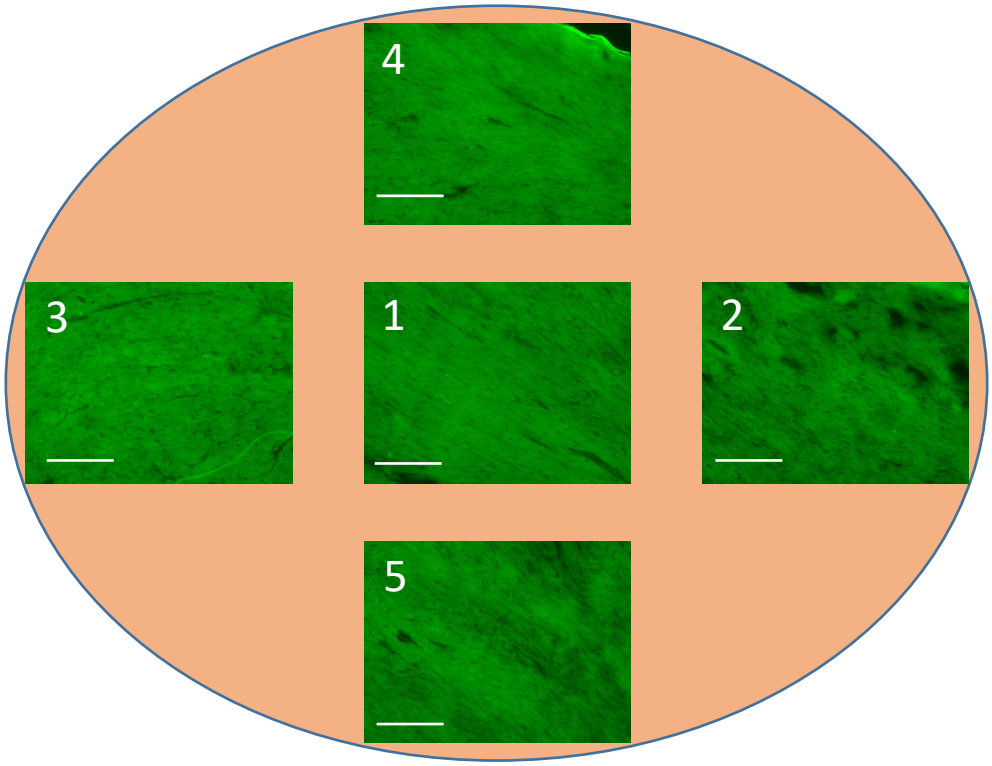

Figure 2.4: Regions of the heart sections imaged for quantitative and qualitative analysis of cell adhesion, oxidative stress or inflammatory adhesion molecule expression. *The central most field of view was imaged and then 4 additional regions above, below and to the left and right of this field were also imaged. Images were taken using the EVOS fluorescent microscope as specified here using a 20x objective. Scale = 100µm.*

2.6.3 Triphenyl Tetrazolium Chloride (TTC) Staining

In order to determine the impact of myocardial IR injury and the potential therapeutic benefits of stem cell therapy on infarct size, TTC staining was conducted on hearts from mice that had undergone either IR injury or IR injury + HPC-7 therapy. This allowed for the determination of final infarct size due to IR injury. Details for the protocol used were as follows [183]:

- Surgery was performed as previously described in **section 2.4**, however reperfusion was allowed to persist for 4 hours. A longer period of reperfusion was necessary in order for NADH to be washed out from the infarct zone for proper delineation of injury.
- After 4 hours of reperfusion had passed, the LAD was re-occluded and 500-800µl of 0.5% Evans Blue dye was injected intra-arterially. This provides a clear demarcation of regions of the heart affected by the IR injury, known as the area at risk (AAR).
- The mouse was then culled using appropriate Schedule 1 techniques and the heart harvested and wrapped in saran film. The heart was then placed in a -20^{o}C freezer for an hour.
- While the heart was freezing down, 20ml of 1% TTC solution was prepared by adding 2,3,5-Triphenyltetrazolium chloride to a phosphate buffer consisting of 77% sodium phosphate dibasic (0.1M) and 23% sodium phosphate monobasic (0.1M). pH was measured at 7.4 and the solution was pre-heated at 37^{o}C before use.
- Once an hour had passed, the frozen heart was removed from the freezer and cut into transverse slices ~2mm in depth.
- The heart slices were then incubated in the 1% TTC solution at 37^{o}C for 20 minutes with continuous agitation.

- After 20 minutes, the heart slices were removed from the 1% TTC solution and fixed in 10% formalin for 20 minutes at room temperature.
- After 20 minutes, the heart slices were then washed in PBS.
- After washing, the heart slices were lightly dried and placed onto a petri dish for imaging under a surgical microscope (Leica Microsystems; Germany). In order to ensure consistent imaging thickness of the heart slices across experiments, a 500g weight was placed on top of the petri dish without restricting the imaging field.

Analysis of images obtained from TTC experiments were carried out using ImageJ. An IR injured heart stained with Evans Blue and TTC will have 3 demarcated regions. The region that is not affected at all by the IR injury will be stained blue. The remaining regions not stained blue are known as the area at risk (AAR). The region affected by the IR injury but with viable myocardium will be stained red. Lastly, the region affected by the IR injury and necrotic will be unstained/white [183]. In ImageJ, the area of these regions was calculated and infarct size was determined by calculating the necrotic area as a percentage of the AAR.

2.7 *In Vitro* Studies – Endothelial-Stem Cell Co-Culture

Further *in vitro* experiments were conducted to investigate the effects of co-culturing SCs with ECs and their ability to reduce oxidative injury induced by hydrogen peroxide (H_2O_2; Sigma).

2.7.1 Endothelial-Stem Cell Co-Culture Assay Setup

In these experiments, 5 x 10^4 stem cells were directly co-cultured with a confluent monolayer of ECs in a 24-well plate while simultaneously being injured with 10µM H_2O_2 [50, 184]. Details of the protocol used for these experiments were as follows:

- Immortomouse vena cava ECs (VCEC) were plated onto a 24-well plate with 1ml EC expansion media as described in **section 2.3.1** and left to grow at 33.5^{o}C in a humidified, 5% CO_2 controlled incubator.
- Once confluent, culture media of the ECs was exchanged from EC expansion media to EC experimental media, as described in **section 2.3.1**, and left for 24 hours at 37^{o}C in a humidified, 5% CO_2 controlled incubator.
- After 24 hours, the culture media was removed from all wells and the wells were washed 3x with PBS.
- After washing, 1ml of fresh EC experimental media was carefully placed in the control wells, where no stem cells are added. For the wells which housed stem cells, 5 x 10^4 stem cells (either HPC-7s, BM MSCs or WJ MSCs) were added to 1ml of fresh EC experimental media and together carefully placed in the experiment wells.
- 110µl of 100µM H_2O_2 was added to all wells to form a final concentration of 10µM H_2O_2.
- The last three steps were repeated every 24 hours for experiments that lasted 72 hours.
- After either 24 hours or 72 hours had lapsed, depending on experiment duration, fluorescent staining was carried out.

2.7.2 Reactive Oxygen Species (Superoxide; $O_2^{\bullet-}$) Staining Protocol using Dihydroethidium

After following the protocol described in **section 2.7.1**, fluorescent staining of the ECs was undertaken to investigate the presence of superoxide ($O_2^{\bullet-}$). The fluorescent dye chosen for this staining was Dihydroethidium (DHE). DHE is a fluorescent probe widely used for specifically detecting the presence of intracellular $O_2^{\bullet-}$ by fluorescence microscopy. The product formed when DHE interacts with $O_2^{\bullet-}$ is a very specific product called 2-hydroxyethidium (2-OH-E^+). With oxidation, 2-OH-E^+ intercalates with DNA, staining the nucleus a bright fluorescent red. Other ROS and RNS do not oxidise DHE to 2-OH-E^+ and so it is considered to be highly specific for detecting superoxide radicals. Details of the protocol used for this experiment were as follows:

- Once the protocol as describe in **section 2.7.1** was completed, culture media was removed from all wells and the wells washed with PBS thoroughly.
- Once washed, 500µl of 10µM DHE solution (diluted in dimethyl sulphoxide (DMSO)) was added to each well carefully. The cells were left to incubate with DHE for 10 minutes in a 37^{o}C, humidified and 5% CO_2 controlled incubator.
- After 10 minutes, the DHE solution was removed and the wells washed with PBS thoroughly.
- Once washed, 500µl of PBS was added to all wells. The cells were now ready for imaging.

2.7.3 Oxidative Damage Staining Protocol (Anti-8-OHdG)

In this study, the ability of stem cells to protect injured ECs through reduction of oxidative damage was assessed. As such, after following the protocol described in **section 2.7.1**, fluorescent antibody staining utilising anti-8-OHdG was undertaken to investigate levels of oxidative damage in ECs. Details of the protocol used for this experiment were as follows:

- Once the protocol as describe in **section 2.7.1** was completed, culture media was removed from all wells and the wells washed with PBS thoroughly.
- Once washed, the cells were fixed and permeabilised using 300µl of cold 70% ethanol. The cells were left to incubate with ethanol for 1 hour in a -20^{o}C freezer.
- After fixing the cells for 1 hour, the ethanol was removed and the cells washed with PBS thoroughly.
- 300µl of a blocking agent was added to each well and left to incubate for 30 minutes at room temperature. The blocking agent used in this experiment was the anti-CD16/CD32 antibody diluted to a ratio of 1:500.
- After 30 minutes, the blocking agent solution was removed and the cells washed with PBS thoroughly.
- The primary antibody, goat anti-mouse 8-OHdG, was diluted to a ratio of 1:500. 300µl of the corresponding solution was carefully added to the cells.
- The plate housing the cells was loosely covered with foil to avoid light interference and allowed to incubate at room temperature for 1 hour.
- After 1 hour, the cells were washed with PBS thoroughly.

- The secondary antibody, AF647-conjugated donkey anti-goat IgG, was diluted to a ratio of 1:250. 300µl of the corresponding solution was carefully added to the cells. The plate housing the cells was loosely covered again with foil to avoid light interference and allowed to incubate at room temperature for 1 hour.
- After 1 hour, the cells were washed with PBS thoroughly. Once washed, 500µl of PBS was added to all wells. The cells were now ready for imaging.

2.7.4 Analysis of Endothelial-Stem Cell Co-Culture Assays

Once the protocols described in **2.7.1**, **2.7.2** and **2.7.3** were completed, the cells were ready for imaging. In this study, imaging was carried out utilising an EVOS Fluorescent Cell Imaging System microscope with a 20x objective lens. Three regions per well were imaged for analytical purposes. The regions chosen for imaging were selected in a manner similar to that shown in ***(Figure 2.1B)***, without regions 4 and 5.

Image analysis was performed using ImageJ software, similar to **section 2.5.4.1**.

2.8 Flow Cytometry Based Studies

2.8.1 Isolation of Cells from Digested Mouse Hearts

For experiments that utilised flow cytometry as a form of analysis, surgery was performed as described in **section 2.4.2** and the mouse heart was removed from the chest cavity and stored in 10ml of cold PBS. In a cell culture hood, the heart and PBS were poured out into a petri dish and excess blood was flushed out by squeezing the heart using forceps. The heart was then

transferred into a new petri dish and manually minced into very small pieces (roughly 1 mm^3) using a scalpel. For enzymatic digestion, 2ml of 0.1% collagenase type-I was added to the minced heart tissue. Once the heart was finely minced in the collagenase solution, the tissue and solution were collected into a 15ml centrifuge tube. The tube was placed into a 37^oC incubator for 45 minutes on a rotator to allow for continuous agitation of the tissue.

After 45 minutes, the tube was removed from the incubator and poured into 10ml of EC experimental media through a 70µm strainer in order to achieve a single cell suspension.

Once the cells were collected, they were centrifuged at 2000 rpm for 10 minutes at room temperature. The supernatant was discarded and the cells resuspended in 10ml of PBS for washing and centrifuged as done previously. After this, the cells were resuspended in 10ml of PBS and a cell count was performed. The cells were now ready for fixation or to be used immediately in flow cytometry (pre-labelled during surgery). For fixation and permeabilisation, the cells were slowly resuspended in cold 70% ethanol. The cells were kept in 70% ethanol at -20^oC for a minimum of 1 hour before staining for cell markers. Where other organs of interest were investigated, such as the lung or liver, the protocol described above was used as well.

2.8.2 Assessing Oxidative Damage Levels in the Murine Heart

These experiments focussed on assessing the level of oxidative damage in coronary ECs and cardiomyocytes after myocardial IR injury. Fluorescent antibodies against markers for these specific cells were utilised and cross-compared with their individual level of oxidative damage in various experimental groups. For these experiments, ECs were labelled with anti-CD31

antibodies whilst cardiomyocytes were labelled with anti-cardiac troponin-T (cTnT) antibodies. Oxidative damage was again determined using the anti-8-OHdG antibody. The protocol conducted in order to perform this experiment was as follows:

- Fixed and permeabilised cells were removed from -20^{o}C.
- Cells were centrifuged for 10 minutes at 2000 rpm at room temperature (standard).
- The supernatant was discarded and cells resuspended in PBS for wash. Cells were centrifuged again.
- The supernatant was discarded and cells resuspended in anti-CD16/CD32 antibody (1:5 dilution) to block non-specific binding of antibodies. Cells were kept on ice and slightly agitated for a minimum of 20 minutes.
- After 20 minutes, cells were centrifuged again.
- The supernatant was discarded and cells resuspended in the desired antibody solution (PE-conjugated anti-CD31 at 1:50, PE-conjugated IgG2a at 1:50, PE-conjugated anti-cTnT at 1:10, PE-conjugated REA Control at 1:10, AF488-conjugated anti-8-OHdG at 1:500, AF488-conjugated IgG at 1:500) as required. Cells were kept on ice and slightly agitated for a minimum of 1 hour away from natural light.
- Samples were centrifuged again.
- The supernatant was discarded and cells washed with PBS again as before.
- The supernatant was discarded and samples resuspended in 300µl of PBS in the appropriate tubes ready for acquisition.

2.8.3 Assessing Upregulation of Adhesion Molecules on ECs after Myocardial IR Injury

These experiments focussed on assessing the presence and upregulation of adhesion molecules on coronary ECs after myocardial IR injury. Fluorescent antibodies against endothelial cells were utilised and the levels of ICAM-1 and VCAM-1 was investigated for various experimental groups. For these experiments, ECs were labelled with anti-CD31 antibodies while ICAM-1 and VCAM-1 were labelled with anti-ICAM-1 antibodies and anti-VCAM-1 antibodies respectively. The protocol conducted in order to perform this experiment was similar to **section 2.8.2** but with the following changes:

- Antibodies used: PE-conjugated anti-CD31 at 1:50, PE-conjugated IgG2a at 1:50, FITC-conjugated anti-ICAM-1 at 1:50, FITC-conjugated IgG2a at 1:50, PECy7-conjugated anti-VCAM-1 at 1:50, PECy7-conjugated IgG2b at 1:50.

2.8.4 Assessing HPC-7 Recruitment to Various Organs during Myocardial IR Injury

These experiments focussed on assessing the homing potential of HPC-7s to the murine heart, lung and liver during cardiac IR injury. HPC-7s were CFSE pre-labelled as described in **section 2.3.4.1**. Once a single cell suspension of cells was obtained as described in **section 2.8.1**, flow cytometry was immediately performed as there was no need to conduct additional cell staining.

2.8.5 Assessing Efficacy of Labelling Circulating Monocytes via Fluorescent Microbeads

These experiments focussed on assessing the efficacy of using fluorescent latex microbeads to label circulating monocytes *in vivo* in various surgical experimental groups. Monocytes were pre-labelled as described in **section 2.5.1.1**. In order to determine labelling efficacy, anti-CD115 antibodies were used as a marker for circulating monocytes using flow cytometry. To achieve this, blood was obtained from mice after surgery as described in **section 2.6.2**. The protocol conducted in order to perform this experiment was similar to **section 2.8.2** but with the following changes:

- Whole fresh blood was incubated in ACK lysing buffer at a 1:10 dilution for 5 minutes at room temperature in order to remove red blood cells prior to initial centrifugation.
- Antibodies used: PECy7-conjugated anti-CD115 at 1:20, PECy7-conjugated IgG2a at 1:20.

2.8.6 Assessing Monocyte Population in the Murine Heart after IR Injury

These experiments focussed on assessing the presence and subsets of monocytes adherent in the heart after IR injury. Monocytes were pre-labelled as described in **section 2.5.1.1**. Anti-CD115 antibodies were also used as an additional co-marker for adherent monocytes. In order to determine polarity of the monocytes, fluorescent antibodies against Ly6C (anti-Ly6C antibodies) were used. Pro-inflammatory murine monocytes express high levels of Ly6C on their surface while anti-inflammatory monocytes express low levels of Ly6C [147]. The protocol conducted in order to perform this experiment was similar to **section 2.8.2** but with the following changes:

- Cells were not fixed/permeabilised prior.
- Antibodies used: PE-conjugated anti-CD115 at 1:20, PE-conjugated IgG2a at 1:20, PECy7-conjugated anti-Ly6C at 1:100, PECy7-conjugated IgG2a at 1:100

2.8.7 Assessment of Whole Blood Counts

These experiments focussed on assessing the cellular make up of blood isolated from the inferior vena cava of mice that had undergone various surgical experiments. Blood was obtained as described in **section 2.6.2**. Without isolating plasma, whole blood was immediately transferred to a haematology analyser, Pentra ES 60 (Horiba; Japan) in order to perform whole blood counts.

2.8.8 Analysis of Flow Cytometry and Whole Blood Counts

Flow cytometry data collection was performed using a FACScalibur (BD Biosciences; USA) flow cytometer. Flow cytometry data analysis was performed using Summit 4.3 software (Beckman Coulter, US). Briefly, data was loaded into the software and relevant gating and compensation strategies were performed in order to generate data that could be compared between the different experimental groups. Collection and analysis of whole blood counts was done by the Pentra ES 60.

2.9 Statistical Analysis

In this study, GraphPad Prism V7.0 software (GraphPad Software Inc; USA) was used to perform statistical analysis of data obtained. Blinding was achieved by randomisation of data obtained during analysis. Once analysis had been completed, data was reorganised into their appropriate experimental groups. Unpaired student's t-tests were performed for direct comparison between two groups of interest. For correlation studies, Pearson's correlation tests were performed. One-way ANOVAs followed by Sidak's post-hoc tests were performed for direct comparisons between three or more groups of interest. For time course studies, two-way ANOVAs followed by Sidak's post-hoc tests were performed. All data is expressed as mean ± standard error of the mean (SEM). Statistical significance was determined when $p<0.05$.

CHAPTER 3:

MICROCIRCULATORY DISTURBANCES IN THE IR INJURED HEART – VASCULOPROTECTIVE EFFECTS OF STEM CELLS AS DETERMINED *IN VITRO*

3.1 Introduction

As coronary heart disease remains a major contributor to mortality and morbidity worldwide, there still exists a need to find new therapeutic options for this disease. One such option is to utilise SCs as a form of cell therapy. SCs provide an interesting therapeutic alternative as they are robust cells, can adapt to the host's requirements and are packed with cytokines/chemokines and enzymes that can modulate the surrounding environment [156]. The question remains as to which SC type to use. Both HSCs and MSCs provide two interesting choices that have been clinically trialled for use in treating heart disease. However, the benefits exerted by these cells have either been poor or transient. The success of SC therapy appears to be dependent on their actual recruitment from the peripheral blood and their subsequent adhesion to the microvessels of the injured organs. Therefore, the degree to which HSCs/MSCs can be recruited to the IR injured heart is an important consideration to make especially as different types of SCs appear to have differing adhesion capabilities. No studies have previously compared the adhesive capabilities of these two different SC types to the IR injured heart. Therefore, this will be assessed in this chapter *in vitro* with the view to taking the more adhesive SC population for further investigation in intravital studies *in vivo*.

Poor clinical success has also been partly attributed to their exact therapeutic mechanistic properties and mode of action remaining poorly understood due to a lack of robust pre-clinical / basic experimental studies. It is therefore important to understand the mechanistic profile and the beneficial effects of these different SCs in order to ascertain how to improve their therapeutic effectiveness in translational and clinical studies. Since endothelial injury as a result of oxidative stress is specifically an important contributor to IR injury in any organ, this

chapter will also focus on identifying whether HSCs and/or MSCs could potentially exert myocardial protection through antioxidant endothelial effects. The ability of HSCs versus MSCs to protect cultured cardiovascular ECs after oxidative injury will therefore be compared *in vitro*. This information will also help provide understanding of the beneficial impacts of SC therapy. Again, the more potent endothelial protective SC will be utilised in intravital studies *in vivo.*

3.1.1 Hypotheses and Aims

- This chapter firstly aimed to establish a working model of murine myocardial IR injury using the temporary LAD coronary artery ligation model. Hearts were removed from these mice for *in vitro* assessment of myocardial injury and SC adhesive capabilities. This same model will also be used in subsequent chapters for intravital imaging of the beating heart coronary microcirculation *in vivo*.
- This chapter therefore aimed to assess oxidative injury and presence of inflammation by immunostaining frozen heart sections for 8-OHdG and the inflammatory adhesion molecule VCAM-1 respectively. This would confirm that the temporary LAD ligation myocardial IR injury did result in ventricular injury. To assess whether the vasculature was a particularly susceptible target of oxidative injury, sections were co-stained with CD31, an endothelial marker. **HYPOTHESIS:** The extent of oxidative and inflammatory stress will be increased in IR injured heart sections when compared to sham heart sections, with the coronary vasculature a particular target of oxidative injury.

- The ability of different SCs, namely murine HSCs (HPC-7s), BM MSCs and WJ MSCs, to adhere to IR injured heart tissue sections was compared to their adhesion to sham tissue sections. This was assessed *in vitro* using frozen tissue Stamper-Woodruff static adhesion assays. Correlations were made with the extent of oxidative tissue damage or inflammatory adhesion molecule expression and SC adhesion. **HYPOTHESIS:** All of the different SCs tested will be more adhesive to IR injured heart tissue sections compared to sham tissue sections.
- The ability of all three types of SCs to rescue cardiovascular ECs from damage induced by hydrogen peroxide (H_2O_2) mediated oxidative stress was also investigated. The ability of SCs to confer vasculoprotection by reducing ROS generation and oxidative damage was assessed by immunostaining vena cava ECs (VCECs) for DHE and 8-OHdG respectively in co-culture experiments *in vitro.* **HYPOTHESIS:** All three types of SCs will be able to rescue cardiovascular ECs from oxidative damage induced by H_2O_2.

3.2 Methods

Detailed methods are described in Chapter 2. Briefly, in order to obtain myocardial IR injured tissue, the LAD artery was temporarily ligated in anaesthetised male mice to induce ischaemia for 45 minutes. The ligation was then removed and the heart was reperfused for 2 hours. After surgery, the mouse was sacrificed by cervical dislocation and the heart was harvested and snap frozen in liquid nitrogen.

Frozen heart tissues were cryostat cut into 10µm sections and stained with antibodies against VCAM-1 and 8-OHdG in order to visualise, and subsequently quantitate, areas of inflammatory

adhesion molecule expression and oxidative stress respectively. Some sections were co-stained with an anti-CD31 antibody to ascertain whether the coronary vasculature underwent greater oxidative damage than the cardiomyocytes. Stamper-Woodruff static adhesion assays were also performed whereby CFSE labelled HPC-7s, BM MSCs or WJ MSCs were incubated on the frozen tissue sections and their adhesive ability subsequently determined.

Co-culture assays with VCECs and SCs were also conducted in order to determine the ability of SCs to confer vasculoprotection by reducing EC damage induced *in vitro* by oxidative stress. Briefly, 10µM of H_2O_2 was used to damage a monolayer of VCECs in 24-well plates. At the same time, CFSE labelled HPC-7s, BM MSCs or WJ MSCs were added to the well. Control wells comprised of similar wells in which no SCs had been added. After 24 hours or 72 hours of co-culture, images were acquired and quantitated to identify the level of superoxide generation or oxidative damage that had been incurred by ECs. Superoxide generation was measured using DHE staining whilst levels of oxidative stress mediated endothelial damage were measured using an antibody against 8-OHdG.

3.3 Results

3.3.1 Stress and Inflammatory Markers on IR Injured Murine Heart Tissue are Increased

Immunohistochemistry assays were carried out, as described in section **2.6.1.2**, to determine the expression of the oxidative injury marker, 8-OHdG, and the endothelial adhesion molecule, VCAM-1, on frozen heart tissue sections. Antibodies against these markers were used to determine their respective expression levels. The expression of 8-OHdG was markedly intense in the IR injured heart tissue compared to the sham counterpart ***(Figure 3.1.1A-1B)***. There was a global and intense increase in 8-OHdG expression throughout the IR injured tissue sections, with staining observed on both myocytes and blood vessels. However, visibly higher expression was observed on the large coronary vessels as determined by co-staining with for CD31, when compared to general myocyte staining ***(Figure 3.1.1C-D)***. Although IR injured large vessel endothelium was a key target of oxidative damage, myocardial capillaries also underwent significant oxidative stress ***(Figure 3.1.1D)***. Quantification of staining intensity and subsequent statistical analysis showed that there was significant ($p<0.05$) difference between the expression of 8-OHdG in IR injured murine heart tissue compared to sham ***(Figure 3.1.1E)***.

The expression of VCAM-1 followed a similar pattern with staining on the sham tissue sections subdued, with few areas of discernible antibody presence ***(Figure 3.1.2A)***. Expression of VCAM-1 on the IR injured tissue sections was higher and could be observed, as anticipated, more concentrated around blood vessels in the tissue ***(Figure 3.1.2B)***. The difference in VCAM-1 expression between the two tissue sections was again statistically significant ($p<0.05$) ***(Figure 3.1.2C)***.

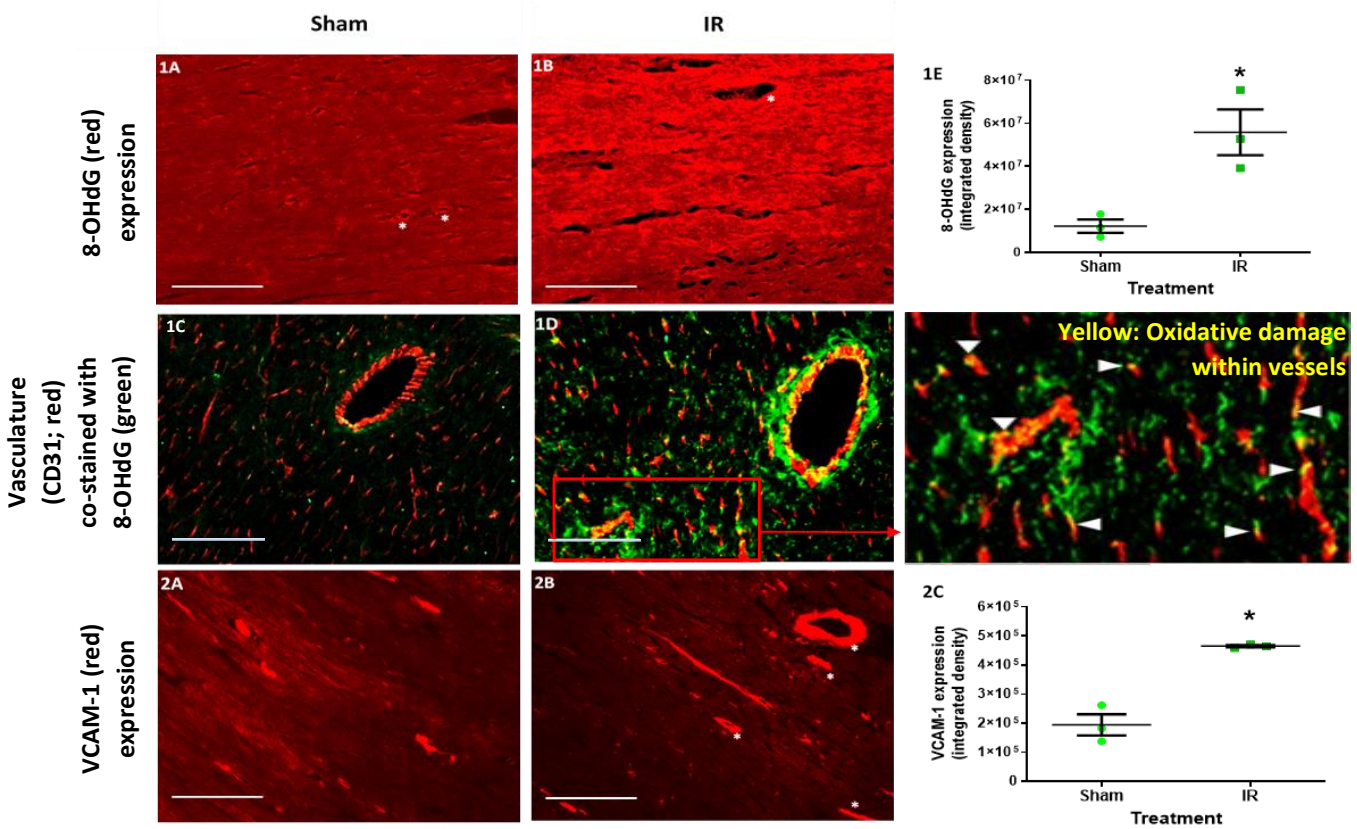

Figure 3.1: Expression of the oxidative injury marker, 8-OHdG, and the endothelial adhesion molecule, VCAM-1, is raised on IR injured heart tissue. *IHC antibody staining was performed on frozen heart tissue sections, which were either directly injured through IR or were sham counterparts, utilising anti-8-OHdG or anti-VCAM-1 antibodies. 8-OHdG (red) expression was low on the sham heart sections, primarily concentrated around blood vessels (asterisks) (**1A**). The expression of 8-OHdG (red) was globally higher on the IR heart sections, with higher concentrations seemingly around blood vessels as well (asterisks) (**1B**). Co-staining of anti-8-OHdG (green) with anti-CD31 (red) showed lower intensity staining of 8-OHdG around blood vessels in sham hearts (**1C**) and higher concentrations in IR injured heart sections **(1D**). Although IR injured large vessel endothelium was a key target of oxidative damage, myocardial capillaries also underwent significant oxidative stress (expanded image - arrowheads). The difference in expression was statistically significant ($p<0.05$) between the sham and IR injured groups (**1E**). VCAM-1 (red) expression was also low on the sham heart sections, with few areas of discernible high concentrations. These were mostly on the microvessels (**2A**). Again, the expression of VCAM-1 (red) was higher on the IR injured heart sections and primarily concentrated around larger blood vessels (asterisks) (**2B**). The difference in expression was statistically significant ($p<0.05$) between the two groups (**2C**). Statistical analysis was performed using unpaired t-tests. N=3 per group. Scale = 100µm*

3.3.2 Adhesion Capabilities of Different Stem Cell Types to Murine Heart Tissue Sections Varies *in vitro*

Static adhesion assays were carried out as described in section **2.6.1.1**. HPC-7s were observed to be capable of adhering to both the IR injured and sham murine heart tissue sections, with a higher affinity for adhering to the IR injured murine heart tissue sections ***(Figure 3.2.1A-1B)***. The difference in adhesion was statistically significant ($p<0.05$) ***(Figure 3.2.1C)***. BM MSCs appeared to favour adherence to IR injured heart tissue compared to sham counterparts ***(Figure 3.2.2A-2B)***. However, there was no statistically significant difference ***(Figure 3.2.2C)***. Interestingly, the adhesion of BM MSCs to IR injured tissue (~13 cells/field of view) was greater than HPC-7s (~6 cells/field of view). WJ MSCs were observed to be the most adhesive to frozen sections (~20-25 cells/field) ***(Figure 3.2.3A-3B)***. However, there was no significant difference between WJ MSC adhesion on sham or IR injured tissues ***(Figure 3.2.3C)***.

3.3.3 Correlation between Stem Cell Adhesion and 8-OHdG Expression

We further investigated whether there was a correlation between the adherent stem cell numbers and the expression levels of 8-OHdG in regions of murine heart tissue sections, regardless of injury. Correlation assays were carried out as described in section **2.6.1.3**. HPC-7s showed an increased likelihood of adhering to regions of the tissue section with a high expression of 8-OHdG, an indicator of oxidative tissue damage ***(Figure 3.3.1A-1B)***. This was confirmed as a significant positive correlation via statistical analysis (Pearson's correlation coefficient (r) = 0.5480; $p<0.05$) ***(Figure 3.3.1C)***. BM MSCs were also observed to more likely adhere to heart tissue regions with a high level of oxidative damage ***(Figure 3.3.2A-2B)***. This positive correlation was statistically significant (r = 0.6482; $p<0.05$) ***(Figure 3.3.2C)***. In

contrast, WJ MSCs were shown to be highly adherent to tissue sections regardless of 8-OHdG expression ***(Figure 3.3.3A-3B)***. Statistical analysis showed a slight but not significant positive correlation between WJ MSCs adhesion and 8-OHdG expression ($r = 0.1653$; $p>0.05$) ***(Figure 3.3.3C)***.

3.3.4 Correlation between Stem Cell Adhesion and VCAM-1 Expression

The correlation between the adherent stem cell numbers and the expression levels of VCAM-1 in regions of murine heart tissue sections, regardless of injury, was also investigated. Correlation assays were carried out as described in section **2.6.1.3**. HPC-7s showed no discernible correlation between adhesion numbers and VCAM-1 expression ***(Figure 3.4.1A-1B)***. Statistical analysis showed there to be almost no correlation between the two factors ($r = 0.2612$; $p>0.05$) ***(Figure 3.4.1C)***. BM MSCs were also observed to not favour adhesion in regions expressing high levels of VCAM-1 ***(Figure 3.4.2A-2B)***. Statistical analysis showed there to be no correlation between the two factors ($r = 0.0433$; $p>0.05$) ***(Figure 3.4.2C)***. WJ MSCs were shown again to be highly adherent to tissue sections regardless of VCAM-1 expression ***(Figure 3.4.3A-3B)***. Statistical analysis again showed there to be no correlation between WJ MSCs adhesion and VCAM-1 expression ($r = 0.0938$; $p>0.05$) ***(Figure 3.4.3C)***.

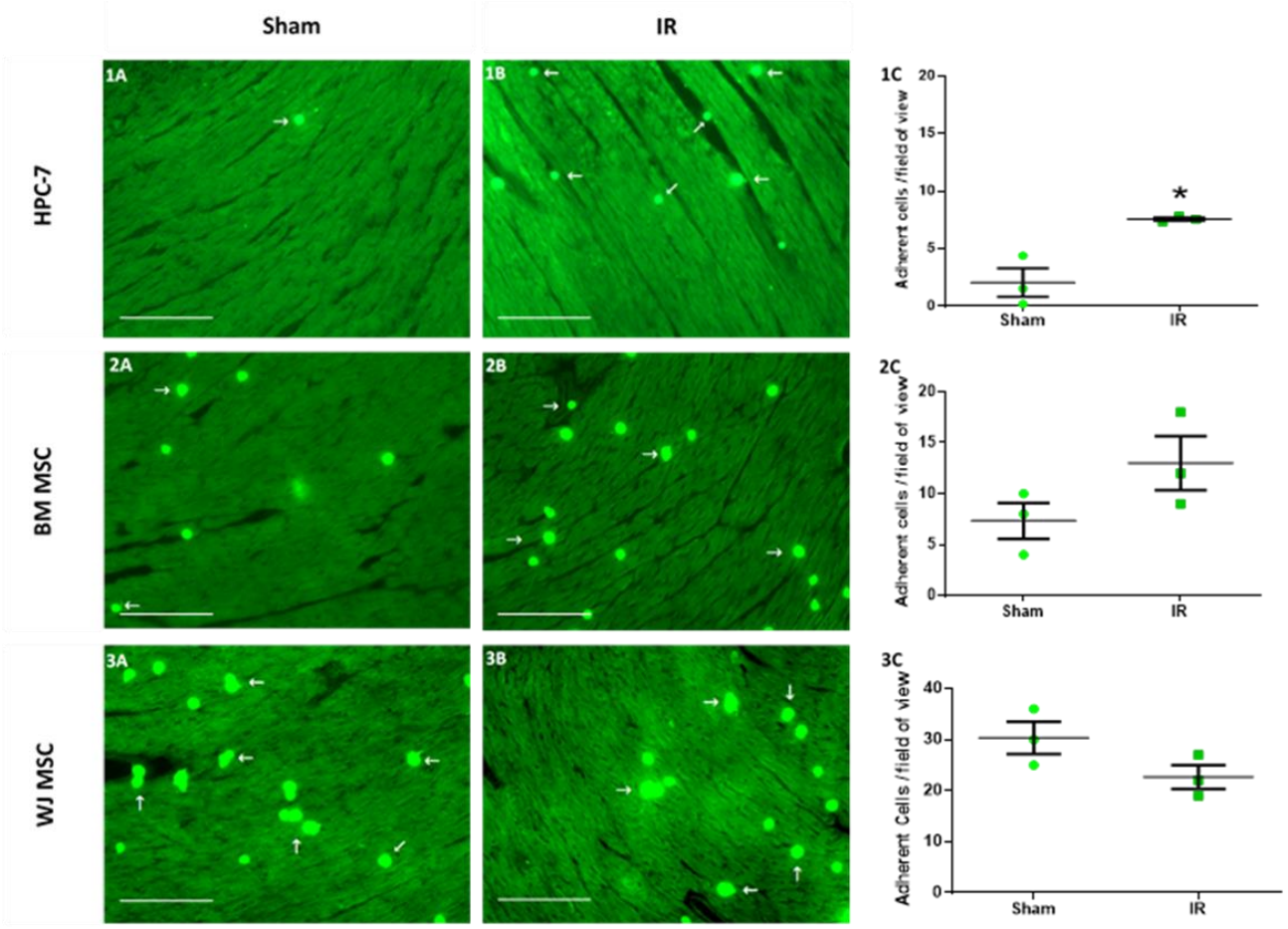

Figure 3.2: Adhesion capabilities of different stem cell types to heart tissue sections in vitro. *Stamper Woodruff assays were performed on frozen heart tissue sections, which were either directly injured through IR or were sham counterparts, utilising HPC-7s, BM MSCs or WJ MSCs stained with CFSE. HPC-7 cells demonstrated small adhesion capabilities to sham heart sections (arrows) (**1A**). These cells demonstrated better adhesion to IR injured heart sections (**1B**). The difference in adhesion was statistically significant ($p<0.05$) between the two groups (**1C**). A similar trend was seen for BM MSCs however there was no statistically significant difference between the two groups. Of note, their adhesive capabilities were better than HPC-7 cells (**2A-C**). WJ MSCs demonstrated very high adhesion to sham heart sections (**3A**). These cells demonstrated similar adhesion capabilities to IR heart sections (**3B**). There was no statistically significant ($p>0.05$) difference between the two groups (**3C**). Statistical analysis was performed using unpaired t-tests. N=3 per group. Scale = 100μm*

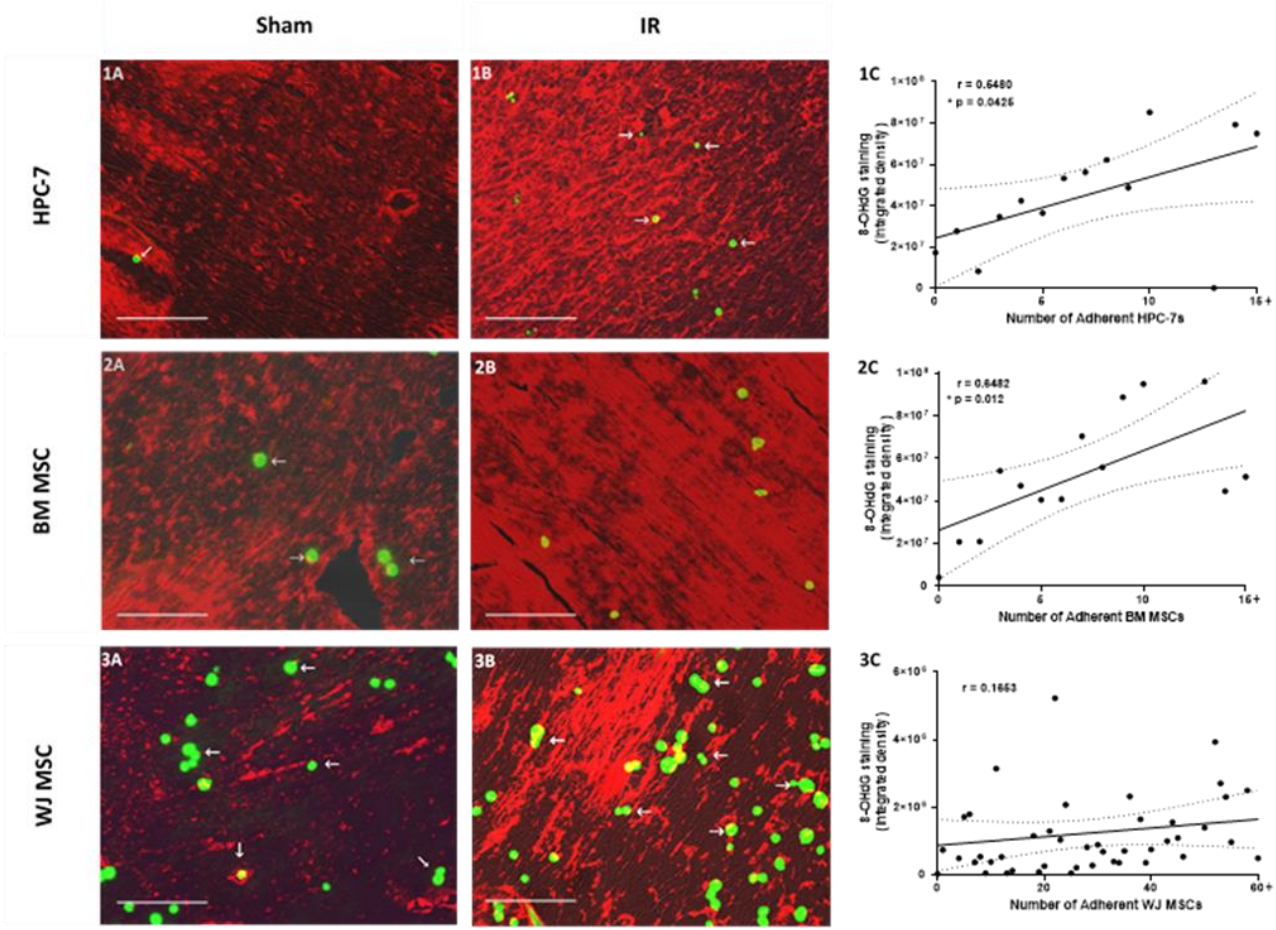

Figure 3.3: Correlation between stem cell adhesion and 8-OHdG expression. *Correlation studies were performed to investigate the relationship between stem cell adhesion and 8-OHdG expression, an indicator of oxidative tissue damage, on heart tissue sections that were either directly injured through IR or were sham counterparts. These studies were conducted using HPC-7s, BM MSCs or WJ MSCs stained with CFSE alongside anti-8-OHdG antibody staining. HPC-7s tended to be more adherent in regions with higher expression of 8-OHdG (**1A-1B**). This correlation was statistically significant (r=0.5480; p<0.05) (**1C**). Similar results were obtained for BM MSCs (r=0.6482; p<0.05) (**2A-C**). However, WJ MSCs were adherent to tissue sections regardless of 8-OHdG expression (**3A-3B**). There was no statistically significant correlation between the two factors (r=0.1653; p>0.05) (**3C**). Statistical analysis was performed using Pearson correlation coefficient. Scale = 100µm*

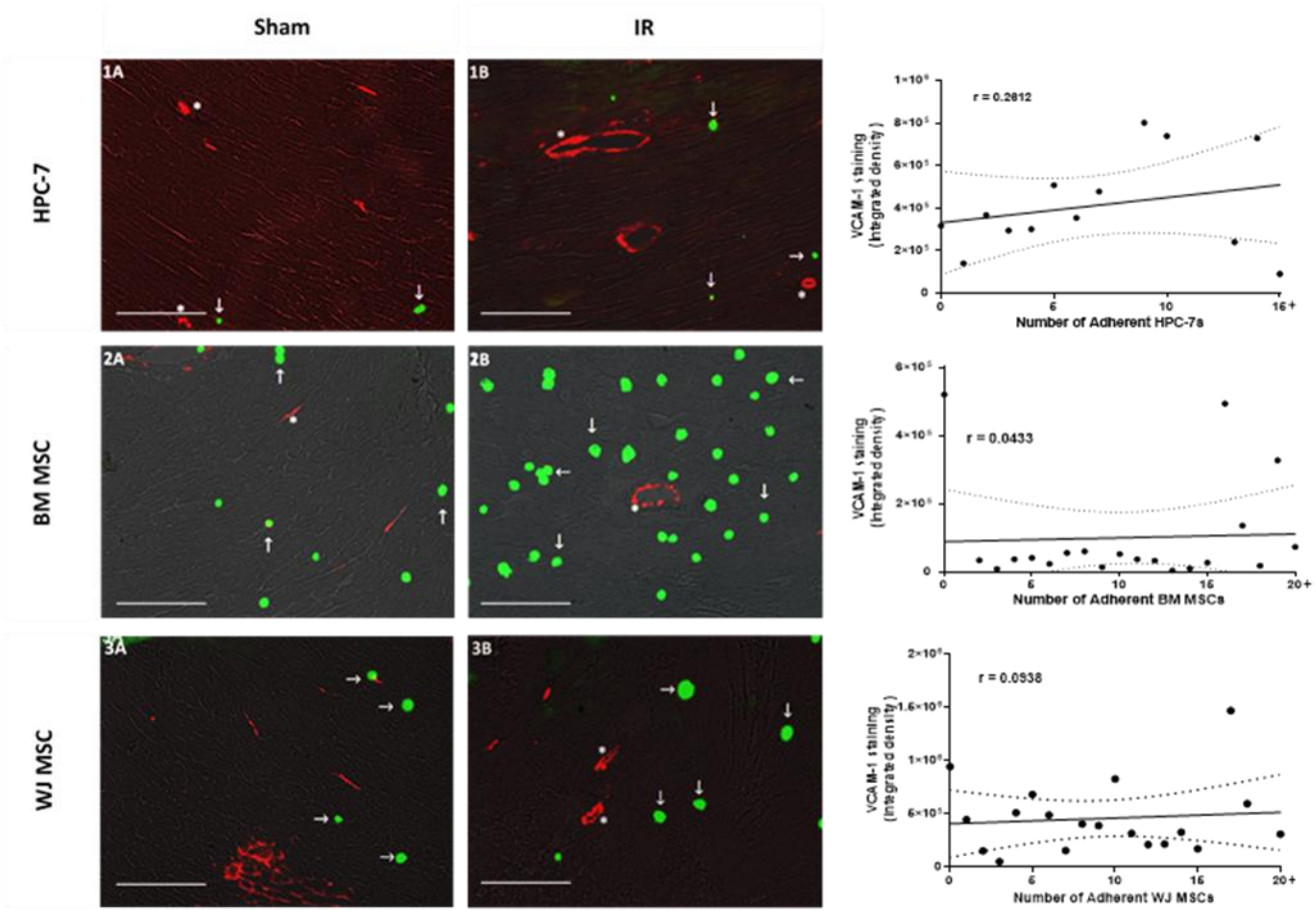

Figure 3.4: Correlation between stem cell adhesion and VCAM-1 expression. *Correlation studies were performed to investigate the relationship between stem cell adhesion and VCAM-1 expression on heart tissue sections that were either directly injured through IR or were sham counterparts. These studies were conducted using HPC-7s, BM MSCs or WJ MSCs stained with CFSE alongside anti-VCAM-1 antibody staining. HPC-7s were adherent to tissue sections (arrows) regardless of VCAM-1 expression (**1A-1B**). There was no correlation between the two factors (r=0.2612) (**1C**). Similar results were obtained with BM MSCs (r=0.0433) (**2A-C**). WJ MSCs were also adherent to tissue sections (arrows) regardless of VCAM-1 expression (**3A-3B**). Similarly, there was almost no correlation between the two factors (r=0.0983) (**3C**). Statistical analysis was performed using Pearson correlation coefficient. Scale = 100µm*

3.3.5 Endothelial-Stem Cell Co-Culture: Protective Effects of HPC-7s as Determined by ROS Generation at 24 & 72 Hours

In this study, further *in vitro* experiments were performed to investigate the potential protective effects of HPC-7 stem cells on vena cava ECs (VCECs) damaged due to exposure to the free radical H_2O_2. Direct co-culture assays were conducted as described in section **2.7**. 24 hours after exposure to H_2O_2, the presence of O_2- was measured using the free radical detecting dye DHE in wells with and without stem cells. VCECs were observed to be damaged after exposure to H_2O_2 when no HPC-7s were added, as demonstrated by an increased DHE red fluorescence. In wells in which HPC-7s were co-cultured, they were seen adherent to the VCECs and appeared to attenuate the production of O_2- compared to the control group of VCECs not receiving any cellular therapy ***(Figure 3.5.1A-1B)***. This trend however was not statistically significant upon analysis ($p>0.05$) ***(Figure 3.5.1C)***. Similar experiments were conducted in which VCECs were exposed to H_2O_2 but for 72 hours. Again VCECs were observed to be damaged after exposure to H_2O_2 when no HPC-7s were added. HPC-7s appeared able to attenuate the production of O_2- compared to the control group of VCECs not receiving any cellular therapy ***(Figure 3.5.2A-2B)***. After 72 hours, the difference was found to be statistically significant when the data was analysed ($p<0.001$) ***(Figure 3.5.2C)***.

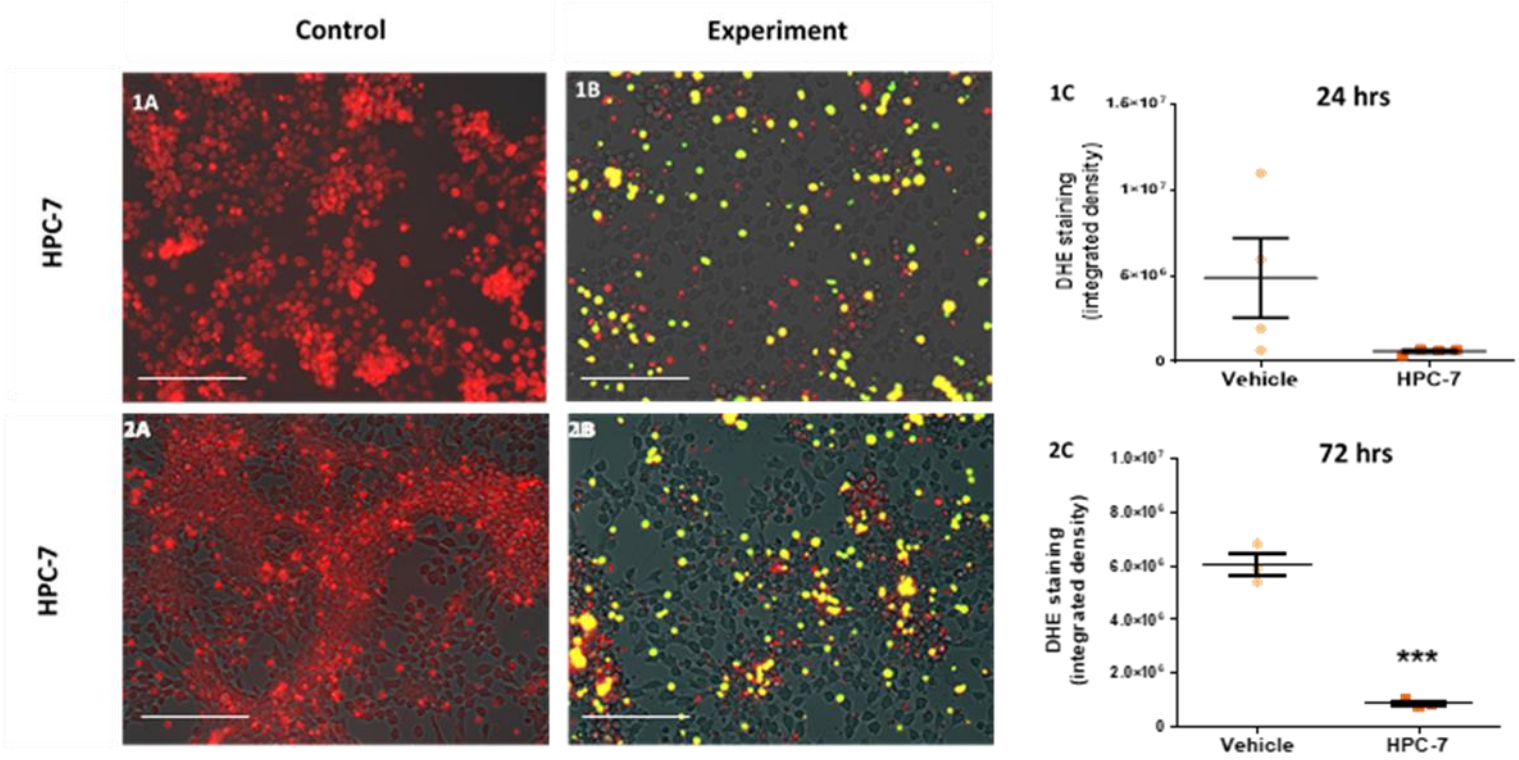

Figure 3.5: Investigating the protective effects of HPC-7s on damaged endothelial by measuring their ability to reduce ROS generation in vitro at <u>24 & 72 hours</u>. *Cellular co-culture assays were performed in 24-well plates utilising mouse vena cava ECs and either no stem cells (control) or HPC-7s stained with CFSE (yellow/green). The ECs were damaged by exposure to 10µM hydrogen peroxide, introduced concurrently with the stem cells. After 24 hours and 72 hours respectively, DHE staining was utilised to measure ROS production (red). HPC-7s appeared to reduce the presence of ROS compared to the control group of ECs not receiving cellular therapy (**1A-1B ; 2A-2B**). This was statistically significant at 72 hours ($p<0.001$) but not at 24 hours (**1C&2C**). Statistical analysis was performed using unpaired t-tests. N=4 per group. Scale = 100µm*

3.3.6 Endothelial-Stem Cell Co-Culture: Protective Effects of BM MSCs as Determined by ROS Generation at 24 & 72 Hours

Similar experiments were conducted to investigate the potential protective effects of BM MSCs on VCECs damaged due to exposure to H_2O_2 over 24 and 72 hours. Co-culture assays were conducted as described in section **2.7**. Interestingly, BM MSCs incorporated themselves into the endothelial layer after 24 hours and appeared elongated. This was in contrast to the HPC-7s which retained their spherical nature when co-cultured with VCECs ***(Figure 3.5.1B-2B)***. However, BM MSCs were not able to affect the production of O_2- and showed the same level of DHE staining as the control group not co-cultured with BM MSCs ***(Figure 3.6.1A-1B)***. Statistical analysis confirmed that there was no significance between the two groups ***(Figure 3.6.1C)***. After 72 hours, BM MSCs were again unable to affect the production of O_2- and showed the same level of DHE staining as the control group ***(Figure 3.6.2A-2B)***. Statistical analysis confirmed that there was no significance between the two groups ***(Figure 3.6.2C)***.

3.3.7 Endothelial-Stem Cell Co-Culture: Protective Effects of HPC-7s as Determined by Oxidative Stress Induced in Endothelial Cells at 24 & 72 Hours

ROS are able to induce oxidative stress or free radical damage in cells. This can be quantitated using dyes that specifically detect oxidative damage. After establishing the protective effects of stem cells, mechanistically by their ability to reduce ROS presence, this study further investigated whether the reduction in ROS generation was accompanied by a reduction in oxidative damage in VCECs damaged by H_2O_2 over a 24- and 72-hour period. Direct co-culture assays were conducted again as described in section **2.7**. 24 hours after exposure to H_2O_2, the

presence of oxidative damage was measured using an anti-8-OHdG ab. HPC-7s appeared to be adherent to the VCECs and the oxidative damage expression appeared similar to the control group ***(Figure 3.7.1A-1B)***. There was no significant difference between the two groups after quantitative analysis ***(Figure 3.7.1C)***. 72 hours after exposure to H_2O_2, the presence of oxidative damage was again measured using an anti-8-OHdG ab. Unlike the effects at 24 hours, HPC-7s were – after a longer incubation period – able to decrease the expression of 8-OHdG compared to the control group receiving no cells ***(Figure 3.7.2A-2B)***. This was confirmed through statistical analysis as there was a significant difference between the two groups ($p<0.05$) ***(Figure 3.7.2C)***.

3.3.8 Endothelial-Stem Cell Co-Culture: Protective Effects of BM MSCs as Determined by Oxidative Stress Induced in Endothelial Cells at 24 & 72 Hours

Similar experiments were conducted to investigate the potential protective effects of BM MSCs on VCECs damaged due to exposure to H_2O_2 over 24 and 72 hours. Direct co-culture assays were conducted as described in section **2.7**. BM MSCs were seen again to incorporate themselves into the endothelial layer ***(Figure 3.8.1A-1B)***. There was an impressive level of reduction in 8-OHdG levels which was statistically significant when compared to controls ($p<0.05$) ***(Figure 3.8.1C)***. After 72 hours, BM MSCs were once again incorporated into the endothelial layer and again, decreased the intensity levels of 8-OHdG when compared to the control group (***Figure 3.8.2A-2B***). As with the 24 hour experiment, there was a significant difference between the two groups on statistical analysis ($p<0.01$) (***Figure 3.8.2C***).

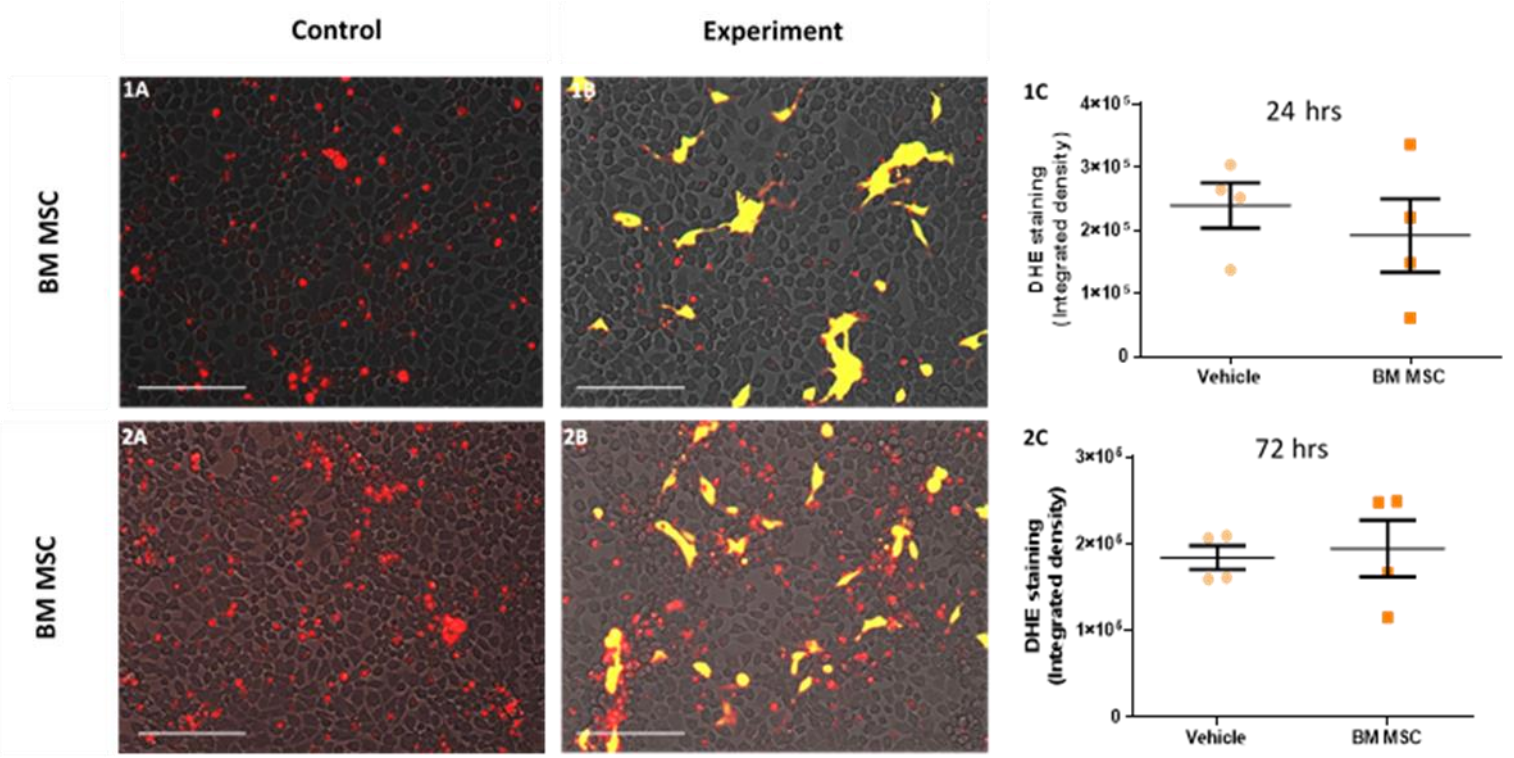

Figure 3.6: Investigating the protective effects of BM MSCs on damaged endothelial by measuring their ability to reduce ROS generation in vitro at <u>24 & 72 hours</u>. *Cellular co-culture assays were performed in 24-well plates utilising mouse vena cava ECs and either no stem cells (control) or BM MSCs stained with CFSE (yellow/green). The ECs were damaged via 10μM hydrogen peroxide, introduced concurrently with the stem cells. After 24 hours and 72 hours respectively, DHE staining was utilised to measure ROS production (red). At both time points, ECs co-cultured with BM MSCs showed similar ROS presence compared to their control counterparts (**1A-1B ; 2A-2B**). There was no statistically significance between the groups (**1C&2C**). Statistical analysis was performed using unpaired t-tests. N=4 per group. Scale = 100μm*

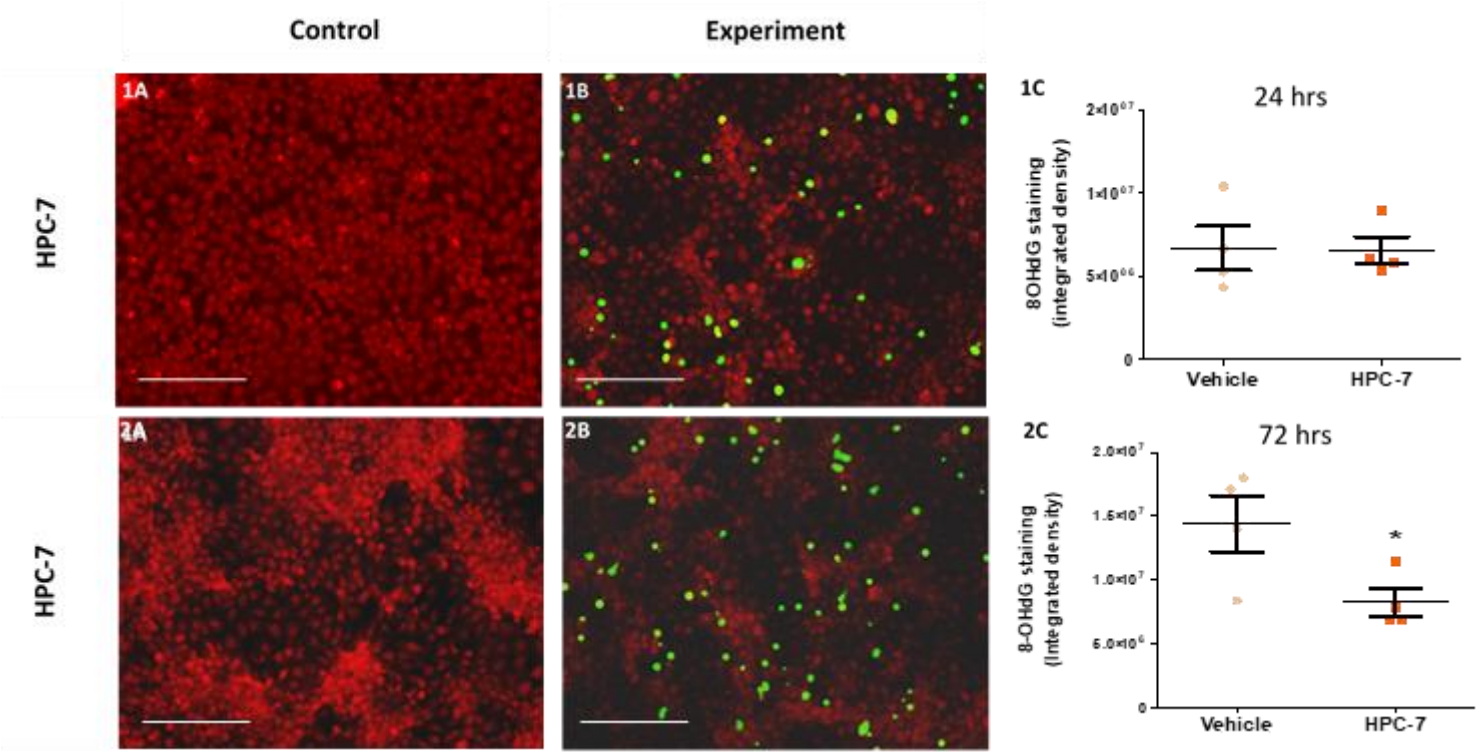

Figure 3.7: Investigating the protective effects of HPC-7s by measuring their ability to reduce ECs oxidative stress in vitro at <u>24 & 72 hours</u>. *Cellular co-culture assays were performed in 24-well plates utilising mouse vena cava ECs and either no stem cells (control) or HPC-7s stained with CFSE (yellow/green). The ECs were damaged via 10µM hydrogen peroxide, introduced concurrently with the stem cells. After 24 hours, anti-8-OHdG antibody staining was utilised to measure oxidative damage (red). HPC-7s did not visually reduce the presence of oxidative damage compared to the control group (**1A-1B**). There was no statistically significant difference (p>0.05) (**1C**). After 72 hours, visually there was a slight reduction in 8-OHdG expression when HPC-7s were used (**2A-2B**). This tendency for decrease was statistically significant between groups (p<0.05) (**2C**). Scale = 100µm*

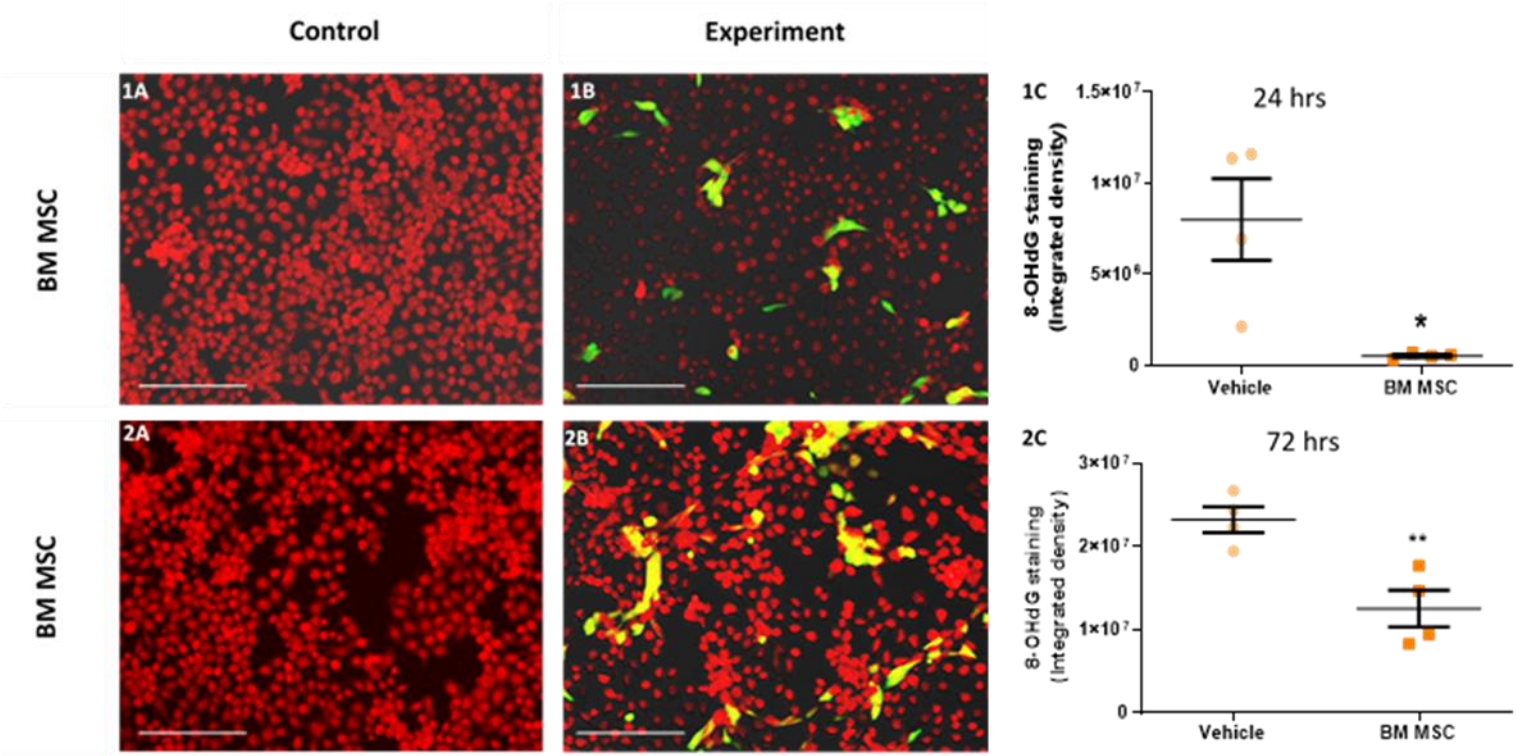

Figure 3.8: Investigating the protective effects of stem cells by measuring their ability to reduce EC oxidative stress in vitro at <u>24 & 72 hours</u>. *Cellular co-culture assays were performed in 24-well plates utilising mouse vena cava ECs and either no stem cells (control) or BM MSCs stained with CFSE (yellow/green). The ECs were damaged via 10µM hydrogen peroxide, introduced concurrently with the stem cells. After 24 hours, anti-8-OhdG ab staining was utilised to measure oxidative damage (red). After 24 hours, BM MSCs visually reduced the presence of oxidative damage compared to the control group (**1A-1B**). This difference was confirmed statistically significant ($p<0.05$) (**1C**). After 72 hours, this trend continued (**2A-2B**). Again, there was a statistically significant difference between the groups ($p<0.01$) (**2C**). Scale = 100µm*

3.3.9 Endothelial-Stem Cell Co-Culture: WJ MSCs Disrupt the Endothelial Cell Monolayer

Co-culture experiments were also attempted using WJ MSCs. Direct co-culture assays were conducted as described in section **2.7**. However, in these experiments the outcome with WJ MSCs was drastically different. After 24 and 72 hours of co-culturing, the VCEC layer was majorly disrupted by the WJ MSCs. The VCECs in the control group remained healthy, formed a monolayer and were more robust than those co-cultured with WJ MSCs ***(Figure 3.9A-B)***. When imaged microscopically, far less VCECs were observed adherent in those wells in which WJ MSCs were also added. Although the WJ MSCs still appeared spherical at 24 hours ***(Figure 3.9C)*** their morphology was very different at 72 hours ***(Figure 3.9D)***. As this outcome was repeatedly encountered, this limited our capability to continue experiments analysing ROS generation with DHE or oxidative damage with 8-OHdG expression as was carried out with HPC-7s and BM MSCs.

3.3.10 Stem Cell Morphology

Determining which type of stem cell would prove the most beneficial in homing to the heart as a form of cell therapy was an essential aim in these initial *in vitro* experimentations. Whilst investigating the various potential protective properties of the three types of stem cells was important, the morphology of the cells would also be an important consideration. Through our co-culture experiments, we found the HPC-7s to consistently maintain their size and shape ***(Figure 3.10A)***. They were not only much smaller than the two different types of MSCs, but importantly maintained their shape and size with co-culture even at 72 hours. However, the BM MSCs and WJ MSCS were not only much larger, but both had tendencies to elongate in *in*

vitro conditions particularly at 72 hours co-culture with VCECs ***(Figure 3.10 B-C)***. These observations were repeatedly noticed through our experiments.

3.4 Discussion

SCs have been shown to improve IR injury in multiple organs [150, 185-187]. Within the heart, commonly measured experimental outputs of success in treating IR injury include improvements in ventricular contraction and a reduction in infarct size. Although similar improvements have been demonstrated clinically, these are modest and/or transient and so the results of utilising SCs as a form of cell therapy in MI and heart failure has been mixed. It is unclear whether this is due to a limited ability of circulating, systemically injected SCs to interact with coronary microvessels to result in their firm adhesion and thus retention within the IR injured heart. Microcirculatory perturbations are increasingly recognised as critical contributors to myocardial IR injury. However, we do not know if the poor success of SC therapy is related to an inability of SCs to 'protect' microvessels from injury i.e. to confer vasculoprotection. It is also unclear whether the poor retention of systematically injected SCs within the heart contribute to this lack of success. Common mediators that contribute to microvascular injury post-reperfusion injury include oxidative stress, inflammation and endothelial dysfunction [4]. However, little is known about whether HSCs or MSCs can moderate these events in a therapeutic manner. Importantly, no studies have compared the adhesive and vasculoprotective propensity of HSCs and different MSC populations.

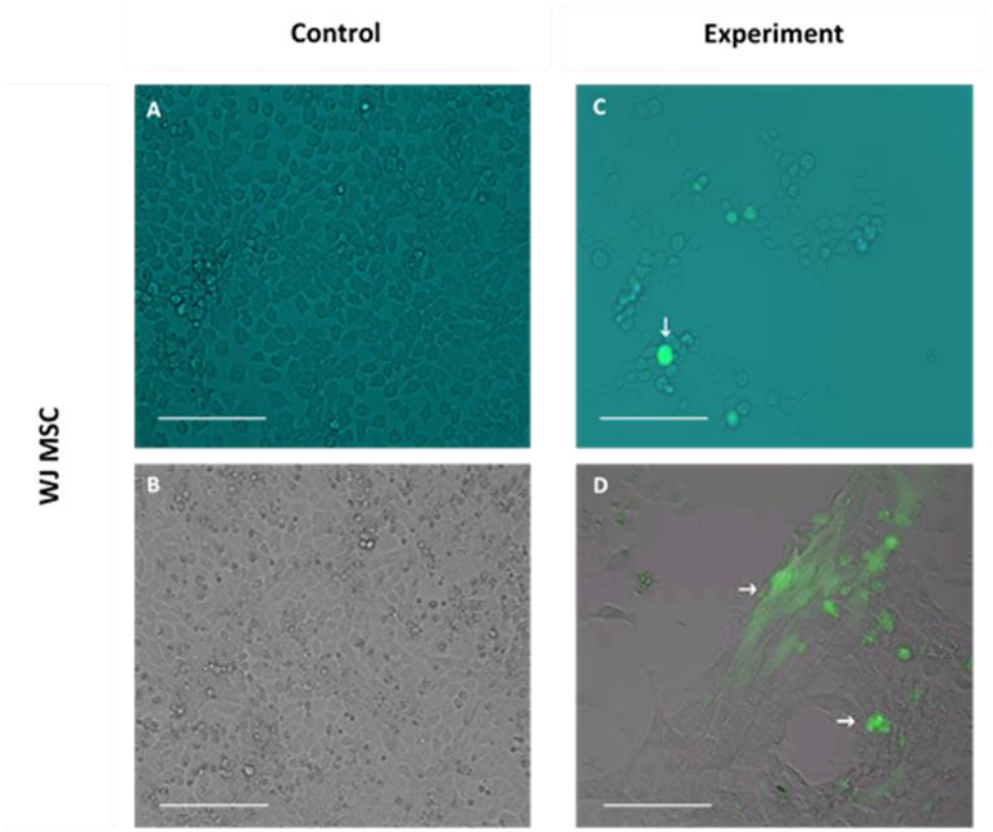

Figure 3.9: WJ MSCs cause disruption to endothelial cells. *Cellular co-culture experiments were also conducted to investigate the effects of CFSE-labelled WJ MSCs on levels of free radical generation and oxidative stress induced damage to VCECs after stimulation with 10µM hydrogen peroxide. VCECs again formed a confluent monolayer in 24-well plates. 24 and 72 hours after co-culture assay stimulation, wells that were co-cultured with no cells (vehicle) were still viable (**A-B**). However, wells that were co-cultured with WJ MSCs (arrows) demonstrated a significant disruption in the EC monolayer with few viable VCECs visible (**C-D**). Although the WJ MSCs still appeared spherical at 24 hours (arrows) (**C**), their morphology was very different at 72 hours (**D**). This halted the experiment and so no DHE or 8-OhdG labelling was performed. No data was collectible from this set of experiments as was possible with HPC-7 or BM MSC co-culture experiments. Scale = 100µm*

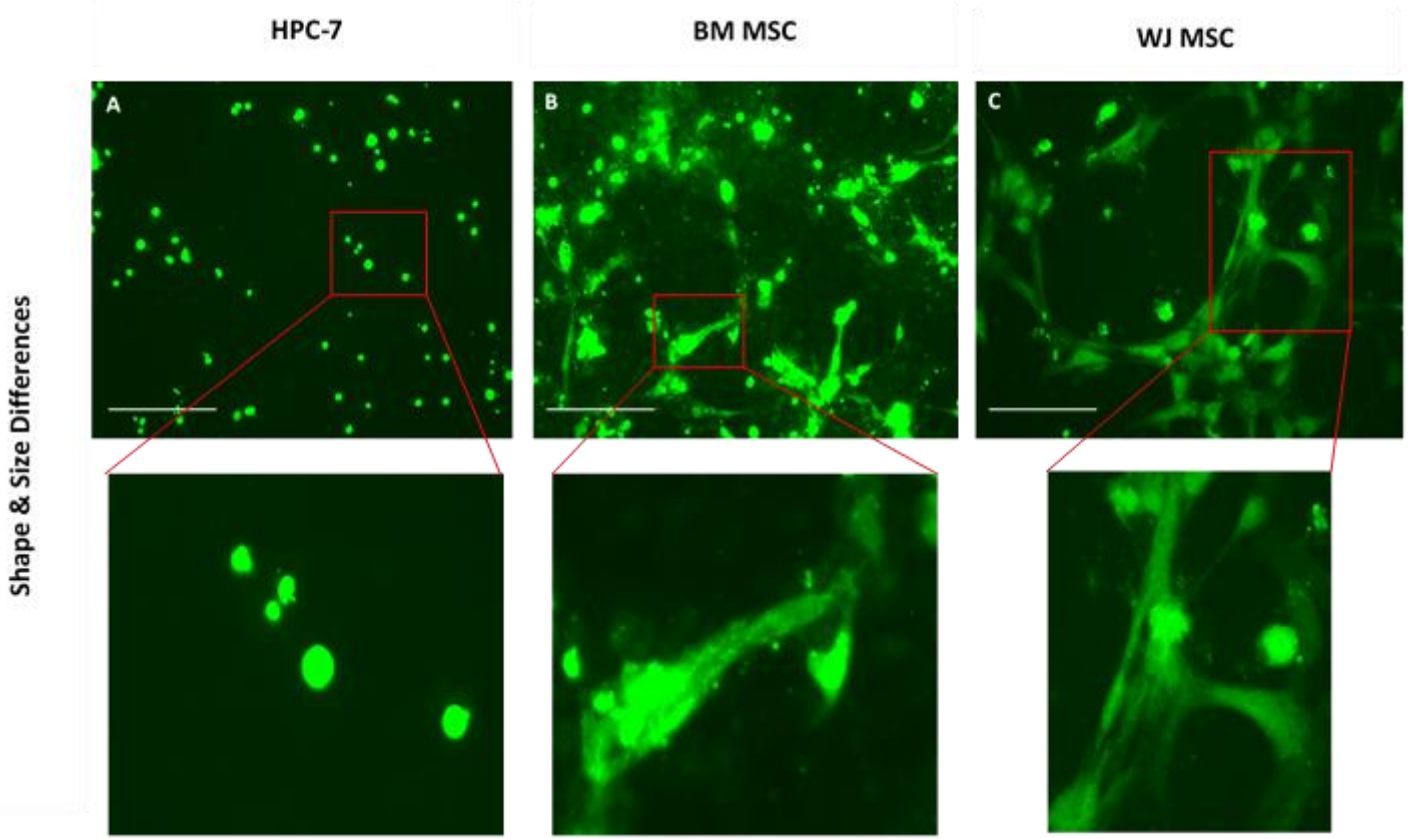

Figure 3.10: Differing shapes and sizes of stem cells in culture conditions. *An important aspect under consideration when deciding which stem cell type to take forward into intravital experiments is the size and morphology of the cells. As seen in* ***Figure 3.2****, HPC-7s were observed to be much smaller in size compared to BM MSCs and WJ MSCs. Furthermore, during in vitro cell co-culture assays, HPC-7s maintained their size and spherical shape even at 72 hours co-culture with VCECs (****A****) whilst BM MSCs and WJ MSCs had the propensity to become elongated, stretching their cellular body (****B-C****). This was Scale = 100µm*

In this chapter, we show murine HPC-7s and BM MSCs share similar adhesive capabilities to murine injured heart sections. Interestingly, although human WJ MSCs were the most adhesive cells, they did not discriminate between healthy and injured tissue. Furthermore, we show that the adhesion of HPC-7s and BM MSCs positively correlated with the extent of oxidative tissue damage. Interestingly, co-culture experiments suggested that HPC-7s were the only cell type that could reduce ROS presence and EC oxidative damage. These beneficial effects were not demonstrated with either of the MSC populations tested. This data suggests HPC-7s are worthy candidates to test in the beating IR injured heart model *in vivo*.

3.4.1 Establishing a Myocardial Ischaemia/Reperfusion Injury Mouse Model

We firstly ensured the heart demonstrated signs of injury post-LAD ligation and reperfusion through histological evaluation of frozen tissue sections immunostained for VCAM-1 and 8-OHdG. VCAM-1 was assessed as its upregulation is known to contribute to the inflammatory response which plays an important role in myocardial IR injury. VCAM-1 is generally not constitutively expressed on vascular endothelium or its expression is low. Interestingly, Henninger and colleagues were the first to show in mice that, (similar to ICAM-1), the highest levels of constitutive VCAM-I expression, as measured using radiolabelled monoclonal antibody accumulation, were present in the heart [188]. VCAM-1 expression is upregulated upon endothelial activation in order to support β_1 integrin CD49d/CD29-dependent circulating neutrophil recruitment to the damaged region [189]. As such, it was not a surprise to see a significantly higher expression of VCAM-1 in IR injured hearts at 2 hours post-reperfusion compared to sham hearts. Only the medium to large blood vessels primarily expressed high

levels of VCAM-1 in a patchy manner in IR injured tissues, with no myocyte staining. This may be attributed to the fact that the medium/large blood vessels would be the first to be impacted by the ischaemia and subsequent reperfusion of the LAD artery, and thus more likely to display a response. Furthermore, this seems to fit with the well-known phenomenon that leukocyte adhesion and subsequent extravasation takes place in post-capillary venules rather than from the smallest capillaries. Hence endothelial adhesion molecule expression would be expected on these 'larger' vessels/venules rather than coronary capillaries.

Bowden and colleagues also presented a similar patchy increase in VCAM-1 immunostaining in IR injured hearts at 3 hours post-reperfusion [190]. The images in the Bowden study were of a small field of view, so it was not easy to discern whether the staining was located on both capillaries and medium/large coronary blood vasculature. They also demonstrated that by 24 hours post-reperfusion, VCAM-1 expression increased further [190]. Therefore, it is possible that the presence of VCAM-1 may have increased, even on smaller vessels, with time in our study. Jaakkola and colleagues also showed similar results in human hearts where P-selectin, ICAM-1 and vascular adhesion protein-1 (VAP-1) were more highly expressed in human samples post-MI with VCAM-1 expression faint [191]. Collectively, our pattern of VCAM-1 immunostaining fits with other limited immunostaining descriptions made, but importantly demonstrates that we were able to successfully establish a myocardial IR injury model in which the vasculature demonstrated signs of being inflamed.

We also found IR injured murine hearts had significantly more oxidative damage present as evidenced by increased expression of 8-OHdG, a well-used marker for oxidative DNA damage. In contrast to VCAM-1 expression which was primarily vascular, signs of oxidative stress appeared more diffuse in nature with both myocytes and vasculature staining intensely

positive for 8-OHdG. As discussed earlier, an increase in ROS generation is a by-product of the reperfusion state [192], hence it was not surprising to detect a higher degree of oxidative damage in the IR injured hearts compared to the sham hearts. 8-OHdG has previously been used in a limited number of studies to demonstrate oxidative heart tissue damage post-reperfusion injury. Inafuku and colleagues imaged reperfused Langendorff rat hearts immunohistochemically using the avidin-biotin-peroxidase complex to detect 8-OHdG positive areas and demonstrated that the nuclei of cardiomyocytes stained brown [193]. Although not stated by the author, from their images it appeared that endothelial cell nuclei also appeared oxidatively damaged. Hu and colleague also stained paraffin embedded myocardial IR injured rat heart sections for 8-OHdG and again identified brown stained myocyte nuclei [194]. However, our study appears to be the first to have co-stained frozen heart tissue vascular endothelium with CD31 to precisely demonstrate significant microcirculatory and macrovessel damage. 8-OHdG expression in our IR injured sections was diffuse and very intense throughout the whole heart due to both myocytes and vasculature experiencing oxidative damage from IR injury. However, the larger blood vessels tended to display the most intense staining in tissue sections.

3.4.2 Haematopoietic Stem Cells

Having successfully established the LAD ligation model of myocardial IR injury, we further assessed the adhesion capabilities of different SC types to frozen sections *in vitro.* The first SC type that will be discussed is the HSC group. In this chapter, HPC-7s were utilised to demonstrate the capabilities of HSCs. As stated earlier, HPC-7s are an immortal murine cell

line that were generated by growing LIM-homeobox 2(LH2)-transduced embryonic stem cells *in vitro* [169]. As such, these cells share characteristics with murine foetal haematopoietic progenitor cells. This study investigated the adhesion capabilities of these cells and their ability to protect against oxidative stress induced EC damage.

3.4.2.1 HPC-7s are More Adherent to IR Injured Murine Heart Tissue

HPC-7s were observed to be significantly more adherent to IR injured heart tissue compared to the sham heart tissue. Indeed, HPC-7s were found to be almost three times more likely to adhere to IR injured heart tissue compared to sham heart tissue. We have previously shown that these same cells can also preferentially adhere to frozen tissue sections of IR injured liver, small intestine, colon and kidney when compared to healthy shams [150, 151, 170, 195]. As stated previously, adhesion molecules are upregulated during an IR injury and as such, it is reasonable to observe increased adhesion capabilities of HPC-7s on IR injured heart tissue. Adhesion of HPC-7s to tissue sections can occur through a variety of interactions. P- and E-selectin has been shown to help HSCs adhere to ECs and are important for trans-endothelial migration [196]. HSC surface integrin subunits such as CD49d, CD49e and CD11a have also been shown to play a role in allowing HSCs to adhere to ECs and migrate through tissue [197]. Studies such as that by Huygen et al. and Grassinger et al. showed that HSCs can bind to fibronectin and truncated osteopontin through integrins such as VLA-4 and α9β1 [198, 199]. These same integrins can readily bind to VCAM-1 as well, indicating the potential for HPC-7s to bind to IR heart tissue expressing high levels of VCAM-1 [190, 200]. The presence of these

molecules and their ligands may account for the observations seen of increased adhesion of HPC-7s in IR injured hearts compared to sham hearts.

However, the Stamper-Woodruff assay has several limitations. It is difficult to distinguishing whether the applied cells of choice are adherent to the endothelial layer, sub-endothelial layer or other non-endothelial cells. It is also difficult to determine whether adherence is to the surface of cells in the tissue section or to the exposed cytoplasm/nucleus. Endothelial receptors (ex. JAMs) that specifically promote leukocyte transmigration in an *in vivo* environment, instead may become exposed and promote binding/capture in an *in vitro* environment. The process of fixation, done with acetone in this study, may also impact negatively upon endothelial adhesion molecules. These factors limit the interpretations that can be made from Stamper-Woodruff assays [201].

3.4.2.2 Adhesion of HPC-7s is Related to Oxidative Damage

Further experiments were conducted in order to gain a more precise understanding of the mechanisms behind increased adhesion of HPC-7s in IR injured heart tissue compared to sham heart tissue. Correlation analyses were performed to investigate the relationship between HPC-7 adhesion and the degree of oxidative damage or VCAM-1 expression. This study is the first to demonstrate a significant positive relationship between HPC-7 adhesion and the level of oxidative damage present in heart tissue. Essentially, more HPC-7s were found adherent in regions expressing high levels of oxidative damage, regardless of whether the heart had undergone IR injury or not. As cells become injured via oxidative damage, they will upregulate adhesion molecules [200]. As such, the positive correlation between HPC-7 adhesion and level

of oxidative damage is a reasonable finding. However, there was no significant relationship between HPC-7 adhesion and VCAM-1 expression. VCAM-1 is a ligand for VLA-4, which is comprised of the integrin subunits α4β1 (CD49d/CD29) and found on HSCs and as such, is an important molecule for permitting HSC-endothelial interactions [170]. Our lab has previously shown that HPC-7s express CD49d and CD18 through flow cytometry analysis and that clustering of CD49d was a potential mechanism for enhanced recruitment of these cells towards target organs such as the gut and liver [150, 170]. As this experiment found no correlation between HPC-7 adhesion and VCAM-1 expression, it is likely that the adhesion observed is mediated by other relevant molecules. This does not diminish the importance of the VLA-4-VCAM-1 interaction for HSC adhesion - merely that in an *in vitro* static adhesion assay, it did not favour that particular interaction. It should be reiterated that these static adhesion assays are not fully representative of the dynamic homing process that takes place in an *in vivo* environment. As such, some findings in this study may be attributable to the nature of static adhesion assays and may not be observed to a similar degree *in vivo*.

3.4.2.3 HPC-7s are Protective of Endothelial Cells Damaged by Oxidative Stress

Having demonstrated that HPC-7s could adhere to the injured heart, we further examined their ability to confer a vasculoprotective effect to cardiovascular ECs in culture. In order to achieve this, immortomouse vena cava ECs were damaged with H_2O_2 and the effects of HPC-7s on the subsequent production of O_2- (DHE staining) and the development of oxidative damage (8-OHdG staining) was investigated. HPC-7s were able to significantly reduce the production of O_2- in ECs at 72 hours. Furthermore, HPC-7s also reduced the subsequent

oxidative damage in ECs, but again this effect took time to materialise as it was only noted at 72 hours. HSCs are known to be able to resist oxidative stress which may explain why despite being exposed to H_2O_2 in the co-culture environment, they were able to protect the ECs from damage [202]. Their protective effect was only apparent after 72 hours and not 24 hours, possibly due to the initial damage caused by H_2O_2 being too early for the HPC-7s to have an influence. As DHE is a specific marker for O_2-, the protective effects of HPC-7s can be partly explained by their ability to modulate the generation of this particular ROS.

This study is the first to directly demonstrate the antioxidant ability of HPC-7s in culture using DHE staining. This data has important *in vivo* implications as it suggests that not only can HPC-7s decrease oxidative vascular damage, but they can also survive in an environment where they will be challenged by high levels of ROS, such as in the IR injured heart. Although we did not investigate how HPC-7s were able to reduce ROS presence, others have shown that various SCs can release antioxidant enzymes which can protect against oxidative stress [203, 204]. The antioxidant effect of HSCs can either be directly or indirectly afforded. After an injury stimulus, direct scavenging of free radicals can be undertaken by N-acetyl cysteine (NCA; a glutathione precursor) or resveratrol that are stored in HSCs [205]. These two small molecule antioxidants function to reduce ROS levels. The indirect antioxidant action of HSCs can be mediated through the nuclear factor erythroid 2-related factor 2 (Nrf2) pathway and Sirtuin activation that increases production and activity of antioxidant enzymes such as SOD, glutathione peroxidase and catalase [205]. Romeo et al. showed that $Nrf2^{-/-}$ HSCs were unable to efficiently reduce intracellular ROS levels after irradiation injury when compared to WT HSCs [206]. High levels of these antioxidant molecules and enzymes may allow for the reduction of oxidative stress within the environment surrounding HSCs through paracrine

actions. More research is required however, as very few studies have actually delved into understanding the mechanisms behind the beneficial antioxidant capabilities of HSCs.

3.4.3 Mesenchymal Stem Cells

This study also investigated and compared the adhesive and vasculoprotective effects of murine BM MSCs and human WJ MSCs in similar assays. As there are obvious differences between BM MSCs and WJ MSCs, such as age of the tissue of origin (adult vs neonatal) and the species (murine vs human), they will be discussed separately.

3.4.3.1 Adherence of BM MSCs to IR Injured Murine Heart Tissue

BM MSCs demonstrated a trend to adhere more to IR injured heart tissue compared to sham heart tissue. Although almost a doubling in the numbers of adherent BM MSCs was observed on IR tissue, there was no statistically significant difference between groups. Similar to HSCs, a number of adhesion molecules are present on MSCs that enable them to adhere to ECs and transmigrate through the endothelium. Examples of adhesion molecules present on MSCs include PSGL-1, L-selectin, P-selectin, VLA-4 and CD44 [207]. MSCs are unique in that they also express adhesion molecules normally present on ECs such as ICAM-1, ICAM-2 and VCAM-1 [208]. Similar to the HPC-7 experiment, these adhesion molecules may play a role in the adhesion of the BM MSCs on IR injured heart tissue.

Interestingly, WJ MSCs did not show any significant difference in their adhesion capabilities between IR injured and sham heart tissue. Furthermore, adhesion of WJ MSCs was very high

on all tissue types, with ~20-25 WJ MSCs adherent per field of view. In contrast, approximately 12-14 BM MSCs and 5-8 HPC-7s were generally adherent on IR injured heart tissue. This indicated that WJ MSCs were quite 'sticky' but in a non-discriminatory manner. Previous studies have shown that MSCs in general are more adherent in a static environment and this may account for the results seen with WJ MSCs [173]. Furthermore, as WJ MSCs are obtained from a neonatal source, they are potentially more readily adherent and more readily differentiable compared to adult MSCs like BM MSCs [160, 209]. A study by Donders and colleagues recently demonstrated that genes associated with cell adhesion were enriched in WJ MSCs [210]. Our intravital studies will aim to investigate whether different SC types home to the IR injured heart more effectively than others once injected into the peripheral blood. This homing process requires that cells attach to ECs of target injured tissue only. The fact that WJ MSCs do not differentiate between healthy and injured cardiac tissue *in vitro* raises concerns with regards to delivering them systemically and their selective homing to injured sites. This is more worrisome as an ongoing problem encountered with systemic MSC delivery into the peripheral blood is non-specific retention of cells in non-injured tissue such as the lungs. It may be that the delivery of WJ MSCs should be restricted to direct injections into the injured tissue (eg. intramyocardial), rather than systemically. However, it is important to consider the limitations of the Stamper-Woodruff assay, as discussed in section **3.4.2.1**.

3.4.3.2 Adhesion of BM MSCs is Related to Oxidative Damage

Similar to the observations seen with HPC-7s, BM MSC adhesion was found to have a significantly positive correlation with oxidative damage levels in murine heart tissue. An

increased number of BM MSCs were seen in regions that had high levels of oxidative damage, regardless of whether the heart had undergone IR injury or not. This is a reasonable finding as cells showcasing oxidative damage are more likely to upregulate adhesion molecules. Again, there was no significant correlation between BM MSC adhesion and VCAM-1 expression. It is therefore possible that BM MSC adhesion in these *in vitro* experiments is mediated by other adhesion molecules aside from the VLA-4-VCAM-1 interaction.

WJ MSCs showed no correlation in terms of adhesion numbers with either the levels of oxidative damage or expression of VCAM-1 in heart tissue, suggesting that its adhesion was not an active process dependent upon injury. This is not entirely unexpected given that no significant difference was observed in the adhesion capabilities of WJ MSC between IR injured and sham heart tissue. As discussed earlier, the increased characteristics of WJ MSCs that favour adhesion and differentiation may play a role in the number of adherent cells seen in this experiment, regardless of level of oxidative damage or VCAM-1 expression.

3.4.3.3 BM MSCs Reduce Endothelial Oxidative Damage Over 24 & 72 Hours; WJ MSCs Disrupt Endothelial Monolayer

EC oxidative stress assays were also conducted with BM MSCs and WJ MSCs. In contrast to HPC-7s, BM MSCs could not decrease the presence of ROS in the co-culture, as evidence by similar DHE staining throughout test and control wells. However, despite this, BM MSCs could significantly reduce the oxidative damage inflicted upon ECs at 24 hours and maintained this effect up until 72 hours. The mechanism behind this reduction was unlikely to be specifically due to the O_2- radical attenuation as no significant reduction was seen in DHE staining.

Therefore, potential mechanisms for this beneficial outcome could possibly include direct inhibition of H_2O_2 mediated damage or involve the increase of antioxidant enzyme activity that was not affecting superoxide [211]. The ability of BM MSCs to confer/maintain an anti-oxidative effect at 72 hours suggest they can continue to be beneficial long after they are introduced to a damaged environment in culture. This has important *in vivo* implications as it suggests that if their myocardial presence can be maintained, either through survival or delivery of more MSCs at later time points, they can continue conferring vasculoprotective benefits.

WJ MSCs were observed to be heavily disruptive on the endothelial layer in the culture experiments performed. Quantitative results were therefore not obtainable and proper interrogation of WJ MSCs in this assay setup was not achievable. This detrimental effect of WJ MSCs on the endothelial layer was most evident in the 72-hour experiments where the entire endothelial layer was seen to have dislodged from the plate well it was housed in. Interestingly, there were more adherent WJ MSCs in the place of the lifted endothelial layer at that time. Further investigation would be required to provide an explanation for this phenomenon. A possible theory is that WJ MSCs were releasing enzymes such as matrix metalloprotease 2 (MMP-2) that would cleave the adhesion between the ECs and the plastic well surface [160] allowing them access to adhere instead. A study by Munir et al. also directly co cultured WJ MSCs with ECs on pre-coated channel slides for over 24 hours with no disruption shown towards the EC layer [212]. A key difference with the co-culture approach in that study was the seeding of WJ MSCs on the EC layer for one hour only before washing, allowing only immediately adherent MSCs to persist in the co-culture. This would reduce the number of MSCs within each channel (from an initial seeding of ~13,500 cells), further

reducing its potential disruptive effect on the EC layer. A similar protocol adopted in our study might have allowed us to ascertain the impact of WJ MSCs without disrupting the EC layer.

3.4.4 Shape Considerations of HPC-7s, BM MSCs and WJ MSCs

An important observation made throughout this chapter was the size and shape of HPC-7s. They consistently appeared as small, spherical cells in culture. The obvious advantage of this for *in vivo* studies is that it would ensure that their systemic delivery would be less harmful and potentially enable more efficient homing to sites of injury and thus increase their therapeutic efficacy. In contrast, both types of MSCs were observed to be much bigger in size and shape compared to HPC-7s. This could become an issue in *in vivo* experiments. Indeed, one of the difficulties in enhancing recruitment of MSCs to the injured target tissue of interest is the sheer size of the cells being introduced, whereby bigger cells end up 'trapped' elsewhere in the circulation, particularly in the pulmonary capillaries [213]. A study by Kraitchman et al. showed that not only do MSCs injected intravenously initially localise to the lungs, it takes over 24 hours for them to redistribute to other organs due to their size [214]. HSCs may become 'entrapped' in the lungs too, such as shown by Dooner et al. in a study that suggested that the lungs may be a 'hotspot' for SCs through immunohistological and flow cytometry analysis, especially during certain cell cycle phases [215]. However, redistribution of HSCs occurs much quicker: within 24 hours [216]. As our intravital experiments would be focussed on the acute phase of myocardial IR injury and that homing of these cells to the target organ was deemed important, this was another benefit of using HPC-7s over MSCs.

3.4.5 Conclusion

The two main aims of this chapter were to firstly establish a successful injury to the left ventricle of the heart using the LAD ligation model and secondly determine which SC type could adhere more to the injured heart and confer greater endothelial protection. The latter was important as this allowed us to 'triage' which SC would have the highest likelihood of being therapeutic when taken forward into future *in vivo* intravital experiments. It is unfortunate that in the past decade or so, the field of regenerative medicine and cellular therapy for cardiovascular diseases has moved from the use of HSCs to a focus on MSCs. Our presented data suggests that HPC-7s are more adhesive and vasculoprotective than BM MSCs in the assays used. In conclusion, we found that HPC-7s were the candidate to take forward as they (i) were able to discriminate between healthy sham and injured heart tissue with regards to their adhesion capabilities (ii) provided the highest level of adhesion onto IR injured heart tissue and (iii) were able to protect ECs from the impact of oxidative stress, a known component of IR injury. We present novel data here showing the correlation between HPC-7s adhesion and oxidative damage levels in frozen heart tissue sections, further establishing a potential mechanism by which HPC-7s could provide vasculoprotection. We speculated that the enhanced opportunity for these cells to home towards the injured heart would allow the cells to confer their protective benefits onto the heart, in comparison to MSCs that were judged to be more likely to also adhere to non-injured organs. The following chapter will examine the vasculoprotective effects of HSCs by investigating the real-time beneficial effects of using HPC-7s as a form of cell therapy during cardiac IR injury utilising intravital microscopy.

CHAPTER 4: MICROCIRCULATORY DISTURBANCES IN THE IR INJURED HEART – VASCULOPROTECTIVE EFFECTS OF STEM CELLS AS DETERMINED *IN VIVO*

4.1 Introduction

The role that the coronary microcirculation plays in MI is not well appreciated due to a lack of understanding of the dynamic events that occur at the microvessel level *in vivo* during an MI. Clinical imaging techniques such as an angiogram only allow visualisation of large coronary vessels, leaving the microcirculation untouched. Pre-clinical studies have also encountered difficulty in visualising the changes that occur at this level, as the beating mouse heart is notoriously difficult to image. Technological limits have also hampered acquisition of high-quality images from these experimental studies. Recent microscopy advancements however, have allowed us to modify existing surgical techniques in order to accommodate real-time imaging of a beating mouse heart.

In the previous chapter we demonstrated that the temporary LAD ligation model for inducing myocardial IR injury did indeed lead to microvascular perturbations in the left ventricle. These included increased oxidative stress and the presence of inflammation as evidenced by increased endothelial adhesion molecule expression. These damaging effects were assessed using conventional immunohistological methodology. However, in this chapter we present data using a novel model we have recently developed that allows real-time imaging of the dynamic microcirculatory events taking place in the beating mouse heart post-reperfusion *in vivo*. We propose to utilise intravital microscopy of the beating mouse heart to answer three main questions: (i) what are the perturbations that take place in the beating coronary microcirculation post-reperfusion (ii) do stem cells home to heart and adhere to coronary microvessels (discussed in Chapter 5) and (iii) do they specifically protect injured coronary blood vessels from damage i.e. inhibit any inflammatory and thrombotic events that may

arise, improve any disturbances in myocardial blood perfusion etc. Events such as the trafficking / homing of circulating cells, be they stem cells or blood cells, and changes in blood flow and myocardial perfusion are a range of dynamic events that cannot be captured with conventional immunohistochemical analysis, which simply provides a 'static' snapshot in time. Dynamic data of this nature can only be acquired through intravital imaging and not histologically. Although the presence of circulating cells within coronary microvessels can be imaged in tissue sections using immunostaining, these images do not inform us whether cells are genuinely adherent in the heart or simply caught in time passing through it. We also obtain no indication of exogenously injected potentially therapeutic cells causing blockage of blood flow in the blood vessels in which they are captured – if this is significant, it may cause more damage than good and impact on their therapeutic effectiveness. More importantly, this chapter will investigate the vasculoprotective effects of stem cells in the beating heart. Immunohistochemical analysis can, at most, provide information on neutrophil / platelet / monocyte infiltration. It cannot indicate whether the heart has adequate blood perfusion, alterations in functional capillary density, whether the velocity of circulating cells has been reduced to a level that is conducive to being pro-adhesive, whether coronary microvessels are viable and not 'leaky' etc.

Therefore, in this chapter we will show data acquired through intravital microscopy of the beating mouse heart. High-end microscopes coupled together with the creation of a 3D-printed stabiliser have allowed us to obtain direct images of the microcirculation of the mouse heart. This has allowed us to image the dynamic changes that occur in the microcirculation in the immediate aftermath of our *in vivo* myocardial IR injury model, which replicates the reperfusion that takes place post-PCI in the setting of MI. Understanding the changes that

occur during this period of reperfusion-mediated injury is important in order to investigate the most suitable form of therapy to diminish, if not reverse, the microvascular effects of IR injury.

As discussed previously, the thrombo-inflammatory response is an important component of IR injury [4, 65]. Understanding the role and impact of cells such as platelets, neutrophils and monocytes in myocardial IR injury will allow us to consider appropriate targeted therapy. For instance, the use of stem cells for its therapeutic benefits has been hotly debated in the research community due to its limited success in the clinical setting. There is a lack of understanding regarding the mechanisms behind any beneficial effects that stem cells may provide in cardiovascular disease, including MI. As such, we sought to investigate the vasculoprotective effects of stem cells through the use of IVM. In particular, we chose to investigate the potential of HSCs as cell therapy in myocardial IR injury due to our findings in the previous chapter which highlighted a number of positive aspects of HPC-7s for use in this regard.

4.1.1 Hypotheses and Aims

This chapter therefore focussed on firstly characterising in detail the impact of myocardial IR injury on the mouse beating heart coronary microcirculation *in vivo* through IVM. We further investigated whether the ability of HPC-7s to potentially be beneficial relied on a vasculoprotective mechanism of action. The main aims and hypotheses of this chapter are shown below.

- This chapter aimed to firstly establish a novel method whereby myocardial stabilisation of a small region of the beating heart left ventricle would subsequently allow real-time intravital imaging of the coronary microcirculation *in vivo*.

- This imaging model would then be used to assess the healthy and IR injured coronary microcirculation. Specifically, the coronary microvessels, functional capillary density and the recruitment of endogenous inflammatory cells (neutrophils, platelets, monocytes and macrophages) would be visualised using fluorescent labels to allow the impact of IR injury on these components to be determined. To further investigate changes in ventricular blood perfusion, laser speckle contrast imaging (LSCI) would also be combined with intravital imaging. **HYPOTHESIS:** Myocardial IR injury leads to tissue infarction by promoting a thrombo-inflammatory response specifically within the coronary microvessels and through causing disorganisation of microvessels of the heart. These multiple events would lead to a decrease in effective ventricular blood perfusion in the injured area due to a decrease in the functional capillary density.

- The ability of HPC-7s to provide any benefit to the IR injured beating heart through effects on the microcirculation will also be assessed. **HYPOTHESIS:** HPC-7s will reduce infarct size in the IR injured heart by inhibiting any thrombo-inflammatory events, protect the structural integrity of the microvessels and increase regional blood flow perfusion through the heart.

4.2 Methods

Detailed methods are described in Chapter 2. Briefly, in order to determine infarct size after myocardial IR injury, dual Evans Blue/TTC staining was utilised. The LAD artery was ligated for 45 minutes to induce ischaemia followed by 4 hours of reperfusion in an anaesthetised mouse. The LAD was re-ligated and Evans Blue dye was injected intra-arterially to delineate the AAR from IR injury. The heart was harvested and frozen at -80^{o}C for one hour. The heart was then sliced transversely at ~2 mm thickness and incubated with TTC for 10 minutes. After staining, the heart slices were washed in PBS and imaged.

In order to perform IVM, IR injury was similarly induced in the anaesthetised mouse. As soon as the LAD was un-ligated, a 3D-printed stabiliser was attached to the reperfused left ventricle using biological glue. As the time taken to attach the stabiliser varied, the first recording was always taken 30 minutes into reperfusion, standardising timings between experiments. Thereafter, 2-minute videos were taken every 15 minutes for 2 hours. For some experiments, intravital imaging of a sterile burn injury inflicted on the left ventricle using a microcautery was performed. A 3D-printed stabiliser was first attached to the heart and then a 2-minute video was captured. After 5 minutes, a small burn injury was performed inside the stabilised region. Videos were then taken every 20 minutes for 2 hours.

For IVM, to fluorescently label endogenous neutrophils and platelets, fluorescent antibodies were used. A PE-conjugated rat anti-mouse Ly6G antibody and an APC-conjugated rat anti-mouse CD41 antibody were injected intra-arterially in order to label neutrophils and platelets respectively. Exogenous platelets obtained from donor mice were isolated and then fluorescently labelled using CFSE before being injected intra-arterially into experimental mice.

In the imaged mice, these labelled antibodies or donor platelets were given 5 minutes prior to reperfusion whilst in mice undergoing cardiac sterile burn injury, these were given 10 minutes prior to the initial pre-injury video capture. To label endogenous monocytes, fluorescent microparticles/beads were injected intra-arterially 10 minutes prior to ischaemia or 10 minutes prior to the initial pre-burn injury video capture. Attempts were also made to label macrophages using an APC-conjugated rat anti-mouse F4/80 antibody injected 5 minutes prior to reperfusion. Vascular patency was investigated in some experiments too, where FITC-BSA was injected 2 hours after reperfusion had elapsed in order to observe the perfusion state of the coronary microvasculature.

In order to investigate any potential dynamic changes in regional myocardial blood flow during injury, LSCI was utilised. Myocardial IR injury was induced as described above. An LSCI device was positioned above the anaesthetised mouse beating heart and videos (1000 frames) were captured during pre-ischaemia, ischaemia and reperfusion. During reperfusion, videos were captured every 15 minutes for 2 hours.

HSCs were provided as a form of cell therapy in several experiments. To achieve this, 2 x 10^6 HPC-7s were injected intra-arterially into mice undergoing IR injury. This was performed within 5 minutes of reperfusion in order to maximise the potential benefits of cell therapy.

4.3 Results

4.3.1 Developing a Successful Protocol for Imaging the Mouse Beating Heart Coronary Microcirculation *in vivo*

As our work in this chapter focussed heavily on utilising IVM to investigate myocardial IR injury, it was necessary for us to optimise our surgical protocol in order to produce reliable and reproducible results. Conducting IVM of the mouse heart was very challenging. Indeed, very few researchers have attempted this technique, and even less so whilst investigating IR injury. There were no guidelines that we could easily refer to or a trained specialist that we could gain advice from in order to optimise our methods. Our optimisation methods came through our own experience working with the model.

A number of changes occurred during the optimisation of our model. One such example was changing our surgical technique by cutting through and removing the left 3rd rib in order to gain a larger exposure of the heart. This proved necessary as attempting to place the stabiliser without removing a rib was needlessly difficult, even when using a tissue retractor. Another change we made was to utilise a micromanipulator in order to slowly lower and accurately attach the 3D stabiliser to the mouse heart. Initially, we used a fixed/rigid stand connected to our surgical board to hold our 3D stabiliser. However, the micromanipulator provided a more delicate approach to this which was necessary in order to safely attach our 3D stabiliser. We also adjusted the design and size of the 3D stabiliser created. Our initial model was similar to the version created by Vinegoni and colleagues in their beating heart imaging model [166]. We found that the diameter of this version was larger than necessary, as the confocal microscope would only focus on less than half of the area stabilised. As such, we reduced the

dimensions of the stabiliser, making it smaller and lighter. This proved beneficial in allowing us to more accurately attach our stabiliser to the mouse heart. The various stabiliser designs used by the Kalia group, some of which were initially developed and tested as part of this thesis, are shown in ***Figure 4.1.***

Overall, it took the better part of a year for us to optimise our surgical protocol in order to obtain reliable and reproducible results. This was a very challenging technique to setup and conduct, but was ultimately fruitful in providing us with novel data that enriches our understanding of cardiac IR injury.

4.3.2 HPC-7 Therapy Reduces Infarct Size after Myocardial IR Injury

Although the studies conducted in Chapter 3 confirmed that the LAD ligation protocol used was eliciting an injury to the heart and coronary vasculature, we further confirmed in this chapter that this resulted in the development of an infarct. TTC staining experiments were carried out in order to outline the infarcted area and to determine whether HPC-7 therapy would reduce the infarct size after IR injury. White necrotic areas, indicative of infarct size, were much larger in IR injured hearts as compared to IR injured hearts that had been treated with HPC-7s ***(Figure 4.2A)***. Necrotic areas were still present in the treated hearts, however, conservation of red viable tissue was more pronounced. Statistical analysis of this data showed that there was a significant ($p<0.01$) reduction in infarct size as a percentage of area at risk in the IR injured hearts treated with HPC-7s ***(Figure 4.2B)***. Notably, this reduction was 2-fold, from ~45% in IR injured hearts to ~22% in HPC-7 treated IR injured hearts.

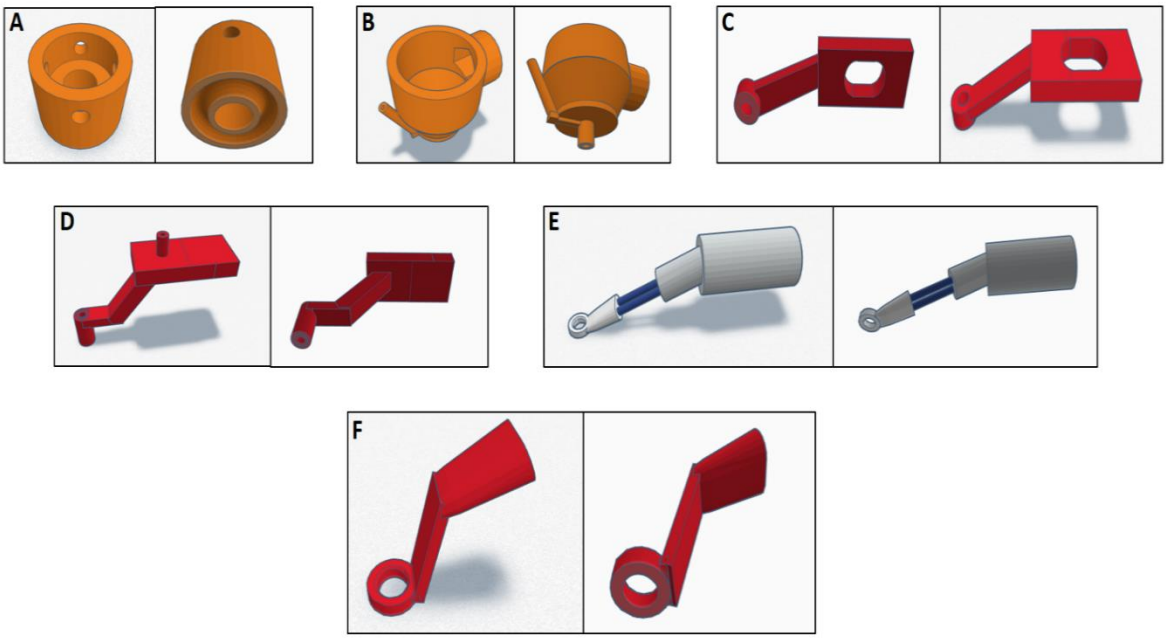

Figure 4.1. Optimisation of the Beating Heart Stabiliser. *A number of design changes were made to optimise the heart stabiliser which primarily involved moving from suction attachment to the heart to glue adhesion and making the stabiliser dimensions smaller and lighter. This proved beneficial in allowing us to more accurately attach our stabiliser to the mouse heart.* ***(A)*** *Original version (not used as part of this thesis) which had holes for string to pass through and be attached to the animal board. The recess in the base was for the glue to dissipate if too much was added. This version moved too much in the up and down directions and was difficult to hold tight on XY.* ***(B)*** *In this version, the objective went inside the central cavity with imaging taking place through the central channel. The arm was for the application of a vacuum – early designs used vacuum suction to attach the stabiliser to the heart.* ***(C)*** *This was the first design in which an arm that entered 'into' the chest cavity. The hole in the middle of the rectangular component was to bolt the stabiliser onto the stand which was also custom designed and used with it.* ***(D)*** *Another version of a vacuum held stabiliser. The vacuum channel came through the top and down to the base of the stand. Although this design worked well, the suction action tended to leave a mark on the surface of the heart.* ***(E)*** *This design was used in the current thesis. It had a* smaller *imaging window, with an attached holder for a metal rod that connected it to a micromanipulator.* ***(F)*** *Subsequent research in the Kalia lab have used this newer version which has a longer arm allowing it to get into the chest cavity further.* ***Dr Dean Kavanagh, Microcirculation Research Group, Institute of Cardiovascular Sciences, UoB, is thanked for providing these images.***

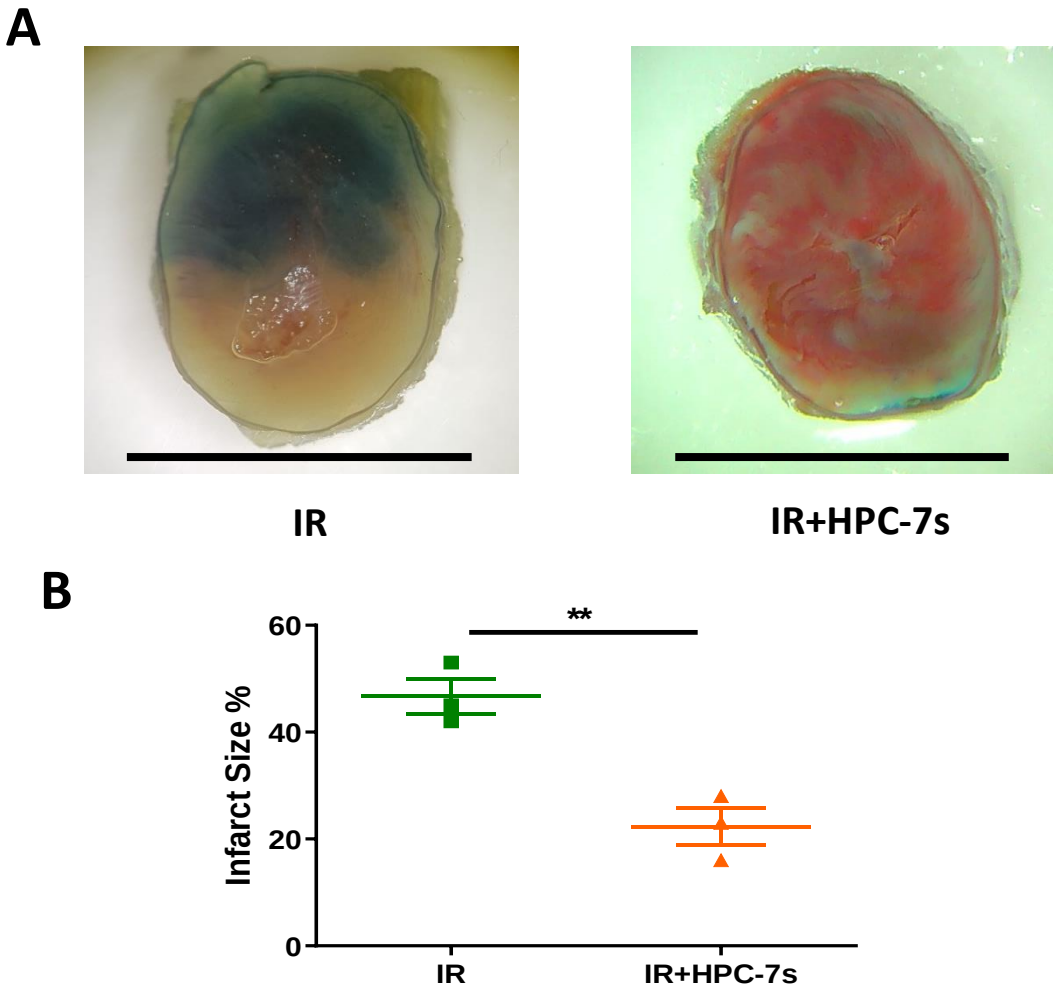

Figure 4.2: HPC-7 therapy reduced infarct size after myocardial IR injury. (A) *Dual Evans Blue / TTC staining showed (i) areas not affected by IR injury (blue) (ii) area at risk of IR injury (red) and (iii) necrotic areas due to IR injury (white) in both IR injury alone and IR injury + HPC-7s hearts. Necrotic areas were still present in the HPC-7s pre-treated hearts, however, conservation of red viable tissue was more pronounced* ***(B).*** *HPC-7s were able to significantly reduce the infarct size as detected using TTC after myocardial IR injury (~22%) when compared to IR injury alone (~45%). Statistical analysis was performed using an unpaired t-test. ** p<0.01; N=3 per group. Scale bar = 5mm.*

4.3.3 Analysing Regional Blood Flow Dynamics in Beating Mouse Hearts using Full Field Laser Speckle Contrast Imaging

Perturbations in blood flow are a common occurrence during myocardial IR injury. Understanding how HPC-7s may impact upon this required investigation of the overall changes in blood flow dynamics within the injured left ventricle during myocardial IR injury. Quantification of left ventricular myocardial blood flow was conducted utilising an LSCI device. This is the first time this imaging modality has been applied to the mouse beating heart and the acquired data analysed. Interpretation of data obtained was challenging due to heart motion and the dynamics of ventricular myocardial blood flow during systole and diastole. Fortunately, left ventricular diastolic and systolic events corresponded nicely with characteristic peaks and troughs on flux recordings respectively. These represented a time point in the cardiac cycle when the heart muscle was highly and poorly perfused respectively (***Figure 4.3A****)*. During diastole, the left ventricular chamber blood volume is high due to ventricular filling and since the muscle is relaxed, myocardial blood flow was at its highest. As the heart contracts during systole, the left ventricular chamber blood volume is low due to blood ejection. Muscle contraction compresses the microvessels of the heart and decreases flow (***Figure 4.3B***). *Basic Speckle Analysis* software (SpAn) was written in-house (Dr Dean Kavanagh, Institute of Cardiovascular Sciences, UoB) and allowed easy identification and collation of the high and low points from flux images (***Figure 4.3C***).

As flux readings obtained contained some component derived from heart motion, it was necessary to viably distinguish readings due to blood flow. To achieve this, we covered part of the left ventricle with a tissue paper in order to capture flux readings purely due to heart

movement ***(Figure 4.4A)***. When flux readings were compared between covered and uncovered area, we were able to attribute flux changes to genuine blood flow. This was because muscle contraction provided a fairly consistent reading between experimental groups ***(Figure 4.4B)***.

4.3.4 Laser Speckle Contrast Imaging Revealed a Sustained Reactive Myocardial Hyperaemia in Response to IR injury Alone and IR injury + HPC-7s

Having established a method to image myocardial perfusion and analyse flux data, we then went on to apply the LSCI method to investigate the dynamic changes that occurred to blood flow in the left ventricle during IR injury. For comparative purposes, we focussed on diastolic events only. In mice undergoing IR injury, a baseline level of flux was obtained during pre-ischaemia indicative of good perfusion and demonstrated by a more yellow/red heat-map. During ischaemia, as expected, a noticeable decrease in flux was observable as demonstrated by a change in the heat map image to a primarily cooler blue hue. After reperfusion, there was a noticeable surge in flux as the heat-map image obtained displayed the heart in a much warmer red hue. The raw data displayed live on the LSCI monitor showed that ischaemia reduced flow with arbitrary flux values decreasing from ~1700 to ~1400. This nicely confirmed that the LAD ligation was successfully reducing blood flow in the myocardium. An increase to an arbitrary value of ~2000 was noted after reperfusion ***(Figure 4.5A).***

The raw data of arbitrary values was presented graphically as mean normalised flow flux and showed that in sham mice, ventricular blood flux did not change throughout the course of imaging. In IR injured mice, as expected, ischaemia decreased this value. Reperfusion was

associated with a rapid and significant ($p<0.001$) increase in this value when compared to pre-ischaemic values. Interestingly, this reactive hyperaemic response was sustained throughout the 2-hour period of reperfusion. A similar pattern of events was observed in IR injured mice receiving HPC-7s therapy ***(Figure 4.5B)***. Statistical analysis showed that there was a significant overall increase in myocardial blood flow in the IR injured hearts when compared to sham hearts ($p<0.0001$) and also between the IR+HPC-7s injured hearts and sham hearts ($p<0.05$) during the period of reperfusion ***(Figure 4.4B)***. However, there was no difference between the two IR injured groups.

4.3.5 Intravital Microscopy Revealed Myocardial IR Injury was Associated with Impaired Capillary Perfusion which was Improved with HPC-7s

LSCI was only able to assess the overall regional blood flow and perfusion of the left ventricle. Therefore, IVM was used to image the coronary microcirculation at a much higher resolution and at a cellular level. In the first set of experiments, FITC-BSA was injected at 2 hours post-reperfusion into mice undergoing sham, IR injury alone and IR injury with infused HPC-7s. In sham mice, FITC-BSA labelling showed a well perfused extensive network of capillaries. The capillaries were seen sitting parallel to the muscle fibres, with cross connections along their length. The field of view obtained showed no areas devoid of perfused capillaries with medium-sized vessels also visibly well perfused (***Figure 4.6A***). In IR injury however, the extensive network of capillaries had become disorganised (loss of structure) and multiple areas of non-perfused capillaries were seen. These patchy areas implied poor functional capillary density. The extent of this was substantial at times, where half the field of view

appeared non-perfused. Some capillaries were also identified as slightly wider, due to accumulation of FITC-BSA. Interestingly, medium-sized vessels were still visibly well perfused (***Figure 4.6B***).

Utilising HPC-7s as a form of cell therapy preserved the structure of the microvessels in the heart during IR injury. Fewer patchy 'gaps' were observed in comparison to purely IR injured hearts ***(Figure 4.6C)***. Statistical analysis of data obtained showed a significant ($p<0.05$) reduction in microvascular perfusion in IR injured hearts compared to sham with a significant ($p<0.05$) increase in HPC-7s treated IR injured hearts compared to IR injured hearts not receiving therapy ***(Figure 4.6D)***.

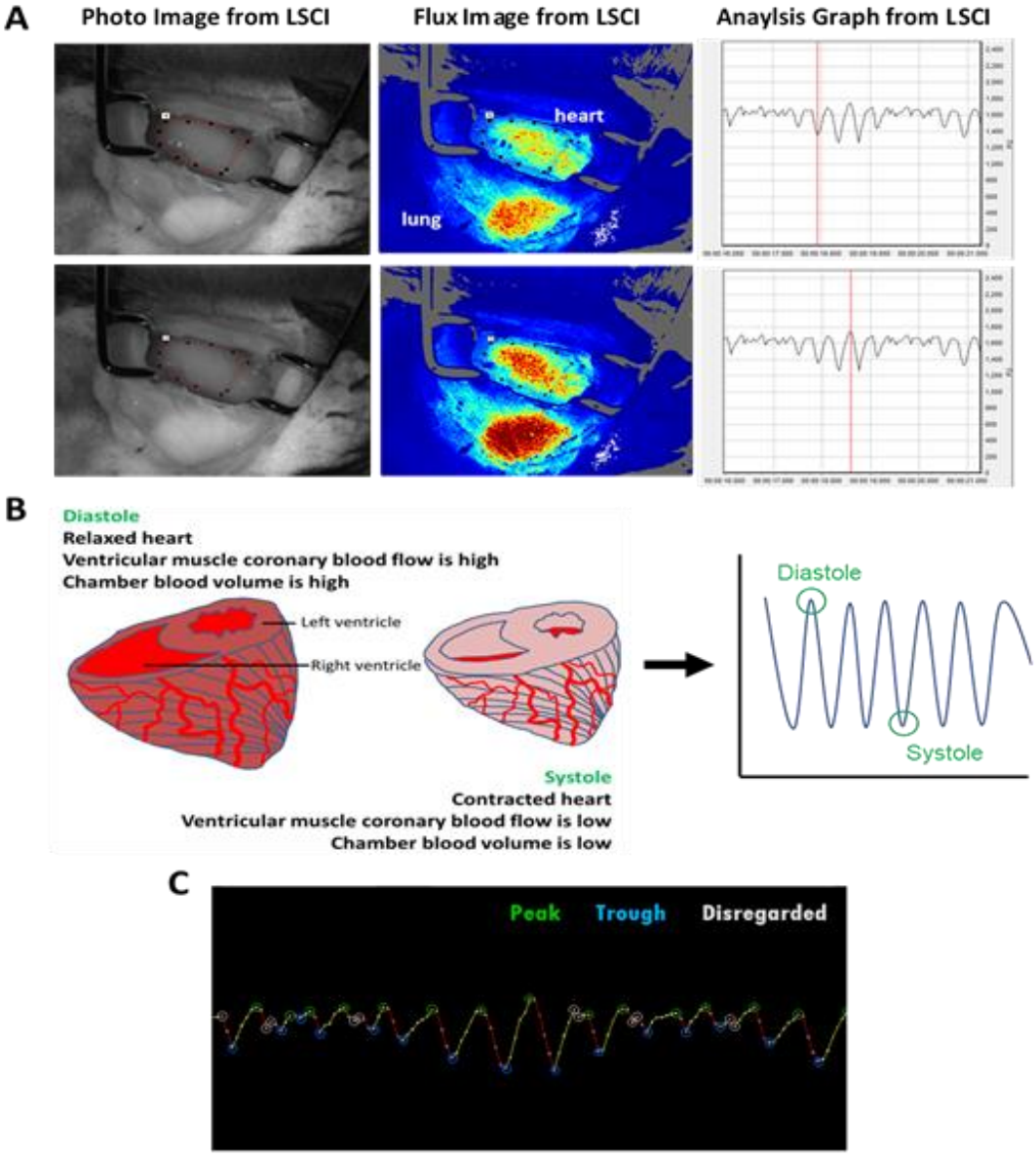

Figure 4.3. Full-field laser speckle contrast imaging (LSCI) and subsequent analysis of the beating mouse heart blood flow following myocardial IR injury. (A) *Diastole and systole presented as peaks and troughs respectively. These can be clearly seen on the analysis graphs. Left panel = Photo; Middle panel = Flux image; Right panel = Flux graph for the area demarked on the flux image. In the upper analysis image, a trough is highlighted by a red line and in the bottom analysis image, a peak is highlighted by a red line. These clearly correspond to moments when the heart is poorly and highly perfused respectively.* ***(B)*** *During diastole, chamber blood volume is high due to ventricular filling. Since the heart muscle is relaxed, myocardial blood flow is also at its highest - peaks. During systole, the heart contracts and chamber blood flow is low due to blood ejection. Muscle contraction compresses the microvessels of the heart and decreases flow - troughs. LSCI does not penetrate the ventricular wall, thus cannot image chamber flow.* ***(C)*** *Basic Speckle Analysis software (SpAn) was written in-house and allowed easy identification and collation of the high and low points from flux images. High peaks (green circle) were confirmed as such by the presence of two decreasing flux points thereafter. Low peaks (blue circle) followed a similar logic. If this condition was not satisfied, the peak was disregarded (white circle). Data presented hereafter analyses flux values during diastole.*

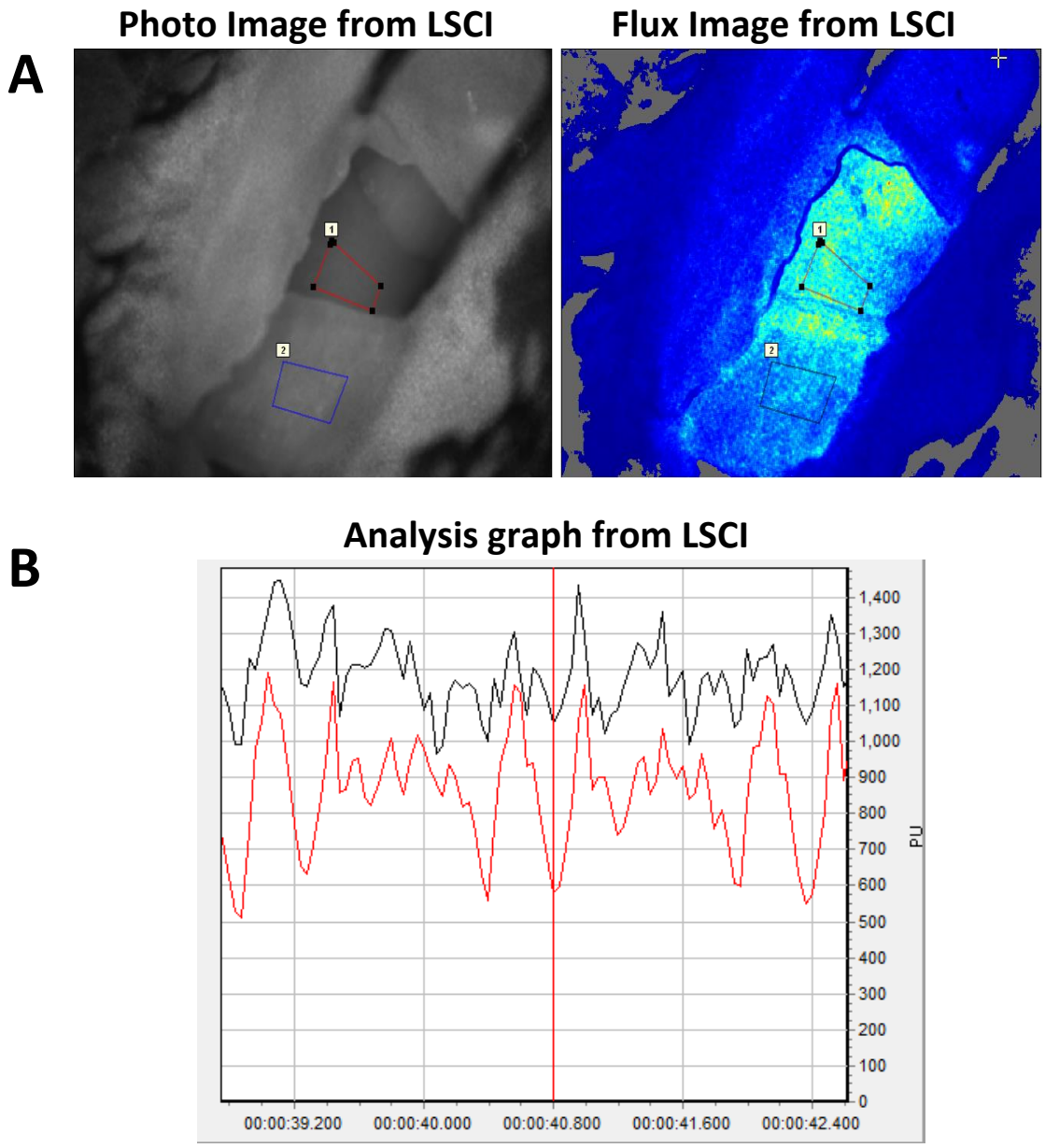

Figure 4.4. LSCI flux values due to heart movement versus flux values due to actual myocardial blood perfusion. ***(A)*** *As flux readings obtained contained some component derived from heart motion, it was necessary to viably distinguish readings due to blood flow. To achieve this, we covered part of the left ventricle with a tissue paper in order to capture flux readings purely due to heart movement. The uncovered heart region (measuring heart motion + perfusion) is represented by the red box while the tissue covered heart region (measuring heart motion only) is represented by the blue/black box.* ***(B)*** *The analysis graph shows a clear difference between recordings obtained from heart motion alone (red) and that obtained from heart motion + perfusion (black). This difference in flux is attributable to blood flow.*

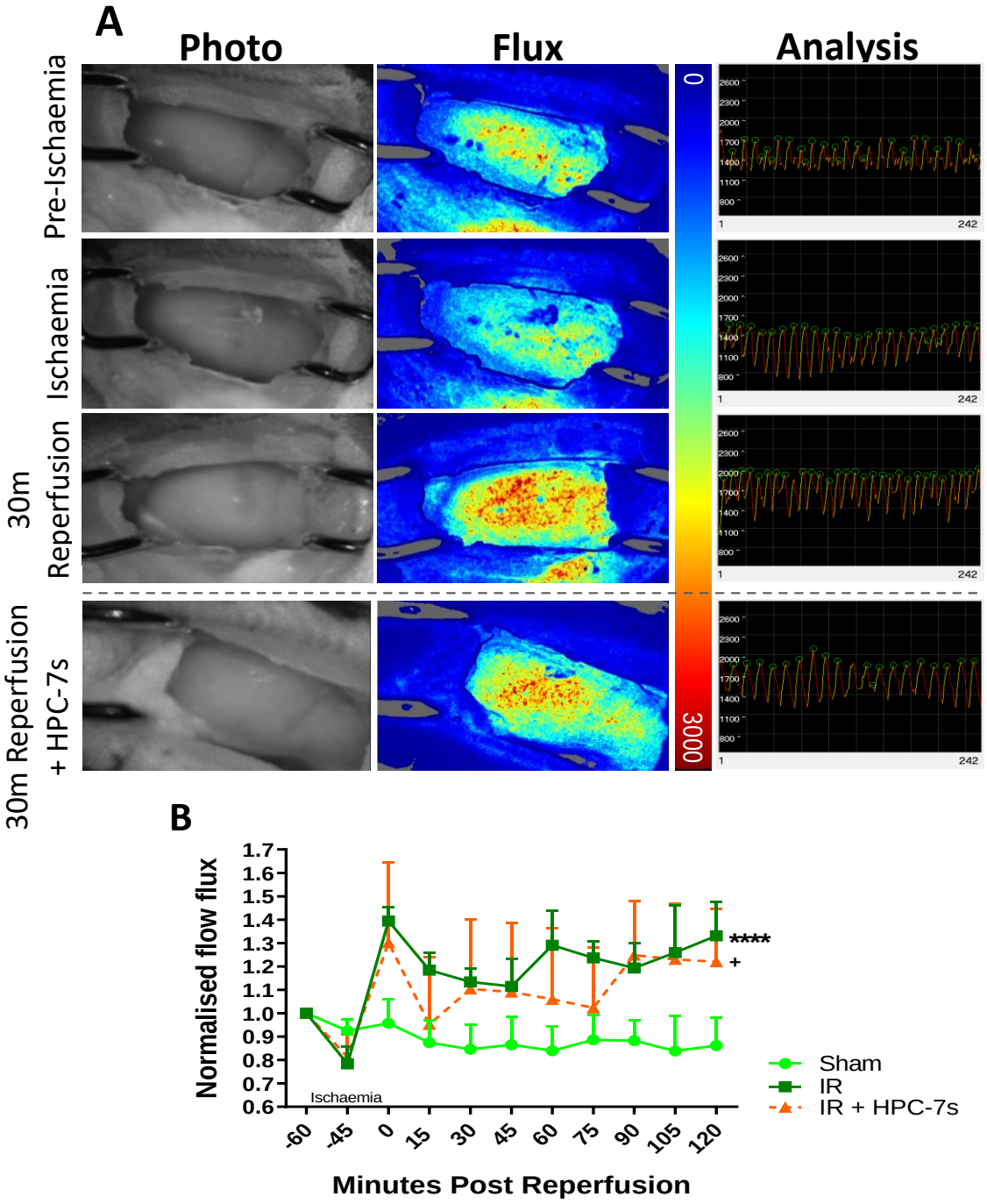

Figure 4.5. LSCI revealed a sustained reactive myocardial hyperaemia in response to IR injury and IR injury + HPC-7s. (A) *Representative photos obtained during LSCI experiments of the beating heart and analysis graph. All flux images have been normalised on the same palette settings. In mice undergoing IR injury, a baseline level of flux was obtained during pre-ischaemia indicative of good perfusion and demonstrated by a more yellow/red heat-map. During ischaemia, as expected, a noticeable decrease in flux was observable as demonstrated by a change in the heat map image to a primarily cooler blue hue. After reperfusion, there was a noticeable surge in flux as the heat-map image obtained displayed the heart in a much warmer red hue. The raw data displayed live on the LSCI monitor showed that ischaemia reduced flow with arbitrary flux values decreasing from ~1700 to ~1400. An increase to an arbitrary value of ~2000 was noted after reperfusion.* ***(B)*** *Normalisation of raw data obtained (mean normalised flow flux). Flux values remain consistent in sham mice. This drops during ischaemia. A rapid and sustained reactive hyperaemic response is seen during reperfusion. IR injury induces a significant flux difference to sham mice regardless of HPC-7 presence however, there was no difference between the two IR injury groups. ****p<0.0001, + p<0.05; ANOVA with Sidak's multiple comparison test. N=3 per group.*

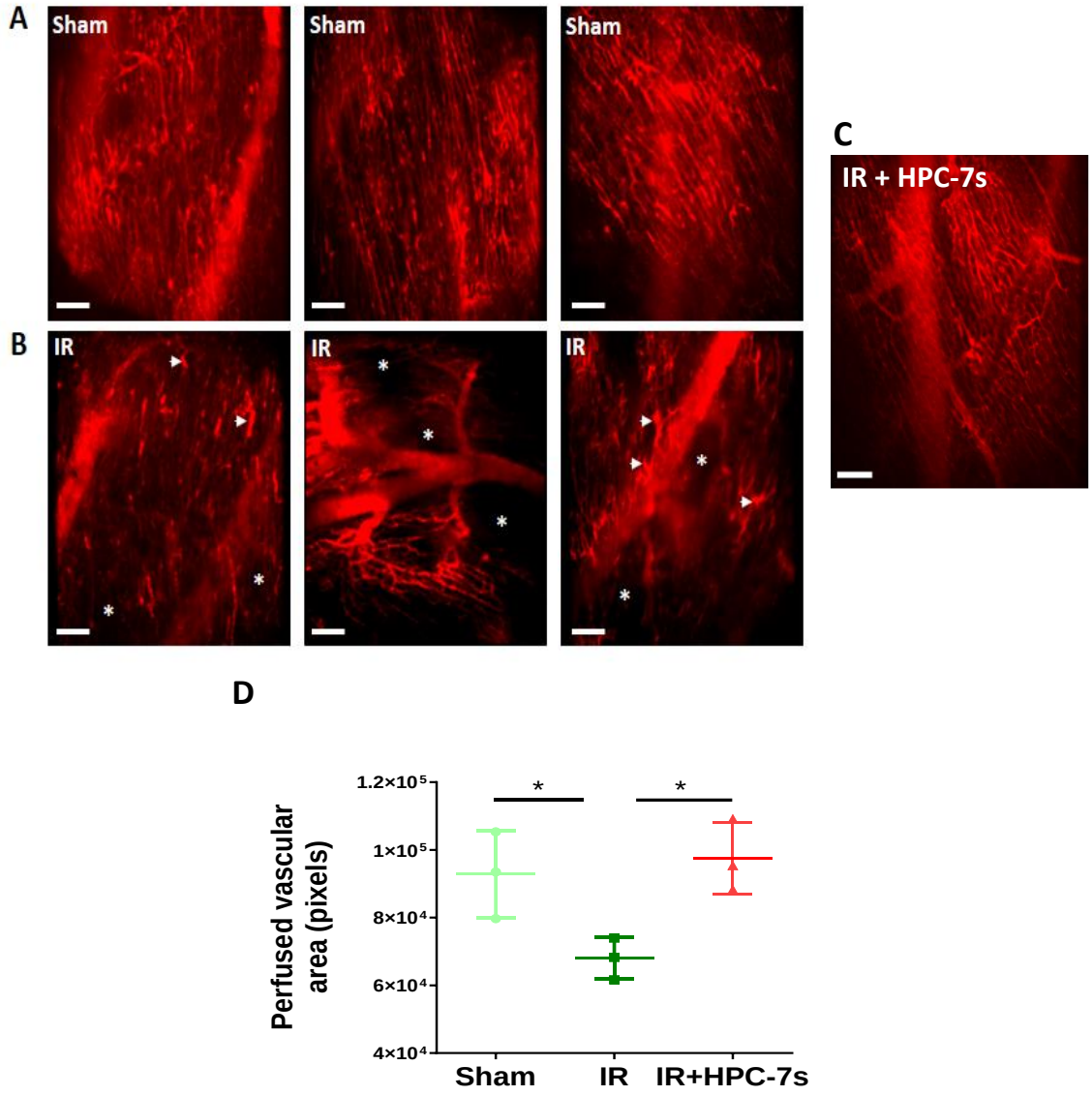

Figure 4.6. Intravital microscopy demonstrated that myocardial IR injury is associated with impaired capillary perfusion and a disturbed microvascular organisation. HPC-7s therapy significantly improves microvascular perfusion. *Representative intravital images obtained when FITC-BSA was administered 2hrs post-reperfusion.* ***(A)*** *In sham mice, FITC-BSA labelling showed a well perfused extensive network of capillaries. The capillaries were seen sitting parallel to the muscle fibres, with cross connections along their length. The field of view obtained showed no areas devoid of perfused capillaries with medium-sized vessels also visibly well perfused (out of focus in some of the images).* ***(B)*** *This well organised structure is lost in IR injury. Patchy areas devoid of vasculature (*) are observable. Some capillaries were also identified as slightly wider, due to accumulation of FITC-BSA. Interestingly, medium-sized vessels were still visibly well perfused.* ***(C)*** *These perturbations are not demonstrated in mice undergoing IR injury and receiving cellular therapy.* ***(D)*** *The difference in microvascular perfusion was significant between the hearts of sham and IR injured mice ($p<0.05$) and IR injured vs IR injured + HPC-7s mice ($p<0.05$). Statistical analysis was performed using a one-way ANOVA with Sidak's multiple comparison test. N=3 per group. Scale bar = 100µm.*

4.3.6 Intravital Microscopy Revealed an Increase in Endogenous Neutrophil Adhesion Following Myocardial IR injury but these did not Appear to Compromise Blood Flow

Clearly, perfusion was disrupted in the myocardium of IR injured hearts. In order to determine the cellular mechanisms behind this, IVM experiments were carried out to investigate the kinetics of endogenous neutrophil recruitment following IR injury. Initial experiments were carried out in sham mice and, interestingly, adherent neutrophils were readily present within coronary capillaries (***Figures 4.7A and 4.8A***). In order to ascertain whether this was due to the placement of a stabiliser causing a local inflammatory response, intravital videos were also captured from exposed beating hearts without the application of a stabiliser. Although images obtained were understandably blurry, difficult to obtain and out-of-focus, adherent neutrophils were still present in sham non-stabilised hearts. As expected, the stabilised hearts provided higher-quality images which could be quantitated and further analysed ***(Figure 4.7A)***. In stabilised sham hearts, neutrophils were found in numbers higher than was expected with approximately 50-60 adherent neutrophils observed per field of view. These were present at 30 minutes, when the first intravital image was taken, and this number did not tend to increase with time ***(Figure 4.8A).*** Some adherent neutrophils, at first glance, appeared to be firmly adherent within coronary capillaries. However, when captured videos were closely inspected, some of these appeared to be patrolling the myocardium in sham mice. Indeed, neutrophils were moving short distances or 'patrolling' the length of the capillary ***(Figure 4.9).***

Whilst adherent neutrophils were present in the sham microcirculation, they did not disrupt blood flow. This was demonstrated by labelling both endogenous neutrophils and injecting FITC-BSA into the same mouse. Adherent neutrophils in sham mice did not compromise blood

flow as evidenced by FITC-BSA perfused capillaries being visible in the whole field of view including in capillaries in which neutrophils were adherent ***(Figure 4.7B)***.

Myocardial IR injury induced a marked and significant ($p<0.0001$) increase in individual neutrophil adhesion, again primarily within coronary capillaries. Neutrophil clusters or aggregates were also identified ***(Figure 4.7C).*** Approximately 150-160 adherent neutrophils were observed per field of view which was a 3-fold increase compared to adherent neutrophils found in sham hearts. Similar to the sham mice, this increased adhesion was present at 30 minutes post-reperfusion and did not increase with time ***(Figure 4.7C and 4.8A).*** Approximately 10 free flowing neutrophils were also identified at each time point trafficking through sham hearts***.*** The number of neutrophils observed trafficking through IR injured hearts was approximately 20-30 at each time point. There was no significant difference between the two groups ***(Figure 4.8B).***

4.3.7 Intravital Microscopy Revealed that Platelet Microthrombi Contributed to Microvascular Occlusive Events Following Myocardial IR injury

Endogenous platelet microthrombus formation was rare in sham mice. However, a significant ($p<0.001$) increase in their generation and presence was noted in IR injured hearts and quantitated as an increase in their integrated fluorescence density ***(Figures 4.10 and 4.11A)***. Platelet aggregates were either small and rounded (more numerous) or formed significant microthrombi that were observed primarily within the capillaries and often stretched along the vessels (less numerous). At times, these microthrombi aggregates were often seen to be comprised of both neutrophils and platelets ***(Figure 4.10A)***.

As shown previously, blood flow was compromised in IR injured hearts ***(Figure 4.6B)***. Interestingly, this was observed to be more common in areas with striking aggregates of platelet and neutrophil microthrombi. These were deemed occlusive as they were often identified upstream of areas in which perfusion was absent (no FITC-BSA) ***(Figure 4.7D)***. The occlusive nature of these platelet-rich aggregates was also further demonstrated by the fact they appeared to occassionaly 'block' the circulation of trafficking or free-flowing neutrophils within coronary capillaries ***(Figure 4.10B).***

Similar to the adhesion of neutrophils, microthrombi were already present within the IR injured heart at 30 minutes post-reperfusion, the first time point of intravital imaging, and their presence did not increase with time. However, there was a gradual accummulation of both neutrophils and platelet microthrombi folowing myocardial IR injury ***(Figures 4.8A, 4.11A and 4.12).***

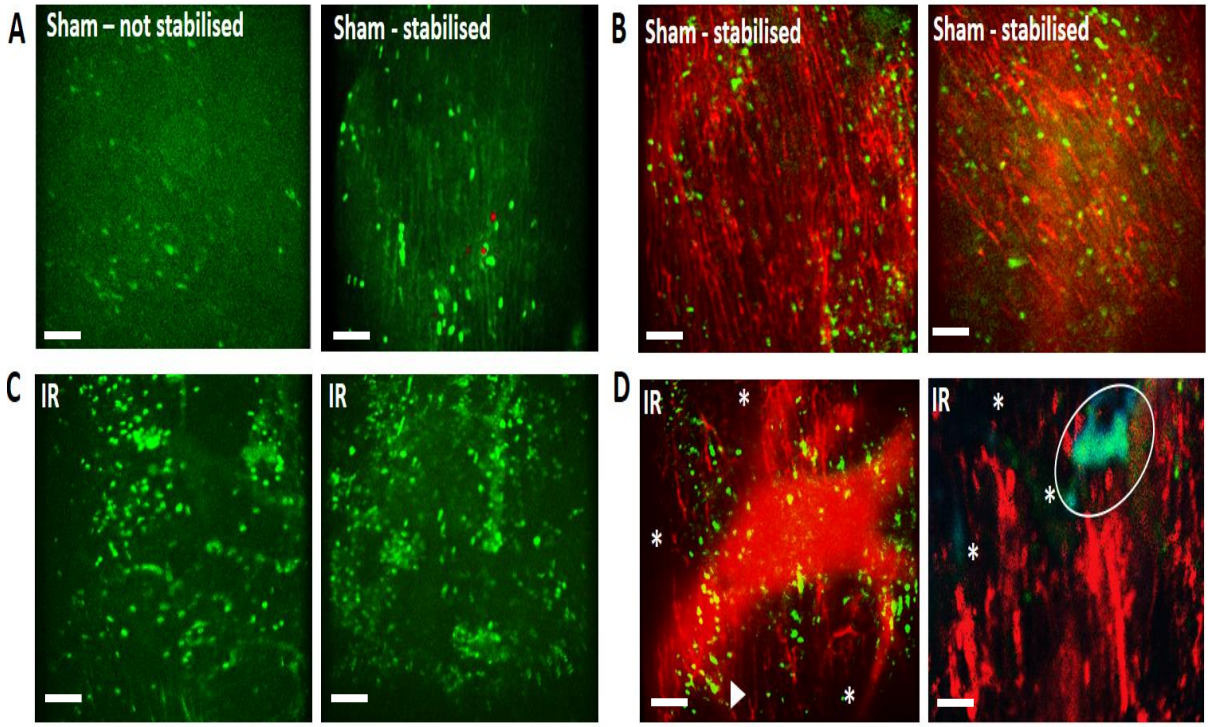

Figure 4.7. Intravital Microscopy Revealed a Significant Increase in Endogenous Neutrophil Adhesion Following Myocardial IR injury but these did not Compromise Blood Flow. (A) *In order to determine whether application of a stabiliser recruited adherent neutrophils, images were obtained from 'non-stabilised' hearts. These images were blurry and out-of-focus. Adherent neutrophils were still observed sham myocardial microcirculation. Stabilised hearts provided higher quality and more easily quantifiable images confirming neutrophil adhesion in sham hearts.* ***(B)*** *Microcirculatory perfusion was not compromised by the presence of adherent neutrophils. Green: neutrophils (PE+anti-Gr-1ab); Red: FITC-BSA.* ***(C)*** *Images obtained from IR injured hearts showed an increase in neutrophil adhesion. Most of these were singular, although aggregates were noted as well.* ***(D)*** *Patchy, non-perfused areas were observed in IR injured hearts (lack of FITC-BSA). However, this was not always associated with areas of neutrophil adhesion. Some capillaries 'end' abruptly (arrowhead). Neutrophils were often seen trapped within platelet microthrombi as seen in the magnified image (right) forming mixed occlusive aggregates. These could occlude capillaries as seen by a lack of FITC-BSA staining (*) downstream of a microthrombus (blue/green - circle) comprised of platelets (blue) and neutrophils (green). Scale bars represent 100µm.*

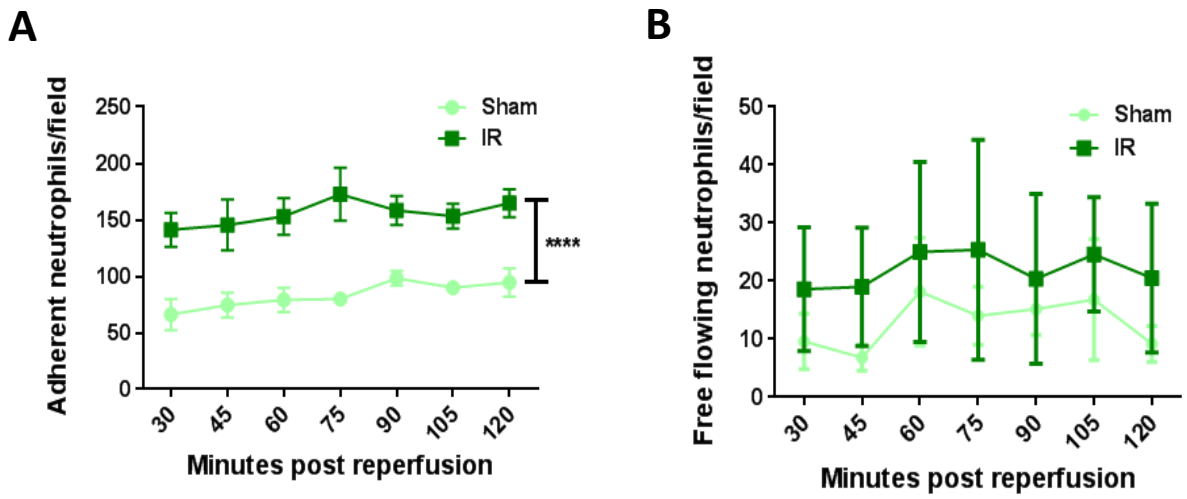

Figure 4.8. Intravital Microscopy Revealed a Significant Increase in Endogenous Neutrophil Adhesion Following Myocardial IR injury. (A) *In sham hearts, neutrophils were found in numbers higher than was expected with approximately 50-60 adherent neutrophils observed per field of view. These were present at 30 minutes, when the first intravital image was taken, and this number did not tend to increase with time. Myocardial IR injury induced a marked and significant increase in individual neutrophil adhesion. Approximately 150-160 adherent neutrophils were observed per field of view which was a 3-fold increase compared to adherent neutrophils found in sham hearts. Similar to the sham mice, this increase was adhesion was present at 30 minutes post-reperfusion and did not increase with time.* ***(B)*** *Approximately 10 free flowing neutrophils were identified at each time point trafficking through sham hearts. The number of neutrophils trafficking through IR injured hearts was approximately 20-30 observed at each time point. There was no significant difference between groups. Statistical analysis was performed using two-way ANOVA with Sidak's multiple comparison test. ****p<0.0001; N=5 per group.*

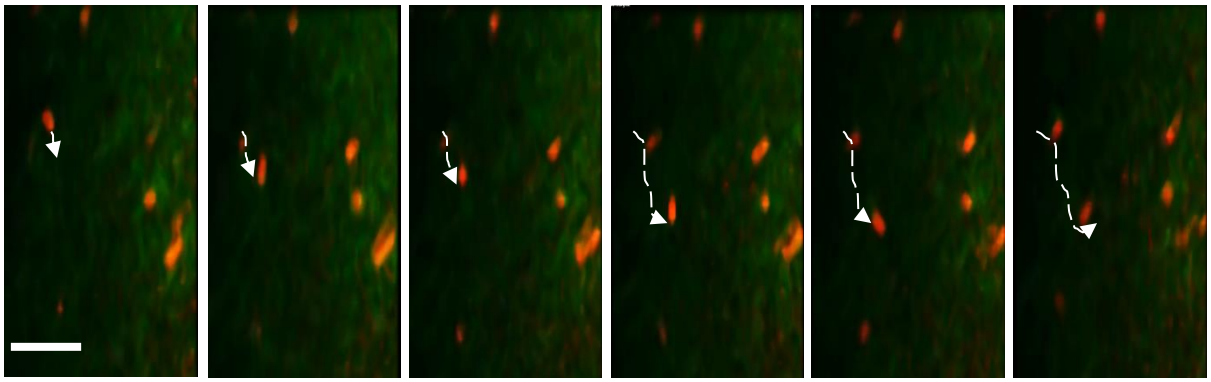

Figure 4.9. 'Patrolling' neutrophils crawling within the coronary capillaries of sham mice – an unusual event. *Some adherent neutrophils, at first glance, appeared to be firmly adherent within coronary capillaries. However, when captured videos were closely inspected, some of these appeared to be patrolling the myocardium in sham mice. Indeed, neutrophils were actually moving short distances or 'patrolling' the length of the capillary as indicated by the arrow showing the trail these neutrophils moved. Representative time lapse images from a sham beating heart showing the tracked movement of a 'patrolling' neutrophil (dotted lines). Scale bar = 100µm.*

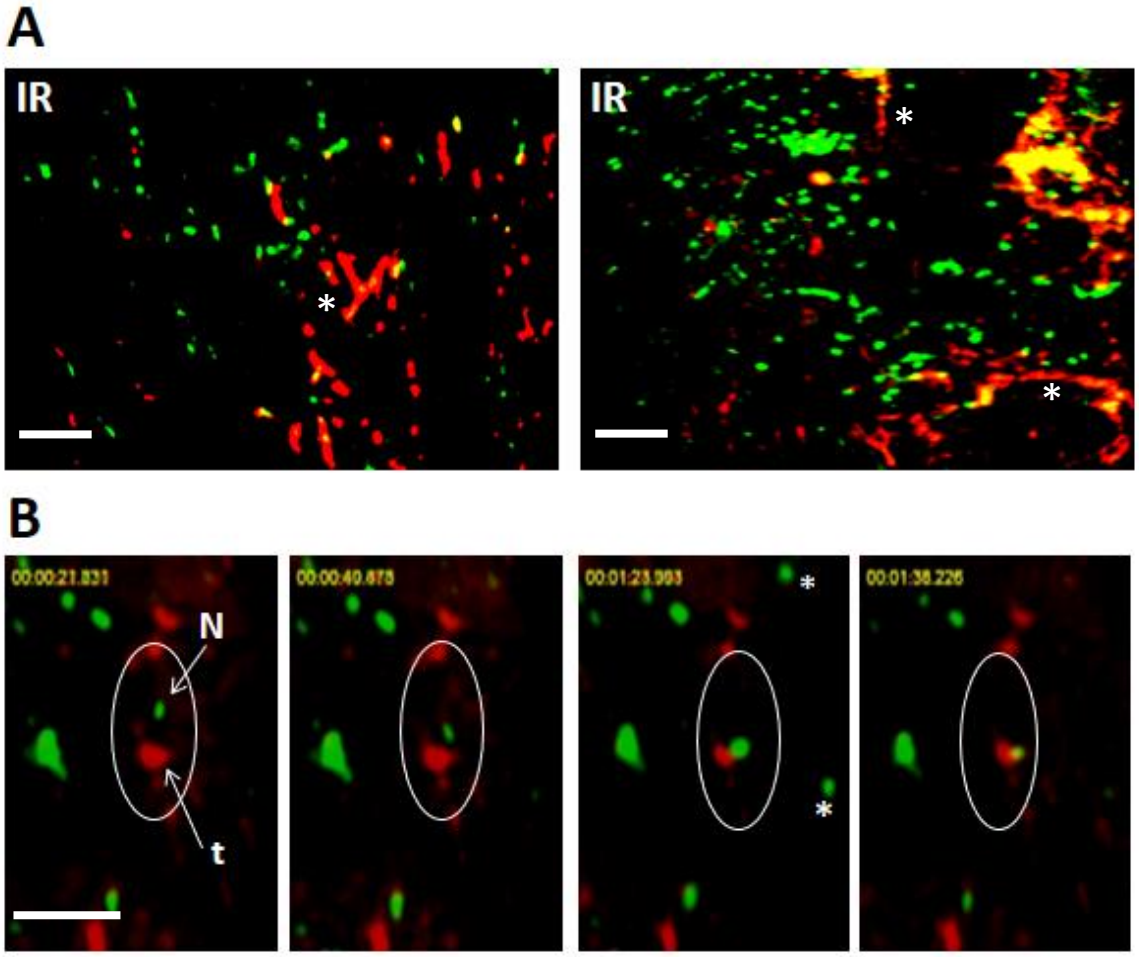

Figure 4.10. **Intravital Microscopy Revealed that Significant Platelet Microthrombi Contributed to Microvascular Occlusive Events Following Myocardial IR injury.** ***(A)*** *Representative intravital images showing neutrophil adhesion (green), platelet aggregation / microthrombus formation (red) following myocardial IR injury. Microthrombi often occupied and followed the contours for a decent length of a capillary (*). These microthrombi are often made up of both neutrophils and platelets - co-localisation (yellow). Numerous smaller and more rounded platelet aggregates were also found dispersed within the field of view. Green: neutrophils (PE+anti-Gr-1ab); Red: endogenous platelets (APC+anti-CD41ab).* ***(B)*** *The occlusive nature of platelet-rich aggregates was demonstrated by the fact they appeared to occassionaly 'block' the circulation of trafficking or free-flowing neutrophils within coronary capillaries. Representative time-lapse images from an IR injured beating mouse heart video are shown. From left to right, within the white circles, a single circulating neutrophil (green, N) is shown unable to move through the capillary as it is occluded by a downstream stationary platelet thrombus (red, t). *= circulating neutrophils only visible in one frame. Scale bar = 100µm.*

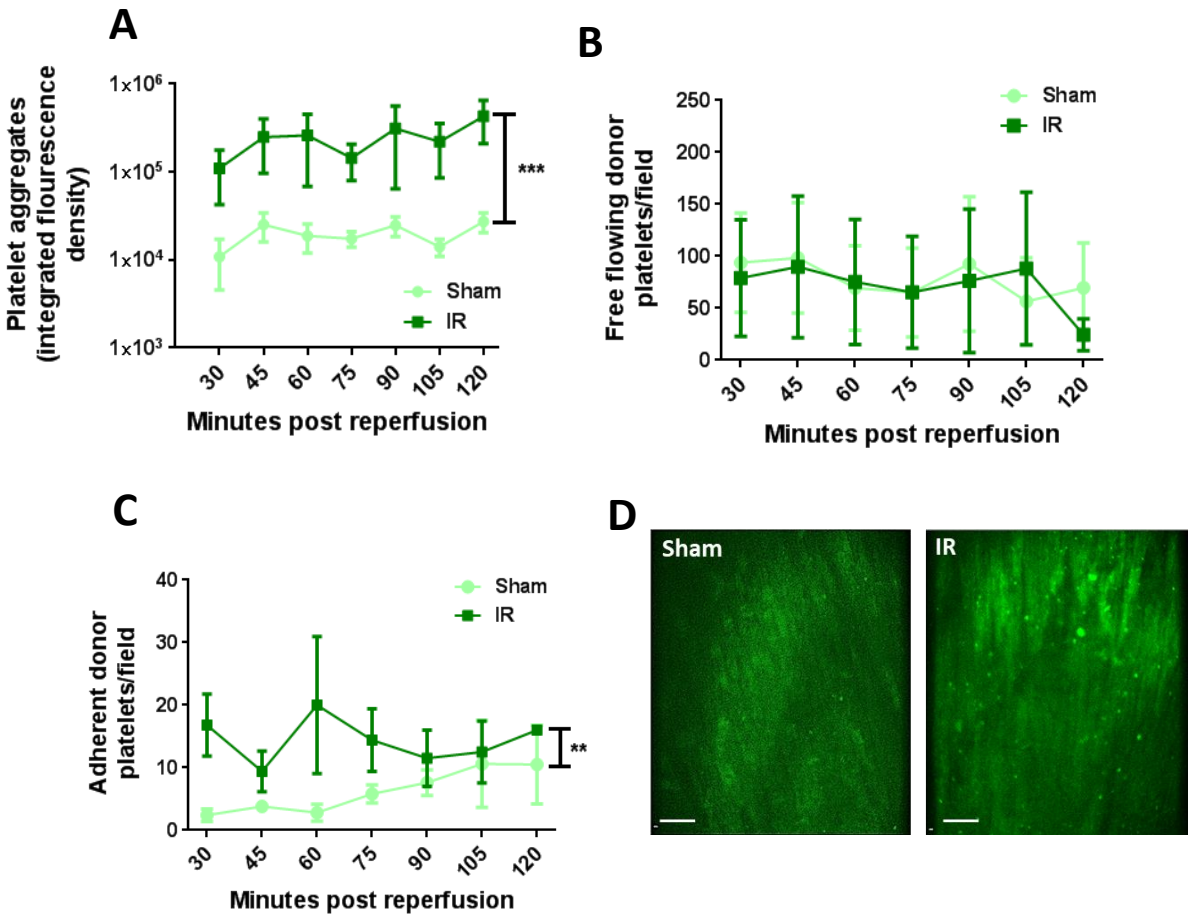

Figure 4.11. Intravital Microscopy Revealed a Significant Increase in Endogenous Microthrombus formation and Individual Donor Platelet Adhesion Following Myocardial IR injury. (A) *Endogenous platelet microthrombus formation was rare in sham mice. However, a significant increase in their generation and presence was noted in IR injured hearts and quantitated as an increase in their integrated fluorescence density.* ***(B)*** *Since labelling of the millions of endogenous platelets could not resolve individual platelets, additional studies were undertaken in which 5% of a donor mouse's platelets were CFSE pre-labelled (green) and injected into experimental mice to measure their activity within the coronary microcirculation. Individual freely flowing or circulating platelets were easily observable in the coronary microcirculation of both sham and IR injured hearts, with approximately 80-90 platelets identified flowing through the field of view at each time point. No significant difference was noted between the two groups.* ***(C)*** *There was a significant increase in individual adherent platelets in the IR injured hearts when compared to sham hearts.* ***(D)*** *Representative intravital images show that the levels of adherent donor platelets increased in IR injured hearts compared to sham. Statistical analysis was performed using two-way ANOVA with Sidak's multiple comparison test. **p<0.01; ***p<0.001; N=5 per group. Scale bar = 100µm.*

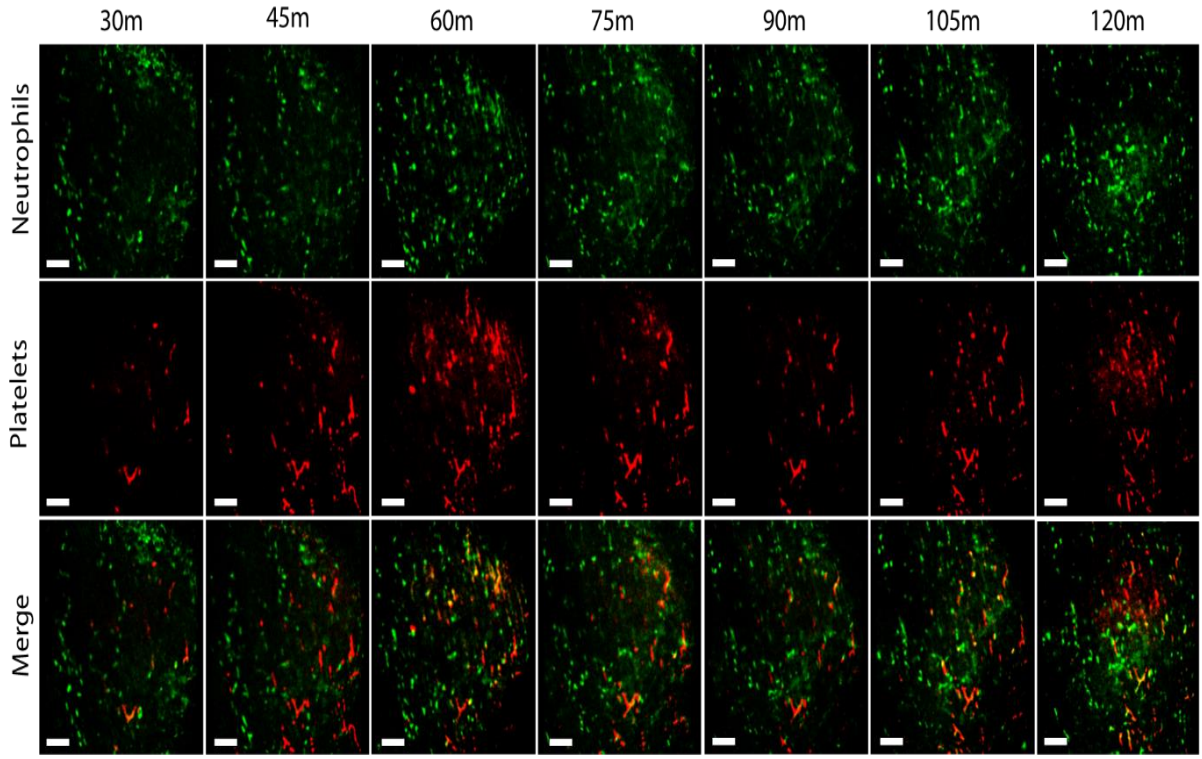

Figure 4.12. Representative intravital images of the beating mouse heart showing rapid recruitment and very gradual increases over time of both adherent neutrophils and platelet microthrombi following myocardial IR injury. *Neutrophils were mainly observed as individual cells while platelets were observed as aggregates. Merged images show microthrombi comprised of both cell types (yellow). Green: Neutrophils (PE+anti-Gr-1ab); Red: endogenous platelets (APC+anti-CD41ab). Scale bars represent 100µm.*

4.3.8 Intravital Microscopy Revealed an Increase in Individual Platelet Adhesion Following Myocardial IR Injury

Since labelling of millions of endogenous circulating platelets could not resolve individual platelets, additional studies were undertaken in which a small volume of CFSE pre-labelled donor platelets were adoptively transferred to experimental mice undergoing intravital experimentation. Individual circulating platelets were easily observable in the coronary microcirculation of both sham and IR injured hearts, with approximately 80-90 platelets identified flowing through the field of view at each time point ***(Figure 4.11B).*** No significant difference was noted between the two groups. There was a significant ($p<0.01$) increase in individual adherent platelets in the IR injured hearts when compared to sham hearts ***(Figures 4.11C and 4.11D)***. However, in comparison to the number of adherent neutrophils, this was a very low number with approximately 10-20 observed per field of view.

4.3.9 HPC-7s Therapy Attenuates the Significant and Rapid Increase in both Neutrophil and Platelet Recruitment Following Myocardial IR Injury

The systemic administration of HPC-7s as a form of cell therapy significantly decreased both endogenous neutrophil recruitment ($p<0.0001$) and platelet microthrombus formation ($p<0.001$) in IR injured hearts ***(Figures 4.13A, 4.13B and 4.13C).*** Indeed, neutrophil adhesion decreased to approximately 60 cells adherent/field of view in mice receiving cellular therapy compared to approximately 150-160 in IR injured hearts of mice receiving no cellular therapy. There appeared a slight increase in free-flowing neutrophils after HPC-7s therapy with approximately 30 cells per field of view trafficking through the heart at each time point.

However, there was no statistically significant difference between groups ***(Figure 4.13D).*** Of note, the IR data presented in ***Figure 4.13*** are the same data presented in ***Figure 4.8*** (neutrophils) and ***Figure 4.11*** (platelet aggregates). Data was separated into different main figures for clarity.

4.3.10 Intravital Microscopy Revealed Myocardial IR Injury was Associated with Increased Monocyte Recruitment which was Decreased with HPC-7s

Intravital microscopy was also utilised for the first time to image the kinetics of monocyte activity within the beating mouse heart ***(Figure 4.14A)***. Using the fluorescent latex bead method, it was possible to image labelled monocytes trafficking through the beating heart, with the numbers noted in sham mice similar to the number of freely circulating neutrophils observed in sham mice. There was no statistically significant difference in free flowing monocytes between the IR injured heart and sham heart ***(Figure 4.14B).*** The number of adherent monocytes was significantly ($p<0.001$) increased in IR injured hearts ***(Figure 4.14C).*** Interestingly, this increase was as rapid and to a similar degree as adherent neutrophils and primarily within the capillaries. Indeed, approximately ~100 monocytes per field of view were observed at all time points compared to ~25 monocytes per field of view in sham hearts. Again, this adhesion was noted mostly in coronary capillaries.

HPC-7s therapy induced a noticeable difference to the recruitment of monocytes during IR injury. There was a noticeable increase in free-flowing monocytes after HPC-7s therapy to ~25 cells per field of view at 30- and 45-minutes post-reperfusion when compared to IR injured hearts ***(Figure 4.14D).*** At these time points this increase was statistically significant ($p<0.05$).

The remaining period of reperfusion showed no significant difference between the two groups. There was a remarkable and significant ($p<0.01$) decrease in adherent monocytes at all time points in the IR+HPC-7s group with ~50 cells observed at each time point ***(Figure 4.14E)***. Of note, the IR data presented in ***Figure 4.14B&C*** are the same in ***Figure 4.14D&E***. Data was separated into different figures for clarity.

4.3.11 Detecting Macrophages in the Mouse Heart

As monocyte recruitment was increased in IR injured beating mouse hearts, we further attempted to investigate the effect of myocardial IR injury on macrophage recruitment as well. Endogenous macrophages were labelled using APC-conjugated rat anti-mouse F4/80 antibodies. Initial attempts to intravitally image macrophages were conducted in sham mice in order to determine the effectiveness of antibody delivery and detection *in vivo*. However, we were unable to obtain useful information as very few cells were observed to be labelled with the antibody even after 3 hours post-labelling (1 or 2 cells/field of view/experiment). We conducted similar experiments within IR injured hearts and again obtained similar results ***(Figure 4.15A)***. In order to determine the viability of the batch of antibodies used, the liver was also imaged in the same mouse after each myocardial experiment to determine whether resident macrophages, the Kupffer cells, were labelled. We found that antibody viability was good as Kupffer cells were easily visible ***(Figure 4.15B)***. Another method was attempted to image macrophages which involved using CD68-eGFP transgenic mice (on a C57BL/6 background) in order to visualise monocytes and macrophages. This resulted in images obtained, from both sham and IR injured hearts, with high background auto-fluorescence. This made it difficult to quantify either population of cells via size ***(Figure 4.15C)***.

Unfortunately, due to these findings and time constraints, we did not pursue further intravital investigations regarding macrophage recruitment in the IR injured heart.

4.3.12 Balloon Ligation as an Alternative Method in Ligating the LAD Artery

Intravital imaging clearly demonstrated that the rapid thrombo-inflammatory response post-IR injury had already taken place at the time of the first recording. This meant that the initial 30 minutes of reperfusion was an important pathophysiological phase. HPC-7s therapy also provided a rapid response during this time period. However, technical limitations meant that we were unable to record IVM images during this time critical period. In order to overcome this, an alternative method of ligating the LAD was created that could feasibly allow us to quickly and easily induce ischaemia and commence intravital imaging immediately upon reperfusion. Instead of tying off the LAD artery using a suture tied against a plastic tube, the balloon ligation method relied on the pumping of saline into a saran wrap 'balloon' placed within the suture loop that would then proceed to constrict the LAD artery upon inflation. This was carried out using a syringe connected to a plastic tube with a saran film balloon firmly wrapped around the opposite end ***(Figures 4.16A-B)***. Importantly, this process could be performed whilst the mouse board was already positioned on the microscope stage ready for immediate imaging after the balloon was deflated and reperfusion initiated.

Successful ligation of the balloon constricted LAD artery was demonstrated using laser speckle imaging. During the period the balloon was fully inflated, the left ventricle appeared a cooler green/yellow hue. Since laser speckle captures 'motion', the fully saline inflated balloon appeared a cold blue hue as the saline inside it was not moving ***(Figure 4.16C).*** The LSCI photo

video showed the balloon being deflated and the LSCI flux heat map showed the balloon changing quickly from blue→green→red→green→blue as the saline moved or emptied from it. Simultaneously, and as a direct result of the balloon emptying, the resumption of blood perfusion towards the apex of the left ventricle was noted by a change from a green/yellow hue towards a redder hue appearing in the left ventricle. This was an important result as it showed the capability of this novel balloon method to induce ischaemia and subsequent reperfusion without the need for a separate surgical microscope to visualise the suture and plastic tubing used to ligate the LAD artery in the more conventional method. This allowed us to gain laser speckle images the moment the heart transferred from a state of ischaemia to reperfusion. However, due to time constraints, we were unable to proceed to intravital imaging of the heart using this balloon IR injury protocol.

4.3.13 Myocardial Sterile Burn Injury Induces a Visible Inflammatory Response which could be Detected using Intravital Microscopy

Intravital imaging using the various labelling methods for endogenous circulating cells that we employed has not previously been performed in the healthy or injured mouse beating heart. We have imaged labelled platelets and neutrophils intravitally in numerous other organs. However, the latex bead method for imaging monocyte trafficking is a relatively new method. Therefore, we felt it was important to determine that fluorescent labelling of both circulating endogenous neutrophils and monocytes was both viable, normal and adequate for beating heart imaging. In order to test this, a small sterile burn injury was performed on the beating left ventricle using a small tip cautery pen to initiate an inflammatory response. In this

experiment, neutrophils and monocytes were labelled using fluorescent antibodies and latex microparticles respectively. Intravital videos/images obtained showed that both cell types were visible during pre-injury and post-injury ***(Figure 4.17A)***. Cells were observed to be free-flowing, rolling and adherent to the coronary microvessel walls, indicating various stages of the cell adhesion cascade was taking place. Interestingly, rolling neutrophils and monocytes were not so readily observed within the coronary microvessels in the myocardial IR injury model. Whilst statistical analysis was not performed for this experiment, graphical comparison of data showed that an increasing number of both neutrophils and monocytes became adherent close to the site of injury over time, peaking at 2 hours post injury ***(Figure 4.17B)***.

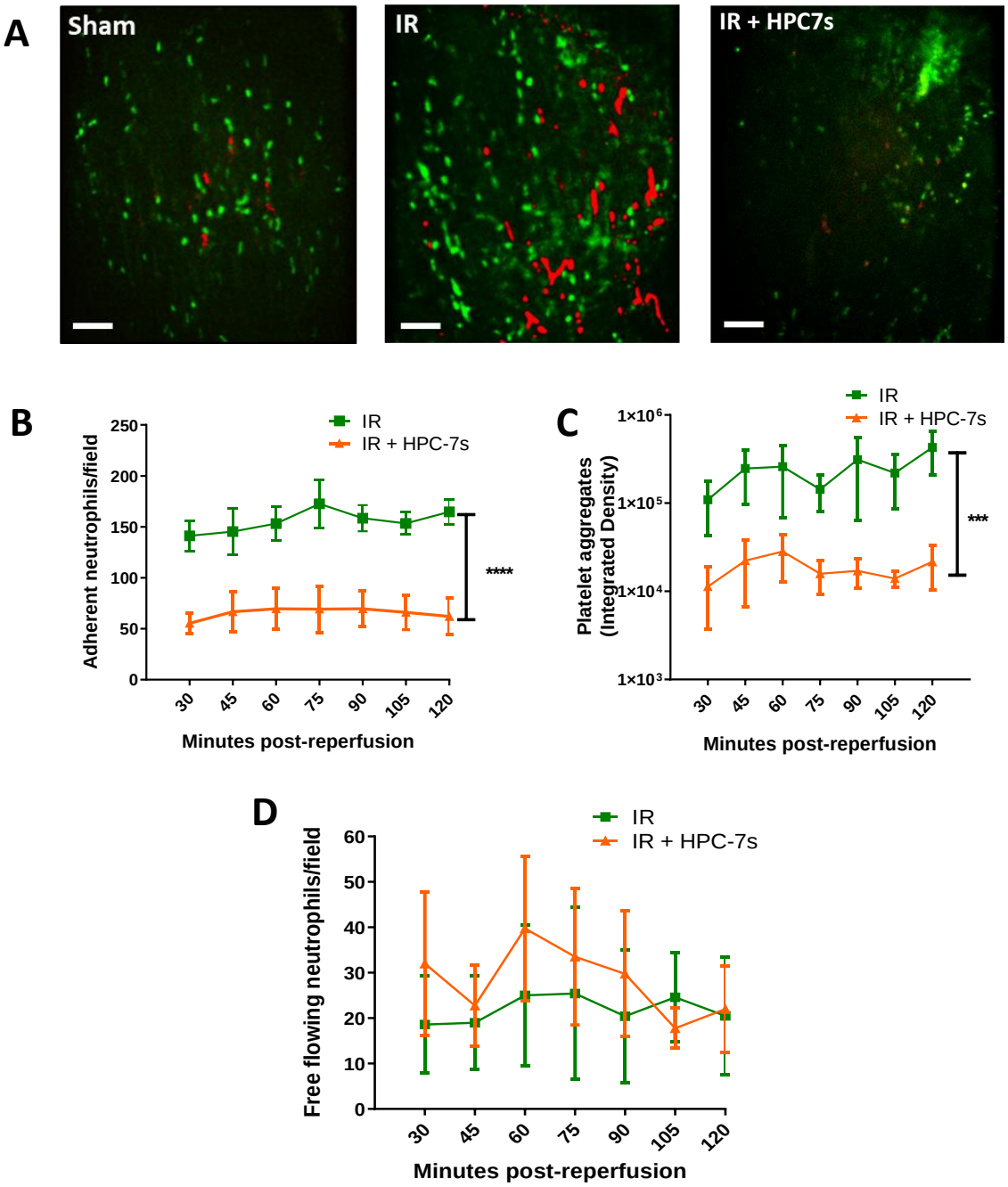

Figure 4.13. HPC-7s Therapy Attenuates the Significant and Rapid Increase in both Neutrophil and Platelet Recruitment Following Myocardial IR Injury. (A) *Representative intravital images to show neutrophil and platelet infiltration in Sham, IR injured and IR injured + HPC-7s beating mouse hearts. Green: Neutrophils (PE+anti-Gr-1ab); Red: endogenous platelets (APC+anti-CD41ab).* ***(B-C)*** *Systemic administration of HPC-7s significantly decreased both endogenous neutrophil recruitment and platelet microthrombus formation in IR injured hearts. Neutrophil adhesion decreased to approximately 60 cells adherent / field of view in mice receiving cellular therapy compared to approximately 150-160 in IR injured hearts of mice receiving no cellular therapy.* ***(D)*** *There was no statistically significant difference in free flowing neutrophils between the two groups. Statistical analysis was performed using two-way ANOVA with Sidak's multiple comparison test. ***p<0.001 ****p<0.0001; N=5 per group. Scale bar = 100µm.*

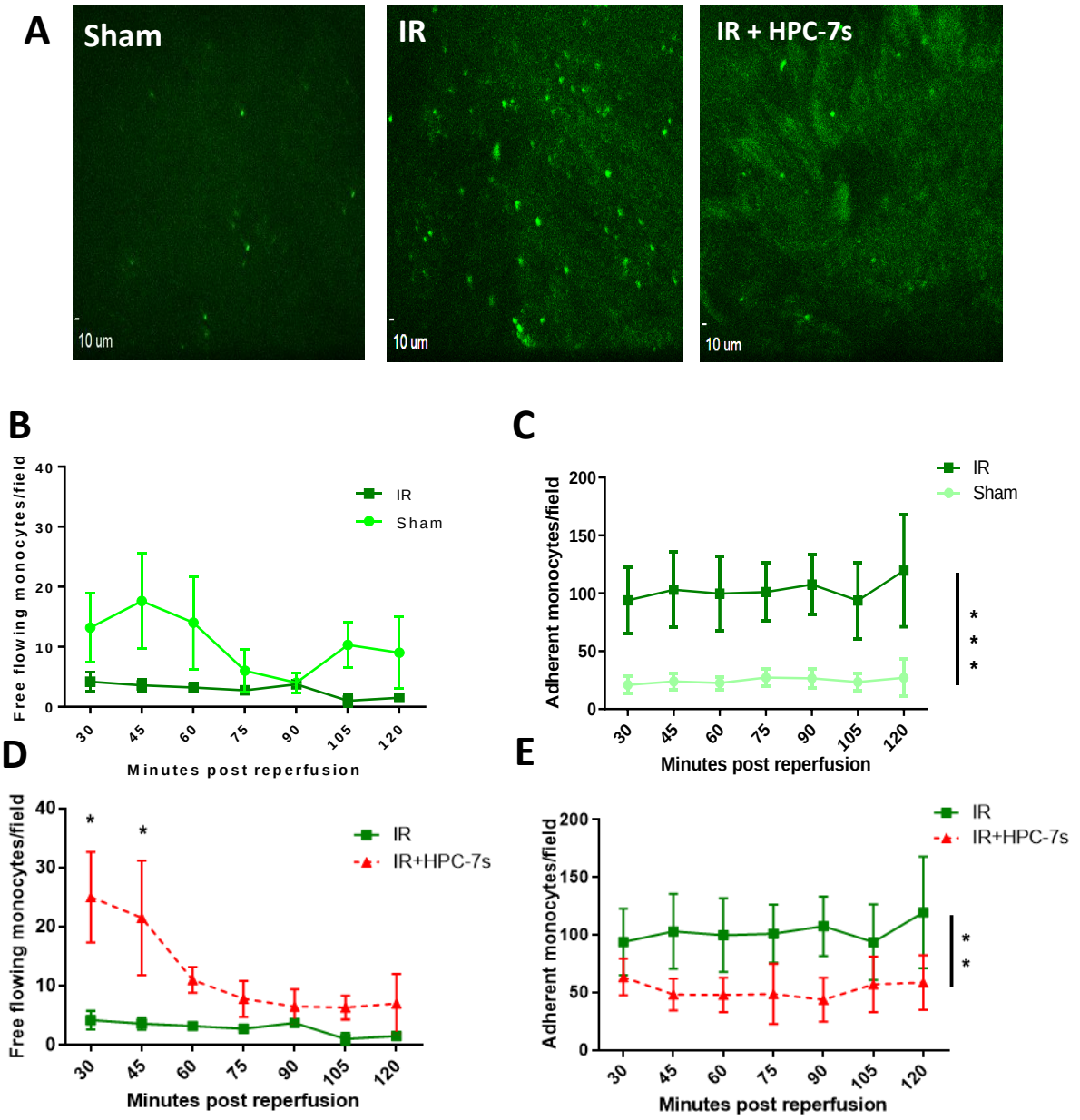

Figure 4.14. Intravital Microscopy Revealed Myocardial IR Injury was Associated with Increased Monocyte Recruitment which was Decreased with HPC-7s. (A) *Representative images showing baseline levels of monocyte recruitment (green) in sham mice. During IR injury, recruitment clearly increases. With HPC-7s therapy, monocyte recruitment returns back close to sham levels. Endogenous monocytes were labelled with non-degradable fluorescent latex beads. 100µl of 1µm diameter Fluoresbrite® FITC-dyed Yellow Green Microspheres were injected intra-arterially at a concentration of 1.15 x 10^{10} particles/ml. The premise behind this method was that circulating monocytes would become labelled after phagocytic uptake of the latex beads.* ***(B)*** *There was no statistically significant difference in free flowing monocytes between the IR injured heart and sham heart.* ***(C)*** *There was a significant increase in adherent monocytes in the IR injured beating hearts compared to sham hearts.* ***(D)*** *There was a slight increase in free-flowing monocytes after HPC-7s therapy to ~25 cells per field of view, which was statistically significant at 30- and 45-minutes post-reperfusion when compared to purely IR injured hearts.* ***(E)*** *There was also a remarkable and significant decrease in adherent monocytes at all time points in the IR+HPC-7s group with ~50 cells observed at each time point. Statistical analysis was performed using two-way ANOVA with Sidak's multiple comparison test. N=5 per group. Scale bar = 10µm.*

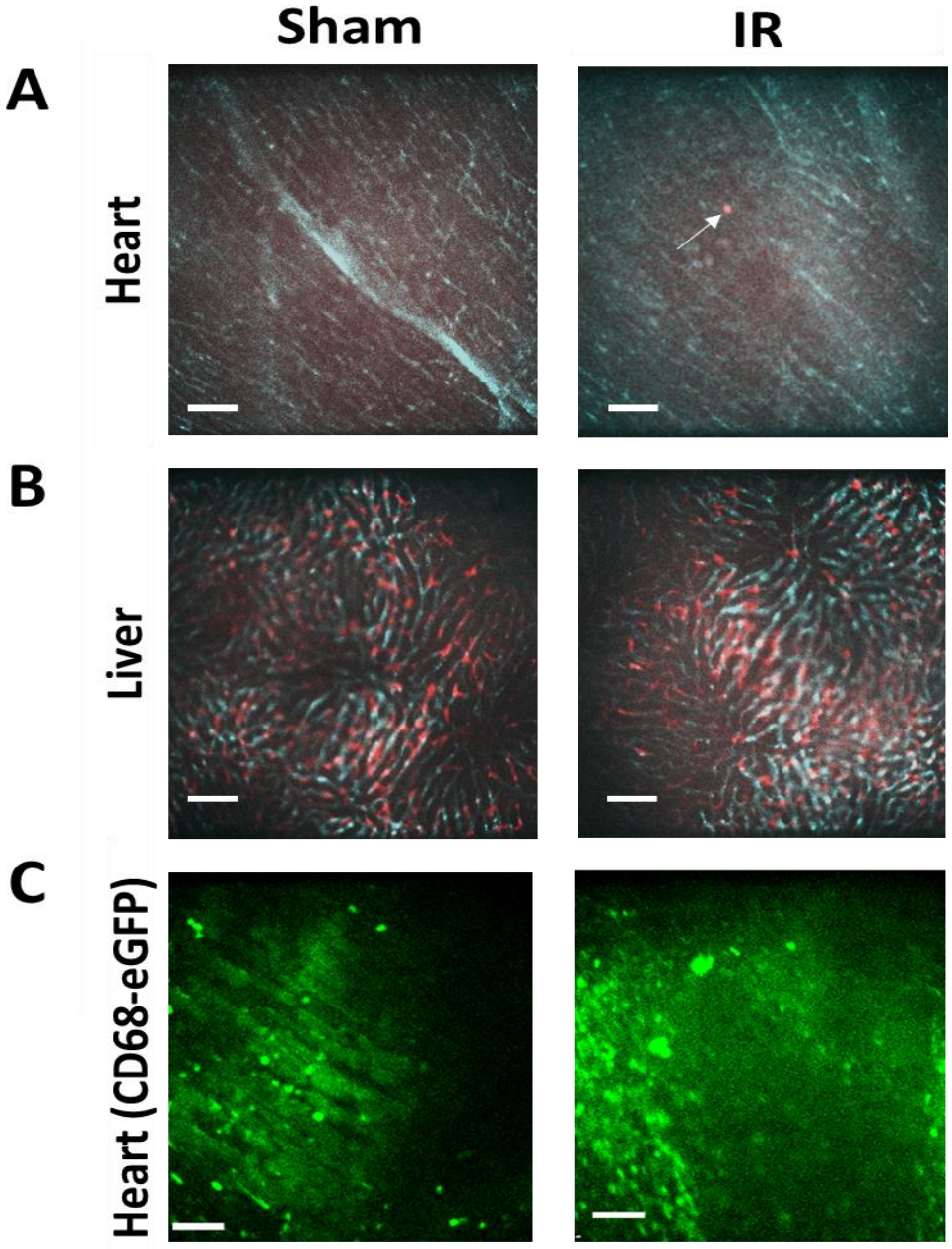

Figure 4.15. Intravital imaging of macrophages in the beating mouse heart in vivo proved to be unsuccessful. ***(A)*** *Attempts were made to visualise macrophage recruitment in the beating mouse heart following myocardial IR injury using APC-conjugated anti-F4/80 antibodies. Endothelial cells (light blue) were simultaneously labelled labelled using PE-conjugated anti-CD31. Visualisation of macrophages (red; arrow) in the heart was unsuccessful as very few positively stained cells were observed even after 3 hours post-labelling with only 1 or 2 cells/field of view visible.* ***(B)*** *The labelling protocol was, however, effective as resident macrophages or Kupffer cells in the liver sinusoids were readily observable in the same mouse. (****C****) Another method was attempted which involved using CD68-eGFP transgenic mice (on a C57BL/6 background) in order to visualise endogenous monocytes and macrophages. This resulted in images obtained, from both sham and IR injured hearts, with high background auto-fluorescence which made it difficult to quantify either population of cells via size. Unfortunately, this meant the intravital imaging and subsequent quantification of macrophages in the setting of myocardial IR injury was not undertaken. Scale bar = 100µm.*

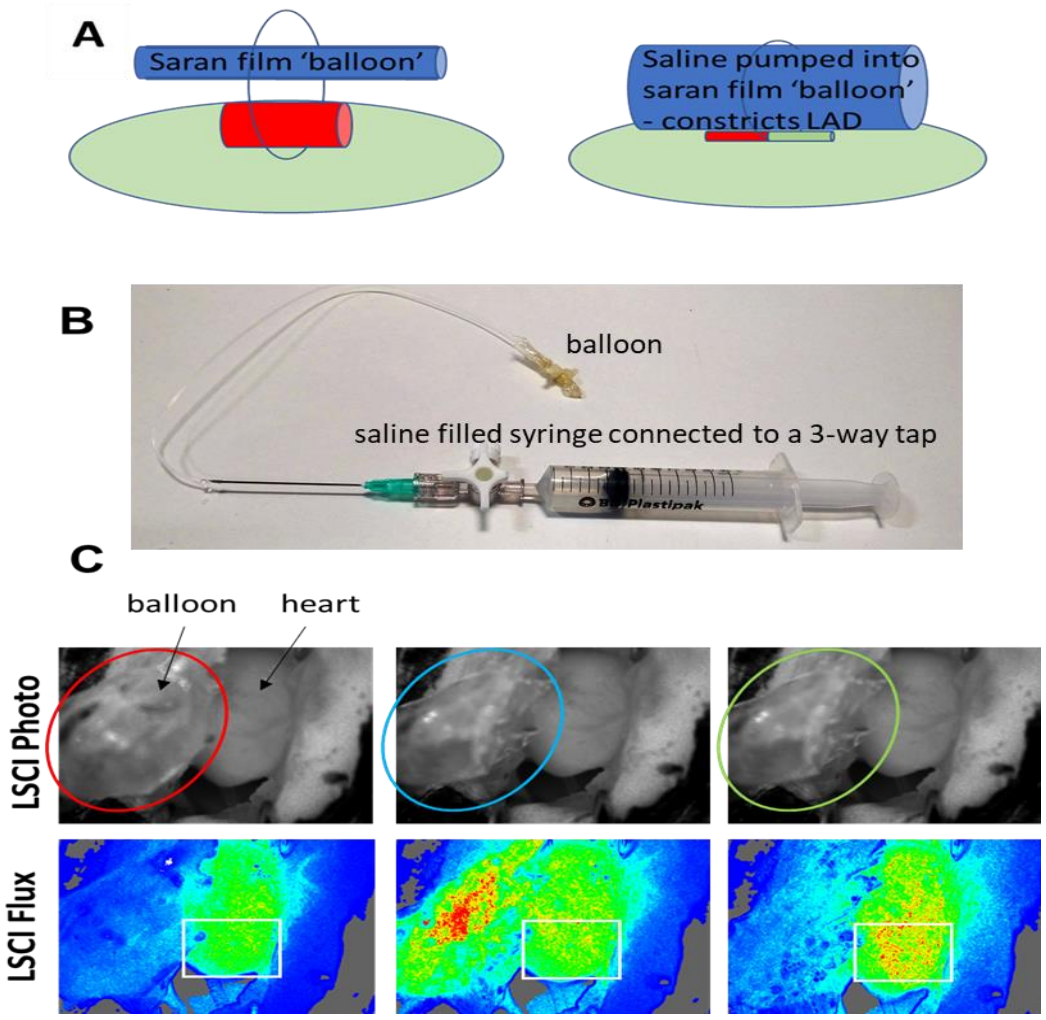

Figure 4.16. Balloon Ligation as an Alternative Method to Ligate the LAD Artery. *Using the conventional 'suture ligated against plastic tubing' method, it was not possible to record images from the reperfused beating heart during the critical immediate first 30 minutes of reperfusion. Therefore, an alternative method was developed in which the coronary LAD artery could be ligated and reperfused on the intravital microscope stage with immediate imaging.* ***(A-B)*** *The balloon ligation method relied on the pumping of saline into a saran wrap 'balloon' placed within the suture loop that would then proceed to constrict the LAD artery upon inflation. This was carried out using a syringe connected to a plastic tube with a saran film balloon firmly wrapped around the opposite end. Importantly, this process could be performed whilst the mouse board was already positioned on the microscope stage ready for immediate imaging after the balloon was deflated.* ***(C)*** *Successful ligation of the LAD artery was demonstrated using LSCI imaging. During the period the balloon was fully inflated, the apical region of the left ventricle (box) appeared a cooler green/yellow hue. Since laser speckle captures 'motion', the fully saline inflated balloon appeared a cold blue hue as the saline inside it was not moving. The representative LSCI video photo showed the balloon being deflated and the and captured LSCI flux heat map showed the balloon changing quickly from blue →green →red →green →blue as the saline quickly moved or emptied from it. Simultaneously, and as a direct result of the balloon emptying, the resumption of blood perfusion towards the apex of the heart was noted by a change from a green/yellow hue towards a redder hue appearing in the left ventricle. The inflated (red oval), half deflated (blue oval) and fully deflated balloon can be seen outlined (green oval).*

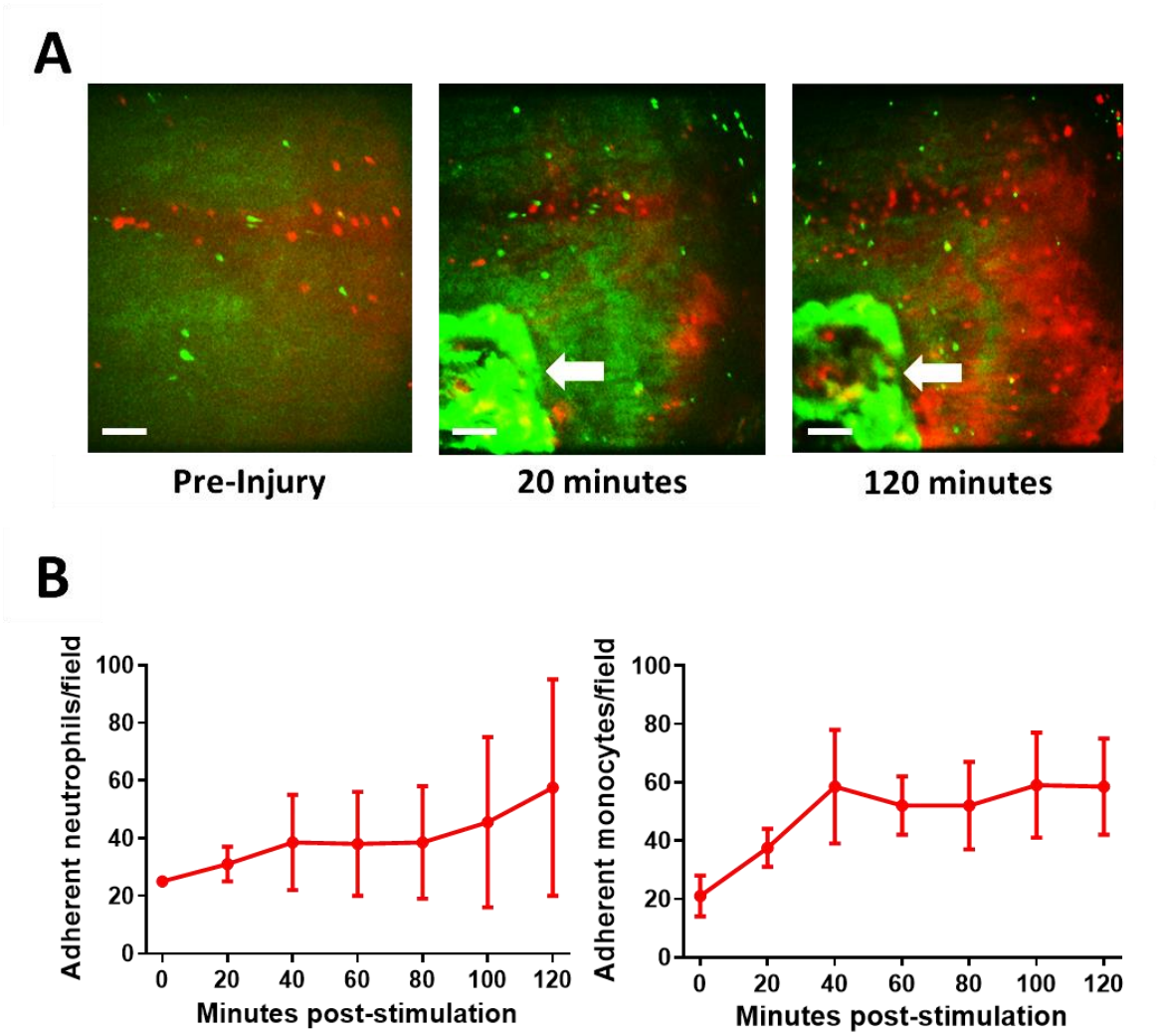

Figure 4.17. Myocardial sterile burn injury induces a visible inflammatory response which could be detected using intravital microscopy. *In order to determine the effectiveness of both circulating endogenous neutrophil and monocyte labelling, a small sterile burn injury was performed on the beating left ventricle using a small tip cautery pen to initiate an inflammatory response.* ***(A)*** *Neutrophils (red) and monocytes (green) were labelled 10 minutes prior to injury using fluorescent antibodies and latex microparticles respectively. Representative intravital images show different stages of the experiment: pre-injury, 20 minutes following injury and 2 hours following injury. Both cell types were visible during pre-injury and post-injury. Cells were observed to be free-flowing, rolling and adherent to the coronary microvessel walls, indicating various stages of the cell adhesion cascade was taking place.* ***(B)*** *Whilst statistical analysis was not performed for this experiment, graphical comparison of data showed that an increasing number of both neutrophils and monocytes became adherent close to the site of injury over time, peaking at 2 hours post injury. N=2 per group. Scale bar = 100µm.*

4.4 Discussion

In order to salvage myocardial tissue post-MI, there needs to exist an adequate level of microcirculatory perfusion, not just the re-opening of an occluded epicardial artery. Imaging of the coronary microvasculature has not previously been conducted directly, creating a 'gap' in our knowledge of the pathophysiological changes in coronary perfusion during IR injury. In this study, we present a novel approach to conduct intravital imaging of the beating mouse heart and visualise multiple coronary microcirculatory perturbations using a 3D-printed stabiliser while assessing the overall blood flow dynamics using laser speckle contrast imaging. We observed a ventricular hyperaemic response during reperfusion that persisted throughout this period. This could have been interpreted as blood flow being adequately re-established to repay the debt acquired during ischaemia. However, it was clear from higher resolution intravital studies that this was poorly transmitted to coronary capillaries and thus did not correspond to adequate perfusion at a microvascular level. The ability to gain high-resolution images allowed us to observe numerous microcirculatory disturbances during IR injury.

In this chapter we have shown that the perturbations that occur post-myocardial IR injury, leading to tissue infarction are, in part, a result of the accumulation of thrombo-inflammatory cells within the coronary capillaries. Rapid accumulation of these cells, especially as platelet-rich microthrombi aggregates, led to areas of non-perfused myocardium within the injured left ventricle. Microvascular obstruction is well-known to exacerbate IR injury, and we have shown how the microcirculation becomes disorganised in cardiac IR injury [5]. The accumulation of inflammatory cells at the area of risk can further aggravate the injury, intensified by the hyperaemic response induced during reperfusion introducing more

thrombo-inflammatory cells to the already inflamed region. HPC-7s were shown to provide remarkable vasculoprotective effects by immediately reducing the accumulation of thrombo-inflammatory cells and attenuating the injury response. This effect in part contributed to the return of a structured microvasculature and adequate perfusion in the microcirculation as well. Ultimately, this resulted in a reduced infarct size after injury. These results showed how HSCs were viable as a form of cell therapy in treating myocardial IR injury.

4.4.1 Establishing a Model for Intravital Imaging of the Murine Beating Heart

Whilst heart disease is a significant burden, our basic understanding of the myocardial microcirculation has been hampered by an inability to image the microvessels of the beating heart experimentally, something which has been possible to do intravitally in other organs for over 100 years. Therefore, there exists a 'black box' with regards our understanding of the dynamic changes that occur in the microcirculation of the heart during IR injury [46]. This stems from a couple of clear and obvious difficulties related to imaging the organ – firstly, the fact that it beats and is moved significantly by the lungs, and secondly, it is located in an anatomically challenging position for microscopy. Although a limited number of studies have attempted to intravitally image the heart, they have all had their limitations. For example, in the first feasible example of cardiac intravital, Martini and Honig performed microscopy on the beating heart of ventilated rats. In this preparation, the heart was exposed via an incision in the chest wall, covered with a glass slip, and illuminated via point-strobe light driven into a ring condenser. While this model generated useable images, it did not control for movement and so poor-quality images were obtained [217]. Other attempts at IVM imaging of the

beating heart have either been carried out in donor hearts transplanted onto the neck of the recipient mouse or in other species such as rats [218, 219]. Additional attempts have included sutures to fix the heart, compression using a coverslip, mechanical or suction-based stabilizers. However, with all of these high resolution imaging of microvascular flow has remained a major challenge [220]. A review detailing all the various attempts to image the beating heart has recently been published [221].

However, we are the first to develop a novel method that not only successfully images the beating mouse heart, but also utilises this method to capture and characterise the multitude of damaging effects of IR injury on the coronary microcirculation and also the vasculoprotective effects of stem cells. Development of an IVM method to visualise the coronary microcirculation of the beating mouse heart *in vivo* was therefore a major component of this Chapter. This was a challenging technique that was initiated and optimised throughout this study. A number of changes were made to our surgical setup and protocol in order to achieve the best high-quality image output. These included creating smaller 3D stabilisers, increasing the exposed heart area by cutting through ribs and utilising a micromanipulator to gently attach the stabiliser to the heart. Optimisation of this technique was challenging however, the ability to successfully and reproducibly gain high-quality images meant that we were able to generate novel data and information. We also utilised a Nipkow spinning disk confocal head that was attached to the intravital microscope in order to capture dynamic microcirculatory events in real-time from the beating heart. This Yokogawa attachment contained approximately 10,000 pinholes in one spinning disk and a second spinning disk with the same number of microlens to focus the excitation laser light into each corresponding pinhole. Both disks then spun to very rapidly raster scan the field of view. This

is in contrast to traditional confocal scanning in which a single laser beam slowly scans the field of view. Hence, spinning disk technology was able to increase scanning speed, allowing high quality images at a high frame rate to be captured of moving cells within the microcirculation [221]. Furthermore, due to multiple laser beams exciting the tissue, low laser power was required resulting in significantly less photobleaching and phototoxicity of the imaged tissue.

In developing this model, we needed to be aware of intrinsic limitations to conducting *in vivo* surgery alongside intravital imaging of the cardiac microcirculation on an anaesthetised mouse. Physiological changes can easily occur in this environment leading to hypothermia, acid-base imbalances, hypoxia and heart rate variability due to anaesthesia delivery, placement of our 3D stabiliser and an exposed thoracic cavity. These changes can affect blood flow. Considerations were made with this in mind, such as body temperature control (37^{o}C) using a heat pad and monitored using a rectal probe. A sterile surgical pad was used to cover the thoracic cavity when videos were not being recorded to prevent excess heat and fluid loss. Medical oxygen was connected to the ventilator during experiments in order to provide high levels of oxygen throughout surgery. Further precautions, such as monitoring of heart rate, blood oxygen saturation and blood pressure could also be undertaken using instruments such as an electrocardiograph, pulse oximetry and a blood pressure monitor.

4.4.2 Mismatch between Global Hyperaemia and Microcirculatory Flow Heterogeneity

Our initial experiments looked into assessing the general perfusion of the left ventricle during IR injury. This was achieved using LSCI, an imaging modality not previously applied to the

beating heart either experimentally or clinically. LSCI utilizes the temporal and spatial blurring of interference patterns of coherent light scattered from moving cellular blood components and thereby allows the measurement of blood flow quantitated as flux. However, motion due to both (i) physical heart movements induced by contraction/relaxation and due to (ii) the heart being moved in the chest cavity by the inflating/deflating lungs, can also interfere with these flux measurements. Therefore, significant efforts were made to analyse the LSCI flux data carefully and we were able to separate flux recordings due to heart movement from flux recording due to blood moving through the left ventricle muscle. We were able to identify two clear responses associated with the systolic and diastolic phases. As far as we are aware, this is the first application of LSCI to the beating mouse ventricle and demonstration of real-time phasic changes associated with the cardiac cycle. However, our main findings from this LSCI study was that reperfusion mediated a very rapid ventricular hyperaemic response. This was not wholly surprising as there exists a deficit in nutrient and oxygen incurred by the ischaemic regions of the heart known as the accumulated oxygen debt [38]. These likely provide signals that modify the vasculature of the heart in order to promote maximum reperfusion benefits and repay the ischaemia-induced oxygen debt [5].

However, what was interesting and not previously demonstrated was the fact that this hyperaemia was sustained throughout the 2 hours of reperfusion. Most studies have demonstrated, using different methods, a marked but transient increase in blood delivery to the heart following ischaemia, lasting only a few minutes and which rapidly returns to baseline. This has been noted both experimentally and clinically [222]. Indeed, in humans it has been shown that due to increased demand, coronary blood flow can increase up to five times basal levels following release of a variety of vasodilatory factors such as adrenalin,

ADP/ATP, adenosine, bradykinin, substance P etc. [223]. Interestingly, in the current study a more sustained reactive hyperaemic response was identified. This discrepancy may possibly be explained by technical differences. Previously, blood flow responses were measured from one of the major coronary arteries using an inserted Doppler flow guide wire. However, in the current study, the full-field optical nature of LSCI was able to image a larger ventricular area, thus averaging macro- and microvascular flow changes, over longer periods of time.

On its own, this increased regional hyperaemic response could have been interpreted as flow being adequately re-established after ischaemia. However, despite this apparent beneficial response, we still demonstrated infarction in the heart. It was therefore, important to determine whether this increase in blood flow actually resulted in adequate perfusion at the microvascular level. It became clear from subsequent intravital studies that this increased blood in the heart myocardium was poorly transmitted to coronary capillaries and thus did not correspond to adequate perfusion at a microvascular level. Indeed, a significant decrease in the functional capillary density was noted when FITC-BSA was injected into mice to identify areas of flow. Therefore, these novel studies in which LSCI was combined with intravital studies suggested that there was a clear mismatch that existed *in vivo* between the global hyperaemic response during reperfusion and microcirculatory flow heterogeneity. As will be discussed later, it was primarily the platelet aggregates that played a critical part in the latter.

4.4.3 Rapid and Sustained Inflammatory Response

Experiments that looked into the recruitment of platelets, neutrophils and monocytes during cardiac IR injury showed a significantly rapid increase in all three cell types throughout the

period of reperfusion. Neutrophil adhesion increased rapidly in IR injured hearts, doubling by 30 minutes post-reperfusion when compared to sham hearts. Neutrophil capture is generally confined to post-capillary venules due to their high and preferential expression of endothelial adhesion molecules [224]. However, in the heart, we noted neutrophil retention mainly within coronary capillaries, a region of the vasculature not usually associated with cellular recruitment. In this study, we characterised cells such as neutrophils as adherent if they were stationary in our imaging field of view for >30seconds. While this provided us with information as to recruitment numbers, it should be noted that some cells can be stationary for reasons other than adherence to the blood vessel. This includes cells that become trapped in a microthrombi, are slowly migrating through tissue or simply immobile during cardiac contracture. Some of these cells can be discerned via co-labelling of platelets (microthrombi) and endothelial cells (blood vessels) alongside the leukocyte of interest. Cells that become immobile during cardiac contracture could be identified via pairing of an electrocardiograph trace with the intravital videos obtained.

In Chapter 3, we demonstrated that VCAM-1 expression was also increased in IR injured vasculature. However, unlike in previously published work, this was observed on the capillaries as well as larger vessels [190]. This suggests active capture mechanisms may also have be involved in mediating capillary-neutrophil interactions in the heart. Neutrophil accumulation has long been recognized histologically as a significant component of myocardial IR injury. However, the impact of their sequestration on coronary perfusion has not been possible to determine from static sections. Intravitally, we show that obstructions in microvessel blood flow do not generally occur in areas with individual adherent neutrophils. This was evidenced by the fact that functional capillary density (FCD) did not decrease in the

whole field of view in parallel with the diffuse neutrophil adhesion. Indeed, only distinct patchy areas lacking FITC-BSA perfusion were observed.

Interestingly, a significant population of adherent neutrophils were observed in sham hearts *in vivo*. This was unusual based on our extensive intravital experience of imaging other solid organs [150, 151, 170, 195]. This may have been due to our experimental setup whereby placement of the 3D stabiliser onto the heart could have invoked a minor inflammatory response. However, this was unlikely as adherent neutrophils were present in sham hearts even in non-stabilised hearts. We speculate that this adhesion may have been due to some trafficking neutrophils becoming trapped within capillaries as blood vessels were compressed during systole. Extravascular compression during isovolumetric contraction markedly reduces coronary flow [225-227]. Indeed, our LSCI studies clearly identified decreased myocardial blood flow during systole, which may have contributed to neutrophil entrapment. Interestingly, these adherent neutrophils did not obstruct blood flow in sham (or indeed IR injured hearts) as evidenced by the ease and ability of FITC-BSA to permeate through the sham heart microvasculature.

Although at first glance these adherent neutrophils appeared firmly adherent, we were able to occasionally detect in both sham and IR injured hearts, some that appeared to slowly 'patrol' short lengths of the capillary. This patrolling behaviour is novel in the heart and the physiological relevance is unclear in sham mice, but following IR injury it may possibly reflect attempts to identify emigration sites. Recent intravital imaging provides evidence that neutrophils also constitutively patrol glomerular capillaries and following injury exhibit a greater dwell time and increased ROS generation [228]. This increase in cellular dwell time

may provide additional benefits in allowing inflammatory cells to be more readily recruited in the advent of cardiac injury. 'Crawling' neutrophils, seeking to provide the first line of defense against infection, have also been identified in pulmonary capillaries [229]. Collectively, our observation of 'patrolling neutrophils' in steady-state conditions, taken together with other studies showcasing this observation as well, seems to suggest a new behaviour for neutrophils that is not site-specific.

Numbers of free-flowing neutrophils circulating through the injured heart also doubled throughout reperfusion, although this to failed to attain statistical significance. This is an interesting observation, particularly in light of the fact that the density of FITC-BSA perfused capillaries decreased. Higher numbers of circulating neutrophils passing through less patent microvasculature can be explained by a possible increase in the blood flow to the injured heart. Indeed, this is supported by the LSCI data. Reactive hyperaemic responses post-occlusion benefit the oxygen-deprived myocardium. However, these responses may also have inadvertently introduced more inflammatory cells into an environment primed for their adhesion. The overall decrease in the perfusion of the microcirculation may thus have potentially aided in the sequestering of neutrophils into the border regions of IR injury.

4.4.4 Intravital Imaging of Monocyte Trafficking in the Beating Mouse Heart *in vivo*

Monocytes are precursors for macrophages and dendritic cells (DCs). Monocytes normally circulate freely or patrol blood vessels for a few days. During inflammatory states, they emigrate across the endothelial lining and rapidly begin the process of terminal differentiation into inflammatory DCs or macrophages [230]. After MI, monocytes have also been shown to

extravasate into the injured tissue and give rise to inflammatory DCs or macrophages [231]. Early elegant work by Nahrendorf and colleagues was the first to show that neutrophils accumulated in the infarcted myocardium within hours of IR injury, peaking after 24 hours. Thereafter, monocytes dominated the cellular infiltrate within the next 2 weeks to aid wound healing, with Ly-6C^{hi} monocytes arriving at day 1 and peaking at day 3 [232]. This work was mainly a histological and flow cytometric analysis of hearts undergoing permanent LAD ligation with the first assessment of the heart at 3-hours, 1-5, 7- and 16-days post-MI.

In this chapter, we studied the dynamic recruitment of endogenous circulating monocytes in the beating heart *immediately* post-reperfusion using a labelling method initially established by the Randolph lab to trace monocytes *in vivo* without the need to rely on their adoptive transfer [233]. This group used flow cytometric analysis to demonstrate that after 4 hours of non-degradable fluorescent latex bead infusion: (i) 1-2% of all circulating cells in the circulation become latex bead positive (ii) these were primarily monocytes and (iii) overall, ~10-12% of blood monocytes were phagocytically labelled after engulfing the beads. Haka and colleagues were the first to utilise this labelling method to image monocytes intravitally in aortic atherosclerotic plaques [179].

Our novel study used the same labelling method to image the dynamics of monocyte recruitment in both sham and IR treated beating mouse hearts. Interestingly, unlike previous studies which showed neutrophils to be the first responders, we found that in the immediate aftermath of reperfusion, monocyte recruitment was as rapid and as extensive as neutrophils. Indeed, the number of neutrophils adherent in the IR injured heart nearly tripled with the number of monocytes nearly quadrupled when compared to sham. Our findings here support

the theory that both neutrophils and monocytes infiltrate the injured heart simultaneously, rather than beginning with neutrophil recruitment followed by monocyte recruitment [234]. This is perhaps not that surprising in light of evidence that monocyte recruitment in the heart appears to be dependent on the same endothelial VCAM-1 utilised by neutrophils for recruitment [231]. This phenomenon was also observed in our sterile injury experiments, where both neutrophils and monocytes were readily recruited to the site of injury. This rapid recruitment of pro-inflammatory and phagocytic cells can be extremely detrimental to the site of injury. The sudden influx of monocytes, whose primary goal is to remove dead tissue, is inherently more harmful to the surrounding healthy tissue [73, 77]. Indeed, both neutrophils and monocytes can release proteolytic enzymes and ROS. Our novel data suggests that since both cell types arrive simultaneously, and in similar numbers, alleviating the recruitment of both cell types may be essential to provide a therapeutic mechanism by which myocardial IR injury is reduced.

4.4.5 Remarkable Thrombotic Events within IR injured Coronary Capillaries

Although individual platelet adhesion was enhanced, a most striking feature noted in IR injured hearts was the presence of multiple platelet aggregates. Similar to neutrophils and monocytes, the elevated recruitment of platelets was again rapid and sustained in the IR injured hearts. These were identified as mostly small rounded aggregates. However, larger, elongated microthrombi that spanned significant lengths of the capillaries were also seen. Some of the larger microthrombi tended to include trapped neutrophils, potentially contributing to its large mass. Indeed, we observed on a number of occasions freely circulating

neutrophils becoming trapped by microthrombi and unable to proceed downstream of a vessel. The presence of these microthrombi tended to coincide with areas of non-perfusion in the heart. Indeed, the major consequence of these was the detrimental effect on capillary perfusion in their immediate vicinity. This was demonstrated by the lack of FITC-BSA presence downstream of microthrombi. Hence multiple non-perfused areas were identified interspersed with perfused microvasculature. Our findings provide the first direct *in vivo* evidence of the often suggested notion that platelet microaggregates impede blood flow in the microvasculature following an MI [63, 235, 236]. Despite reperfusion of the major LAD, this component of the research clearly demonstrated that highly heterogeneous responses in the microvasculature occurred with some areas remaining blocked while others showed hyperaemic responses that were detected by LSCI. This is an important finding from a clinical perspective as seemingly reperfused coronary arteries in patients after a PCI may falsely suggest therapeutic success, when actually a large area of non-reperfused microvasculature can eventually result in severe loss of a functional myocardium [220].

4.4.6 Stem Cells Confer Vasculoprotection in the IR injured Beating Heart

The collective results of Chapters 3 and 4 highlight the coronary microcirculation as an early and principal therapeutic target to prevent ensuing muscle damage. Our model was therefore used for the first time to image whether vasculoprotection was a critical therapeutic mechanism employed by SCs to confer benefit in the reperfused beating heart. We focussed on cellular therapy as there has been intense interest in their use for CVDs. Clinical trials using SCs as a form of cell therapy for treating CVD have not yielded satisfying results. A major

reason behind this is the lack of pre-clinical understanding of the role that SCs can play in CVD [72]. The data presented in Chapter 3 showed that HPC-7s were a promising candidate to use as cell therapy in treating myocardial IR injury potentially through beneficial actions on the coronary microcirculation. We therefore attempted to investigate this possibility by initially investigating the impact that HPC-7s have on the injured microcirculation of the mouse heart using intravital microscopy. This has not previously been undertaken and so this was a novel aspect of the work and allowed the beating heart intravital model to be utilised for answering a specific research question. In this study, we have chosen to utilise a more purified population of HSCs (HPC-7s), although it needs to be acknowledged that most clinical studies utilise total un-fractioned BM mononuclear cells (comprising haematopoietic stem/progenitor cells, mesenchymal stem cells (MSCs), lymphocytes and monocytes).

Our initial experiments looking into the benefits of HPC-7s in treating cardiac IR injury focussed on assessing the impact of these cells on infarct size. The TTC staining method was used to determine the infarct size of IR injured hearts not receiving therapy in comparison to IR injured hearts treated with HPC-7s. Here we showed that HPC-7s were able to provide a significant reduction in infarct size, from ~45% in un-treated hearts to ~22% in HPC-7s treated IR injured hearts, reducing necrotic tissue in the heart. Our findings here agree with the work others have shown that HSCs can be beneficial in the setting of IR injury [150, 151]. Critical evaluation of the TTC stain observed in our experiments did show more necrotic tissue present in the subepicardial region over the subendocardial region, especially in IR injured hearts. This is unusual as many studies have shown that myocardial IR injury tends to cause necrosis to the subendocardial region before effecting the subepicardial region [183]. A possible reason for our results is the impact of prolonged freezing on the heart tissue prior to TTC staining causing

added damage [237]. This would have impacted both the IR and IR+HPC-7s groups and must be noted when considering the results of our findings.

In order to determine the specific impact that HPC-7s therapy had on myocardial IR injury, we also investigated their effects on the blood flow dynamics using LSCI. We found that the hyperaemic response that was present in un-treated IR injured hearts was still present in the treated hearts. This was perhaps not too surprising a result, as the impact of ischaemia would still have inflicted damage onto the myocardium, that would have proceeded to release danger/damage signals encouraging an increase in blood flow to make up for the debt of nutrient and oxygen deprivation. Again, the hyperaemic response was sustained throughout the reperfusion period, indicating that HPC-7s therapy did not affect this response. In addition to this, the microvasculature of the heart was significantly improved with HPC-7s therapy too as assessed intravitally. Delineation of the microcirculation with FITC-BSA showed a return to the well-structured and organised network of capillaries in the heart.

HPC-7s also afforded rapid and remarkable vasculoprotection in the injured heart through limiting neutrophil, monocyte and platelet adhesive events. This reduction is likely a major contributor to maintaining the patency of an intact microvasculature in these hearts. The same HPC-7 cells used in this current study have previously been shown by the Kalia group to produce anti-inflammatory factors to inhibit the recruitment of neutrophils in other IR injured organs [150]. Studies have shown that SCs and progenitor cells derived from the BM are able to secrete a combination of growth factors and anti-inflammatory cytokines. These are then able to influence neighbouring cells and modulate the inflammatory response by a paracrine action [238]. Even without retention in the heart (which will be investigated in Chapter 5),

these factors may be released systemically from remote sites and confer vasculoprotection in the heart. Indeed, remote transplantation of MSCs into the interscapular region protected the IR injured heart [239]. Reducing neutrophil recruitment most likely limits the presence of ROS within the IR heart as neutrophils are key sources of this free radicals. This would protect neighbouring endothelial cells from oxidative damage. A healthy endothelium is better able to modulate inflammatory cell recruitment. Indeed, we demonstrated in Chapter 3 how HPC-7s had the potential to reduce ROS generation and directly protect endothelial cells from oxidative stress. With the presence of antioxidants such as SODs, HSCs may be able to rebalance oxygen consumption and reduce the production of superoxide and hydrogen peroxide [148]. In Chapter 3 we also showed that HPC-7s inhibited ICAM-1/VCAM-1 up-regulation. This is probably the most likely mechanistic explanation for the decreased neutrophil and monocyte infiltration.

The impact of HPC-7s therapy on the reduction in platelet aggregation is harder to explain. One possibility that may explain our findings is that platelet activation and aggregation occurred due to endothelial damage and denudation that was instigated by inflammatory cells such as neutrophils. However, as our earliest ability to conduct intravital imaging only began at 30 minutes post-reperfusion, it is not clear which of the thrombotic or inflammatory events occurred first. Indeed, HSCs may harbour direct anti-thrombotic capabilities. A recent study by Peng et al. described how MSCs were linked to the modification of urokinase-type plasminogen activator (UPA) [240] UPA is known to play a role in the early resolution of a thrombus. The ability of HSCs to also modify this pathway is unknown and would require further investigation. Interestingly, we found that the number of circulating neutrophils and monocytes trafficking through the injured heart was higher in HPC-7s treated IR injured hearts

when compared to untreated mice. Indeed, at 30- and 45-minutes post-reperfusion, monocytes were found in significantly higher numbers circulating through the heart. We speculate that by preventing the formation of platelet-rich microthrombi and thus the occlusion of capillaries, the leukocytes could freely circulate through coronary microvessels. However, in the absence of appropriate adhesion molecules, and in the presence of a possible plethora of soluble anti-inflammatory agents released in a paracrine manner by HPC-7s, these cells were simply not recruited despite readily circulating through the site of injury.

4.4.7 Technical Limitations of the Study

Our desire to understand the inflammatory response during myocardial IR injury also led us to investigate the role that macrophages played in this model immediately post-reperfusion. Unfortunately, we were unable to successfully label resident or infiltrating macrophages in our experiments. Systemic injection of the rat anti-mouse F4/80 antibody did not adequately label macrophages in the beating mouse heart. The failure to image resident macrophages was most likely explained by the inability of the antibody to penetrate through the blood vessel and bind to macrophages in the myocardium. Infiltrating macrophages were also unlikely to have appeared within the acute timeframe that we used in our experiments. We do not believe that problems with the labelling protocol was a likely explanation as the same staining protocol was effective in the liver, as evidenced by us and others, to use it to successfully label Kupffer cells [182]. Kupffer cells are specialized hepatic macrophages that line the walls of the sinusoidal capillaries. This meant that they had easy access to the systemically injected fluorescently tagged F4/80 antibody.

Another method of visualising cardiac macrophages was by using genetically altered mice with the enhanced-GFP gene attached to CD68 (CD68-eGFP) [241]. CD68 expression is restricted to monocyte/macrophages and is commonly used as an immunostain to label infiltrating monocyte-derived macrophages in atherosclerotic plaques [241]. However, when CD68-eGFP transgenic mice were used intravitally, we found that the auto-fluorescent level in the hearts of these mice was high, given that both monocytes and macrophages – and even a small number of neutrophils – were brightly labelled [241]. Quantification of data was difficult, especially in IR injured hearts. Differentiating monocytes and macrophages based purely on size proved fruitless, necessitating additional concessions in order to specifically demarcate macrophages. This would have included simultaneous labelling of neutrophils and monocytes as well. As such, and due to time constraints, we were not able to further investigate the role that macrophages played in myocardial IR injury.

Due to our surgical protocol and setup, another limitation of our work was the inability to acquire IVM images within the first 30 minutes post-reperfusion. This was a shame in light of the fact that the rapid increase in thrombo-inflammatory cell recruitment had already taken place within those first 30 minutes. In order to overcome this issue, attempts were made to alter the surgical model by replacing the conventional method of tying off the LAD artery with a suture tied against a plastic tube with a new model termed ‘balloon ligation’. This model was similar in surgical preparation up until the placement of the plastic tube, where instead a small inflatable balloon was placed within the loosely tied off suture. This balloon was connected to a syringe and then inflated using saline. This caused it to compress the LAD artery and induce ischaemia with reperfusion initiated as soon as the balloon was deflated. The advantage of this model was that it allowed us to safely, quickly and easily induce ischaemia and reperfusion

whilst the mouse was on the intravital microscope ready for imaging (and therefore without the need to place the mouse under a surgical microscope).

Although inflating the balloon proved trickier than deflating, using LSCI we were still able to safely and successfully induce ischaemia and subsequent reperfusion and simultaneously acquire real-time flux images. We observed that the heart did not move during the period of deflation either, an important aspect to consider if IVM experiments using our 3D stabiliser were to be carried out using this method. This potentially could allow us to safely deflate the balloon while the beating heart was being imaged under the intravital confocal microscope, with the 3D stabiliser already in place. Whilst only a small success, further improvements to this model could very feasibly allow us to obtain valuable data from the missing critical 30 minutes post-reperfusion. Ultimately, we could even look to obtain images during the whole experiment, from pre-ischaemia to ischaemia to reperfusion. Unfortunately, as this setup was challenging and the creation of the device underwent many changes, we did not have enough time to test this model using IVM in this study.

Although spinning Nipkow disk intravital imaging allows high-quality and high resolution, real-time videos to be captured, one limitation of this tool is the relatively superficial imaging depth of 25-35µm. This impedes our ability to understand the workings of the microcirculation in the depths of the myocardium from the epicardial surface through to the endocardial layer lining the chamber. Even the use of a multiphoton microscope in order to conduct beating heart experiments, if this was possible, would only result in a slight increase in depth of around 70-80µm. As such, global assessment of any microcirculatory changes would require additional investigations such as full imaging of sliced tissue sections or flow cytometry.

4.4.8 Conclusion

In conclusion, this chapter has provided us with valuable information with regards to the real-time and dynamic coronary microcirculatory changes that occur post-reperfusion injury and the vasculoprotective benefits of HPC-7s therapy in alleviating those perturbations. Indeed, our novel work which combines intravital imaging of the beating mouse hear with laser speckle microscopy, provides a wealth of dynamic information on the coronary microcirculation that was not possible to obtain with conventional immunohistological approaches. We show for the first time that although myocardial IR injury is associated with an overall hyperaemic response in the injured left ventricle, this may be deceptive as at a microvascular level, increased flow heterogeneity exists due to occluded coronary capillaries. To the best of our knowledge, this is the first detailed *in vivo* characterisation of multiple microcirculatory perturbations taking place in the IR injured beating heart. We further show that HPC-7s can prevent deleterious myocardial thromboinflammatory events. Our findings provide never before seen images of the thromboinflammatory response and changes in microvascular structure in both IR injured hearts and injured hearts that received HPC-7s therapy.

The work outlined in this chapter was published in *Cardiovascular Research* and was followed by an Editorial in which the authors stated: “The combination of three new developments, namely high-end intravital microscopy, 3D-printing of stabilisers and laser speckle contrast imaging (LSCI) has now provided long-awaited insights in the mechanisms underlying micro-obstructions and other vascular pathologies of the microcirculation in mouse hearts undergoing ischaemia/reperfusion.” [220].

CHAPTER 5: MECHANISMS BEHIND THE VASCULOPROTECTIVE EFFECTS OF HPC-7s THERAPY IN MYOCARDIAL IR INJURY

5.1 Introduction

Cellular therapy utilising BM-derived HSCs in clinical trials for the treatment of various cardiovascular conditions has been ongoing for years. Indeed, many trials have demonstrated that stem cells are both a feasible treatment option and safe to use [242]. However, although considered a promising approach, particularly for ischaemic heart diseases, their success has been limited clinically. It is generally agreed that major obstacles still need to be solved before stem cell therapy can be fully applied. These include a thorough understanding of the therapeutic mechanisms they employ to confer benefit, which for the treatment of MI remain poorly understood. This is due to a lack of preclinical studies assessing the actual beneficial effects of HSCs. Although a major focus has been on their ability to reduce infarct size, whether they can protect the coronary microcirculation from IR injury has not previously been investigated *in vivo.*

In Chapter 4 we demonstrated that HPC-7s can be remarkably vasculoprotective. However, there are further important questions that still need to be answered. These are centred on the mechanisms they have employed in order to confer this vasculoprotection. It is not, for example, well documented whether HSCs are actually required to home to the heart in order to impart any kind of benefit to coronary blood vessels. This is because it has not been possible to image, at a cellular level, the trafficking and subsequent retention of individual HSCs within the coronary microcirculation. The ability of pre-treatment strategies to visibly enhance HSC retention within the heart is also unknown. The Kalia group have previously shown that HPC-7 pre-treatment with H_2O_2 can increase their homing and retention in the IR injured gut and so this was worth considering in the IR injured heart too [150]. It is plausible

that retention is not essential and the simple activation of HSCs as they circulate through the heart produces a paracrine effect that leads to an overall benefit to the microvasculature. HSCs may even localise to other organs, such as the lungs, and provide therapeutic benefit from a remote site. It is also unclear whether the whole cell is required for vasculoprotection of whether secreted pro-repair molecules may be sufficient on their own. Indeed, stem cell-derived cultured medium, containing various growth factors and anti-inflammatory cytokines, appears promising for regenerative medicine and has gained significant pharmaceutical company interest [243]. All of this will be possible to investigate using intravital imaging of the beating mouse heart.

In addition to investigating the above raised questions regarding HSC homing to the heart, this current chapter will also determine in more detail the specific mechanisms involved that may explain the ability of HSCs to be vasculoprotective post-IR injury. We have previously demonstrated in Chapter 3 that oxidative stress and endothelial inflammatory changes such as adhesion molecule up-regulation were prominent events. Both could mediate the microcirculatory thromboinflammatory events described in Chapter 4. Therefore, in this chapter we will further assess the ability of HPC-7s to modify these two events in the IR injured heart using a novel flow cytometry protocol we have developed to detect both oxidative damage and adhesion molecule expression on coronary endothelial cells of the digested injured heart.

Whether HPC-7s can modify the levels of a whole host of inflammatory cytokines will also be assessed. This chapter will focus on the role of a new member of the IL-1 superfamily, namely IL-36, in mediating inflammatory responses in the heart. This has not previously been

determined. Indeed, the ability of IL-36 to directly affect circulating cell recruitment has not previously been assessed intravitally in any organ or vascular bed. The ability of this cytokine to induced both neutrophil and/or monocyte adhesion within coronary microvessels of the beating mouse heart will therefore be determined intravitally. Importantly, whether HPC-7s can prevent IL-36 from having a pro-inflammatory effect will be assessed *in vivo.* An exciting potential for HPC-7s to modulate IL-36 activity in the heart would be a novel finding.

In Chapter 4, it was clear that myocardial IR injury could recruit monocytes immediately upon reperfusion in numbers similar to neutrophils. However, what was not deciphered was which sub-population of monocyte was recruited – in other words, which of the $Ly6C^{hi}$ inflammatory or $Ly6C^{lo}$ non-inflammatory monocytes became immediately adherent in reperfused coronary capillaries. Therefore, in this chapter, this detail will be provided by making use of monoclonal antibodies and flow cytometry to clearly define and enumerate murine classical and non-classical monocyte subsets based on the differential expression of cell surface markers like CD115 and Ly6C (Gr1) [244, 245]. Importantly, whether the anti-inflammatory mechanism of HPC-7s relies on their ability to modify a specific monocyte sub-population in the IR injured heart will be investigated.

5.1.1 Hypotheses and Aims

This chapter therefore focussed on eliciting the mechanisms behind HPC-7s therapy in protecting the heart during myocardial IR injury. The main aims and hypotheses of this chapter are shown below.

1. This chapter firstly aimed to investigate the homing potential of HPC-7s to the IR injured heart using IVM and assess whether this event could be enhanced with pre-treatment strategies known to be effective in other organs. The level of non-site-specific retention within non-injured organs will also be determined. **HYPOTHESIS:** HPC-7s recruitment to the injured heart will be higher than in sham hearts, with H_2O_2 increasing their retention further.
2. The ability of HPC-7s cultured media to confer vasculoprotection and thus provide any tangible benefits to HPC-7s therapy in myocardial IR injury will be assessed intravitally. **HYPOTHESIS:** Soluble factors released from HPC-7s are all that is required for HPC-7s to be beneficial.
3. The level of oxidative damage and up-regulation of adhesion molecules (ICAM-1 / VCAM-1) on coronary endothelial cells post-IR injury will be compared with the injury incurred by cardiomyocytes using flow cytometric analysis. Attempts will be made to also image VCAM-1 intravitally. **HYPOTHESIS:** Coronary vascular cells will be more susceptible to oxidative and inflammatory injury and this will be inhibited in the presence of HPC-7s.
4. Detailed analysis of which monocyte subset is present in the heart following IR injury will be performed and the impact of HPC-7s on their presence determined.

HYPOTHESIS: Myocardial IR injury will induce a pro-inflammatory shift in the recruited monocyte population with HPC-7s therapy reversing this towards a non- or anti-inflammatory monocyte response.

5. The role of IL-36 as a novel inflammatory stimulus in the coronary microcirculation will be assessed intravitally and the effect of HPC-7s on inhibiting any response they elicit determined. **HYPOTHESIS:** HPC-7s will attenuate any potential pro-inflammatory activity of IL-36.

5.2 Methods

Detailed methods are described in Chapter 2. Briefly, in order to determine the homing capabilities of HPC-7s in the IR injured beating heart using IVM, surgery was performed in anaesthetised mice to ligate the LAD artery for 45 minutes of ischaemia followed by 2 hours of reperfusion. Following reperfusion, a 3D-printed stabiliser was attached to the heart using biological glue. The first intravital video (2 minutes) was captured at 30 minutes post-reperfusion and thereafter every 15 minutes until 2 hours of reperfusion elapsed. In order to visualise HPC-7s homing to the heart, these cells were labelled with CFSE and injected intra-arterially (2 x10^6 cells) during the initial video capture. This allowed us to image the first pass of these cells through the heart. In some studies, 200µL of cultured media (CM) sourced from HPC-7s was injected intra-arterially at 5 minutes post-reperfusion. Briefly, CM was obtained after HPC-7s that were seeded between 3 to 5 x 10^6 cells in 3 to 5ml (1 x 10^6 cells/ml) of fresh culture media experienced a 2-fold growth after a single day. Media was then collected and stored at -80^{o}C until use.

IVM experiments were also performed looking at the effect of a topical application of the three IL-36 isoforms (IL-36α, IL-36β and IL-36γ) on inflammatory cell recruitment. A 3D-printed stabiliser was attached to the surface of the left ventricle as previously described. A waterproof well was created in the centre of the stabiliser that was conducive to the topical application of solutions to the heart surface. Initially, 3µl of PBS was applied and left for 20 minutes before removal and imaging. This initial timepoint provided a point of comparison for IL-36 cytokine topical treatment within the same mouse. After the PBS treatment, 3µl of either IL-36α, β or γ (100ng/ml) was added into the well and left for 20 minutes before removal and imaging. This was repeated until 2 hours had elapsed. An IL-36 receptor antagonist (IL-36RA) was tested in one mouse. Briefly, 3µl of IL-36RA (250 µg/ml) was added to 100µl of PBS and injected intra-arterially 5 minutes post-reperfusion.

In order to fluorescently label endogenous neutrophils or endothelial VCAM-1 for intravital imaging, APC-conjugated rat anti-mouse Ly6G or APC-conjugated rat anti-mouse CD106 (VCAM-1) antibodies were injected intra-arterially respectively. In mice undergoing IR injury, these were administered 5 minutes prior to reperfusion whilst in topical application experiments, these were given 10 minutes prior to PBS application. To label monocytes, fluorescent microparticles/beads were injected intra-arterially 10 minutes prior to ischaemia in IR injury experiments or 10 minutes prior to PBS application in topical application studies.

Flow cytometry was utilised to quantitate VCAM-1 (CD106), ICAM-1 (CD54) and oxidative stress (using 8-OHdG) on coronary endothelial cells ($CD31^+$) or cardiomyocytes ($cTnT^+$) or quantitate monocyte sub-populations (using surface markers for CD115 and Ly6C). Hearts were harvested from experimental mice and then manually sliced into $1mm^3$ pieces in order

to facilitate enzymatic digestion. The slices of heart were incubated in collagenase type-1 solution (0.1%) at 37^{o}C for 45 minutes to obtain a single cell suspension. If labelling was required, the cells were resuspended in blocking buffer consisting of rat anti-mouse CD16/32 antibody. Once washed, the cells were incubated with either PE-conjugated rat anti-mouse CD115 antibody, PECy7-conjugated rat anti-mouse Ly6C antibody, PE-conjugated rat anti-mouse CD31 antibody, AF488-conjugated rat anti-mouse CD54 antibody, PE-Cy7-conjugated rat anti-mouse CD106 antibody, PE-conjugated rat anti-mouse cTnT antibody or unconjugated goat anti-mouse 8-OHdG antibody (with AF488 donkey anti-goat secondary). The cells were then stored at 4^{o}C until analysis. Similar steps were undertaken when the blood, lungs or liver were harvested for flow cytometric analysis.

To assess the inflammatory cell profile within peripheral blood collected after myocardial IR injury experiments, 500µl of anti-coagulated blood was collected and run through a Horiba blood counter machine. To assess the inflammatory cytokine profile within plasma, similarly, 500µl of anti-coagulated blood was collected and centrifuged (2000 rpm, 10 min) to obtain plasma. Circulating cytokine concentrations were identified in plasma samples from experimental mice. Samples were loaded in triplicate onto a Bio-Plex pro mouse cytokine 23-plex assay plate and analysed using a Luminex 200 plate reader. The protocol supplied by the manufacturer for mouse cytokine assay preparation and analysis was followed for accurate measurements.

5.3 Results

5.3.1 HPC-7s Demonstrate Low Levels of Adhesion within the Coronary Microcirculation following Myocardial IR Injury

We firstly assessed whether the vasculoprotective effects of HPC-7s following myocardial IR injury could mechanistically be explained by an increase in their homing and retention within the injured coronary microvessels. Intravitally, the adhesion of HPC-7s in IR injured hearts was low and not significantly different to that observed in sham mice. Pre-treatment of HPC-7s for an hour with 100μM H_2O_2 did not enhance their retention ***(Figures 5.1A and 5.1B)***. Unlike the very high numbers of adherent neutrophils and monocytes (100-150 cells) described in Chapter 4, only 5-10 firmly adherent HPC-7s were seen in IR injured hearts in the imaged field of view. However, there appeared an almost four-fold increase in the number of free flowing naïve and H_2O_2 pre-treated HPC-7s in IR injured hearts (~90 cells/field of view) compared to in sham hearts (~25 cells/field of view) at the initial imaging time point of 30 minutes into reperfusion. However, this was not significantly different between all three groups. Thereafter, the number of free-flowing HPC-7s was generally maintained at ~25 cells/field of view for the remainder of reperfusion, which was not significantly different to sham mice ***(Figure 5.1C)***.

5.3.2 Non-Specific HPC-7s Retention Identified Within Non-Injured Lungs and Liver

Intravital experiments observed a single, small region of the epicardial surface of the left ventricle continuously throughout reperfusion. Therefore, it was possible that the small

number of adherent HPC-7s identified intravitally was not truly representative of adhesive events taking place in the whole heart. Therefore, flow cytometric analysis of digested whole hearts, as well as the lungs and liver removed from the same mouse, was also undertaken in order to determine HPC-7s presence. The gating strategy for isolating CFSE labelled HPC-7s from digested whole heart tissue is provided ***(Figure 5.2A)***. Again, a low retention of HPC-7s was observed in IR injured hearts, confirming the intravital data, which was not statistically different to sham hearts. Approximately 0.14% and 0.09% of all the viable cells in the heart were HPC-7s in sham and injured hearts respectively ***(Figure 5.2B)***.

In contrast, more HPC-7s appeared retained in remote organs, with 0.76% and 1.10% of all viable cells identified as HPC-7s in the liver and lungs respectively of mice undergoing sham myocardial surgery. This was at least a 5-fold increase in HPC-7s present within sham livers and an 8-fold increase in the sham lungs compared to the sham heart. There was also a trend for an increase in HPC-7s retained in the liver and lungs removed from mice undergoing myocardial IR injury. Indeed, 7.26% and 3.11% of all viable cells were identified as HPC-7s in the liver and lungs respectively of mice undergoing myocardial IR injury. These numbers were almost double that compared to the same organs' sham tissue however, this was not statistically significant. Furthermore, this was at least an 80-fold increase in HPC-7s retained in IR livers and a 35-fold increase in the IR lungs compared to the IR heart ***(Figure 5.2C)***.

5.3.3 HPC-7s Cultured Media (CM) Is Not Vasculoprotective

In the previous chapter, we demonstrated that infusion of HPC-7s was able to modify thrombo-inflammatory events. This could mechanistically be explained by active soluble factors released from HPC-7s. Furthermore, the previous figures demonstrated that HPC-7s retention was not high, indicating their local retention was not necessary for a therapeutic effect. We therefore went on to investigate whether CM sourced from cultured HPC-7s would have similar effects on platelet and neutrophil recruitment as the HPC-7s themselves. 200µl of CM from HPC-7s was injected systemically 5 minutes into reperfusion of the heart, a time point similar to when HPC-7s themselves were injected. IVM images obtained showed that even after 2 hours of reperfusion, there was still a visibly high recruitment of both neutrophils and platelets/microthrombi ***(Figure 5.3A-C)***. This was noted in two separate experiments. As there appeared no reduction in the recruitment of neutrophils and platelets, the experiment was halted and no statistical analysis was performed.

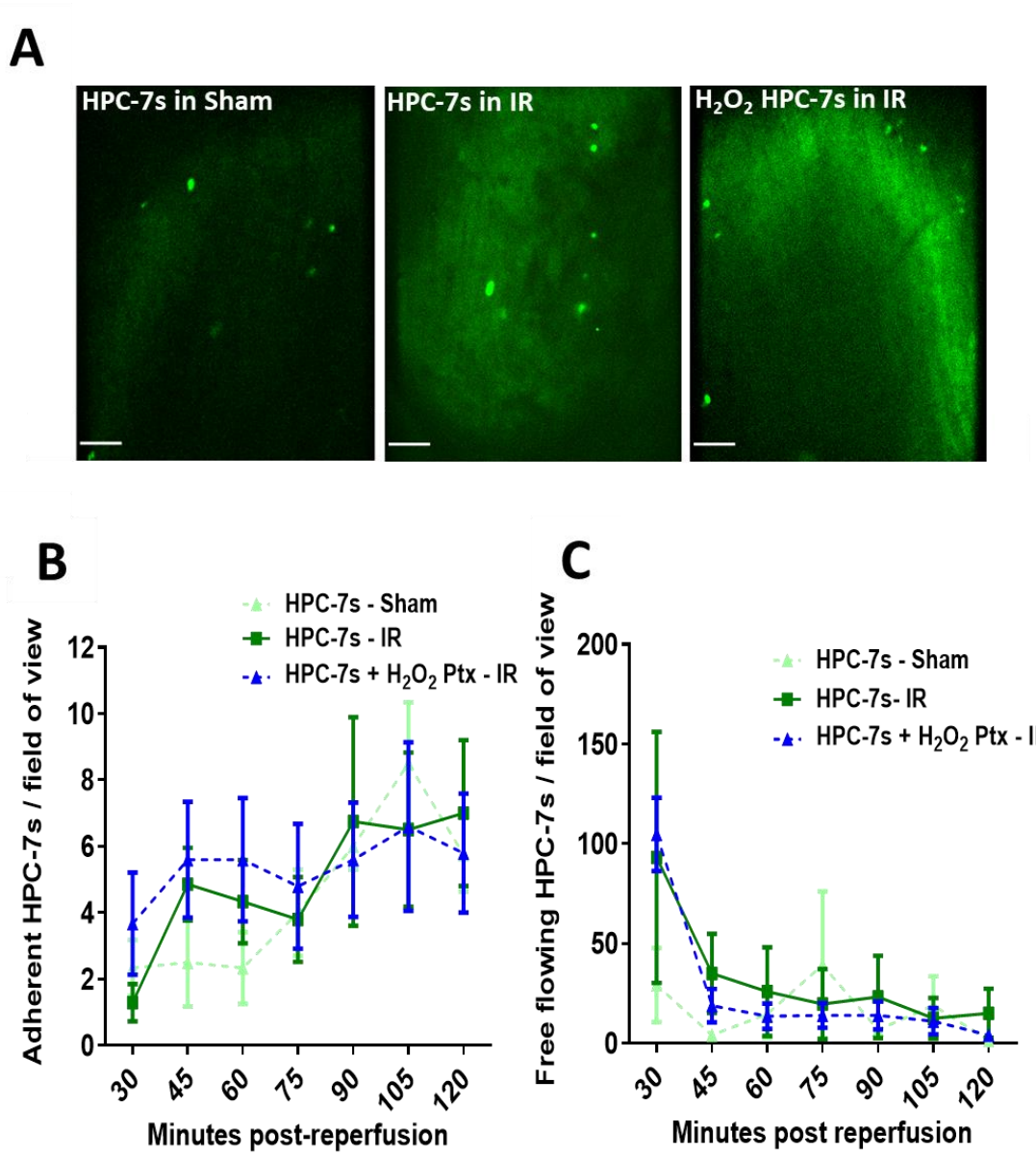

Figure 5.1. Intravitally assessing the homing capabilities of HPC-7s to the IR injured heart - HPC-7s Demonstrate very Low Levels of Adhesion within the Coronary Microcirculation following Myocardial IR Injury. ***(A)*** *In order to determine whether recruitment of HPC-7s into the heart was required to impart their vasculoprotective benefits, IVM experiments were undertaken whereby CFSE labelled HPC-7s (green) were imaged in sham and IR injured beating hearts. Representative intravital images obtained showed no obvious differences in the recruitment of naïve or H_2O_2 pre-treated HPC-7s to the heart after IR injury.* ***(B)*** *HPC-7s adhesion in IR injured hearts was low and not significantly different to that observed in sham mice. Pre-treatment of HPC-7s for an hour with 100µM H_2O_2 did not enhance their retention.* ***(C)*** *Whilst there appeared an initial burst of free-flowing HPC-7s in the IR injured hearts at 30 minutes post-reperfusion, statistical analysis of the data obtained showed no significant difference in free-flowing HPC-7s between all three groups. Statistical analysis was performed using two-way ANOVA with Sidak's multiple comparison test. N=5 per group. Scale bar = 100µm.*

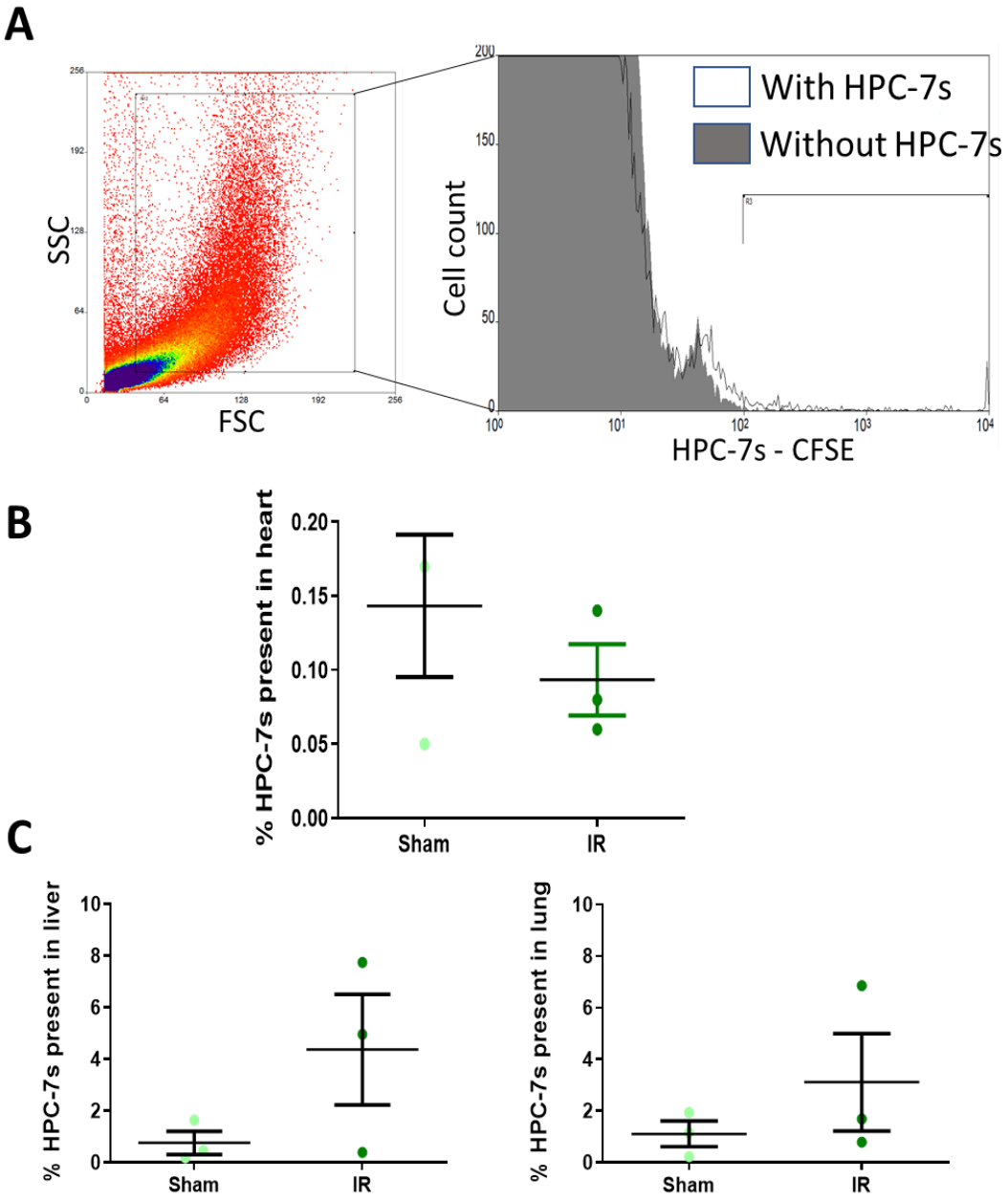

Figure 5.2. Non-Specific HPC-7s Retention Identified Within Non-Injured Lungs and Liver. *Flow cytometry was utilised to determine the level of HPC-7s recruitment in the whole heart, liver and lungs after myocardial IR injury.* ***(A)*** *An example of the gating strategy used to isolate CFSE-labelled HPC-7s from digested whole heart tissue is provided.* (***B***) *Data obtained from the heart indicated very few HPC-7s were retained and that there was no significant difference in sham or IR injured hearts.* ***(C)*** *The liver and lungs showed a much higher retention of HPC-7s, even in the sham group. There appeared an increase in HPC-7s retained in the liver and lungs removed from mice undergoing myocardial IR injury with numbers almost double compared to sham. However, there was no significant difference between the two groups. Statistical analysis was performed using unpaired t-test. N=3 per group.*

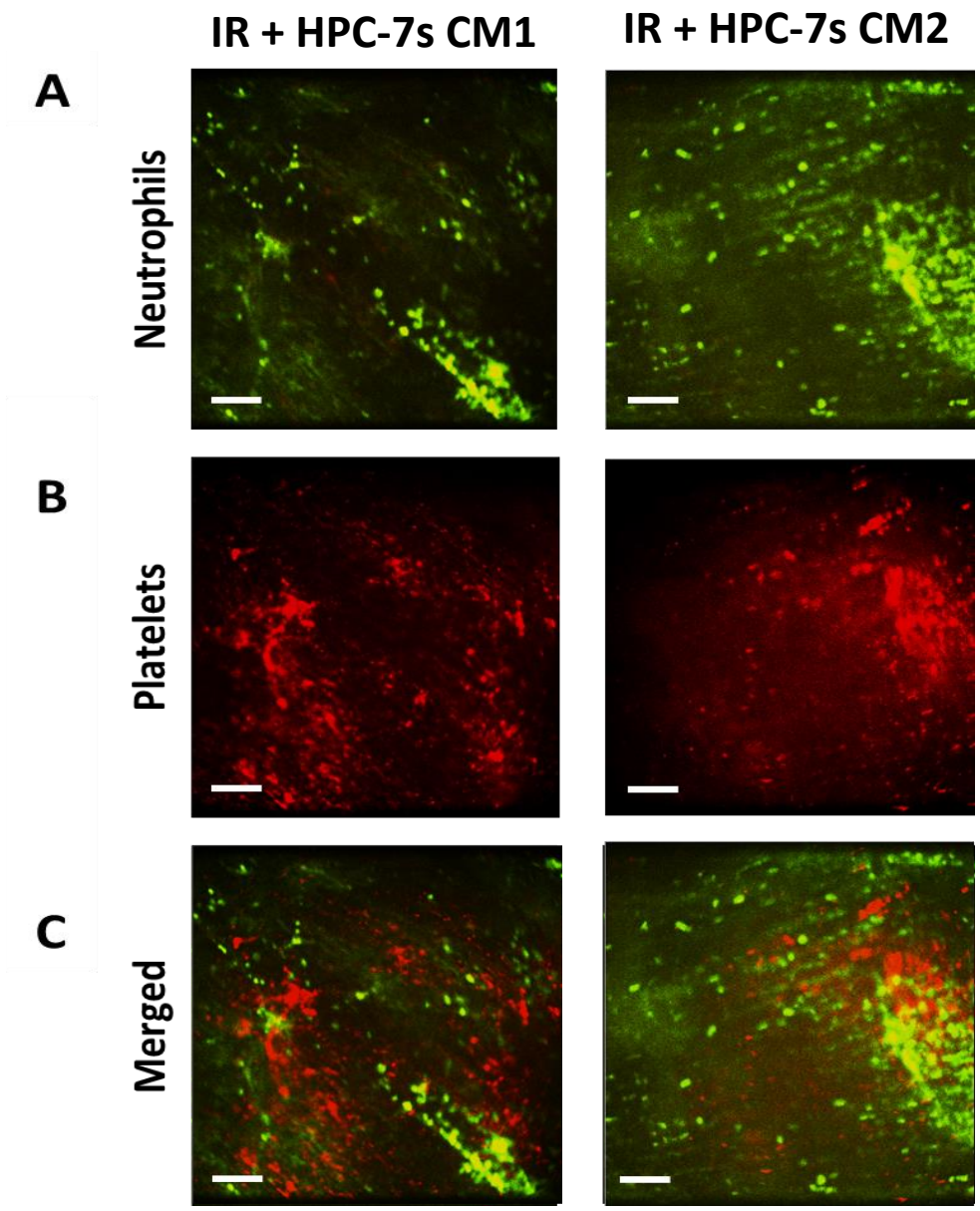

Figure 5.3. Intravitally determining the effects of HPC-7s cultured media (CM) on platelet and neutrophil recruitment in myocardial IR injury*. As the homing of HPC-7s to the heart was not necessary to invoke a significant reduction in the thrombo-inflammatory cellular recruitment during IR injury, we investigated whether CM obtained from cultured HPC-7s would be adequate to elicit a similar response. 200µl of CM from HPC-7s was injected systemically 5 minutes into reperfusion.* ***(A-C)*** *Representative intravital images show platelet and neutrophil recruitment appeared high after 2 hours of reperfusion in 2 separate experiments. As the use of CM from HPC-7s appeared ineffective, the experiment was halted and statistical analysis was not performed. Green: neutrophils (PE+anti-Gr-1ab); Red: endogenous platelets (APC+anti-CD41ab). N=2. Scale bar = 100µm.*

5.3.4 Flow Cytometric Analysis of Oxidative Stress and ICAM-1/VCAM-1 in Whole Hearts

As our previous IHC experiments described in Chapter 3 had shown that endothelial inflammatory dysfunction and oxidative stress were relevant events that occurred during myocardial IR injury in the mouse heart, experiments focussing on identifying the level of oxidative damage and endothelial dysfunction in *whole* hearts were carried out utilising flow cytometry. The ability of HPC-7s to confer vasculoprotection through modifying these events in the whole heart was also investigated. Whole hearts were digested in order to obtain a high yield of a single cell suspension. However, this digestion process required optimisation. The different protocols utilised are described below.

5.3.4.1 Optimisation of the Heart Digestion Protocol - Optimisation Protocol 1

Flow cytometry experiments were initially conducted on mice hearts that were digested utilising an enzymatic combination of 0.1% collagenase and 1x trypsin-EDTA. These hearts were then fixed and permeabilised using 2% formalin and 0.1% triton x-100 respectively (Protocol A). These experiments produced results that were incomprehensible as it became difficult to discern positive antibody staining for $CD31^+$ endothelial cells and $cTnT^+$ cardiomyocytes from IgG labelled control samples ***(Figure 5.4A)***. The protocol was slightly modified and optimised by changing the method for digesting the whole mouse heart in order to obtain substantial cell yields for subsequent analysis. This involved using the protocol described in **Section 5.2** whereby only 0.1% collagenase was used to digest whole mouse hearts and 70% ethanol (cold) was used to fix and permeabilise cells (Protocol B). This protocol

provided better results that could be used for data analysis as the $CD31^+$ endothelial cells and $cTnT^+$ cardiomyocytes were clearly distinct from IgG labelled control cells ***(Figure 5.4B)***.

5.3.4.2 Optimisation of the Heart Digestion Protocol – Optimisation Protocol 2

Another protocol optimisation was necessary in order to determine levels of oxidative damage in heart tissue. During initial flow cytometry experiments, it was found that the anti-8-OHdG antibody used to determine the presence of oxidative cell damage, at a high concentration or 1:50 dilution, would skew data and bleach into adjacent fluorescent channels at high concentrations. These experiments produced results that could therefore not be adequately analysed ***(Figure 5.5A)***. This issue was resolved by utilising a lower concentration of the anti-8-OHdG antibody at a 1:500 dilution. With this antibody dilution factor, cells were still being positively stained without bleaching ***(Figure 5.5B)***.

5.3.5 Endothelial Cells are More Susceptible to Oxidative Stress than Cardiomyocytes following IR Injury - HPC-7s Therapy Reduces this Oxidative Damage in Endothelial Cells

Flow cytometric analyses were performed on digested whole hearts in sham, ischaemic, IR injured and IR injured + HPC-7s experiments. The gating strategy used to isolate $CD31^+$ ECs and $cTnT^+$ cardiomyocytes, and their corresponding oxidative damage levels as evidence by being $8\text{-}OHdG^+$, is provided ***(Figure 5.6A)***. The percentage of ECs obtained was approximately 12% of the total viable cells obtained from the digested heart regardless of the experimental group. The percentage of cardiomyocytes obtained was much higher at around 70% of the

total viable cells obtained from the digested heart, again regardless of the experimental group as well ***(Figure 5.6B)***.

The level of oxidative damage in ECs was significantly ($p<0.01$) higher in IR injured hearts compared to sham hearts. For these experiments, we also aimed to determine if this damage was incurred early during the ischaemic phase, in which case, hearts were removed from some mice after 45 minutes of LAD artery ligation. Although oxidative damage was increased on ECs as a result of the ischaemia compared to sham, this was not statistically significant. HPC-7s therapy significantly ($p<0.05$) reduced the level of endothelial oxidative damage in IR injured hearts when compared to injured hearts not receiving cellular therapy to a level similar to sham hearts ***(Figure 5.7A)***. The level of oxidative damage incurred by the cardiomyocytes was also assessed. Although there was a slight increase in oxidative damage following ischaemia and IR injury, this was not significantly different. HPC-7s did not affect this response ***(Figure 5.7B)***.

5.3.6 Myocardial IR Injury Induces an Upregulation of ICAM-1 and VCAM-1 in Endothelial Cells – HPC-7s Therapy Reduces this Adhesion Molecule Upregulation

In order to better understand the impact of myocardial IR injury on the coronary microcirculation, we further investigated the modulation of endothelial adhesion molecules within digested whole hearts. The gating strategy used to isolate $CD31^+$ ECs and the adhesion molecules ICAM-1 ($CD54^+$) and VCAM-1 ($CD106^+$) is provided ***(Figure 5.8A)***. ICAM-1 expression was significantly increased as a result of ischaemia ($p<0.05$) and reperfusion injury ($p<0.01$) compared to sham. HPC-7s therapy significantly ($p<0.05$) reduced their expression in

comparison to the IR injured group ***(Figure 5.8B)***. Generally, VCAM-1 expression was lower than ICAM-1. Although its expression was elevated in IR injured hearts, this was not significant when compared to sham. Again, HPC-7s therapy reduced this expression of VCAM-1 ***(Figure 5.8C)***. VCAM-1 expression *in vivo* in the beating mouse heart was also imaged intravitally at the end of 2 hours reperfusion. Interestingly, it observed in the larger microvessels but to a much lesser extent in the coronary capillaries ***(Figure 5.8D)***.

5.3.7 HPC-7s Therapy Reduces Plasma Levels of Multiple Inflammatory Cytokines but Increased Levels of IL-10

Circulating plasma levels of 10 out of 23 investigated inflammatory cytokines were significantly ($p<0.05$) elevated in the IR injured group compared to sham ***(Table 1)***. The highest increases – more than 6-fold – were seen for IL-6, IL-12(p40), G-CSF, CXCL1, CCL2 and CCL4 cytokines. HPC-7s therapy significantly reduced 9 of these 10 pro-inflammatory cytokines elevated in the IR injury group ($p<0.05$-0.001). The only one increased by IR injury but not reduced by HPC-7s was IL-10. Interestingly, HPC-7s induced a further significant ($p<0.001$) increase in IL-10. This was the only cytokine to be significantly increased in IR injured hearts receiving HPC-7s therapy. HPC-7s therapy also significantly reduced 11 other cytokines not elevated in IR injury, including IL-1α, IL-1β, IL-2, IL-3, IL-5, IL-9, IL-12(p70), IL-13, IL-17, GM-CSF and IFNγ ($p<0.05$-0.001).

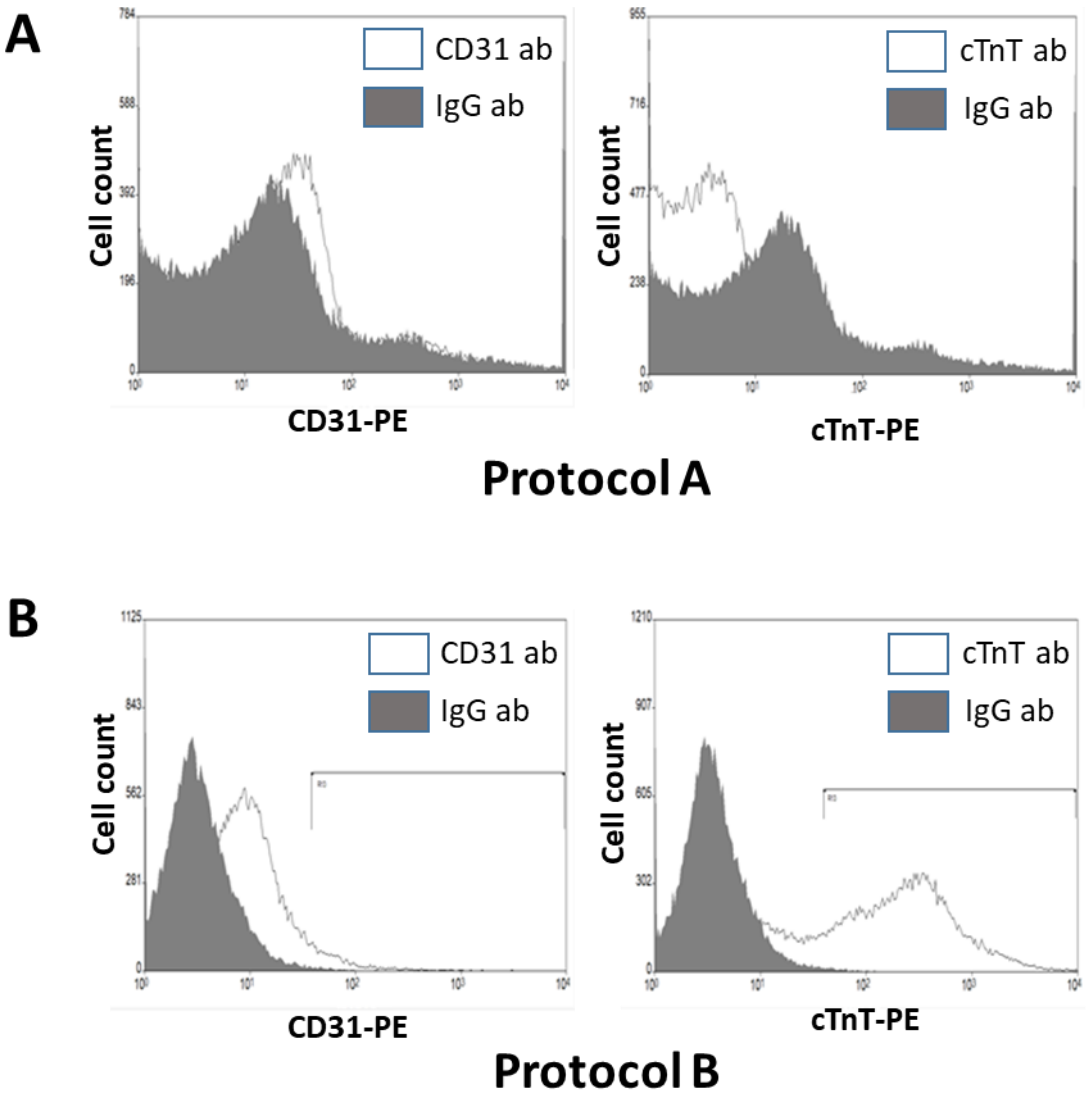

Figure 5.4. Optimisation of the Heart Digestion Protocol for Subsequent Flow Cytometric Analysis - Optimisation Protocol 1. (A) Protocol A: *Initial experiments followed a protocol utilising 1x trypsin-EDTA + 0.1% collagenase to digest the heart tissue. This was followed by fixation and permeabilisation of cells isolated with 2% formalin and 0.1% triton x-100 respectively. This combination yielded results that were incomprehensible. Staining of cells for CD31 and cTnT did not provide a clear region of positively stained cells that were distinct from IgG labelled control cells.* ***(B) Protocol B:*** *Experiments conducted using only 0.1% collagenase to digest the heart tissue and 70% ethanol (cold) to fix and permeabilise cells yielded results showcasing positively stained CD31^{+} endothelial cells and cTnT^{+} cardiomyocytes that were distinct from IgG labelled control cells. Representative flow cytometry histograms are provided.*

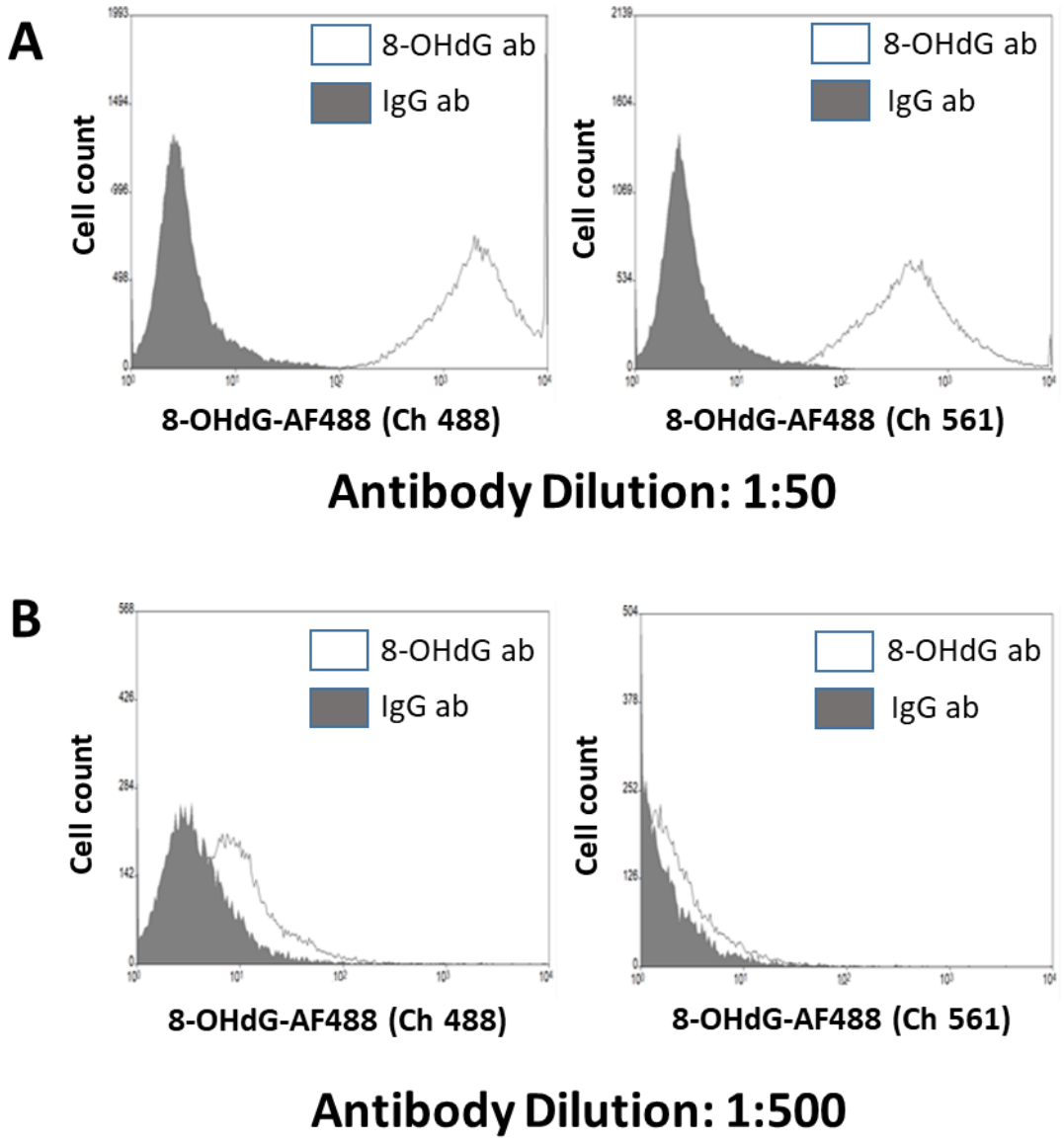

Figure 5.5. Optimisation of the Heart Digestion Protocol for Subsequent Flow Cytometric Analysis - Optimisation Protocol 2. (A) *Staining of cells with an anti-8-OHdG antibody at a high concentration or a 1:50 dilution resulted in skewed data and bleaching of fluorescence into adjacent emission channels.* ***(B)*** *A dilution factor of 1:500 resulted in cells still being positively stained without bleaching.*

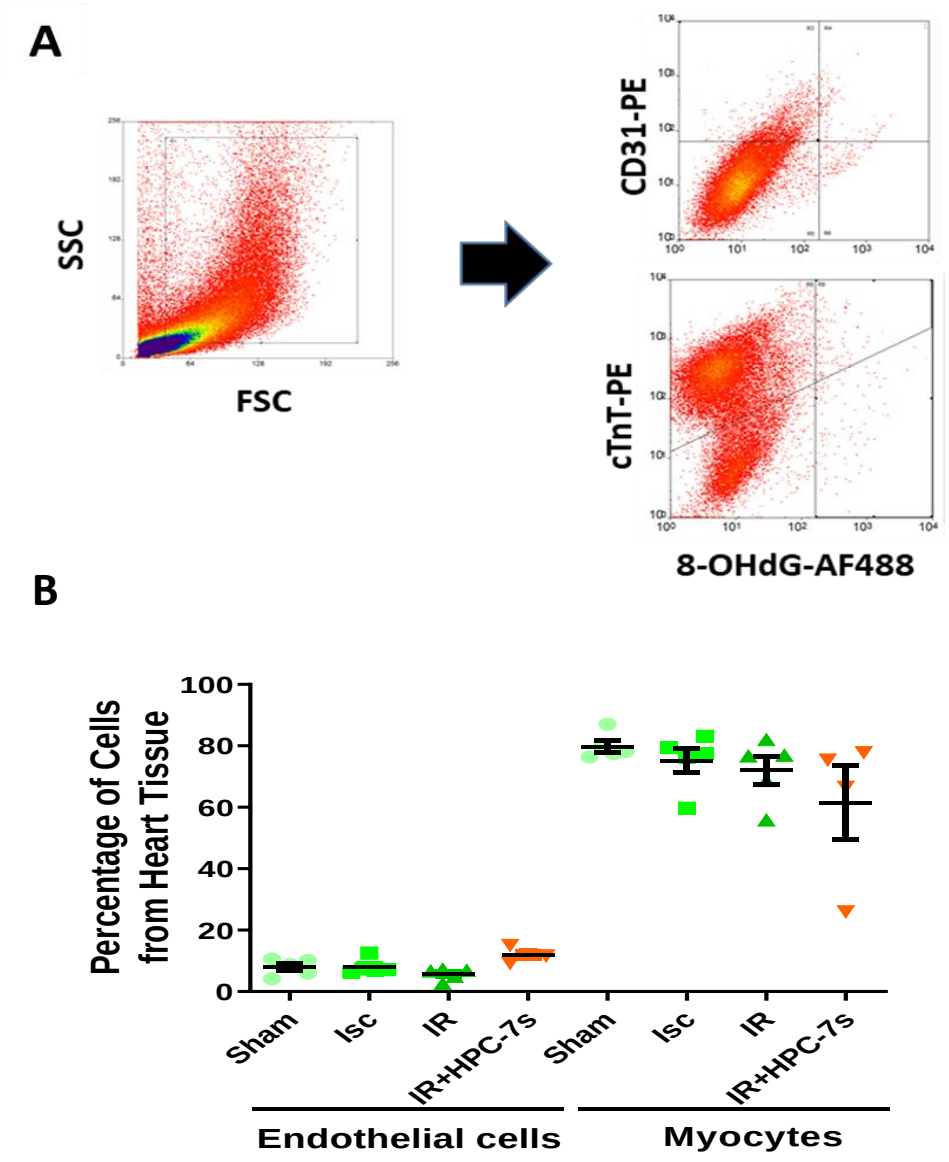

Figure 5.6. Flow cytometric analyses were performed on digested whole hearts in sham, ischaemic, IR injured and IR injured + HPC-7s experiments. (A) *Representative scatter plot showing the gating strategy used to identify CD31⁺ coronary ECs and cTnT⁺ cardiomyocytes from digested whole hearts and their oxidative damage levels as detected using an anti-8-OHdG antibody.* ***(B)*** *The percentage of endothelial cells obtained was approximately 12% of the total viable cells obtained from the digested heart regardless of the experimental group. The percentage of cardiomyocytes obtained was much higher at around 70% of the total viable cells obtained from the digested heart, again regardless of the experimental group as well. Data obtained was from a total of 30,000 events. N≥4 per group.*

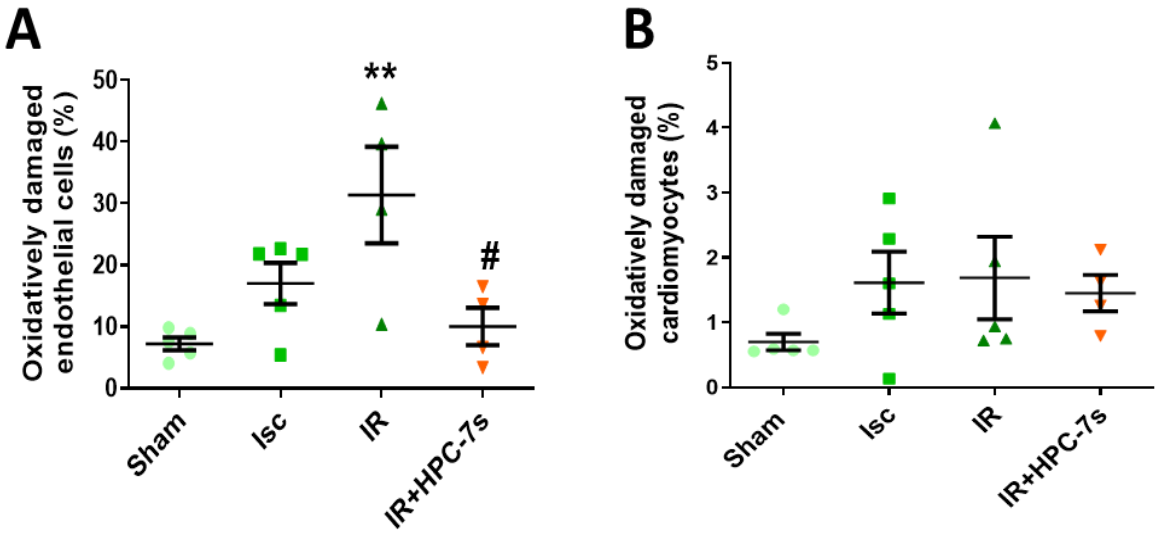

Figure 5.7. Endothelial cells (ECs) are more susceptible to oxidative stress than myocytes following cardiac IR injury but HPC-7s are able to inhibit this damage. (A) *Myocardial IR injury, but not ischaemia alone, significantly increased EC oxidative damage levels. This increase was significantly reduced by HPC-7s therapy to levels similar to sham heart ECs.* ***(B)*** *Cardiomyocyte levels of oxidative damage did not significantly alter between groups. Data obtained was from a total of 30,000 events. Statistical analysis was performed using one-way ANOVA with Sidak's multiple comparison test. **p<0.01; #p<0.05; N≥4 per group.*

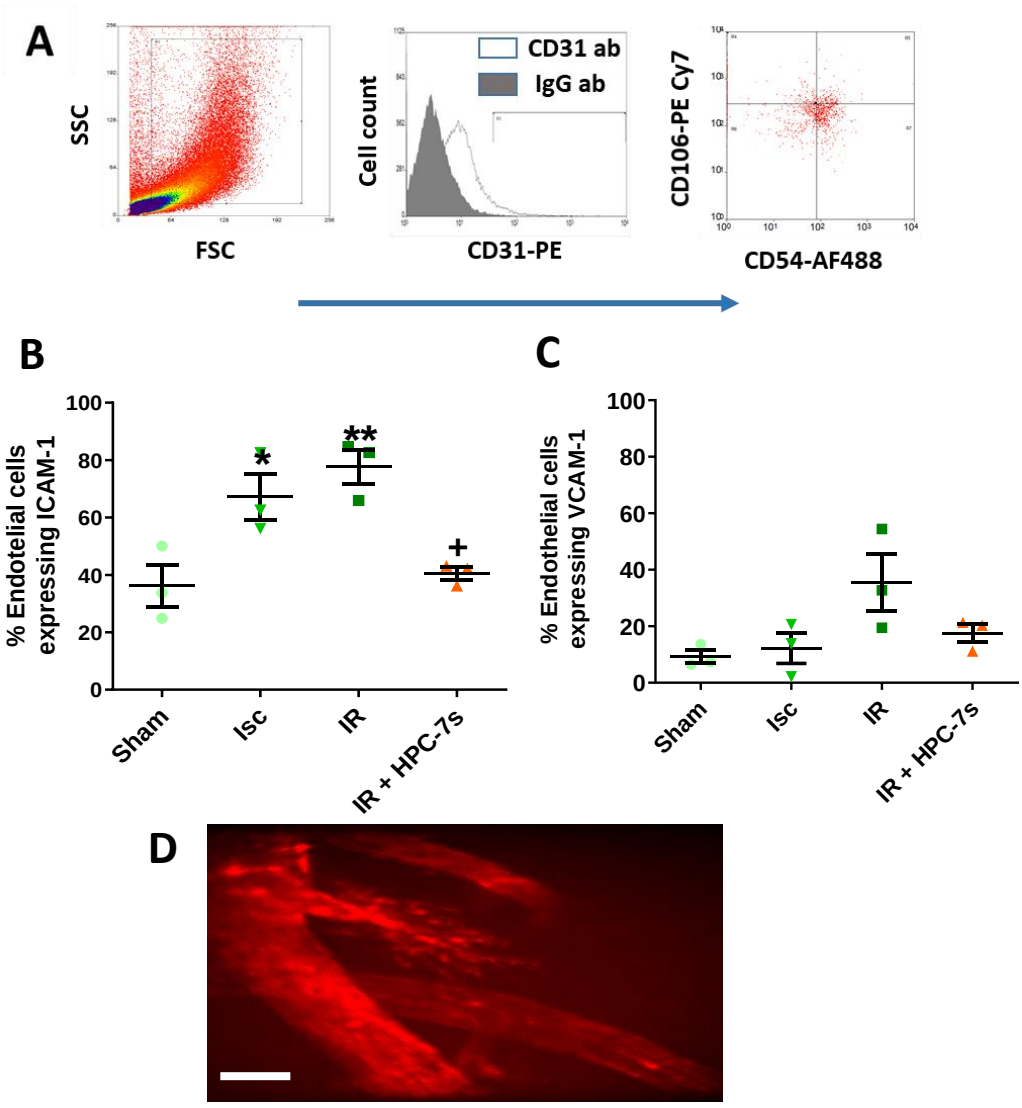

Figure 5.8. Myocardial IR Injury Induces an Up-regulation of ICAM-1 and VCAM-1 expression in Endothelial Cells – HPC-7s Therapy Reduces this Adhesion Molecule Up-Regulation. (A) *Example of the flow cytometric gating strategy used to identify the expression levels of ICAM-1 ($CD54^+$) and VCAM-1 ($CD106^+$) on ECs ($CD31^+$) from digested whole hearts.* ***(B)*** *Both ischaemia and IR injury significantly increased the expression levels of ICAM-1 on ECs which was reduced with HPC-7s therapy.* ***(C)*** *Only IR injury increased the expression levels of VCAM-1 on ECs which was again reduced with HPC-7s therapy.* ***(D)*** *VCAM-1 expression in vivo in the beating mouse heart was also imaged intravitally at the end of 2 hours reperfusion. VCAM-1 was interestingly observed in the larger microvessels but to a lesser extent in the coronary capillaries. Flow cytometric data obtained was from a total of 30,000 events. Statistical analysis was performed using one-way ANOVA with Sidak's multiple comparison test. N=3 per group. Scale bar = 100µm.*

Cytokines	Sham (pg/mL)	IR injury (pg/mL)	IR injury + HPC-7s (pg/mL)
Interleukin-1α	14.07 ± 2.90	18.62 ± 3.95	10.63 ± 0.67$^{\#}$
Interleukin-1β	37.18 ± 5.06	42.84 ± 4.37	24.94 ± 2.40$^{\#\#}$
Interleukin-2	14.92 ± 3.00	11.65 ± 0.86	8.17 ± 0.48$^{\#\#}$
Interleukin-3	17.13 ± 2.45	16.46 ± 1.67	10.93 ± 0.93$^{\#\#}$
Interleukin-4	13.61 ± 3.48	10.27 ± 2.77	6.76 ± 4.29
Interleukin-5	32.63 ± 11.95	31.56 ± 5.69	17.78 ± 2.91$^{\#}$
Interleukin-6	316.138 ± 118.21	1993.53 ± 841.45*	425.07 ± 78.19$^{\#}$
Interleukin-9	51.29 ± 7.54	45.76 ± 4.83	34.22 ± 2.64$^{\#}$
Interleukin-10	143.57 ± 9.06	222.70 ± 45.84*	452.48 ± 41.06$^{\#\#\#}$
Interleukin-12(p40)	2253.75 ± 350.50	14 588.86 ± 5889.30*	2424.66 ± 179.39$^{\#}$
Interleukin-12(p70)	501.84 ± 85.43	555.36 ± 57.31	350.24 ± 38.07$^{\#\#}$
Interleukin-13	278.182 ± 51.10	337.87 ± 38.67	159.26 ±25.87$^{\#\#\#}$
Interleukin-17	18.70 ± 2.68	14.50 ± 1.22	11.36 ± 1.06$^{\#}$
CCL11	992.67 ± 113.83	1607.58 ± 50.43*	1020.15 ± 90.44$^{\#\#\#}$
G-CSF	395.23 ± 97.79	2720.72 ± 1272.80*	200.29 ± 36.04$^{\#}$
GM-CSF	54.52 ± 7.25	61.95 ± 6.50	41.09 ± 4.75$^{\#\#}$
IFNγ	46.44 ± 7.28	42.25 ± 4.50	30.55 ± 2.20$^{\#}$
CXCL1	326.15 ± 93.22	1769.48 ± 783.47*	227.52 ± 28.93$^{\#}$
CCL2	638.92 ± 121.67	5016.62 ± 2117.35*	704.97 ± 93.02$^{\#}$
CCL3	21.84 ± 8.95	48.51 ± 21.69	37.30 ± 10.35
CCL4	169.46 ± 56.60	1545.83 ± 736.81*	250.28 ± 58.80$^{\#}$
CCL5	108.06 ± 15.03	248.96 ± 79.09*	85.75 ± 10.29$^{\#}$
TNFα	191.95 ± 29.16	369.49 ± 95.21*	154.62 ± 19.28$^{\#}$

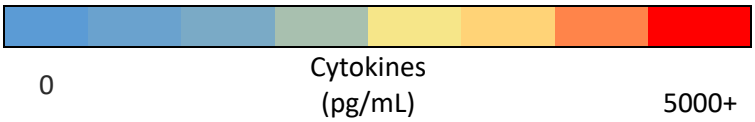

Table 1: Heatmap showing HPC-7s Therapy in myocardial IR injury significantly reduces plasma levels of multiple pro-inflammatory cytokines but significantly increased levels of IL-10. *Using a Luminex cytokine array kit, a number of pro-inflammatory cytokines in the plasma were significantly increased following myocardial IR injury. Indeed, 10 out of 23 cytokines tested were higher in the IR injury group when compared to sham plasma. Of these, IL-6, IL-12, G-CSF, CXCL1, CCL2, and CCL4 showed greater than 6-fold increases. HPC-7s therapy significantly reduced 9 of the 10 cytokines increased in the IR injury group. The only one increased by IR injury but not reduced by HPC-7s was IL-10. Interestingly, HPC-7s induced a further significant (p<0.001) increase in IL-10. This was the only cytokine to be significantly increased in IR injured hearts receiving HPC-7s therapy. HPC-7s therapy also significantly reduced a number of cytokines not increased in IR injury. */# p<0.05; ## p<0.01; ### p<0.001. Statistical analysis was performed using unpaired t-test. N=9 per group.*

5.3.8 Circulating Cell Profile in Murine Peripheral Blood following Myocardial IR Injury

The concentration of circulating inflammatory cells in peripheral blood was determined after experiments using a Horiba blood count machine. Following myocardial IR injury, there appeared a tendency for the total number of circulating white blood cells and platelets to decrease when compared to sham numbers ***(Table 2)***. This decrease appeared most marked for neutrophils (~2-fold) and monocytes (~4-fold). HPC-7s therapy appeared to increase the number of neutrophils and lymphocytes following myocardial IR injury, but did not modify the reduced number of monocytes or basophils. With regards to circulating platelets, myocardial IR injury also appeared to decrease their circulating numbers which was also reversed by HPC-7s therapy. However, none of the data collected in this experiment was statistically significant.

5.3.9 Verification of Circulating Monocytes Population Labelling with Fluorescent Latex Microparticles

In Chapter 4, fluorescent latex beads or microparticles (MPs), which were phagocytosed by circulating monocytes after systemic infusion, were used as a means of intravitally imaging their trafficking *in vivo* in the beating heart. In this Chapter, we aimed to investigate in detail which sub-population of monocytes were recruited and whether the anti-inflammatory mechanism of HPC-7s relied on their ability to modify a specific monocyte sub-population in the IR injured heart. Since the same latex MP method was used, we used flow cytometry to actually verify the efficiency of fluorescent MPs to label blood monocytes. Initial gating of live cells was undertaken followed by detection of monocytes via surface expression of CD115.

Backgating of fluorescent MP^+ and $CD115^-$ cells showed that a small number were likely to be neutrophils or monocytes not labelled by the CD115 antibody. The presence of fluorescent MPs within the $CD115^+$ monocytes could then be ascertained ***(Figure 5.9A)***. Of all circulating leukocytes detected, ~3% were monocytes. Of all circulating monocytes, ~15% were fluorescently labelled. We also investigated whether monocytes were the only cells to phagocytose the MPs and found that ~70% of the phagocytosed MPs were taken in by monocytes ***(Figure 5.9B)***. As mentioned earlier, the remaining ~30% were taken up primarily by neutrophils and monocytes not labelled with CD115, as identified via backgating.

Fluorescent monocytes were also visualised at a cellular level using a fluorescent microscope. $CD115^+$ cells obtained from the peripheral blood of mice could be seen packed with MPs under immunofluorescence ***(Figure 5.9C)***. Importantly, intravital imaging of the beating heart showed clear separation between the fluorescently labelled monocytes and fluorescently labelled neutrophils ***(Figure 5.9D)***.

5.3.10 Myocardial IR Injury Causes Recruitment of a Pro-Inflammatory Monocyte Sub-Population but HPC-7s Therapy Induces a Generalised Reduction of all Monocytes

Flow cytometry of digested whole heart tissue was utilised to assess the differences in monocyte subset recruitment following myocardial IR injury. Initial gating of live cells was undertaken followed by gating on cells fluorescently labelled with MPs. It was then possible to isolate $CD115^+$ cells in this population and whether these cells were $Ly6C^+$ (pro-inflammatory) or $Ly6C^-$ (anti-inflammatory). Quantification of both subsets were determined in sham, IR injured and IR injured + HPC-7s groups ***(Figure 5.10A)***. Unsurprisingly, the total

percentage of fluorescently labelled monocytes in the sham mouse heart was very low at ~0.04%. The total percentage of fluorescently labelled monocytes recruited to the heart significantly ($p<0.001$) increased in the IR injured group to ~0.12%, nearly triple the sham group percentage. This increase was significantly ($p<0.01$) reduced back to sham levels or ~0.05% when HPC-7s were introduced to IR injured mice ***(Figure 5.10B)***.

With regards to the subset breakdown, in sham hearts, $Ly6C^+$ cells accounted for ~30% of the fluorescently labelled monocytes. There was a significant ($p<0.01$) shift in this ratio in the IR injured hearts where ~60% of the fluorescently labelled monocytes were $Ly6C^+$. Interestingly, we found that in IR injured hearts treated with HPC-7s, although the overall total percentage of recruited cells decreased as compared with purely IR injured hearts, the ratio between subsets remained the same with ~60% still $Ly6C^+$. As expected, this shift was still significant ($p<0.01$) when compared to sham hearts ***(Figure 5.10B)***.

The general increase in the recruitment of fluorescent monocytes was also shown by immunofluorescence conducted on frozen heart tissue sections ***(Figure 5.10C)***. Quantification of this data showed ~2 cells / field of view in sham sections, which significantly ($p<0.05$) increased in the IR injured group to ~8 cells / field of view. In the IR injured + HPC-7s group, there was a trend towards a reduction of this number to ~5 cells / field of view but this was not statistically significant when compared to the IR injured group ***(Figure 5.10D)***.

5.3.11 Topical Application of Either IL-36 α or β to the Beating Mouse Heart Promotes Monocyte Recruitment *in vivo* while IL-36β + HPC-7s Therapy Inhibited this Effect.

As the recently discovered IL-36 family of cytokines have been shown to increasingly play a role in other inflammatory conditions, we investigated intravitally whether direct topical application of the three different IL-36 isoforms onto the beating heart left ventricle *in vivo* would initiate an inflammatory response with regards to monocyte recruitment. Representative intravital images of the mouse heart after either topical PBS treatment or 2 hours post-IL-36α, IL-36β or IL-36γ treatments were obtained ***(Figure 5.11A)***. Quantification of the data obtained showed that after 2 hours of treatment, only IL-36α ($p<0.05$) and IL-36β ($p<0.05$) significantly increased monocyte recruitment when compared to PBS control (time point 0) whilst IL-36γ did not ***(Figure 5.11B).*** As IL-36β treatment induced a striking increase in monocyte recruitment with time, we further investigated intravitally whether IL-36β topical treatment combined with simultaneous HPC-7s administration would prevent any monocyte increases. Indeed, administration of HPC-7s was able to significantly ($p<0.001$) attenuate the recruitment of monocytes in hearts after 2 hours of IL-36β topical treatment ***(Figure 5.11A&C)***.

Cell Type ($10^3/mm^3$)	Sham	IR injury	IR injury + HPC-7s
All WBCs	6.275 ± 2.721	4.525 ± 1.435	7.375 ± 2.018
Neutrophils	3.487 ± 1.891	1.918 ± 0.811	3.173 ± 0.946
Monocytes	1.03 ± 0.805	0.263 ± 0.116	0.273 ± 0.042
Lymphocytes	2.67 ± 0.524	2.230 ± 0.567	3.808 ± 1.009
Eosinophils	0.053 ± 0.027	0.035 ± 0.013	0.048 ± 0.017
Basophils	0.118 ± 0.085	0.068 ± 0.021	0.075 ± 0.024
Atypical Lymphocytes	0.08 ± 0.054	0.048 ± 0.009	0.048 ± 0.013
Large Immature Cells	0.19 ± 0.147	0.155 ± 0.094	0.238 ± 0.156
Platelets	601.7 ± 179.7	382.3 ± 156.9	528.0 ± 40.9

Table 2: Circulating cell profile in murine blood following myocardial IR injury. *Using a Horiba blood count machine, the concentration of different types of white blood cells were quantified in the peripheral blood of sham, IR injured and IR+HPC-7s mice. Overall, the trend of a general decrease in WBCs, most notably in neutrophils and monocytes was observed following IR injury to the heart. This trend was reversed following HPC-7s therapy except for monocytes and basophils. A similar trend where a decrease in circulating platelet numbers was also noted in IR injury which was again reversed with HPC-7s therapy. Statistical analysis of the data obtained indicated that these trends were not statistically significant. Statistical analysis was performed using a one-way ANOVA with Sidak's multiple comparison test. N=4 per group.*

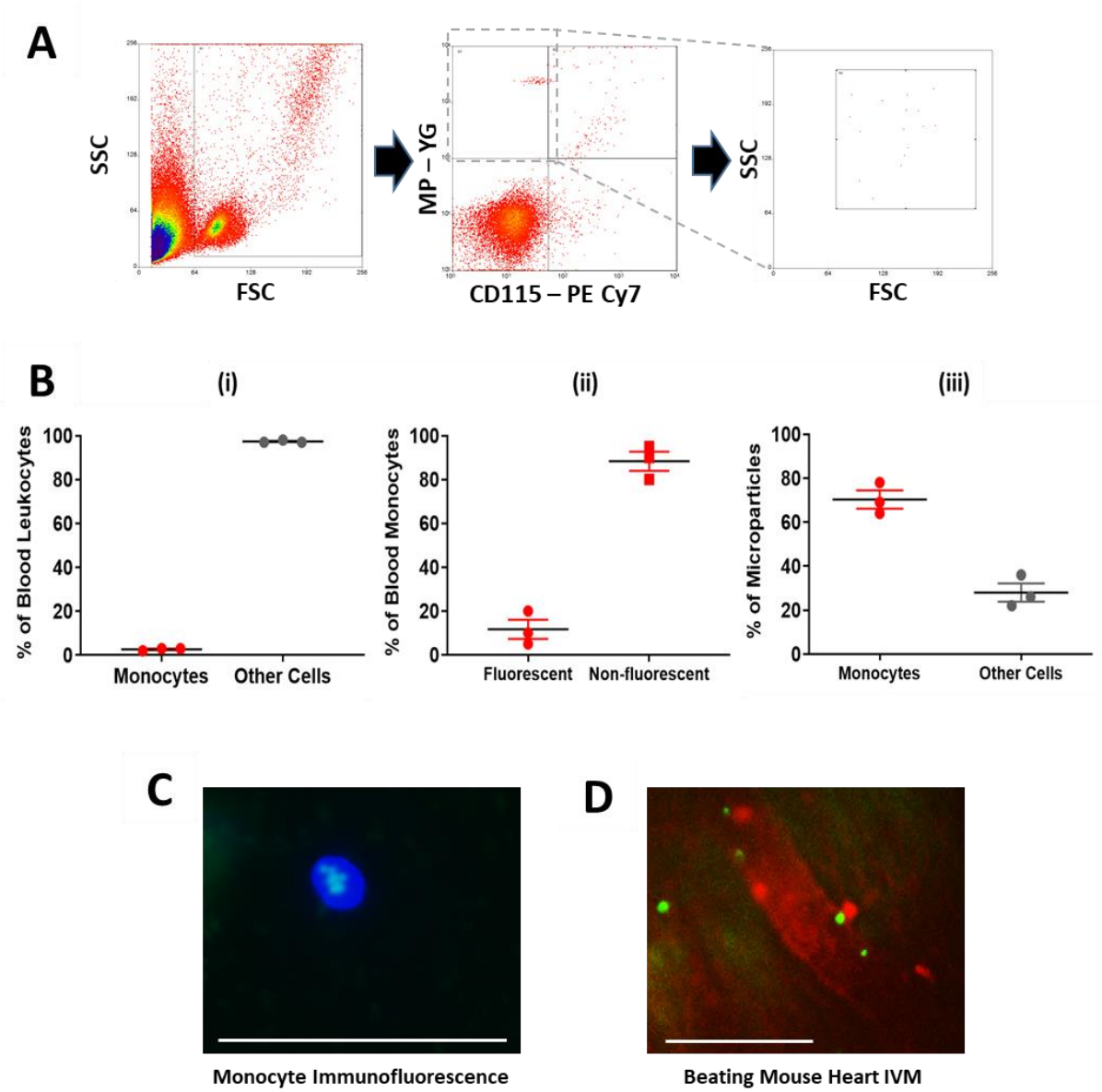

Figure 5.9. Circulating monocyte labelling efficiency utilising fluorescent latex microparticles (MP). (A) *The gating strategy utilised in order to determine the monocyte population that become fluorescently labelled via microparticles. Backgating of MP^+ and $CD115^-$ population indicated that other phagocytic cells were most likely neutrophils.* ***(B)*** *Of all circulating leukocytes detected (i) ~3% were identified as being monocytes (ii) ~15% of all circulating monocytes were fluorescently labelled and (iii) ~70% of fluorescent MPs were phagocytosed by monocytes.* ***(C)*** *Image shows a $CD115^+$ monocyte with engulfed fluorescent MPs.* ***(D)*** *Intravital image showing distinctive staining of neutrophils (red) and monocytes (green) trafficking as separate entities through the coronary microcirculation in a beating mouse heart. Flow cytometric data was obtained from 100,000 events. N=3 per group. Scale bar = 100µm.*

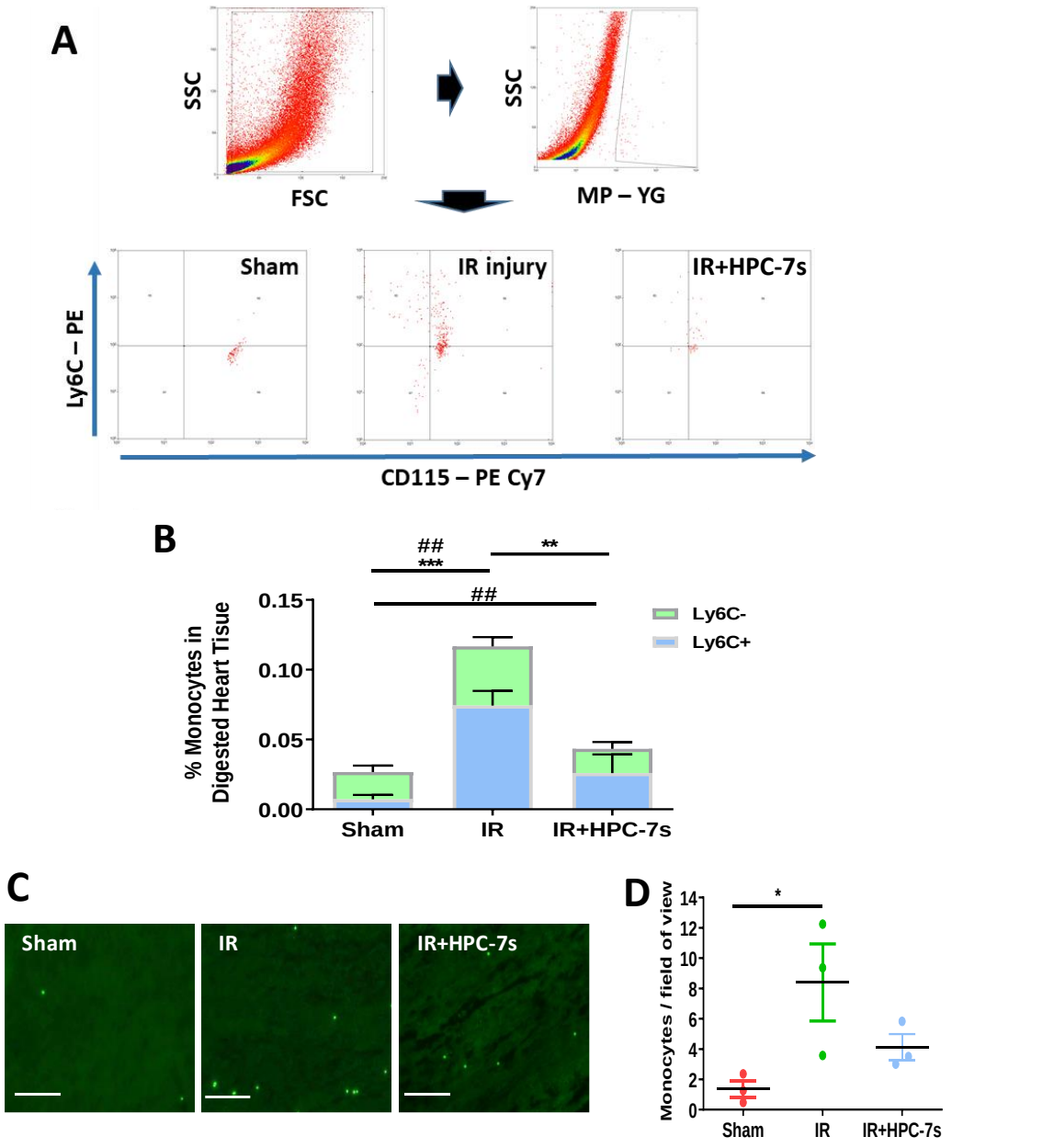

Figure 5.10. Myocardial IR Injury Causes Recruitment of a Pro-Inflammatory Monocyte Sub-population but HPC-7s Therapy Induces a Generalised Reduction of all Monocytes. (A) *The gating strategy utilised to determine pro-inflammatory (Ly6C$^+$) and anti-inflammatory (Ly6C$^-$) monocyte subpopulations in different groups.* ***(B)*** *There was a significant increase in overall monocyte numbers in IR injured hearts compared to sham that was attenuated by HPC-7s therapy. There was a significant increase in the pro-inflammatory population of these monocytes in IR injured hearts compared to sham that remained high even with HPC-7s therapy. Data was obtained form 100,000 events.* ***(C)*** *Representative IHC images of frozen heart tissue samples showing the presence of fluorescent monocytes in sham, IR injured and IR+HPC-7s groups.* ***(D)*** *Quantification of these IHC images showed a significant increase in the presence of monocytes in IR injured sections compared to sham but with no significant difference to IR+HPC-7s sections. Statistical analysis was performed using one-way ANOVA with Sidak's multiple comparison test. *p<0.05, **/## p<0.01,***p<0.001 ; N=3 per group. Scale bar = 100µm.*

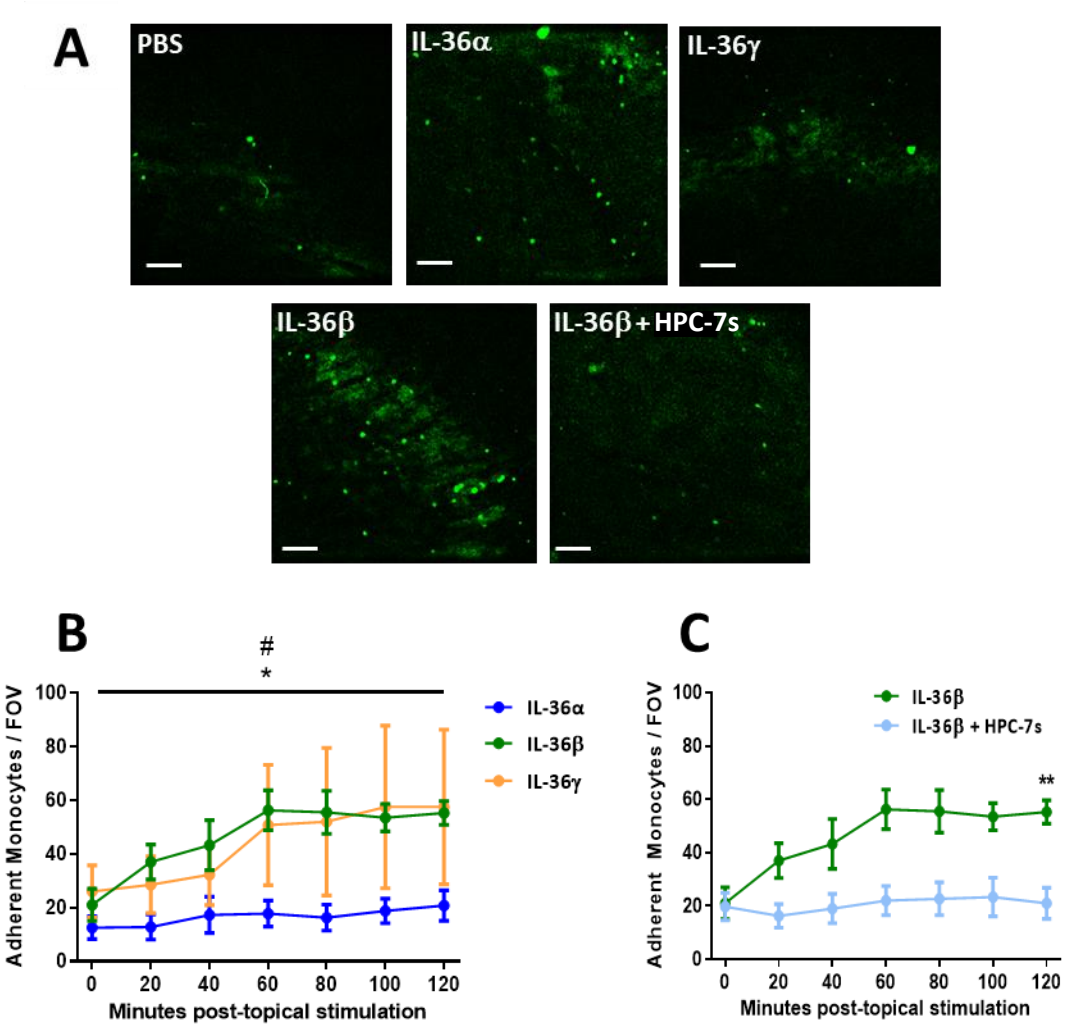

Figure 5.11. Topical application of either IL-36 α or β to the beating mouse heart promotes monocyte recruitment in vivo while IL-36β + HPC-7s therapy inhibited this effect. (A) *Intravital images showing recruitment of latex bead labelled fluorescent monocytes (green) after topical PBS, IL-36α, IL-36γ, IL-36β only and IL-36β application with concurrent injection of HPC-7s.* ***(B)*** *There was a significant increase in monocyte recruitment over time after topical application of only IL-36α (#p<0.05; despite looking as if it was not significant – error bars are tight) or IL-36β (*p<0.05) after 2 hours when compared to PBS (time point = 0 minutes). For IL-36γ, there was more variability in the data, so despite a trend to increase, it was not statistically significant.* ***(C)*** *HPC-7s were able to significantly attenuate this increased monocyte recruitment induced by IL-36β topical application (**p<0.05). Statistical analyses were performed using unpaired t-tests. N=4 per group. Scale bar = 100 µm.*

5.3.12 Topical Application of Either IL-36 α or β to the Beating Mouse Heart Promotes Neutrophil Recruitment *in vivo* while IL-36β + HPC-7s Therapy did not Inhibit this Effect

The impact of topical application of IL-36 isoforms on neutrophil recruitment was also investigated in the beating heart intravitally. Representative intravital images of the mouse heart after either PBS treatment or 2 hours post-IL-36α, IL-36β or IL-36γ treatments were obtained ***(Figure 5.12A)***. Similar to the monocyte results, quantification of the data obtained showed that after 2 hours of treatment, only IL-36α ($p<0.05$) and IL-36β ($p<0.05$) significantly increased the recruitment of neutrophils to the heart in comparison to PBS control (time point 0) while IL-36 γ did not ($p<0.05$) ***(Figure 5.12B)***. As IL-36β treatment induced a striking increase in neutrophil recruitment with time, we further investigated intravitally whether IL-36β topical treatment combined with simultaneous HPC-7s administration would prevent any neutrophil increases. However, unlike the effect seen on monocytes, we found that the administration of HPC-7s was not able to attenuate the recruitment of neutrophils in hearts after 2 hours of IL-36β topical treatment ***(Figure 5.12A&C)***.

5.3.13 IL-36RA Treatment Reduces Inflammatory Recruitment following Myocardial IR Injury

Our final investigation focussed on assessing whether using the IL-36 receptor antagonist as a form of therapy for alleviating the inflammatory response following myocardial IR injury would be effective. 3µl of IL-36RA (250 µg/ml) was added to 100µl of PBS and injected intraarterially 5 minutes post-reperfusion. Representative intravital images showed a slightly reduced level of neutrophil and monocyte recruitment, compared to the level of recruitment previously seen in IR injured hearts ***(Figure 5.13)***. The effects seemed more pronounced for neutrophils. Unfortunately, due to time constraints only one experiment was completed in this investigation**.**

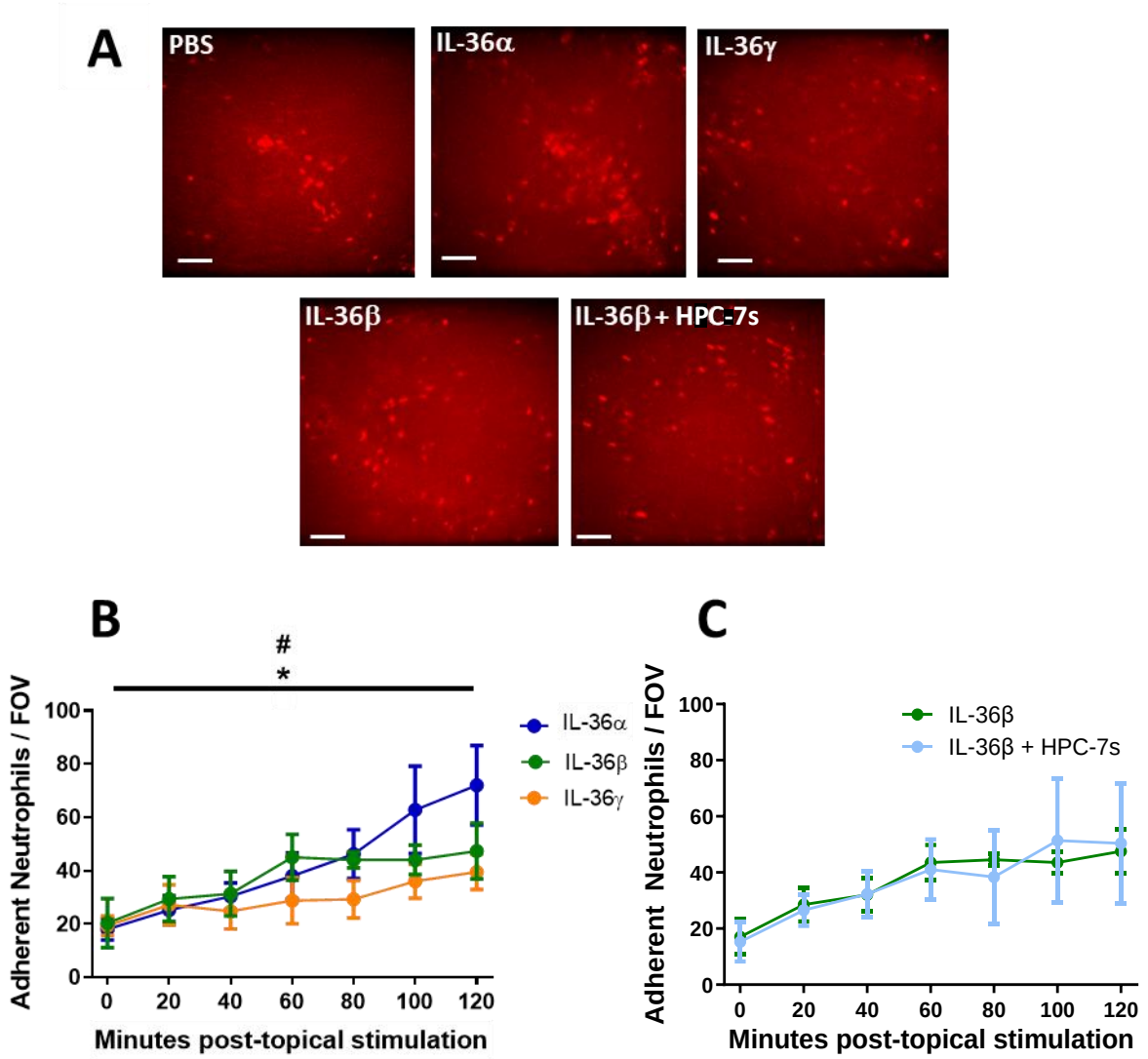

Figure 5.12. Topical application of either IL-36 α or β to the beating mouse heart promotes neutrophil recruitment in vivo while IL-36β + HPC-7s therapy did not inhibit this effect. (A) *Intravital images showing recruitment of neutrophils (red) fluorescently labelled using APC+anti-Ly6G antibodies after topical PBS, IL-36α, IL-36γ, IL-36β only and IL-36β application with concurrent injection of HPC-7s.* ***(B)*** *There was an increase in neutrophil recruitment over time after topical application of only IL-36α (#p<0.05) or IL-36β (*p<0.05) which was significant after 2 hours when compared to PBS (time point = 0 minutes).* ***(C)*** *HPC-7s were not able to significantly attenuate this increased neutrophil recruitment induced by IL-36β topical application. Statistical analyses were performed using unpaired t-tests. N=4 per group. Scale bar = 100 µm.*

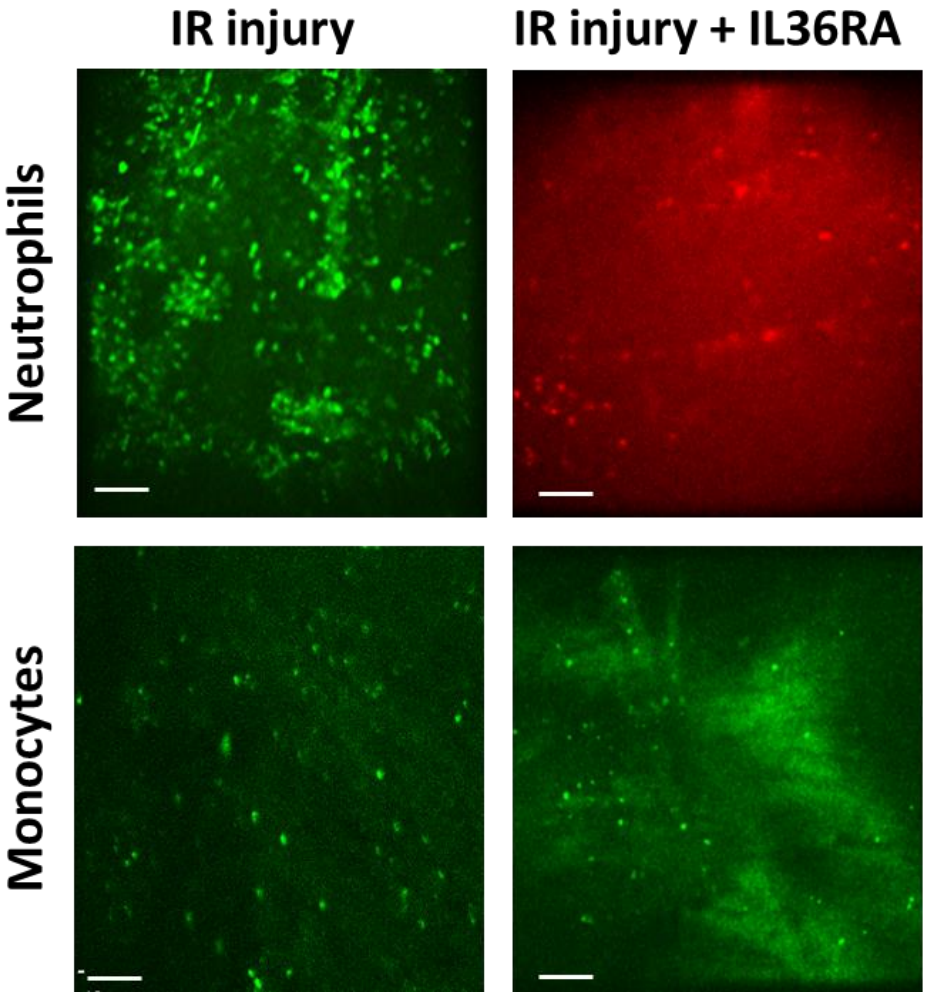

Figure 5.13. IL-36 Receptor Antagonist (IL-36RA) Reduces Neutrophil and Monocyte Recruitment after Myocardial IR injury. *Intravital experiments were conducted to investigate whether the IL-36RA could potentially reduce the recruitment of neutrophils and monocytes in the beating heart following myocardial IR injury. The antagonist was injected intra-arterially 5 minutes post-reperfusion. Although this was only attempted in one mouse, both neutrophil and monocyte recruitment appeared to be slightly less than had previously been observed in mice undergoing only myocardial IR injury – the effect appeared more pronounced for neutrophils. Red or Green in upper panels are neutrophils stained using PE+anti-Gr-1ab. Green in the lower panels are monocytes labelled with Fluoresbrite® FITC-dyed yellow green microspheres. N=1 per group. Scale bar = 100µm.*

5.4 Discussion

As mentioned previously, the pre-clinical assessment of HSC therapy in CVD has been minimal [72]. As such, little is known about their ability to contribute towards coronary vasculoprotection or even how they may achieve this. In Chapter 4 we clearly demonstrated a beneficial impact of HPC-7s therapy in inhibiting thromboinflammatory events and improving functional capillary density in the IR injured beating heart coronary microcirculation. Furthermore, this resulted in a reduction in infarct size. In order to tease out potential mechanisms by which this could be achieved, we conducted additional intravital and flow cytometric experiments. We present in this chapter novel data that suggests the beneficial effects of exogenously administered HPC-7s could stem from their ability to reduce the degree of oxidative damage incurred by coronary endothelial cells and also reduce the upregulation of inflammatory endothelial adhesion molecules.

Furthermore, HPC-7s also decreased circulating levels of a plethora of well-established inflammatory cytokines, although increased levels of IL-10, a naturally occurring potent anti-inflammatory cytokine. Interestingly, these benefits were imparted without a need for HPC-7s to actually become locally retained in any significant numbers within the IR injured coronary microvasculature. This indicates that the protection afforded by HPC-7s is delivered in a paracrine fashion, rather than by directly adhering within local microvessels at the site of injury. IL-36, a novel member of the IL-1 superfamily, was also shown for the first time to be directly pro-inflammatory *in vivo*. This was particularly novel work as no previous studies have imaged the direct effects of IL-36 isoforms in any vascular bed intravitally, let alone in the beating mouse heart. Furthermore, we speculate that the vasculoprotective effects of HPC-

7s following IR injury could potentially be linked to their ability to inhibit the pro-inflammatory actions of IL-36 isoforms on neutrophils and monocytes – this is a novel mechanism that we propose which will require further detailed investigation. These results will help inform any future translational studies investigating ways of optimising the beneficial effects of HSC therapy.

5.4.1 HPC-7s Do Not Adhere within the Heart During Reperfusion

Our initial hypothesis with regards to how HPC-7s conferred their vasculoprotection was that they directly homed and became locally retained within the injured heart. This was based on the fact that the Kalia lab had previously shown the propensity of HPC-7s to become more adherent in IR injured organs such as the liver and gut, and that their ability to be beneficial increased as retention was improved [150]. However, our beating heart IVM studies clearly showed that HPC-7s were no more adherent in IR injured hearts than in sham hearts. Indeed, only 4-5 HPC-7s were adherent per field of view. Flow cytometric analysis of digested whole hearts confirmed these intravital findings. Furthermore, pre-treating or pre-activating HPC-7s with H_2O_2, a strategy previously found by the Kalia group to be very effective in the injured gut, did not increase HPC-7s adhesion in the setting of myocardial IR injury [150, 195]. Poor stem cell retention in the heart has also been shown clinically. Indeed, Hofmann and colleagues demonstrated <2.6% retention of unselected BM-derived cells in MI patients when delivered 5-10 days after stenting [246]. Poor adhesion may be due to the fact that the level of endothelial adhesion molecules, required to capture circulating HPC-7s and permit firm endothelial interactions, were reduced in HPC-7s treated IR injured hearts, which would have

reduced the ability for HPC-7s to become adherent. However, it is not clear why there is this difference between the IR injured heart and other similarly injured organs.

As HSCs and other stem cells are known to become non-specifically entrapped in the microvasculature of non-injured organs such as the lungs [72], the presence of HPC-7s in two remote organs was also investigated flow cytometrically. It was interesting to note that in general, there was a larger number of HPC-7s present in the lungs and liver compared to the heart. There was also a trend for more HPC-7s to be present in the lungs and liver of mice undergoing myocardial IR injury than the respective sham organ, however, this was not statistically significant. Pulmonary entrapment is well known to be a major obstacle for systemic stem cell delivery for therapeutic purposes both experimentally and clinically [213]. Indeed, patients receiving exogenous HPC-7s for hematologic disorders experience post-transplant pulmonary injury due to cells becoming trapped in lung capillaries [213, 247]. In addition to promoting lung damage, pulmonary entrapment significantly reduces the available pool of circulating transplanted HPC-7s available for recruitment to the actual injured organs. However, the Kalia Group previously demonstrated that the H_2O_2 pre-treatment strategy not only enhanced recruitment within the gut, the actual site of tissue injury, but also concomitantly decreased their entrapment within lungs. They speculated that this was simply related to cell availability i.e. enhanced intestinal recruitment meant less cells were available for pulmonary entrapment. However, in the current study, H_2O_2 did not improve specific injury site retention. This may be due to some unique, as yet unknown, characteristic of the heart.

Even without retention in the heart, HPC-7s were able to protect the coronary microvessels from thrombo-inflammatory injury as was shown clearly in Chapter 4. This suggested

beneficial soluble factors may have been released systemically from remote sites in order to confer vasculoprotection in the heart. Indeed, remote transplantation of MSCs into the interscapular region has been shown to protect the IR injured heart [239]. Since a paracrine anti-inflammatory effect appeared likely, we also chose to investigate whether simply providing CM sourced from HPC-7s, rather than whole cells, would be adequate to provide vasculoprotection. However, it was interesting to note from our intravital studies that CM was not able to reduce the thrombo-inflammatory response. This indicates that the presence of whole and viable HPC-7s themselves is necessary and that their physical response to the microenvironmental changes during IR injury is pivotal in order to provide vasculoprotection. Although stem cell derived CM has been shown to be effective in many studies, a similar outcome to our own was shown by Xing and colleagues in the IR injured kidney, whereby MSC-derived CM did not demonstrate any favourable effects [248]. It has been demonstrated that different microenvironments can stimulate stem cells to release different types and concentrations of cytokines. Indeed, stimulants in a culture system would vary from those found in injured tissue leading to secretion of different soluble mediators. Our CM was not generated in a hypoxia/reoxygenation culture system which would have better mimicked the IR microenvironment of the heart. Regardless, our findings here show the need for HPC-7s to become activated by the microenvironment in order to confer vasculoprotection; this protection is not afforded constitutively.

Additional information we obtained about the kinetics of HPC-7s trafficking to the beating heart *in vivo* was the observed initial 4-fold increase in circulating HPC-7s identified in IR injured hearts in the immediate aftermath of being introduced. This may have been related to the hyperaemic response that was described using LSCI in Chapter 4. Indeed, 25-30 circulating

cells were consistently observed throughout reperfusion at all time points. This was unusual as we have shown in other organs that HPC-7s were only observed on the 'first pass' immediately after infusion and not thereafter [150, 151, 170, 195]. Again, this continual passing of freely circulating HPC-7s through the heart may be related to the maintained hyperaemic response identified in Chapter 4. It is also possible that these freely circulating HPC-7s became activated to release paracrine factors locally as they passed the injured coronary microvessels.

5.4.2 Cellular Mechanisms by Which HPC-7s Confer Vasculoprotection

5.4.2.1 Optimisation of Flow Cytometry

Intravital microscopy focussed on imaging HPC-7s kinetics in the same randomly pre-selected, small field of view throughout reperfusion. Therefore, to confirm that these represented events taking place in the whole heart, we also investigated the role of HPC-7s in the whole heart using flow cytometry. We found that using a protocol which included digestion of heart tissue with type-I collagenase for 45 minutes followed by fixation and permeabilization of cells with ice cold 70% ethanol provided more robust results that we could then analyse effectively. There are a number of published protocols available for digesting whole heart tissue that provide various advantages, which we were required to modify in order to extract our cells of interest [249]**.** From our optimised digestion protocol, we were consistently able to acquire around 12% ECs and 70% cardiomyocytes from digested whole hearts. By comparison, Banerjee et al. observed similar cell populations using flow cytometry as well, where they acquired around 7% ECs and 56% cardiomyocytes from adult mice digested whole hearts

[250]. The slight difference in cell populations observed is accountable by the differing protocol used to isolate cardiac cells. The use of anti-8-OHdG antibodies to identify oxidative damage in the heart also required optimisation. As this antibody was not routinely used in flow cytometry, we had to adjust the concentration of the antibody used as we found that it easily influenced the fluorescence output of other channels during sample acquisition using the flow cytometer. These adjustments were necessary in order to obtain reliable and reproducible data.

5.4.2.2 HPC-7s Reduce Coronary Endothelial Cell Oxidative Damage

In Chapter 3, we demonstrated that HPC-7s were able to significantly reduce the generation of free radicals and the oxidative stress damage they induced in H_2O_2 damaged VCECs *in vitro.* We therefore investigated in this Chapter whether this could mechanistically explain their ability to protect microvessels in the IR injured heart *in vivo.* Whilst there appeared an increase in the level of oxidative damage in cardiomyocytes after IR injury, this was not statistically significant. There was, however, a significant increase in oxidative damage in ECs with nearly 30% experiencing oxidative damage. Oxidative damage of some population of myocardial cells was not in itself surprising as the role of oxidative stress in myocardial IR injury is well reported [38]. However, the fact that flow cytometry demonstrated coronary endothelium, rather than cardiomyocytes, as the primary and initial target of oxidative injury was interesting. Others have also shown this differential susceptibility to injury with endothelial and cardiomyocyte apoptotic death occurring at 5 and 60 minutes respectively in isolated perfused hearts [251, 252]. This, in conjunction with the high degree of correlation between

capillary CD31 and 8-OHdG immunostaining noted histologically in Chapter 3, collectively highlights the coronary microcirculation as an early and principal therapeutic target to prevent ensuing muscle damage. It was therefore exciting to see that HPC-7s could significantly reduce the burden and impact of oxidative stress on coronary ECs, reducing the level of oxidative damage back down to around 10%, which was close to sham levels.

5.4.2.3 HPC-7s Prevent the Up-Regulation of Endothelial Adhesion Molecules

Our IVM findings in Chapter 4 indicated a remarkable reduction in the recruitment of inflammatory neutrophils and monocytes in IR injured hearts treated with HPC-7s. Since leukocyte-endothelial interactions are mediated by endothelial integrins ICAM-1 and VCAM-1, we further analysed whether HPC-7s modified their expression on IR injured coronary ECs using flow cytometry. Oxidatively stressed or damaged ECs can upregulate adhesion molecules in order to attract inflammatory cells to repair the said damage [253]. As such, it is not surprising, firstly, to see the expression of both ICAM-1 and VCAM-1 increased on ECs after myocardial IR injury. Interestingly, even after just a 45-minute period of ischaemia, expression of ICAM-1 was significantly elevated. The introduction of HPC-7s attenuated the increased expression noted in reperfused hearts, reducing the expression of both ICAM-1 and VCAM-1. As we had also shown that HPC-7s reduced the level of oxidative damage experienced by ECs, this was a likely contributing factor in the results obtained here.

5.4.2.4 HPC-7s Reduce Circulating Levels of Multiple Inflammatory Cytokines

Myocardial IR injury generates a remarkable pro-inflammatory environment locally in the heart [5]. Consequently, the recruitment of platelets, neutrophils and monocytes as shown in Chapter 4 cause significant microvessel disruption. Indeed, the build-up of platelet-rich microthrombi impaired perfusion by obstructing blood flow in the tiny capillaries of the heart. HPC-7s therapy was able to significantly inhibit the recruitment of these cells leading to a more patent and healthier microvasculature. In this Chapter, we found that a number of circulating pro-inflammatory cytokines were significantly increased during myocardial IR injury, particularly IL-6, IL-12, G-CSF, CXCL1, CCL2, CCL4 and TNF-α. Not only did HPC-7s therapy reduce these circulating cytokines back down to sham levels, it also reduced the levels of other pro-inflammatory cytokines that weren't significantly increased during IR injury, such as IL-1, IL-2, GM-CSF and IFNy. It is well known that IL-6, IL-1 and TNF-α are classic cytokines that can aggravate myocardial IR injury [254]. Hence, the reduction of multiple cytokine pathways may explain the anti-inflammatory and associated therapeutic effects of HPC-7s.

Interestingly, we noted a significant increase in one plasma cytokine out of the 23 investigated. IL-10 is a naturally occurring, potent anti-inflammatory cytokine which can suppress secretion of various pro-inflammatory cytokines both *in vitro* and *in vivo* via inhibition of NF-κβ [255]. A number of immunohistochemical studies have demonstrated that exogenous IL-10 can suppress myocardial inflammation as evidenced by decreased neutrophil infiltration in similar injury models [256, 257]. Indeed, the beneficial effects of remote ischaemic pre-conditioning in the heart have also been demonstrated to be mediated via increases in IL-10 [258]. Furthermore, genetically engineering mesenchymal stem cells (MSC)

to overexpress IL-10 has been shown to better reduce infarct size and cardiac impairment compared to individual treatments of MSC or IL-10 administration [259]. It is therefore likely that increased plasma levels of IL-10 in mice receiving HPC-7s may mechanistically explain the vasculoprotective effects observed in the current study. The demonstration that stem cells may secrete therapeutic factors provides a potential breakthrough in that, rather than administering cells, one may be able to administer specific proteins produced by these cells for cardiac therapy.

5.4.2.5 HPC-7s Reduce Monocyte Infiltration in a Non-Selective Manner

In Chapter 4 we had intravitally shown a very rapid and significant infiltration of monocytes into the IR injured beating mouse heart using a fluorescent latex bead labelling method. This was the first time this method had been applied to track endogenous monocytes in real-time in the heart. However, without adoptive transfer of specific donor-derived cells, it was not possible to image endogenous sub-populations of monocytes. Therefore, it was not possible to ascertain intravitally whether the beneficial effects of HPC-7s were potentially due to the increase or decrease in the presence of a specific inflammatory or non-inflammatory sub-population of monocytes.

Circulating peripheral blood monocytes are precursors for macrophages and dendritic cells [233]. Once they transmigrate out of the blood vessels, they rapidly differentiate into one or the other of these terminal cells types which can then mediate innate and adaptive immune responses to disease or injury. Different sub-populations of monocytes can give rise to one or the other [230]. Mouse monocytes can be divided into sub-populations depending on the

variable presence of lymphocyte antigen 6C (Ly6C). Monocytes expressing high levels of Ly6C ($Ly6C^{hi}$) are referred to as classical or 'inflammatory monocytes' and represent approximately 2-5% of circulating white blood cells. They are rapidly recruited to sites of infection and inflammation and differentiate into M1 macrophages and DCs. Similar to neutrophils, these monocytes are necessary for eliminating foreign invaders but can have detrimental effects in sterile IR injuries. Hence, they are also considered key therapeutic targets for disease treatment. Ly6C low ($Ly6C^{lo}$) monocytes are less prevalent than $LY6C^{hi}$ monocytes in the bloodstream and are known as 'patrolling' monocytes. These monocytes constantly crawl along the blood vessel lumen searching for and clearing damaged ECs and debris to maintain vasculature integrity. In pathological conditions, $Ly6C^{lo}$ monocytes can also transmigrate into surrounding tissue and differentiate into M2 non-inflammatory macrophages, which possess the ability to secrete anti-inflammatory cytokines and repair damaged tissue [244].

To assess whether HPC-7s reduced the recruitment of the inflammatory $Ly6C^{hi}$ and increased infiltration of $Ly6C^{lo}$ monocytes or resulted in the population of monocytes shifting towards an anti-inflammatory phenotype, we digested whole hearts and alongside co-labelling for CD115 (macrophage CSF receptor) and latex beads, quantitated levels of monocyte sub-populations. We firstly demonstrated that there was a significant increase predominantly in the pro-inflammatory $Ly6C^{hi}$ monocytes in IR injured hearts. However, the level of increase noted was likely an underestimation [179] as the method used to label monocytes in our experiments was only labelling around 15% of circulating monocytes with fluorescent microparticles, leaving the majority unlabelled (alternatively, it could be an accurate assessment as the phagocytic activity of monocytes may be correlated with their ability to become more readily adherent to the vessel wall). As such, while the absolute number of

monocytes recruited is not known, the changes observed during IR injury and with HPC-7s therapy are still vitally important and relevant to understanding the inflammatory response in this setting.

Interestingly, we found that in IR injured hearts treated with HPC-7s, although the overall total percentage of recruited cells decreased as compared with non-treated injured hearts, the ratio between subsets remained the same – i.e. HPC-7s reduced both sub-populations and not just one type. Similar to what we found, Nakano et al. conducted a study which showed that in IR injured mice hearts, there was an increase in the infiltration of monocytes dominated by the pro-inflammatory sub-population (~80% of total infiltrating monocytes) within 3-hours of reperfusion [260]. This is not a surprising outcome and mirrors what we have found in our study. They went on to investigate the effects of myocardial IR injury in C-C chemokine receptor type 2 knockout mice ($CCR2^{-/-}$) in order to specifically ascertain the role of $Ly6C^{hi}$ monocytes in IR injury without impacting on recruitment of $Ly6C^{lo}$ monocytes [244, 261]. They found that while recruitment of $Ly6C^{hi}$ monocytes was inhibited, delaying infarct enlargement, there was no increased recruitment of $Ly6C^{lo}$ monocytes to compensate for this. In fact, recruitment of $Ly6C^{lo}$ monocytes was not observed even after 48 hours of reperfusion. The role of $Ly6C^{lo}$ monocytes is believed to begin around day 4/5 after myocardial IR injury [232]. This is commonly referred to as the biphasic recruitment of monocytes to the IR injured heart. As such, the reduction of monocyte recruitment exhibited when we utilised HPC-7s as a form of cell therapy in our model is very promising. Whilst we still showed a dominance in the pro-inflammatory monocyte sub-population after HPC-7s therapy, this appears to be due to the biphasic nature of monocyte recruitment to the injured heart and the early favouring of pro-inflammatory monocyte recruitment, not because of inhibition of the anti-inflammatory sub-

population. To properly assess the effects of HPC-7s therapy on the recruitment of anti-inflammatory monocytes in myocardial IR injury, tissue samples would need to be obtained a few days after the insult.

5.4.2.6 Critical Evaluation of Flow Cytometry Results

Critical evaluation of flow cytometry results observed in this study show that a more complex/robust panel setup alongside more stringent gating out of doublets and dead cells would yield more conclusive results. The FACScalibur flow cytometer used here features a single 488nm excitation laser with three emission detectors at 530/30nm, 585/42nm and 650nm. It only captures the height parameter for side/forward scatter of events, but not additional parameters such as width or area. The presence of doublets and dead cells may provide false positives and can be more accurately excluded for instance by plotting the height against the area for side/forward scatter of events (for doublet removal) and by using the dead cell markers propidium iodide and annexin v (for necrotic and apoptotic dead cell removal). As mentioned, a more complex panel setup to characterise the different cell populations within the mouse heart would provide more accurate information. Additional markers could be used to help specify endothelial cells (anti-CD31 ab) and cardiomyocytes (anti-CTnT ab) in this study, such as the anti-CD144 ab and anti-alpha Sarcomeric Actinin ab respectively. The use of an anti-CD45 antibody would also help identify the inflammatory cell population within the heart, of which some may express CD31 (separating them from ECs). The inflammatory population can then be further assessed by using an anti-CD11b ab alongside anti-Ly6G ab, anti-CD68 ab and anti-F4/80 ab to help define neutrophils, monocytes

and macrophages. These additions would help solidify the results obtained in our study. Representing the data obtained using mean/median fluorescence intensity (MFI) would also help solidify the results shown of cell population percentages.

5.4.2.7 IL-36: A Novel Inflammatory Cytokine Capable of Mediating Inflammation in the Beating Mouse Heart

The Kalia group developed an interest in IL-36, a new cytokine with similar characteristics to IL-1, after their novel data showed that the expression of the IL-36 receptor (IL36R / 1L1Rrp2) was significantly increased in the IR injured heart. Interestingly, its expression was further enhanced in the aged mouse heart (data unpublished). Expression was primarily vascular in nature as determined by immunohistological co-staining with CD31. Increased levels of IL-36α and IL36β were also shown in response to myocardial IR injury (ongoing research - data unpublished). As far as we are aware, this was the first clear experimental evidence of a role for the IL-36/IL-36R pathway in the murine heart. As IL-36 isoforms are a newly recognised family of pro-inflammatory cytokines, their role in myocardial inflammation is not well understood. The results described in this chapter showed that during myocardial IR injury, the level of multiple pro-inflammatory cytokines was increased, indicating that IL-36 cytokines may also be potentially increased. However, as these are novel cytokines, there is currently no commercially available mouse ELISA based assay to quantify their presence in the plasma without substantial optimisation.

With this in mind, we decided to conduct intravital studies in which the three isoforms of IL-36 were topically applied to the otherwise healthy beating heart. We show for the first time

that directly applying IL-36α and IL-36β to the heart caused a gradual but significant increase in both neutrophil and monocyte recruitment. IL-36γ also showed an increased trend for neutrophil and monocyte recruitment, however this was not statistically significant. This is a highly novel aspect of our research as it is the first intravital demonstration of IL-36 isoforms being pro-inflammatory *in vivo,* within a few minutes of exposure, in any tissue bed let alone the beating heart. Surprisingly, even basic studies using *in vitro* adhesion assays to assess the pro-adhesive effects of IL-36 have not been conducted. The inflammatory nature of IL-36 cytokines has primarily been demonstrated in immunohistological studies. For example, Milora and colleagues showed a reduced infiltration of neutrophils in the skin in IL-36 knockout mice [262]. Although the impact on neutrophils is well described, the ability of IL-36 to affect monocytes was investigated by Foster and colleagues who showed that murine monocytes expressed the IL-36R and could be recruited to skin exposed to IL-36α. Furthermore, monocytes have been shown to be a very good source of the IL-36 cytokine itself [263]. However, the current intravital studies are the first to provide exciting data on the kinetics of IL-36 mediated pro-adhesive events in microvessels in real-time *in vivo.*

We further demonstrated that pre-administration of HPC-7s could attenuate the recruitment of monocytes, but not neutrophils, in the presence of stimulation with IL-36β. This provides another potential mechanistic method by which HPC-7s may modulate the inflammatory response. The difference in the ability of HPC-7s to modify only the monocyte response is interesting and requires further investigation, particularly since HPC-7s could reduce IR mediated neutrophil increases. The use of the IL-36 receptor antagonist was the next logical step in our investigation. However, due to time constraints, we only managed to conduct this experiment once, but promising results were obtained.

5.4.3 Conclusion

In conclusion, this chapter has provided us with valuable information with regards to the mechanistic actions behind the vasculoprotective effects of HPC-7s therapy in myocardial IR injury. We provide novel and conclusive visual evidence that HPC-7s are not required to directly home to the injured heart in order to confer their vasculoprotective benefits. Either through release of soluble factors from a remote site, or though being activated whilst circulating through the injured heart, HPC-7s were able to protect the coronary endothelium through paracrine actions. This was partly achieved by reducing the levels of oxidative damage experienced by the endothelium and by reducing the inflammatory response as well. We also showed how HPC-7s were able to attenuate the general recruitment of all monocytes in myocardial IR injury without shifting the sub-population imbalance that favours pro-inflammatory monocytes after insult. There is also a potential pathway for the modulation of IL-36 pro-inflammatory cytokines, whether by HPC-7s or by the IL-36RA, to reduce myocardial IR injury.

CHAPTER 6:

GENERAL DISCUSSION

6.1 Summary of Main Findings

As CVD is still the leading cause of morbidity and mortality worldwide, with MIs contributing the most to CVD, it remains imperative that better treatment strategies are pursued [38, 264]. Current treatment strategies include the use of pharmacotherapies, percutaneous coronary intervention (PCI) and surgical procedures that limit the ischaemia injury, instigate timely reperfusion and aim to improve patient outcomes. However, it is well accepted that despite PCI and other contemporary pharmacotherapies which successfully reperfuse the heart, a significant proportion of MI patients still incur extensive muscle damage and develop heart failure. Microvascular obstruction post-PCI and/or IR injury (due to thromboinflammation, oedema, endothelial dysfunction etc.) can impair myocardial reperfusion. To date, no treatments targeting this process have shown conclusive benefit. Strategies to alleviate reperfusion injury therefore remains of interest in cardiovascular research. The use of alternative therapies to deal with this is critical and one of the options available is in using cellular therapy. Although clinical trials have used cell therapy, specifically SC therapy, in treating MI, their effectiveness in the clinical setting has generally been poor [149]. Reasons for this include:

- Inadequate standardisation of procedures with a need for more rigorous trial designs
- Uncertainty over the appropriate SC population for use and route of delivery
- A lack of a robust method for imaging the beating mouse heart *in vivo* for pre-clinical assessment of disease and treatment options
- A lack in the pre-clinical assessment of the mechanisms explaining the beneficial role of SC therapy in MI

The use of SC therapy has primarily been with the aim of regenerating lost tissue. This is an attractive proposition in the heart as the heart has generally been seen as a post-mitotic organ. SC therapy however, can be of more use than just as a form of regenerative medicine. SCs harbour many additional protective characteristics such as modulation of the inflammatory response, reducing levels of oxidative stress and enhancing revascularisation of tissue [156, 157]. The use of SC therapy as a reparative tool is an ongoing research question that we have attempted to address in this thesis with a specific focus on coronary microcirculatory vasculoprotection.

One of the main aims of this study was to determine the vasculoprotective effects of haematopoietic stem cells (HSCs) in myocardial IR injury (mimicking an MI). We undertook this study by attempting to answer some of the questions thrown up by the list of reasons behind its limited clinical success. We optimised an intravital imaging technique allowing us to visualise the microcirculation of the mouse heart *in vivo* in real-time. This allowed us to understand the kinetics of endogenous thromboinflammatory cells in myocardial IR injury and the recruitment of HPC-7s to the heart microvessels. Novel data has also been gathered on the microcirculatory disturbances that occur during myocardial IR injury. This novel data is accompanied by a robust evaluation of the mechanisms employed by HPC-7s therapy to potentially protect coronary microvessels *in vivo* including their ability to inhibit oxidative stress and the inflammatory response. The major findings from this study are:

- Microcirculatory perturbations are a major concern in myocardial IR injury. IVM is a powerful tool for the assessment of the coronary microcirculation, notably during IR injury, and for testing therapeutic options.

- Although global myocardial perfusion appears improved, this is not matched by adequate perfusion at a microcirculatory level. Under normal conditions, innate immune cells readily patrol the heart vasculature. During IR injury, both neutrophils and monocytes are rapidly recruited in large numbers with their presence primarily within coronary capillaries. At times these cells become entrapped within platelet aggregates forming mixed microthrombi. The platelet microthrombi are the main contributors to the blocking of blood flow in coronary microvessels which leads to a significant decline in the functional capillary density within the myocardium.
- HPC-7s are a viable, suitable and appropriate population to study in cardiac IR injury. Their small size and spherical shape allow them to readily mobilise through the microcirculation. They attenuate most of the microcirculatory disturbances that occur post-reperfusion in the beating heart, affording the return of organised capillaries, inhibiting microthrombus formation and inflammatory cell infiltration and reducing oxidative endothelial cell damage. Protecting the endothelium from oxidative stress maintains a healthy endothelium and is less likely to cause activation of platelets and inflammatory cells. Consequently, this leads to a smaller infarct size.
- The vasculoprotective action of HPC-7s in cardiac IR injury is not achieved via direct homing and subsequent retention of the cells to the injured heart. Even pre-treating HPC-7s with hydrogen peroxide did not aid in their recruitment in this model. As such, their reparative actions likely stem from paracrine mechanisms. This may include their ability to reduce circulating levels of inflammatory IL-6, IL-12(p40), G-CSF, CXCL1, CCL2 and CCL4 cytokines (markedly increased during IR injury) and several other pro-

inflammatory cytokines. Circulating IL-10, an anti-inflammatory cytokine, was markedly elevated after HPC-7s therapy.

- Topical application of pro-inflammatory IL-36 cytokines elicits a pronounced inflammatory response in the beating heart and may be a potential candidate in the future for treating reperfusion-mediated inflammatory disturbances in the coronary microcirculation.

The major body of work presented in this thesis includes data obtained from novel intravital experiments conducted on the beating mouse heart undergoing myocardial IR injury. For the first time, we have been able to directly show the substantial damage that occurs within the cardiac microcirculation *in vivo*. Indeed, we demonstrated in real-time the concept of 'no-reflow' occurring during the period of reperfusion. We were able to categorically state that microthrombi made up primarily of activated platelets, with the occasional inflammatory cell, occupied significant lengths of the capillaries, blocking blood flow through the vessel during the period of reperfusion. These areas devoid of blood flow continue to be injured and we show that the microvascular structure becomes more disorganised in this period. Importantly, these events have not previously been observed clinically in MI patients post-reperfusion due to limitations of current diagnostic and imaging tools.

This information is supplemented by our LSCI data indicating that there is an immediate and persistent hyperaemic response in the heart during the period of reperfusion. Unsurprisingly, the blood flow 'debt' built-up during the period of ischaemia incurs a response from the tissue, leading towards signals promoting vasodilation with the intention of increasing blood flow to the hypoxic area [5]. This leads to a generalised increase in blood flow through the left ventricle. However, as we have noted, this does not necessarily translate into reperfusion at

the microcirculatory level. Areas that are reperfused however, are subject to an increased amount of blood cells than usual, overcompensating for the earlier 'debt'. This also leads to a return of oxygen in a higher capacity than usual, aggravating the microenvironment by inducing oxidative stress.

Our novel flow cytometry data shows endothelial cells are more susceptible to oxidative stress compared to cardiomyocytes during the initial period of reperfusion. Again, this emphasises the importance of the coronary microcirculation as a key target for potentially salvaging the ischaemically damaged myocardium. The early susceptibility of endothelial cells can be explained by the fact that they are the first cells to come into contact with the returning oxygen supply, meaning they are one of the first tissue resident cells to be exposed to oxidative stress. It is important to note however, that others have claimed that cardiomyocytes are more susceptible to oxidative stress compared to endothelial cells. This is reportedly due to their reliance on high energy usage [265]. Our data is perhaps a reflection of the acute stage in reperfusion, where early on, endothelial cells appear to be more susceptible. This can also be reasoned by the difference in mitochondrial numbers in these cells. As cardiomyocytes have more mitochondria within the cell, this provides them with a higher resistance to oxidative stress as compared to endothelial cells, especially in the acute stage [266]. Stressed and damaged endothelial cells will activate surrounding platelets and inflammatory cells, and the upregulation of adhesion molecules – as we have shown with ICAM-1 and VCAM-1 – invokes their recruitment.

Activation of platelets and inflammatory cells during the period of reperfusion is not surprising. These events have been observed before by others [62, 73]. Through IVM experiments however, we have been able to show the rapid and substantial increase in cell

recruitment that occurs in real-time. Within 30 minutes of reperfusion, peak levels of platelets, neutrophils and monocytes are observed within the injured site. We also show that for the duration of 2 hours of reperfusion, these levels remain stable and do not fluctuate much. Through these experiments, we have also been able to show how inflammatory cells naturally patrol the myocardium in steady-state conditions. During IR injury, these cells become trapped in platelet aggregates, contributing somewhat to microthrombi size and composition.

It is interesting to note the patrolling behaviour of neutrophils and monocytes in healthy hearts, impossible to detect without *in vivo* imaging. This behaviour is not unique to the heart, being described in other organs such as the lungs and kidneys [178, 267]. As the heart is an organ in constant motion, it is perhaps unsurprising that cells may become temporarily immobile during systole/contraction, contributing to their patrolling behaviour. In the case of monocytes, it is generally the anti-inflammatory Ly6C^{lo} subset that patrol the vasculature and function to remove dead cells or debris from the vasculature [268]. Data that we have provided here in our sham experiments agrees with this notion, as more Ly6C^{lo} monocytes were found in digested whole heart tissue compared to the Ly6C^{high} population. As we have shown however, during IR injury, the pro-inflammatory Ly6C^{high} monocytes are more readily recruited to the heart, significantly shifting the subset balance towards more Ly6C^{high} monocytes compared to Ly6C^{lo} monocytes.

This pro-inflammatory microenvironment that occurs during cardiac IR injury is known to exacerbate the final level of damage inflicted [3]. Our findings further demonstrate this by the increased levels of circulating pro-inflammatory cytokines such as IL-6, IL-12, G-CSF, CXCL1, CCL2 and CCL4 cytokines. Mobilisation of inflammatory cells to the site of injury is important

and reservoirs of these cells can be found in the bone marrow and spleen [135, 269]. The significant increase in IL-10 levels is interesting as well, indicating that there exists an attempt to balance the inflammatory response in cardiac IR injury. This was an unexpected finding but could potentially be exploited as a form of therapeutic intervention.

Another major part of the work presented in this thesis involves the use of HPC-7s as a form of cell therapy to alleviate the microvascular damage caused during myocardial IR injury. Using primary HSCs from mice is not feasibly possible due to the low number of cells present in the bone marrow of mice, where only around 5000 cells (Kit^+, $Sca\text{-}1^+$, Lin^- ; KSL cells) can be acquired from one mouse [270]. As such, here we have used a murine HSC line known as HPC-7s to investigate the homing and protective effects of HSC therapy. These cells have been used to model murine primary HSCs by a number of studies that involve molecular assessment of HPC-7s and their cellular signalling pathways [151, 169, 271]. As such, we feel confident in its use in modelling primary HSCs. This study shows HPC-7s therapy is effective in the immediate aftermath of reperfusion injury, a time point not previously investigated for beneficial effects – in fact most cell therapy studies both clinical and experimental look for long-term benefits particularly on heart function and infarct size. Here we show that these cells limit thromboinflammatory events at both a cellular and molecular level which ultimately reduced infarct size. This effect was immediate, within 30 minutes of reperfusion, and sustained. Although anti-inflammatory capabilities have been ascribed to stem cells, it was somewhat surprising to see that even microthrombus formation, a hallmark in injured hearts, were no longer present. Impressive also was the return of functional perfused microvessels. Interestingly, these effects were achieved whilst still maintaining the general hyperaemic response noted in non-treated IR injured hearts.

In both our *in vitro* and *in vivo* studies, we have shown how HPC-7s protect endothelial cells against oxidative stress. This capability in HSCs is not surprising, as their natural habitat in the bone marrow niche has very low oxygen levels. As such, HSCs are naturally resistant to oxidative stress and have anti-oxidant capabilities, such as via superoxide dismutase 2, to deal with such an environment [272]. Oxidative stress is a major component of IR injury and this protection afforded by HPC-7s appears to be important in explaining the beneficial changes observed in our study. As mentioned previously, stressed and damaged endothelial cells can exacerbate the thromboinflammatory response in IR injury. This can be achieved either directly, via activation of local circulating blood cells, or indirectly, via paracrine/endocrine mechanisms that instigate a systemic response [47].

Studies have shown that extracellular vesicles from endothelial cells from IR injured hearts can travel to distant organs, such as the spleen, in order to elicit a systemic inflammatory response [273]. The spleen may subsequently release its reservoir of inflammatory cells and may also initiate the increased production of pro-inflammatory cytokine and chemokine receptor gene transcripts [274]. Of note, HSCs have been shown to counter this effect on the spleen when used as treatment for cerebral ischaemia [274]. It is therefore very possible that the protection afforded to endothelial cells by HSCs has regional and systemic benefits. As we have shown, the healthier endothelium has a markedly lower level of ICAM-1 and VCAM-1 expression compared to the IR injured endothelium, directly inhibiting excessive inflammatory infiltration.

Studies have intimated that the paracrine effects of various stem cells produce similar therapeutic benefits [275]. Researchers using MSCs, HSCs and EPCs independently as forms of cell therapy have produced similar beneficial results on ventricular function after cardiac

injury [270, 276, 277]. As such, a known vasculoprotective effect of MSCs and EPCs – the production of NO – may also be attributable to HSCs [278, 279]. NO is a known vasculoprotective agent, inhibiting leukocyte-endothelial cell adhesion and platelet aggregation in order to maintain vascular health [280]. Increased production of NO in our IR+HPC-7s model, whether directly released from HPC-7s or indirectly by inhibition of eNOS uncoupling (via reduction of oxidative stress), could help explain our findings.

It is interesting to note that the subset shift in monocyte population during IR injury is maintained in the HPC-7s treated hearts. The benefit in HPC-7s therapy was in the generalised reduction of infiltrating monocytes, without shifting the monocyte subset balance towards the anti-inflammatory population. This is despite the microenvironmental shift from a pro-inflammatory environment to an anti-inflammatory environment. The highly elevated circulating pro-inflammatory cytokines listed earlier, IL-6, IL-12, G-CSF, CXCL1, CCL2 and CCL4, were all significantly reduced following HPC-7s therapy. In fact, a number of other circulating pro-inflammatory cytokines were also lower in the HPC-7s therapy group. As mentioned before, the circulating anti-inflammatory IL-10 cytokine was markedly higher in the HPC-7s therapy group. The anti-inflammatory propensity of HSCs is not surprising, having been observed when applied as treatment for IR injury in other organs [150, 151].

If, however, a major contribution of HSCs in the setting of myocardial IR injury is the protection afforded against oxidative stress, then the window of therapeutic benefit may be small. Once damage due to oxidative stress has accumulated, the effectiveness of HSC therapy could be compromised. This is an important consideration that will inform how best to provide HSCs in the clinical setting. Alongside this, another important consideration is the method of cell delivery in the clinical setting.

Method of cell delivery for any cell therapy option is important as the local presence of these cells at the site of injury may be necessary. Our group hypothesised that any vasculoprotective benefit of HSCs in the setting of myocardial IR injury would be related to its ability to home to the site of injury. However, we have provided novel real-time data in this study showing that systemically delivered HPC-7s are not recruited to the injured heart. Even pre-treating our HPC-7s with hydrogen peroxide did not affect its recruitment. Despite this, we have still shown tremendous benefit in HPC-7s therapy for cardiac IR injury. This indicates that the primary form for conferring vasculoprotection is through paracrine means. It is also important to note that HPC-7s require exposure to the IR environment in order to become activated and confer protection. This was shown in this study as using cultured media from inactivated HPC-7s as a treatment option had no effect on the thromboinflammatory response.

The final part of this thesis was centred on investigating the role that HPC-7s may play in modulating the IL-36 cytokine pro-inflammatory response. Novel mechanistic work currently being conducted in our group has shown that the IL-36 receptor expression in the murine heart was elevated after IR injury. Therefore, we wanted to determine the potency of IL-36 cytokines in directly initiating an inflammatory response in the heart and the modulating effects of HPC-7s in such a circumstance. Here we have shown novel data indicating that topically treating the heart with IL-36 cytokines elicits an inflammatory response as the recruitment of both neutrophils and monocytes was increased. This was especially true with IL-36β. This is the first time an intravital study has been conducted on any vascular bed to directly demonstrate the ability of IL-36 isoforms to be pro-inflammatory. Interestingly, HPC-7s therapy in this circumstance only inhibited the recruitment of monocytes, not neutrophils. Unfortunately, more research into the role that HSCs can play in attenuating the pro-

inflammatory response of IL-36 cytokines is necessary before any real conclusion can be drawn.

6.2 Imaging the Beating Mouse Heart with Intravital Microscopy

An important aspect of our work was utilisation of IVM in order to detail for the first time the role of the coronary microcirculation in myocardial IR injury *in vivo*. IVM is not a new technique, having been used to investigate the microcirculation in other murine tissues such as the gut, kidney, liver and cremaster muscle. Whilst others have used these models to infer parallels to cardiovascular disease, in order to fully comprehend the workings of the heart however, we believed that directly imaging the microcirculation of the heart was important. Moreover, the coronary microcirculation has peculiar site specific characteristics. For example, unlike other organs, the microvessels in the heart can form hairpin loops, T-, Y- and H-shaped junctions [281]. Adjacent capillaries may also have opposite flow [282]. These capillaries are also 'squeezed' during systole, where the lumen diameter decreases by nearly 20% and retrograde flow may occur [283].

Historically, imaging the beating heart has proven difficult for two main reason. Firstly, the contractile nature of the beating heart alongside the movement of the inflating lungs has made stable image acquisition difficult. Secondly, there have been technical issues with performing imaging within the 'tight' thoracic cavity. With recent advancements in microscopy and technology in general, this undertaking has become more feasible. Indeed, recent studies have started to investigate cardiomyocytes [219] and neutrophil trafficking within the healthy cardiac microcirculation [177] and transplanted hearts of mice [218]. Jung

and colleagues used a suction-assisted endoscope attached to a confocal microscope to image monocytes in the permanently ligated LAD MI model [234]. Similar to our own study, they also demonstrated a rapid and abundant recruitment in monocytes during the ischaemic phase. Furthermore, they also identified 'patrolling' monocytes rolling at a slow pace in coronary venules, a phenomenon we also described in the coronary capillaries. Collectively, our two studies provide direct evidence of a population of potentially immune surveillance cells in the heart. Although such cells have been identified intravitally in organs that are constantly exposed to toxins, such as the skin, intestine and lungs, it was interesting to find such 'patrolling' cell behaviour in the heart. Identification of such novel inflammatory cell behaviours is where intravital studies really come into their own. Additional work such as that conducted by Xu et al., have also investigated inflammatory infiltration in the heart after inhibition of adhesion molecules [284].

The current study is certainly the first to image the coronary microcirculation immediately post-reperfusion. This is an important and clinically relevant model as it mirrors the scenario of a patient having their heart reperfused immediately after an intervention such as PCI to open up an obstructed coronary artery. Moreover, this study did not just image inflammatory cell kinetics but also platelet activity *in vivo* and effects on functional capillary density and whole ventricular perfusion. Coronary microvascular disease is an area of research gaining track, such as in cases of acute coronary syndrome without obstruction or in heart failure with preserved ejection fraction [285, 286]. Conducting live imaging in order to assess coronary dysfunction in the pre-clinical setting can only further enhance our understanding of its importance.

6.3 Future Work

The results obtained within this study can be used to inform a number of different research projects going forward. One of our consistent intravital findings was that the thromboinflammatory events described had already occurred within 30 minutes of reperfusion which was the earliest time point at which we could image. To better understand at which time point this actually happened (i.e during ischaemia or immediately after reperfusion), it would be ideal to optimise our stabilisation method such that those critical 30 minutes can be imaged. This has clear clinical implications as it could determine timing of drug delivery in MI patients post-interventions such as a PCI. Therefore, optimisation of our balloon ligation technique is essential as it would provide us with valuable information missing in our current study. Another benefit of this technique is that it would allow us to directly assess the microcirculatory impact of ischaemic pre- and post-conditioning therapies on the IR injured heart. Studies have shown that ischaemic pre- and post-conditioning can lead to better tissue healing in the IR injured heart [287]. Optimising our model would allow us to study this aspect in greater detail.

In recent years, the possibility that cells of the adaptive immune system, and cytokines derived from such cells, can also influence inflammation is emerging. This view suggests lymphocytes cooperate with innate immune cells and both collectively orchestrate the inflammatory response. Moreover, a role for lymphocytes has also been implicated in MI and IR injury in humans [288]. Boag and colleagues noted an early depletion of circulating lymphocytes, particularly highly differentiated T cells, in the peripheral blood of MI patients [289]. They further showed that these cells were likely being sequestered within the reperfused

myocardium. The most critical observation from this study was the fact that the degree of lymphopenia was linked to long-term patient prognosis. In light of these studies, it is important that we experimentally image the role of other trafficking cells in addition to neutrophils, monocytes and platelets. This includes investigating the role that the adaptive immune system plays in this disease model. This would provide a more rounded view of the immune response, especially if the inclusion of possible roles for B cells and NK cells are taken into account as well.

As oxidative stress appears to play an important role in the beneficial impact of HSC therapy, conducting IVM experiments that can spatially and temporally detect ROS *in vivo* in the beating heart would prove beneficial. This would then allow for the assessment of therapeutic strategies that inhibit their presence, and thus subsequent oxidative damage. Studies have used dihydroethidium (DHE) to assess the presence of ROS, specifically superoxide, in other tissues such as the renal glomeruli intravitally [290]. This fluorescent method of labelling oxidative stress works well with IVM. We used this same dye in our *in vitro* studies, but incorporating this technique with IVM is vital in order to understand oxidative stress and its detrimental effects in myocardial IR injury *in vivo* (ongoing studies in the Kalia lab).

With regards to therapeutic research, other forms of cell therapy to treat myocardial IR injury could be investigated. MSCs, EPCs or iPSCs for instance, are viable treatment options that can be examined in our model and their efficacy compared to HSCs. Further investigations into the stem cell paracrine effect may allow for the harnessing of specific proteins or factors that are beneficial without the need for cell therapy. Regardless, cellular therapy is still an exciting field as the ability of the cell to adapt to its environment has inherit advantages. We can also look into pharmacological treatment options alongside possible combination therapy with

stem cells. Our model would also allow us to better understand how contemporary treatment options, such as anti-platelet strategies and anti-hypertensives, effect the coronary microcirculation. Clinical trials are very expensive and intensive studies to conduct, and as such, the more knowledge that can be accumulated in pre-clinical investigations, the better.

6.4 Concluding Remarks

In conclusion, the role of the microcirculation in myocardial IR injury is extremely important. The dysfunction that occurs at this level is only beginning to be appreciated in an *in vivo* setting. However, we have shown in this study that it can no longer be overlooked. The changes in the microvascular structure and integrity during IR injury indicate that the health of the microcirculation is important and that we can no longer simply rely on therapeutic interventions that only focus on reperfusion via unblocking a major coronary artery.

CHAPTER 7:

REFERENCES

1. Wilkins E, W.L., Wickramasinghe K, Bhatnagar P, Leal J, Luengo-Fernandez R, Burns R, Rayner M, Townsend N, *European Cardiovascular Disease Statistics 2017.* European Heart Network, 2017.
2. Rossini, R., et al., *Long-term outcomes of patients with acute coronary syndrome and nonobstructive coronary artery disease.* Am J Cardiol, 2013. **112**(2): p. 150-5.
3. Bulluck, H., D.M. Yellon, and D.J. Hausenloy, *Reducing myocardial infarct size: challenges and future opportunities.* Heart, 2016. **102**(5): p. 341-8.
4. Yellon, D.M. and D.J. Hausenloy, *Myocardial reperfusion injury.* N Engl J Med, 2007. **357**(11): p. 1121-35.
5. Kalogeris, T., et al., *Ischemia/Reperfusion.* Compr Physiol, 2016. **7**(1): p. 113-170.
6. Bolognese, L., et al., *Impact of microvascular dysfunction on left ventricular remodeling and long-term clinical outcome after primary coronary angioplasty for acute myocardial infarction.* Circulation, 2004. **109**(9): p. 1121-6.
7. Camici, P.G. and F. Crea, *Coronary microvascular dysfunction.* N Engl J Med, 2007. **356**(8): p. 830-40.
8. De Maria, G.L., et al., *How does coronary stent implantation impact on the status of the microcirculation during primary percutaneous coronary intervention in patients with ST-elevation myocardial infarction?* Eur Heart J, 2015. **36**(45): p. 3165-77.
9. Ito, H., et al., *Clinical implications of the 'no reflow' phenomenon. A predictor of complications and left ventricular remodeling in reperfused anterior wall myocardial infarction.* Circulation, 1996. **93**(2): p. 223-8.
10. Wang, X., et al., *Metformin attenuates myocardial ischemia-reperfusion injury via up-regulation of antioxidant enzymes.* PLoS One, 2017. **12**(8): p. e0182777.
11. Souktani, R., et al., *Cardioprotection against myocardial infarction with PTD-BIR3/RING, a XIAP mimicking protein.* J Mol Cell Cardiol, 2009. **46**(5): p. 713-8.
12. Sanada, S., I. Komuro, and M. Kitakaze, *Pathophysiology of myocardial reperfusion injury: preconditioning, postconditioning, and translational aspects of protective measures.* Am J Physiol Heart Circ Physiol, 2011. **301**(5): p. H1723-41.
13. Pike, M.M., et al., *NMR measurements of Na+ and cellular energy in ischemic rat heart: role of Na(+)-H+ exchange.* Am J Physiol, 1993. **265**(6 Pt 2): p. H2017-26.
14. Lesnefsky, E.J., et al., *Mitochondrial Dysfunction and Myocardial Ischemia-Reperfusion: Implications for Novel Therapies.* Annu Rev Pharmacol Toxicol, 2017. **57**: p. 535-565.
15. Kurian, G.A., et al., *The Role of Oxidative Stress in Myocardial Ischemia and Reperfusion Injury and Remodeling: Revisited.* Oxid Med Cell Longev, 2016. **2016**: p. 1656450.
16. Borutaite, V., et al., *Inhibition of mitochondrial permeability transition prevents mitochondrial dysfunction, cytochrome c release and apoptosis induced by heart ischemia.* J Mol Cell Cardiol, 2003. **35**(4): p. 357-66.
17. Jennings, R.B., *Historical perspective on the pathology of myocardial ischemia/reperfusion injury.* Circ Res, 2013. **113**(4): p. 428-38.
18. Jennings, R.B., et al., *Myocardial necrosis induced by temporary occlusion of a coronary artery in the dog.* Arch Pathol, 1960. **70**: p. 68-78.
19. Qian, T., et al., *Mitochondrial permeability transition in pH-dependent reperfusion injury to rat hepatocytes.* Am J Physiol, 1997. **273**(6 Pt 1): p. C1783-92.
20. Lemasters, J.J., et al., *The pH paradox in ischemia-reperfusion injury to cardiac myocytes.* EXS, 1996. **76**: p. 99-114.
21. Granger, D.N., *Role of xanthine oxidase and granulocytes in ischemia-reperfusion injury.* Am J Physiol, 1988. **255**(6 Pt 2): p. H1269-75.
22. Raedschelders, K., D.M. Ansley, and D.D. Chen, *The cellular and molecular origin of reactive oxygen species generation during myocardial ischemia and reperfusion.* Pharmacol Ther, 2012. **133**(2): p. 230-55.

23. Talukder, M.A., J.L. Zweier, and M. Periasamy, *Targeting calcium transport in ischaemic heart disease.* Cardiovasc Res, 2009. **84**(3): p. 345-52.
24. Ferran, C., et al., *Inhibition of NF-kappa B by pyrrolidine dithiocarbamate blocks endothelial cell activation.* Biochem Biophys Res Commun, 1995. **214**(1): p. 212-23.
25. Tissier, S., et al., *Calpain inhibitors improve myocardial dysfunction and inflammation induced by endotoxin in rats.* Shock, 2004. **21**(4): p. 352-7.
26. Ibanez, B., et al., *Evolving therapies for myocardial ischemia/reperfusion injury.* J Am Coll Cardiol, 2015. **65**(14): p. 1454-71.
27. Sanchez, J.A., et al., *Effects of a reduction in the number of gap junction channels or in their conductance on ischemia-reperfusion arrhythmias in isolated mouse hearts.* Am J Physiol Heart Circ Physiol, 2011. **301**(6): p. H2442-53.
28. Lauten, A., et al., *Impact of ischemia-reperfusion on extracellular matrix processing and structure of the basement membrane of the heart.* PLoS One, 2014. **9**(3): p. e92833.
29. Romero, J., et al., *CMR imaging for the evaluation of myocardial stunning after acute myocardial infarction: a meta-analysis of prospective trials.* Eur Heart J Cardiovasc Imaging, 2013. **14**(11): p. 1080-91.
30. Niwano, S., et al., *Cardioprotective effects of sarcolemmal and mitochondrial K-ATP channel openers in an experimental model of autoimmune myocarditis. Role of the reduction in calcium overload during acute heart failure.* Int Heart J, 2012. **53**(2): p. 139-45.
31. Ito, H., *No-reflow phenomenon and prognosis in patients with acute myocardial infarction.* Nat Clin Pract Cardiovasc Med, 2006. **3**(9): p. 499-506.
32. Topol, E.J. and J.S. Yadav, *Recognition of the importance of embolization in atherosclerotic vascular disease.* Circulation, 2000. **101**(5): p. 570-80.
33. Manciet, L.H., et al., *Microvascular compression during myocardial ischemia: mechanistic basis for no-reflow phenomenon.* Am J Physiol, 1994. **266**(4 Pt 2): p. H1541-50.
34. Kunichika, H., et al., *Effects of glycoprotein IIb/IIIa inhibition on microvascular flow after coronary reperfusion. A quantitative myocardial contrast echocardiography study.* J Am Coll Cardiol, 2004. **43**(2): p. 276-83.
35. Kocher, A.A., et al., *Neovascularization of ischemic myocardium by human bone-marrow-derived angioblasts prevents cardiomyocyte apoptosis, reduces remodeling and improves cardiac function.* Nat Med, 2001. **7**(4): p. 430-6.
36. Manning, A.S. and D.J. Hearse, *Reperfusion-induced arrhythmias: mechanisms and prevention.* J Mol Cell Cardiol, 1984. **16**(6): p. 497-518.
37. Ter Keurs, H.E. and P.A. Boyden, *Calcium and arrhythmogenesis.* Physiol Rev, 2007. **87**(2): p. 457-506.
38. Hausenloy, D.J. and D.M. Yellon, *Myocardial ischemia-reperfusion injury: a neglected therapeutic target.* J Clin Invest, 2013. **123**(1): p. 92-100.
39. Rochitte, C.E., et al., *Magnitude and time course of microvascular obstruction and tissue injury after acute myocardial infarction.* Circulation, 1998. **98**(10): p. 1006-14.
40. Zhao, Z.Q., et al., *Inhibition of myocardial injury by ischemic postconditioning during reperfusion: comparison with ischemic preconditioning.* Am J Physiol Heart Circ Physiol, 2003. **285**(2): p. H579-88.
41. Niccoli, G., et al., *Coronary microvascular obstruction in acute myocardial infarction.* Eur Heart J, 2016. **37**(13): p. 1024-33.
42. Thackeray, J.T., et al., *Molecular Imaging of the Chemokine Receptor CXCR4 After Acute Myocardial Infarction.* JACC Cardiovasc Imaging, 2015. **8**(12): p. 1417-1426.
43. Bulluck, H., et al., *Cardiovascular Magnetic Resonance in Acute ST-Segment-Elevation Myocardial Infarction: Recent Advances, Controversies, and Future Directions.* Circulation, 2018. **137**(18): p. 1949-1964.

44. Fearon, W.F. and Y. Kobayashi, *Invasive Assessment of the Coronary Microvasculature: The Index of Microcirculatory Resistance.* Circ Cardiovasc Interv, 2017. **10**(12).
45. Sambuceti, G., A. L'Abbate, and M. Marzilli, *Why should we study the coronary microcirculation?* Am J Physiol Heart Circ Physiol, 2000. **279**(6): p. H2581-4.
46. Pries, A.R. and B. Reglin, *Coronary microcirculatory pathophysiology: can we afford it to remain a black box?* Eur Heart J, 2017. **38**(7): p. 478-488.
47. Mehta, D. and A.B. Malik, *Signaling mechanisms regulating endothelial permeability.* Physiol Rev, 2006. **86**(1): p. 279-367.
48. Kolettis, T.M., et al., *Endothelin in coronary artery disease and myocardial infarction.* Cardiol Rev, 2013. **21**(5): p. 249-56.
49. Xu, Y., et al., *Activated platelets contribute importantly to myocardial reperfusion injury.* Am J Physiol Heart Circ Physiol, 2006. **290**(2): p. H692-9.
50. Granger, D.N. and P.R. Kvietys, *Reperfusion injury and reactive oxygen species: The evolution of a concept.* Redox Biol, 2015. **6**: p. 524-551.
51. Lucchesi, B.R., *Myocardial ischemia, reperfusion and free radical injury.* Am J Cardiol, 1990. **65**(19): p. 14I-23I.
52. Camara, A.K., E.J. Lesnefsky, and D.F. Stowe, *Potential therapeutic benefits of strategies directed to mitochondria.* Antioxid Redox Signal, 2010. **13**(3): p. 279-347.
53. Jiang, F., Y. Zhang, and G.J. Dusting, *NADPH oxidase-mediated redox signaling: roles in cellular stress response, stress tolerance, and tissue repair.* Pharmacol Rev, 2011. **63**(1): p. 218-42.
54. Tiefenbacher, C.P., et al., *Restoration of endothelium-dependent vasodilation after reperfusion injury by tetrahydrobiopterin.* Circulation, 1996. **94**(6): p. 1423-9.
55. Zhang, C., et al., *Direct relationship between levels of TNF-alpha expression and endothelial dysfunction in reperfusion injury.* Basic Res Cardiol, 2010. **105**(4): p. 453-64.
56. Masano, T., et al., *Beneficial effects of exogenous tetrahydrobiopterin on left ventricular remodeling after myocardial infarction in rats: the possible role of oxidative stress caused by uncoupled endothelial nitric oxide synthase.* Circ J, 2008. **72**(9): p. 1512-9.
57. Seshadri, G., et al., *The delivery of superoxide dismutase encapsulated in polyketal microparticles to rat myocardium and protection from myocardial ischemia-reperfusion injury.* Biomaterials, 2010. **31**(6): p. 1372-9.
58. Pell, V.R., et al., *Moving Forwards by Blocking Back-Flow: The Yin and Yang of MI Therapy.* Circ Res, 2016. **118**(5): p. 898-906.
59. Ramos, C., et al., *Effects of a novel ascorbate-based protocol on infarct size and ventricle function in acute myocardial infarction patients undergoing percutaneous coronary angioplasty.* Arch Med Sci, 2017. **13**(3): p. 558-567.
60. Tsujita, K., et al., *Long-term efficacy of edaravone in patients with acute myocardial infarction.* Circ J, 2006. **70**(7): p. 832-7.
61. Oyewole, A.O. and M.A. Birch-Machin, *Mitochondria-targeted antioxidants.* FASEB J, 2015. **29**(12): p. 4766-71.
62. Rodrigues, S.F. and D.N. Granger, *Role of blood cells in ischaemia-reperfusion induced endothelial barrier failure.* Cardiovasc Res, 2010. **87**(2): p. 291-9.
63. Barrabes, J.A., et al., *Antagonism of P2Y12 or GPIIb/IIIa receptors reduces platelet-mediated myocardial injury after ischaemia and reperfusion in isolated rat hearts.* Thromb Haemost, 2010. **104**(1): p. 128-35.
64. Lam, F.W., K.V. Vijayan, and R.E. Rumbaut, *Platelets and Their Interactions with Other Immune Cells.* Compr Physiol, 2015. **5**(3): p. 1265-80.
65. Husain, S., et al., *Aspirin improves endothelial dysfunction in atherosclerosis.* Circulation, 1998. **97**(8): p. 716-20.
66. Massberg, S., et al., *Fibrinogen deposition at the postischemic vessel wall promotes platelet adhesion during ischemia-reperfusion in vivo.* Blood, 1999. **94**(11): p. 3829-38.

67. Ziegler, M., et al., *Highly Sensitive Detection of Minimal Cardiac Ischemia using Positron Emission Tomography Imaging of Activated Platelets.* Sci Rep, 2016. **6**: p. 38161.
68. Ziegler, M., X. Wang, and K. Peter, *Platelets in cardiac ischaemia/reperfusion injury: a promising therapeutic target.* Cardiovasc Res, 2019. **115**(7): p. 1178-1188.
69. Liu, Y., et al., *Novel role of platelets in mediating inflammatory responses and ventricular rupture or remodeling following myocardial infarction.* Arterioscler Thromb Vasc Biol, 2011. **31**(4): p. 834-41.
70. Kohler, D., et al., *Phosphorylation of vasodilator-stimulated phosphoprotein prevents platelet-neutrophil complex formation and dampens myocardial ischemia-reperfusion injury.* Circulation, 2011. **123**(22): p. 2579-90.
71. Ziegler, M., et al., *Platelet-Targeted Delivery of Peripheral Blood Mononuclear Cells to the Ischemic Heart Restores Cardiac Function after Ischemia-Reperfusion Injury.* Theranostics, 2017. **7**(13): p. 3192-3206.
72. Ziegler, M., et al., *The pulmonary microvasculature entraps induced vascular progenitor cells (iVPCs) systemically delivered after cardiac ischemia-reperfusion injury: Indication for preservation of heart function via paracrine effects beyond engraftment.* Microcirculation, 2019. **26**(2): p. e12493.
73. Courties, G., et al., *In vivo silencing of the transcription factor IRF5 reprograms the macrophage phenotype and improves infarct healing.* J Am Coll Cardiol, 2014. **63**(15): p. 1556-66.
74. Arai, M., et al., *An anti-CD18 antibody limits infarct size and preserves left ventricular function in dogs with ischemia and 48-hour reperfusion.* J Am Coll Cardiol, 1996. **27**(5): p. 1278-85.
75. Nourshargh, S. and R. Alon, *Leukocyte migration into inflamed tissues.* Immunity, 2014. **41**(5): p. 694-707.
76. Liu, J., H. Wang, and J. Li, *Inflammation and Inflammatory Cells in Myocardial Infarction and Reperfusion Injury: A Double-Edged Sword.* Clin Med Insights Cardiol, 2016. **10**: p. 79-84.
77. Ong, S.B., et al., *Inflammation following acute myocardial infarction: Multiple players, dynamic roles, and novel therapeutic opportunities.* Pharmacol Ther, 2018. **186**: p. 73-87.
78. Arslan, F., et al., *Myocardial ischemia/reperfusion injury is mediated by leukocytic toll-like receptor-2 and reduced by systemic administration of a novel anti-toll-like receptor-2 antibody.* Circulation, 2010. **121**(1): p. 80-90.
79. Latz, E., T.S. Xiao, and A. Stutz, *Activation and regulation of the inflammasomes.* Nat Rev Immunol, 2013. **13**(6): p. 397-411.
80. Martinon, F., K. Burns, and J. Tschopp, *The inflammasome: a molecular platform triggering activation of inflammatory caspases and processing of proIL-beta.* Mol Cell, 2002. **10**(2): p. 417-26.
81. Takahashi, M., *NLRP3 in myocardial ischaemia-reperfusion injury: inflammasome-dependent or -independent role in different cell types.* Cardiovasc Res, 2013. **99**(1): p. 4-5.
82. Sims, J.E. and D.E. Smith, *The IL-1 family: regulators of immunity.* Nat Rev Immunol, 2010. **10**(2): p. 89-102.
83. Suzuki, K., et al., *Overexpression of interleukin-1 receptor antagonist provides cardioprotection against ischemia-reperfusion injury associated with reduction in apoptosis.* Circulation, 2001. **104**(12 Suppl 1): p. I308-I3.
84. Mauro, A.G., et al., *Reduction of Myocardial Ischemia-Reperfusion Injury by Inhibiting Interleukin-1 Alpha.* J Cardiovasc Pharmacol, 2017. **69**(3): p. 156-160.
85. Abbate, A., et al., *Effects of interleukin-1 blockade with anakinra on adverse cardiac remodeling and heart failure after acute myocardial infarction [from the Virginia Commonwealth University-Anakinra Remodeling Trial (2) (VCU-ART2) pilot study].* Am J Cardiol, 2013. **111**(10): p. 1394-400.
86. Ridker, P.M., et al., *Antiinflammatory Therapy with Canakinumab for Atherosclerotic Disease.* N Engl J Med, 2017. **377**(12): p. 1119-1131.

87. Ridker, P.M., et al., *Relationship of C-reactive protein reduction to cardiovascular event reduction following treatment with canakinumab: a secondary analysis from the CANTOS randomised controlled trial.* Lancet, 2018. **391**(10118): p. 319-328.
88. Akdis, M., et al., *Interleukins, from 1 to 37, and interferon-gamma: receptors, functions, and roles in diseases.* J Allergy Clin Immunol, 2011. **127**(3): p. 701-21 e1-70.
89. Ridker, P.M., *From C-Reactive Protein to Interleukin-6 to Interleukin-1: Moving Upstream To Identify Novel Targets for Atheroprotection.* Circ Res, 2016. **118**(1): p. 145-56.
90. Gresnigt, M.S. and F.L. van de Veerdonk, *Biology of IL-36 cytokines and their role in disease.* Semin Immunol, 2013. **25**(6): p. 458-65.
91. Gabay, C. and J.E. Towne, *Regulation and function of interleukin-36 cytokines in homeostasis and pathological conditions.* J Leukoc Biol, 2015. **97**(4): p. 645-52.
92. Ainscough, J.S., et al., *Cathepsin S is the major activator of the psoriasis-associated proinflammatory cytokine IL-36gamma.* Proc Natl Acad Sci U S A, 2017. **114**(13): p. E2748-E2757.
93. Hahn, M., S. Frey, and A.J. Hueber, *The novel interleukin-1 cytokine family members in inflammatory diseases.* Curr Opin Rheumatol, 2017. **29**(2): p. 208-213.
94. Johnston, A., et al., *IL-1 and IL-36 are dominant cytokines in generalized pustular psoriasis.* J Allergy Clin Immunol, 2017. **140**(1): p. 109-120.
95. Bachmann, M., et al., *IL-36gamma/IL-1F9, an innate T-bet target in myeloid cells.* J Biol Chem, 2012. **287**(50): p. 41684-96.
96. Bozoyan, L., et al., *Interleukin-36gamma is expressed by neutrophils and can activate microglia, but has no role in experimental autoimmune encephalomyelitis.* J Neuroinflammation, 2015. **12**: p. 173.
97. Kovach, M.A., et al., *IL-36gamma is secreted in microparticles and exosomes by lung macrophages in response to bacteria and bacterial components.* J Leukoc Biol, 2016. **100**(2): p. 413-21.
98. Martin, U., et al., *Externalization of the leaderless cytokine IL-1F6 occurs in response to lipopolysaccharide/ATP activation of transduced bone marrow macrophages.* J Immunol, 2009. **183**(6): p. 4021-30.
99. Carrier, Y., et al., *Inter-regulation of Th17 cytokines and the IL-36 cytokines in vitro and in vivo: implications in psoriasis pathogenesis.* J Invest Dermatol, 2011. **131**(12): p. 2428-37.
100. Ding, L., et al., *IL-36 cytokines in autoimmunity and inflammatory disease.* Oncotarget, 2018. **9**(2): p. 2895-2901.
101. Sims, J.E., et al., *A new nomenclature for IL-1-family genes.* Trends Immunol, 2001. **22**(10): p. 536-7.
102. Henry, C.M., et al., *Neutrophil-Derived Proteases Escalate Inflammation through Activation of IL-36 Family Cytokines.* Cell Rep, 2016. **14**(4): p. 708-722.
103. Vigne, S., et al., *IL-36R ligands are potent regulators of dendritic and T cells.* Blood, 2011. **118**(22): p. 5813-23.
104. Scheibe, K., et al., *Inhibiting Interleukin 36 Receptor Signaling Reduces Fibrosis in Mice With Chronic Intestinal Inflammation.* Gastroenterology, 2019. **156**(4): p. 1082-1097 e11.
105. Ley, K., et al., *Getting to the site of inflammation: the leukocyte adhesion cascade updated.* Nat Rev Immunol, 2007. **7**(9): p. 678-89.
106. Muller, W.A., *Getting leukocytes to the site of inflammation.* Vet Pathol, 2013. **50**(1): p. 7-22.
107. Mitroulis, I., et al., *Leukocyte integrins: role in leukocyte recruitment and as therapeutic targets in inflammatory disease.* Pharmacol Ther, 2015. **147**: p. 123-135.
108. Burke, J., et al., *Hepatic ischemia-reperfusion injury causes E-selectin upregulation.* Transplant Proc, 1998. **30**(5): p. 2321-3.
109. McEver, R.P. and R.D. Cummings, *Role of PSGL-1 binding to selectins in leukocyte recruitment.* J Clin Invest, 1997. **100**(11 Suppl): p. S97-103.

110. Silva, M., P.A. Videira, and R. Sackstein, *E-Selectin Ligands in the Human Mononuclear Phagocyte System: Implications for Infection, Inflammation, and Immunotherapy.* Front Immunol, 2017. **8**: p. 1878.
111. Picker, L.J., et al., *The neutrophil selectin LECAM-1 presents carbohydrate ligands to the vascular selectins ELAM-1 and GMP-140.* Cell, 1991. **66**(5): p. 921-33.
112. Sperandio, M., et al., *P-selectin glycoprotein ligand-1 mediates L-selectin-dependent leukocyte rolling in venules.* J Exp Med, 2003. **197**(10): p. 1355-63.
113. Seftor, R.E., *Role of the beta3 integrin subunit in human primary melanoma progression: multifunctional activities associated with alpha(v)beta3 integrin expression.* Am J Pathol, 1998. **153**(5): p. 1347-51.
114. Hynes, R.O., *Integrins: versatility, modulation, and signaling in cell adhesion.* Cell, 1992. **69**(1): p. 11-25.
115. Lefer, D.J., et al., *A novel sialyl LewisX analog attenuates neutrophil accumulation and myocardial necrosis after ischemia and reperfusion.* Circulation, 1994. **90**(5): p. 2390-401.
116. Weyrich, A.S., et al., *In vivo neutralization of P-selectin protects feline heart and endothelium in myocardial ischemia and reperfusion injury.* J Clin Invest, 1993. **91**(6): p. 2620-9.
117. Deshmane, S.L., et al., *Monocyte chemoattractant protein-1 (MCP-1): an overview.* J Interferon Cytokine Res, 2009. **29**(6): p. 313-26.
118. Girbl, T., et al., *Distinct Compartmentalization of the Chemokines CXCL1 and CXCL2 and the Atypical Receptor ACKR1 Determine Discrete Stages of Neutrophil Diapedesis.* Immunity, 2018. **49**(6): p. 1062-1076 e6.
119. Eniola, A.O., P.J. Willcox, and D.A. Hammer, *Interplay between rolling and firm adhesion elucidated with a cell-free system engineered with two distinct receptor-ligand pairs.* Biophys J, 2003. **85**(4): p. 2720-31.
120. Metzler, B., et al., *Myocardial ischaemia-reperfusion injury in haematopoietic cell-restricted beta1 integrin knockout mice.* Exp Physiol, 2008. **93**(7): p. 825-33.
121. Nandi, A., P. Estess, and M. Siegelman, *Bimolecular complex between rolling and firm adhesion receptors required for cell arrest; CD44 association with VLA-4 in T cell extravasation.* Immunity, 2004. **20**(4): p. 455-65.
122. Zhuo, L., et al., *SHAP potentiates the CD44-mediated leukocyte adhesion to the hyaluronan substratum.* J Biol Chem, 2006. **281**(29): p. 20303-14.
123. Carman, C.V. and T.A. Springer, *Trans-cellular migration: cell-cell contacts get intimate.* Curr Opin Cell Biol, 2008. **20**(5): p. 533-40.
124. Shaw, S.K., et al., *Coordinated redistribution of leukocyte LFA-1 and endothelial cell ICAM-1 accompany neutrophil transmigration.* J Exp Med, 2004. **200**(12): p. 1571-80.
125. Dejana, E., *Endothelial cell-cell junctions: happy together.* Nat Rev Mol Cell Biol, 2004. **5**(4): p. 261-70.
126. Corada, M., et al., *Junctional adhesion molecule-A-deficient polymorphonuclear cells show reduced diapedesis in peritonitis and heart ischemia-reperfusion injury.* Proc Natl Acad Sci U S A, 2005. **102**(30): p. 10634-9.
127. Mamdouh, Z., G.E. Kreitzer, and W.A. Muller, *Leukocyte transmigration requires kinesin-mediated microtubule-dependent membrane trafficking from the lateral border recycling compartment.* J Exp Med, 2008. **205**(4): p. 951-66.
128. Wang, S., et al., *PECAM-1, alpha6 integrins and neutrophil elastase cooperate in mediating neutrophil transmigration.* J Cell Sci, 2005. **118**(Pt 9): p. 2067-76.
129. Verbeek, M.M., et al., *T lymphocyte adhesion to human brain pericytes is mediated via very late antigen-4/vascular cell adhesion molecule-1 interactions.* J Immunol, 1995. **154**(11): p. 5876-84.
130. Coito, A.J., *Leukocyte transmigration across endothelial and extracellular matrix protein barriers in liver ischemia/reperfusion injury.* Curr Opin Organ Transplant, 2011. **16**(1): p. 34-40.

131. Wang, S., et al., *Venular basement membranes contain specific matrix protein low expression regions that act as exit points for emigrating neutrophils.* J Exp Med, 2006. **203**(6): p. 1519-32.
132. Chandrasekar, B., J.B. Smith, and G.L. Freeman, *Ischemia-reperfusion of rat myocardium activates nuclear factor-KappaB and induces neutrophil infiltration via lipopolysaccharide-induced CXC chemokine.* Circulation, 2001. **103**(18): p. 2296-302.
133. Dewald, O., et al., *CCL2/Monocyte Chemoattractant Protein-1 regulates inflammatory responses critical to healing myocardial infarcts.* Circ Res, 2005. **96**(8): p. 881-9.
134. Hoshida, S., et al., *Attenuation of neutrophil function by inhibitors of arachidonate metabolism reduces the extent of canine myocardial infarction.* Am J Cardiol, 1989. **63**(10): p. 24E-28E.
135. Swirski, F.K., et al., *Identification of splenic reservoir monocytes and their deployment to inflammatory sites.* Science, 2009. **325**(5940): p. 612-6.
136. Puhl, S.L. and S. Steffens, *Neutrophils in Post-myocardial Infarction Inflammation: Damage vs. Resolution?* Front Cardiovasc Med, 2019. **6**: p. 25.
137. Slegtenhorst, B.R., et al., *Ischemia/reperfusion Injury and its Consequences on Immunity and Inflammation.* Curr Transplant Rep, 2014. **1**(3): p. 147-154.
138. Koeth, R.A., V. Haselden, and W.H. Tang, *Myeloperoxidase in cardiovascular disease.* Adv Clin Chem, 2013. **62**: p. 1-32.
139. Kolaczkowska, E. and P. Kubes, *Neutrophil recruitment and function in health and inflammation.* Nat Rev Immunol, 2013. **13**(3): p. 159-75.
140. Ge, L., et al., *Neutrophil extracellular traps in ischemia-reperfusion injury-induced myocardial no-reflow: therapeutic potential of DNase-based reperfusion strategy.* Am J Physiol Heart Circ Physiol, 2015. **308**(5): p. H500-9.
141. Frangogiannis, N.G., *Regulation of the inflammatory response in cardiac repair.* Circ Res, 2012. **110**(1): p. 159-73.
142. Rios-Navarro, C., et al., *Characterization and implications of the dynamics of eosinophils in blood and in the infarcted myocardium after coronary reperfusion.* PLoS One, 2018. **13**(10): p. e0206344.
143. Dutta, P. and M. Nahrendorf, *Monocytes in myocardial infarction.* Arterioscler Thromb Vasc Biol, 2015. **35**(5): p. 1066-70.
144. Nahrendorf, M. and F.K. Swirski, *Abandoning M1/M2 for a Network Model of Macrophage Function.* Circ Res, 2016. **119**(3): p. 414-7.
145. Martinez, F.O. and S. Gordon, *The M1 and M2 paradigm of macrophage activation: time for reassessment.* F1000Prime Rep, 2014. **6**: p. 13.
146. Frangogiannis, N.G., *The inflammatory response in myocardial injury, repair, and remodelling.* Nat Rev Cardiol, 2014. **11**(5): p. 255-65.
147. Sager, H.B., T. Kessler, and H. Schunkert, *Monocytes and macrophages in cardiac injury and repair.* J Thorac Dis, 2017. **9**(Suppl 1): p. S30-S35.
148. Barzegar, M., et al., *Potential therapeutic roles of stem cells in ischemia-reperfusion injury.* Stem Cell Res, 2019. **37**: p. 101421.
149. Madigan, M. and R. Atoui, *Therapeutic Use of Stem Cells for Myocardial Infarction.* Bioengineering (Basel), 2018. **5**(2).
150. Kavanagh, D.P., et al., *Mechanisms of adhesion and subsequent actions of a haematopoietic stem cell line, HPC-7, in the injured murine intestinal microcirculation in vivo.* PLoS One, 2013. **8**(3): p. e59150.
151. White, R.L., et al., *Modulating the Adhesion of Haematopoietic Stem Cells with Chemokines to Enhance Their Recruitment to the Ischaemically Injured Murine Kidney.* PLoS One, 2013. **8**(6): p. e66489.
152. Fitzsimmons, R.E.B., et al., *Mesenchymal Stromal/Stem Cells in Regenerative Medicine and Tissue Engineering.* Stem Cells Int, 2018. **2018**: p. 8031718.

153. Bertrand, J.Y., et al., *Hematopoietic stem cell development during mouse embryogenesis.* Methods Mol Med, 2005. **105**: p. 273-88.
154. Mangel, M. and M.B. Bonsall, *Stem cell biology is population biology: differentiation of hematopoietic multipotent progenitors to common lymphoid and myeloid progenitors.* Theor Biol Med Model, 2013. **10**: p. 5.
155. Kopp, H.G., et al., *The bone marrow vascular niche: home of HSC differentiation and mobilization.* Physiology (Bethesda), 2005. **20**: p. 349-56.
156. Bijkerk, R., et al., *Hematopoietic microRNA-126 protects against renal ischemia/reperfusion injury by promoting vascular integrity.* J Am Soc Nephrol, 2014. **25**(8): p. 1710-22.
157. Li, B., et al., *Mobilized human hematopoietic stem/progenitor cells promote kidney repair after ischemia/reperfusion injury.* Circulation, 2010. **121**(20): p. 2211-20.
158. Magnusson, M., et al., *Expansion on stromal cells preserves the undifferentiated state of human hematopoietic stem cells despite compromised reconstitution ability.* PLoS One, 2013. **8**(1): p. e53912.
159. Bieback, K. and I. Brinkmann, *Mesenchymal stromal cells from human perinatal tissues: From biology to cell therapy.* World J Stem Cells, 2010. **2**(4): p. 81-92.
160. Singh, A., A. Singh, and D. Sen, *Mesenchymal stem cells in cardiac regeneration: a detailed progress report of the last 6 years (2010-2015).* Stem Cell Res Ther, 2016. **7**(1): p. 82.
161. Amado, L.C., et al., *Multimodality noninvasive imaging demonstrates in vivo cardiac regeneration after mesenchymal stem cell therapy.* J Am Coll Cardiol, 2006. **48**(10): p. 2116-24.
162. Zhang, W., et al., *Wharton's jelly-derived mesenchymal stem cells promote myocardial regeneration and cardiac repair after miniswine acute myocardial infarction.* Coron Artery Dis, 2013. **24**(7): p. 549-58.
163. Gavins, F.N. and B.E. Chatterjee, *Intravital microscopy for the study of mouse microcirculation in anti-inflammatory drug research: focus on the mesentery and cremaster preparations.* J Pharmacol Toxicol Methods, 2004. **49**(1): p. 1-14.
164. Kozhura, V.L., et al., *Reperfusion injury after critical intestinal ischemia and its correction with perfluorochemical emulsion "perftoran".* World J Gastroenterol, 2005. **11**(45): p. 7084-90.
165. Yago, T., et al., *Blocking neutrophil integrin activation prevents ischemia-reperfusion injury.* J Exp Med, 2015. **212**(8): p. 1267-81.
166. Vinegoni, C., et al., *Imaging the beating heart in the mouse using intravital microscopy techniques.* Nat Protoc, 2015. **10**(11): p. 1802-19.
167. Weigert, R., et al., *Intravital microscopy: a novel tool to study cell biology in living animals.* Histochem Cell Biol, 2010. **133**(5): p. 481-91.
168. Langley, R.R., et al., *Tissue-specific microvascular endothelial cell lines from H-2K(b)-tsA58 mice for studies of angiogenesis and metastasis.* Cancer Res, 2003. **63**(11): p. 2971-6.
169. Pinto do, O.P., A. Kolterud, and L. Carlsson, *Expression of the LIM-homeobox gene LH2 generates immortalized steel factor-dependent multipotent hematopoietic precursors.* EMBO J, 1998. **17**(19): p. 5744-56.
170. Kavanagh, D.P., et al., *Haematopoietic stem cell recruitment to injured murine liver sinusoids depends on (alpha)4(beta)1 integrin/VCAM-1 interactions.* Gut, 2010. **59**(1): p. 79-87.
171. Houlihan, D.D., et al., *Isolation of mouse mesenchymal stem cells on the basis of expression of Sca-1 and PDGFR-alpha.* Nat Protoc, 2012. **7**(12): p. 2103-11.
172. Kavanagh, D.P., et al., *Pretreatment of Mesenchymal Stem Cells Manipulates Their Vasculoprotective Potential While Not Altering Their Homing Within the Injured Gut.* Stem Cells, 2015. **33**(9): p. 2785-97.
173. Prasanna, S.J., et al., *Pro-inflammatory cytokines, IFNgamma and TNFalpha, influence immune properties of human bone marrow and Wharton jelly mesenchymal stem cells differentially.* PLoS One, 2010. **5**(2): p. e9016.

174. Munir, H., et al., *Analyzing the effects of stromal cells on the recruitment of leukocytes from flow.* J Vis Exp, 2015(95): p. e52480.
175. Dumitriu, I.E., et al., *5,6-carboxyfluorescein diacetate succinimidyl ester-labeled apoptotic and necrotic as well as detergent-treated cells can be traced in composite cell samples.* Anal Biochem, 2001. **299**(2): p. 247-52.
176. Song, G., et al., *[Promoting effect of Fasudil on the proliferation and survival of bone marrow-derived neural stem cells in vitro].* Xi Bao Yu Fen Zi Mian Yi Xue Za Zhi, 2015. **31**(11): p. 1488-91, 1496.
177. Lee, S., et al., *Real-time in vivo imaging of the beating mouse heart at microscopic resolution.* Nat Commun, 2012. **3**: p. 1054.
178. Wang, J., et al., *Visualizing the function and fate of neutrophils in sterile injury and repair.* Science, 2017. **358**(6359): p. 111-116.
179. Haka, A.S., et al., *Quantitative analysis of monocyte subpopulations in murine atherosclerotic plaques by multiphoton microscopy.* PLoS One, 2012. **7**(9): p. e44823.
180. Konopatskaya, O., et al., *PKCalpha regulates platelet granule secretion and thrombus formation in mice.* J Clin Invest, 2009. **119**(2): p. 399-407.
181. Kalia, N., et al., *Effects of hypothermia and rewarming on the mucosal villus microcirculation and survival after rat intestinal ischemia-reperfusion injury.* Ann Surg, 2002. **236**(1): p. 67-74.
182. Wang, J. and P. Kubes, *A Reservoir of Mature Cavity Macrophages that Can Rapidly Invade Visceral Organs to Affect Tissue Repair.* Cell, 2016. **165**(3): p. 668-78.
183. Redfors, B., Y. Shao, and E. Omerovic, *Myocardial infarct size and area at risk assessment in mice.* Exp Clin Cardiol, 2012. **17**(4): p. 268-72.
184. Liu, J.H., et al., *Baicalein significantly protects human retinal pigment epithelium cells against H(2)O(2)-induced oxidative stress by scavenging reactive oxygen species and downregulating the expression of matrix metalloproteinase-9 and vascular endothelial growth factor.* J Ocul Pharmacol Ther, 2010. **26**(5): p. 421-9.
185. Watkins, D.J., et al., *Synergistic effects of HB-EGF and mesenchymal stem cells in a murine model of intestinal ischemia/reperfusion injury.* J Pediatr Surg, 2013. **48**(6): p. 1323-9.
186. Sadek, E.M., et al., *Histological study on effect of mesenchymal stem cell therapy on experimental renal injury induced by ischemia/reperfusion in male albino rat.* Int J Stem Cells, 2013. **6**(1): p. 55-66.
187. Broughton, B.R., et al., *Post-stroke inflammation and the potential efficacy of novel stem cell therapies: focus on amnion epithelial cells.* Front Cell Neurosci, 2012. **6**: p. 66.
188. Henninger, D.D., et al., *Cytokine-induced VCAM-1 and ICAM-1 expression in different organs of the mouse.* J Immunol, 1997. **158**(4): p. 1825-32.
189. Mazo, I.B., et al., *Hematopoietic progenitor cell rolling in bone marrow microvessels: parallel contributions by endothelial selectins and vascular cell adhesion molecule 1.* J Exp Med, 1998. **188**(3): p. 465-74.
190. Bowden, R.A., et al., *Role of alpha4 integrin and VCAM-1 in CD18-independent neutrophil migration across mouse cardiac endothelium.* Circ Res, 2002. **90**(5): p. 562-9.
191. Jaakkola, K., et al., *Vascular adhesion protein-1, intercellular adhesion molecule-1 and P-selectin mediate leukocyte binding to ischemic heart in humans.* J Am Coll Cardiol, 2000. **36**(1): p. 122-9.
192. Raha, S., et al., *Superoxides from mitochondrial complex III: the role of manganese superoxide dismutase.* Free Radic Biol Med, 2000. **29**(2): p. 170-80.
193. Inafuku, H., et al., *Determination of oxidative stress and cardiac dysfunction after ischemia/reperfusion injury in isolated rat hearts.* Ann Thorac Cardiovasc Surg, 2013. **19**(3): p. 186-94.

194. Hu, T., et al., *Synergistic cardioprotective effects of Danshensu and hydroxysafflor yellow A against myocardial ischemia-reperfusion injury are mediated through the Akt/Nrf2/HO-1 pathway.* Int J Mol Med, 2016. **38**(1): p. 83-94.
195. Kavanagh, D.P., et al., *Enhancing the adhesion of hematopoietic precursor cell integrins with hydrogen peroxide increases recruitment within murine gut.* Cell Transplant, 2013. **22**(8): p. 1485-99.
196. Frenette, P.S., et al., *Endothelial selectins and vascular cell adhesion molecule-1 promote hematopoietic progenitor homing to bone marrow.* Proc Natl Acad Sci U S A, 1998. **95**(24): p. 14423-8.
197. Peled, A., et al., *The chemokine SDF-1 activates the integrins LFA-1, VLA-4, and VLA-5 on immature human CD34(+) cells: role in transendothelial/stromal migration and engraftment of NOD/SCID mice.* Blood, 2000. **95**(11): p. 3289-96.
198. Grassinger, J., et al., *Thrombin-cleaved osteopontin regulates hemopoietic stem and progenitor cell functions through interactions with alpha9beta1 and alpha4beta1 integrins.* Blood, 2009. **114**(1): p. 49-59.
199. Huygen, S., et al., *Adhesion of synchronized human hematopoietic progenitor cells to fibronectin and vascular cell adhesion molecule-1 fluctuates reversibly during cell cycle transit in ex vivo culture.* Blood, 2002. **100**(8): p. 2744-52.
200. Cook-Mills, J.M., M.E. Marchese, and H. Abdala-Valencia, *Vascular cell adhesion molecule-1 expression and signaling during disease: regulation by reactive oxygen species and antioxidants.* Antioxid Redox Signal, 2011. **15**(6): p. 1607-38.
201. Fukuda, M., *Cell Surface Carbohydrates and Cell Development*. 1991: CRC Press. 352.
202. Nakamura, S., et al., *Bmi1 confers resistance to oxidative stress on hematopoietic stem cells.* PLoS One, 2012. **7**(5): p. e36209.
203. Valle-Prieto, A. and P.A. Conget, *Human mesenchymal stem cells efficiently manage oxidative stress.* Stem Cells Dev, 2010. **19**(12): p. 1885-93.
204. Kim, Y., et al., *Antioxidant and anti-inflammatory effects of intravenously injected adipose derived mesenchymal stem cells in dogs with acute spinal cord injury.* Stem Cell Res Ther, 2015. **6**: p. 229.
205. Hu, L., et al., *Reactive Oxygen Species and Nrf2: Functional and Transcriptional Regulators of Hematopoiesis.* Oxid Med Cell Longev, 2019. **2019**: p. 5153268.
206. Rodrigues-Moreira, S., et al., *Low-Dose Irradiation Promotes Persistent Oxidative Stress and Decreases Self-Renewal in Hematopoietic Stem Cells.* Cell Rep, 2017. **20**(13): p. 3199-3211.
207. Ruster, B., et al., *Mesenchymal stem cells display coordinated rolling and adhesion behavior on endothelial cells.* Blood, 2006. **108**(12): p. 3938-44.
208. Majumdar, M.K., et al., *Characterization and functionality of cell surface molecules on human mesenchymal stem cells.* J Biomed Sci, 2003. **10**(2): p. 228-41.
209. Hass, R., et al., *Different populations and sources of human mesenchymal stem cells (MSC): A comparison of adult and neonatal tissue-derived MSC.* Cell Commun Signal, 2011. **9**: p. 12.
210. Donders, R., et al., *Human Wharton's Jelly-Derived Stem Cells Display a Distinct Immunomodulatory and Proregenerative Transcriptional Signature Compared to Bone Marrow-Derived Stem Cells.* Stem Cells Dev, 2018. **27**(2): p. 65-84.
211. Jeong, S.G. and G.W. Cho, *Trichostatin A modulates intracellular reactive oxygen species through SOD2 and FOXO1 in human bone marrow-mesenchymal stem cells.* Cell Biochem Funct, 2015. **33**(1): p. 37-43.
212. Munir, H., et al., *Comparative Ability of Mesenchymal Stromal Cells from Different Tissues to Limit Neutrophil Recruitment to Inflamed Endothelium.* PLoS One, 2016. **11**(5): p. e0155161.
213. Fischer, U.M., et al., *Pulmonary passage is a major obstacle for intravenous stem cell delivery: the pulmonary first-pass effect.* Stem Cells Dev, 2009. **18**(5): p. 683-92.

214. Kraitchman, D.L., et al., *Dynamic imaging of allogeneic mesenchymal stem cells trafficking to myocardial infarction.* Circulation, 2005. **112**(10): p. 1451-61.
215. Dooner, M., et al., *Homing and conversion of murine hematopoietic stem cells to lung.* Blood Cells Mol Dis, 2004. **32**(1): p. 47-51.
216. Brenner, W., et al., *111In-labeled CD34+ hematopoietic progenitor cells in a rat myocardial infarction model.* J Nucl Med, 2004. **45**(3): p. 512-8.
217. Martini, J. and C.R. Honig, *Direct measurement of intercapillary distance in beating rat heart in situ under various conditions of O 2 supply.* Microvasc Res, 1969. **1**(3): p. 244-56.
218. Li, W., et al., *Intravital 2-photon imaging of leukocyte trafficking in beating heart.* J Clin Invest, 2012. **122**(7): p. 2499-508.
219. Matsuura, R., et al., *Intravital imaging with two-photon microscopy reveals cellular dynamics in the ischeamia-reperfused rat heart.* Sci Rep, 2018. **8**(1): p. 15991.
220. Bienvenu, L.A., X. Wang, and K. Peter, *Prime time viewing of the ischaemic heart: new technologies allow imaging and flow assessment of the microvasculature in the beating heart.* Cardiovasc Res, 2019. **115**(13): p. 1817-1819.
221. Kavanagh, D.P.J. and N. Kalia, *Live Intravital Imaging of Cellular Trafficking in the Cardiac Microvasculature-Beating the Odds.* Front Immunol, 2019. **10**: p. 2782.
222. Olivecrona, G.K., et al., *Coronary artery reperfusion: The ADP receptor P2Y(1) mediates early reactive hyperemia in vivo in pigs.* Purinergic Signal, 2004. **1**(1): p. 59-65.
223. Vassalli, G. and O.M. Hess, *Measurement of coronary flow reserve and its role in patient care.* Basic Res Cardiol, 1998. **93**(5): p. 339-53.
224. Ley, K., *Molecular mechanisms of leukocyte recruitment in the inflammatory process.* Cardiovasc Res, 1996. **32**(4): p. 733-42.
225. Gregg, D.E. and D.C. Sabiston, Jr., *Effect of cardiac contraction on coronary blood flow.* Circulation, 1957. **15**(1): p. 14-20.
226. Panerai, R.B., J.H. Chamberlain, and B.M. Sayers, *Characterization of the extravascular component of coronary resistance by instantaneous pressure-flow relationships in the dog.* Circ Res, 1979. **45**(3): p. 378-90.
227. Sabbah, H.N., et al., *Coronary extravascular compression influences systolic coronary blood flow.* Heart Vessels, 1986. **2**(3): p. 140-6.
228. Devi, S., et al., *Corrigendum: Multiphoton imaging reveals a new leukocyte recruitment paradigm in the glomerulus.* Nat Med, 2016. **22**(4): p. 446.
229. Harding, M.G., et al., *Neutrophil crawling in capillaries; a novel immune response to Staphylococcus aureus.* PLoS Pathog, 2014. **10**(10): p. e1004379.
230. Ziegler-Heitbrock, H.W., *The biology of the monocyte system.* Eur J Cell Biol, 1989. **49**(1): p. 1-12.
231. Nahrendorf, M., M.J. Pittet, and F.K. Swirski, *Monocytes: protagonists of infarct inflammation and repair after myocardial infarction.* Circulation, 2010. **121**(22): p. 2437-45.
232. Nahrendorf, M., et al., *The healing myocardium sequentially mobilizes two monocyte subsets with divergent and complementary functions.* J Exp Med, 2007. **204**(12): p. 3037-47.
233. Tacke, F., et al., *Immature monocytes acquire antigens from other cells in the bone marrow and present them to T cells after maturing in the periphery.* J Exp Med, 2006. **203**(3): p. 583-97.
234. Jung, K., et al., *Endoscopic time-lapse imaging of immune cells in infarcted mouse hearts.* Circ Res, 2013. **112**(6): p. 891-9.
235. Pachel, C., et al., *Inhibition of Platelet GPVI Protects Against Myocardial Ischemia-Reperfusion Injury.* Arterioscler Thromb Vasc Biol, 2016. **36**(4): p. 629-35.
236. Takaya, N., et al., *Platelets activated by collagen through the immunoreceptor tyrosine-based activation motif in the Fc receptor gamma-chain play a pivotal role in the development of myocardial ischemia-reperfusion injury.* J Mol Cell Cardiol, 2005. **39**(6): p. 856-64.

237. Bohl, S., et al., *Refined approach for quantification of in vivo ischemia-reperfusion injury in the mouse heart.* Am J Physiol Heart Circ Physiol, 2009. **297**(6): p. H2054-8.
238. Korf-Klingebiel, M., et al., *Bone marrow cells are a rich source of growth factors and cytokines: implications for cell therapy trials after myocardial infarction.* Eur Heart J, 2008. **29**(23): p. 2851-8.
239. Preda, M.B., et al., *Remote transplantation of mesenchymal stem cells protects the heart against ischemia-reperfusion injury.* Stem Cells, 2014. **32**(8): p. 2123-34.
240. Peng, X., et al., *Therapeutic effectiveness of bone marrow-derived mesenchymal stem cell administration against acute pulmonary thromboembolism in a mouse model.* Thromb Res, 2015. **135**(5): p. 990-9.
241. Iqbal, A.J., et al., *Human CD68 promoter GFP transgenic mice allow analysis of monocyte to macrophage differentiation in vivo.* Blood, 2014. **124**(15): p. e33-44.
242. Young, P.P. and R. Schafer, *Cell-based therapies for cardiac disease: a cellular therapist's perspective.* Transfusion, 2015. **55**(2): p. 441-51; quiz 440.
243. Pawitan, J.A., *Prospect of stem cell conditioned medium in regenerative medicine.* Biomed Res Int, 2014. **2014**: p. 965849.
244. Shi, C. and E.G. Pamer, *Monocyte recruitment during infection and inflammation.* Nat Rev Immunol, 2011. **11**(11): p. 762-74.
245. Ziegler-Heitbrock, L., *Blood Monocytes and Their Subsets: Established Features and Open Questions.* Front Immunol, 2015. **6**: p. 423.
246. Hofmann, M., et al., *Monitoring of bone marrow cell homing into the infarcted human myocardium.* Circulation, 2005. **111**(17): p. 2198-202.
247. Kotloff, R.M., V.N. Ahya, and S.W. Crawford, *Pulmonary complications of solid organ and hematopoietic stem cell transplantation.* Am J Respir Crit Care Med, 2004. **170**(1): p. 22-48.
248. Xing, L., et al., *Mesenchymal stem cells, not conditioned medium, contribute to kidney repair after ischemia-reperfusion injury.* Stem Cell Res Ther, 2014. **5**(4): p. 101.
249. Jian, Z., et al., *In Vivo Cannulation Methods for Cardiomyocytes Isolation from Heart Disease Models.* PLoS One, 2016. **11**(8): p. e0160605.
250. Banerjee, I., et al., *Determination of cell types and numbers during cardiac development in the neonatal and adult rat and mouse.* Am J Physiol Heart Circ Physiol, 2007. **293**(3): p. H1883-91.
251. Scarabelli, T., et al., *Apoptosis of endothelial cells precedes myocyte cell apoptosis in ischemia/reperfusion injury.* Circulation, 2001. **104**(3): p. 253-6.
252. Singhal, A.K., et al., *Role of Endothelial Cells in Myocardial Ischemia-Reperfusion Injury.* Vasc Dis Prev, 2010. **7**: p. 1-14.
253. Huang, R.B. and O. Eniola-Adefeso, *Shear stress modulation of IL-1beta-induced E-selectin expression in human endothelial cells.* PLoS One, 2012. **7**(2): p. e31874.
254. Sharma, H.S. and D.K. Das, *Role of cytokines in myocardial ischemia and reperfusion.* Mediators Inflamm, 1997. **6**(3): p. 175-83.
255. Saxena, A., et al., *Interleukin-10 paradox: A potent immunoregulatory cytokine that has been difficult to harness for immunotherapy.* Cytokine, 2015. **74**(1): p. 27-34.
256. Jung, M., et al., *IL-10 improves cardiac remodeling after myocardial infarction by stimulating M2 macrophage polarization and fibroblast activation.* Basic Res Cardiol, 2017. **112**(3): p. 33.
257. Krishnamurthy, P., et al., *IL-10 inhibits inflammation and attenuates left ventricular remodeling after myocardial infarction via activation of STAT3 and suppression of HuR.* Circ Res, 2009. **104**(2): p. e9-18.
258. Cai, Z.P., et al., *Remote ischemic preconditioning confers late protection against myocardial ischemia-reperfusion injury in mice by upregulating interleukin-10.* Basic Res Cardiol, 2012. **107**(4): p. 277.
259. Meng, X., et al., *Transplantation of mesenchymal stem cells overexpressing IL10 attenuates cardiac impairments in rats with myocardial infarction.* J Cell Physiol, 2018. **233**(1): p. 587-595.

260. Nakano, Y., et al., *Nanoparticle-Mediated Delivery of Irbesartan Induces Cardioprotection from Myocardial Ischemia-Reperfusion Injury by Antagonizing Monocyte-Mediated Inflammation.* Sci Rep, 2016. **6**: p. 29601.
261. Tacke, F., et al., *Monocyte subsets differentially employ CCR2, CCR5, and CX3CR1 to accumulate within atherosclerotic plaques.* J Clin Invest, 2007. **117**(1): p. 185-94.
262. Milora, K.A., et al., *Unprocessed Interleukin-36alpha Regulates Psoriasis-Like Skin Inflammation in Cooperation With Interleukin-1.* J Invest Dermatol, 2015. **135**(12): p. 2992-3000.
263. Foster, A.M., et al., *IL-36 promotes myeloid cell infiltration, activation, and inflammatory activity in skin.* J Immunol, 2014. **192**(12): p. 6053-61.
264. McMurray, J.J., et al., *ESC guidelines for the diagnosis and treatment of acute and chronic heart failure 2012: The Task Force for the Diagnosis and Treatment of Acute and Chronic Heart Failure 2012 of the European Society of Cardiology. Developed in collaboration with the Heart Failure Association (HFA) of the ESC.* Eur J Heart Fail, 2012. **14**(8): p. 803-69.
265. Li, T., et al., *Resveratrol alleviates hypoxia/reoxygenation injuryinduced mitochondrial oxidative stress in cardiomyocytes.* Mol Med Rep, 2019. **19**(4): p. 2774-2780.
266. Bartz, R.R., H.B. Suliman, and C.A. Piantadosi, *Redox mechanisms of cardiomyocyte mitochondrial protection.* Front Physiol, 2015. **6**: p. 291.
267. Kuligowski, M.P., A.R. Kitching, and M.J. Hickey, *Leukocyte recruitment to the inflamed glomerulus: a critical role for platelet-derived P-selectin in the absence of rolling.* J Immunol, 2006. **176**(11): p. 6991-9.
268. Thomas, G., et al., *Nonclassical patrolling monocyte function in the vasculature.* Arterioscler Thromb Vasc Biol, 2015. **35**(6): p. 1306-16.
269. Scapini, P. and M.A. Cassatella, *Location in the spleen dictates the function of murine neutrophils.* J Exp Med, 2017. **214**(5): p. 1207-1209.
270. Orlic, D., et al., *Bone marrow cells regenerate infarcted myocardium.* Nature, 2001. **410**(6829): p. 701-5.
271. Pinto do, O.P., K. Richter, and L. Carlsson, *Hematopoietic progenitor/stem cells immortalized by Lhx2 generate functional hematopoietic cells in vivo.* Blood, 2002. **99**(11): p. 3939-46.
272. Miao, W., et al., *Hematopoietic stem cell regeneration enhanced by ectopic expression of ROS-detoxifying enzymes in transplant mice.* Mol Ther, 2013. **21**(2): p. 423-32.
273. Akbar, N., et al., *Endothelium-derived extracellular vesicles promote splenic monocyte mobilization in myocardial infarction.* JCI Insight, 2017. **2**(17).
274. Schwarting, S., et al., *Hematopoietic stem cells reduce postischemic inflammation and ameliorate ischemic brain injury.* Stroke, 2008. **39**(10): p. 2867-75.
275. Ratajczak, M.Z., et al., *Pivotal role of paracrine effects in stem cell therapies in regenerative medicine: can we translate stem cell-secreted paracrine factors and microvesicles into better therapeutic strategies?* Leukemia, 2012. **26**(6): p. 1166-73.
276. Kucia, M., et al., *Cells expressing early cardiac markers reside in the bone marrow and are mobilized into the peripheral blood after myocardial infarction.* Circ Res, 2004. **95**(12): p. 1191-9.
277. Quevedo, H.C., et al., *Allogeneic mesenchymal stem cells restore cardiac function in chronic ischemic cardiomyopathy via trilineage differentiating capacity.* Proc Natl Acad Sci U S A, 2009. **106**(33): p. 14022-7.
278. Ren, G., et al., *Mesenchymal stem cell-mediated immunosuppression occurs via concerted action of chemokines and nitric oxide.* Cell Stem Cell, 2008. **2**(2): p. 141-50.
279. Abou-Saleh, H., et al., *Endothelial progenitor cells bind and inhibit platelet function and thrombus formation.* Circulation, 2009. **120**(22): p. 2230-9.

280. Sullivan, J.C. and J.S. Pollock, *Coupled and uncoupled NOS: separate but equal? Uncoupled NOS in endothelial cells is a critical pathway for intracellular signaling.* Circ Res, 2006. **98**(6): p. 717-9.
281. Kassab, G.S., et al., *Morphometry of pig coronary arterial trees.* Am J Physiol, 1993. **265**(1 Pt 2): p. H350-65.
282. Steinhausen, M., H. Tillmanns, and H. Thederan, *Microcirculation of the epimyocardial layer of the heart. I. A method for in vivo observation of the microcirculation of superficial ventricular myocardium of the heart and capillary flow pattern under normal and hypoxic conditions.* Pflugers Arch, 1978. **378**(1): p. 9-14.
283. Toyota, E., et al., *Dynamic changes in three-dimensional architecture and vascular volume of transmural coronary microvasculature between diastolic- and systolic-arrested rat hearts.* Circulation, 2002. **105**(5): p. 621-6.
284. Xu, H., et al., *Leukocytosis and resistance to septic shock in intercellular adhesion molecule 1-deficient mice.* J Exp Med, 1994. **180**(1): p. 95-109.
285. Paulus, W.J. and C. Tschope, *A novel paradigm for heart failure with preserved ejection fraction: comorbidities drive myocardial dysfunction and remodeling through coronary microvascular endothelial inflammation.* J Am Coll Cardiol, 2013. **62**(4): p. 263-71.
286. Schindler, T.H. and V. Dilsizian, *Coronary Microvascular Dysfunction: Clinical Considerations and Noninvasive Diagnosis.* JACC Cardiovasc Imaging, 2019.
287. Ormerod, J.O., et al., *Human Second Window Pre-Conditioning and Post-Conditioning by Nitrite Is Influenced by a Common Polymorphism in Mitochondrial Aldehyde Dehydrogenase.* JACC Basic Transl Sci, 2017. **2**(1): p. 13-21.
288. Yang, Z., et al., *Myocardial infarct-sparing effect of adenosine A2A receptor activation is due to its action on CD4+ T lymphocytes.* Circulation, 2006. **114**(19): p. 2056-64.
289. Boag, S.E., et al., *T lymphocytes and fractalkine contribute to myocardial ischemia/reperfusion injury in patients.* J Clin Invest, 2015. **125**(8): p. 3063-76.
290. Finsterbusch, M., et al., *Patrolling monocytes promote intravascular neutrophil activation and glomerular injury in the acutely inflamed glomerulus.* Proc Natl Acad Sci U S A, 2016. **113**(35): p. E5172-81.